

The Mineralogy, Geochemistry and Microbiology of Cobalt-bearing Mine Tailings from the
Cobalt Mining Camp in Northeastern Ontario, Canada

by

Brittaney Courchesne

A thesis submitted in partial fulfillment
of the requirements for the degree of
Master of Science (MSc) in Geology

The Faculty of Graduate Studies
Laurentian University
Sudbury, Ontario Canada

© Brittaney Courchesne, 2020

THESIS DEFENCE COMMITTEE/COMITÉ DE SOUTENANCE DE THÈSE

Laurentian University/Université Laurentienne
Faculty of Graduate Studies/Faculté des études supérieures

Title of Thesis

Titre de la thèse The mineralogy, geochemistry and microbiology of Cobalt-bearing mine tailings from the Cobalt mining camp in Northeastern Ontario, Canada

Name of Candidate

Nom du candidat Courchesne, Brittany

Degree

Diplôme Master of Science

Department/Program

Département/Programme Geology

Date of Defence

Date de la soutenance November 23, 2020

APPROVED/APPROUVÉ

Thesis Examiners/Examineurs de thèse:

Dr. Nadia Mykytczuk

(Co-Supervisor/Co-directrice de thèse)

Dr. Michael Schindler

(Co-Supervisor/Co-directeur de thèse)

Dr. Graeme Spiers

(Committee member/Membre du comité)

Approved for the Faculty of Graduate Studies
Approuvé pour la Faculté des études supérieures

Dr. Lacey Marie Brogden

Madame Lacey Marie Brogden

Acting Dean, Faculty of Graduate Studies

Doyenne intérimaire, Faculté des études supérieures

Dr. Jeanne Pervical

(External Examiner/Examineur externe)

ACCESSIBILITY CLAUSE AND PERMISSION TO USE

I, Brittany Courchesne, hereby grant to Laurentian University and/or its agents the non-exclusive license to archive and make accessible my thesis, dissertation, or project report in whole or in part in all forms of media, now or for the duration of my copyright ownership. I retain all other ownership rights to the copyright of the thesis, dissertation or project report. I also reserve the right to use in future works (such as articles or books) all or part of this thesis, dissertation, or project report. I further agree that permission for copying of this thesis in any manner, in whole or in part, for scholarly purposes may be granted by the professor or professors who supervised my thesis work or, in their absence, by the Head of the Department in which my thesis work was done. It is understood that any copying or publication or use of this thesis or parts thereof for financial gain shall not be allowed without my written permission. It is also understood that this copy is being made available in this form by the authority of the copyright owner solely for the purpose of private study and research and may not be copied or reproduced except as permitted by the copyright laws without written authority from the copyright owner.

Abstract

Advancements in the field of biotechnology have proven bioleaching processes as an economic and environmentally safe form of mining. Most bioleaching studies to date however have been focused on Fe, Cu, and Au-sulfidic mine tailings, rather than metalloid-rich, neutral-pH tailings. This thesis will apply a multidisciplinary and multi-variate statistical approach to explore whether the neutral, Co and As-rich tailings material within the Cobalt mining camp can be efficiently bioleached. Tailings material within 30-cm depth profiles from three tailings sites (sites A, B and C) were characterized for their mineralogical, chemical and microbial community compositions, followed by the execution of bench-scale oxidative and reductive bioleaching experiments. Tailings material from sites A, B and C are composed primarily of quartz, albite, clinocllore, calcite and dolomite with minor safflorite, arsenopyrite, erythrite and annabergite. The material at site A contains on average more (sulf-)arsenides and higher concentrations of Fe than site B. Site C however is altogether geochemically and mineralogically dissimilar, with the presence of distinct reduced and oxidized zones. Variations in the Co+As+Sb+Zn (Co#), Fe (Fe#), and total S (S#) have been identified as geochemical markers for the presence of Fe, Co-arsenides versus secondary Co, Ni, Zn-arsenates, e.g. tailings material with a high Co# and low Fe# tend to have a higher proportion of secondary arsenate minerals. In the tailings material of sites B and C, a lower average As valence coincides with a higher S#. Three distinct site-specific groupings are observed for 1) the Co vs Fe and S#'s and 2) the microbial communities. The Cobalt tailings are primarily composed of Actinobacteria and Proteobacteria and N, S, Fe, methane, and (possible) As-cycling bacteria. The tailings from sites B and C have a larger abundance of Fe- and S-cycling bacteria (e.g. *Sulfurifustis* and *Thiobacillus*), of which are more abundant at greater depths, whereas the tailings of site A have a higher proportion of potential

As-cycling and -resistant genera (e.g. *Methylocystis* and *Sphingomonas*). The microbial communities appear to be highly correlated to depth, S#, Fe#, pH, and the average valence of As. The variation in the average valence of As correlates well with the abundances of N, S, Fe, and methane-cycling bacteria (e.g. *Nitrospira* sp., the order Thermodesulfobionia, and *Methylocystis* sp.). Aerobic and anaerobic bioleaching experiments were conducted on three samples (in duplicate) from each site, with six samples characterized by high and/or low Co, Fe and S#'s and three bulk, site-specific samples. The experiments used the tailings native consortia and had three methods/treatments. The first two were for chemolithotrophic and heterotrophic bacteria enrichment, with the third serving as a control or baseline experiment. The experiments ran for 18-weeks, with (1) biweekly measurements of pH, Eh, and total and dissolved metals, and (2) analysis of the microbial community composition through 16S rRNA DNA extraction at experiment completion. The highest abundance of As-reducing and -oxidizing genera (i.e. *Delftia* and *Dechloromonas*) were observed in the heterotroph-enrichments, which was additionally characterized as having the highest Co and As recovery (0.94 and 29.8 %, respectively). Samples that were composed of a higher proportion of Co, Ni, Zn-arsenates and Fe, Co-arsenides were observed to be enriched in Fe-reducing bacteria or As-reducing and -oxidizing genera, respectively. The enrichments were able to successfully shift the microbial communities to those involved in As-cycling. However, further work is required to determine what hindered the metal recovery process, i.e. future micro- and/or nano-scale studies may indicate that Co and As precipitated as Co-phosphates.

Acknowledgements

To Dr. Nadia Mykytczuk, first off, thank you for being my supervisor on this project, and for your willingness to take me on as a student with no microbiological background. Thank you for your understanding, support and patience throughout the many hurdles I faced during the completion of this project, and for teaching me all about microbes! They truly are fascinating.

To Dr. Michael Schindler, thank you for being my supervisor, for your guidance in helping me choose an undergraduate degree, for taking me under your wing after my second year of said undergraduate degree, for and showing me how exciting and challenging environmental geochemistry can be. Thank you for your support, patience, for all of the very enjoyable trips to labs in different provinces, and, of course, for your very fast, 24-hour email response.

To Dr. Graeme Spiers, thank you for all of your help over the years, for accompanying me during sampling for my undergraduate project, for the lab work, and for all of the wonderful and exciting stories.

Thank you to Anthony Story of Story Environmental Inc. for showing me around Cobalt, ON and aiding in my tailings sample collection, also to Chris Kennedy of Agnico Eagle for providing me with informative data on Cobalt.

Thank you to all of the lab technicians that have helped me see this Masters project through. To Willard Desjardins, thank you for the hilarious chats, chocolate, and of course helping to prepare my SEM samples. To William Zhe, thank you for all of your help on the SEM during both my undergraduate degree as well as my Masters degree. To Troy Maki and Alex Withers, thank you for processing my tailings samples and for all of your help. To Peter Blanchard and Renfei Feng of the Canadian Light Source in Saskatoon, thank you so much for all of your help, and for answering my emails very promptly. A special thank you to Alan Lock and Heather Dufour at the Perdue Central Analytical Facility for re-processing my samples time and time again in order to get the best possible data. Alan Lock, thank you so much for all of your help, and Heather

Dufour, I simply can't thank you enough for working around the clock, even on your vacation time, so that I could complete my data analysis on time, as well as your friendship along the way.

Thank you to the Basiliko and Mykytczuk lab at the Vale Living with Lakes Centre as well as my fellow graduate students in the Harquail Earth Science department. It was through your support and friendship that made these last two years truly enjoyable.

An additional special thank you to: the R guru, Emily Smenderovac for teaching me the ways of statistics and the R programming language, James Seward for teaching me about the anaerobic world, Katlyn Mitchell for always being around to answer my millions of questions, ensuring me that, despite my many experimental setbacks, it would all work out in the end, and for joining me in Cobalt for a day of sampling. To Gretchen Lescord, thank you for helping me in the ICP lab and for being a wonderful person to talk to about academia politics. To Nathalie Tremblay, thank you for teaching me about microbiology, coming from a geological background, I truly knew nothing; it was also sincerely a pleasure going through this Masters alongside you. Extra special thank you to Robert Meek for joining me in field sampling, keeping me on my toes during the seminar question period, and finally, for accompanying me to Saskatoon, enduring sleep-deprivation due to lab work, and helping me so much with the data collection and processing. Thank you to Madison Cooper and Saskia Hart for helping me with my bioleaching experiment re-start and analyses. Also, thank you to Roxane Mehes and Edda Bozzato for always helping me with anything in the WGMC when I needed help, and for the delicious snacks that were always available. Thank you all for your friendship along the way.

And finally, thank you to my family, friends, and partner Jeff for all of your non-stop understanding, love, and support during this, at times, very difficult, but ultimately rewarding, journey.

Brittaney

Table of Contents

Abstract	iii
Acknowledgements	v
List of Figures	xiii
List of Tables	xv
Abbreviations	xvi
Chapter One: Introduction	1
1 General Introduction	1
1.1 Arsenic-bearing Mine Tailings in Canada	1
1.2 Thesis Objectives	5
1.3 Original Contributions	6
Chapter Two: Literature Review	7
2 Biogeochemistry of Arsenic, Cobalt and Silver	7
2.1 Arsenic	7
2.1.1 Occurrence, Abundance and Use	7
2.1.2 Chemistry and Geochemistry of Arsenic	8
2.1.3 Primary and Secondary Arsenic Minerals	10
2.1.4 Microbial-driven Arsenic Processes	11
2.1.5 Remediation and Disposal of Arsenic	14
2.2 Cobalt	16
2.2.1 Occurrence, Abundance and Use	16
2.2.2 Primary and Secondary Co-bearing Minerals	17
2.2.3 Cobalt in Soils	18
2.2.4 Bioremediation of Cobalt-ores	19
2.3 Silver	21
2.3.1 Occurrence, Abundance and Use	21
2.3.2 Silver Mineralogy	22
2.3.3 Silver in the Soil Environment	23
2.3.4 Microbial Interaction with Silver	24
2.3.5 Silver Nanoparticles	25
2.3.6 Silver-bearing Waste	26
3 Mineral-Microbe Interactions	26
3.1 Overview	26
3.2 Microbe-mineral Contact Mechanisms	28

3.3	Microbial-mediated Mineral Precipitation.....	29
3.4	Microbial-mediated Mineral Dissolution and Transformation	30
3.5	Metal(loid) Mobilization and Immobilization	31
3.6	Applications for Bioremediation.....	32
Chapter Three: The geochemistry, mineralogy and microbiology of selected alkaline, legacy mine tailings sites from Cobalt, Ontario		
4	Introduction.....	33
4.1	Background information	36
4.1.1	Past studies on the relationships between microbial communities and geochemical-mineralogical parameters	36
4.1.2	Previous microbial studies on sediments around the Cobalt mining camp	38
4.1.3	Past studies on the speciation of As in natural waters and sediments around the Cobalt mining camp.....	39
5	Materials and Methods.....	40
5.1	Study Area	40
5.2	Sampling methods and storage	41
5.3	Field measurements	42
5.4	Total Carbon and Sulfur Analysis.....	43
5.5	Chemical analysis - Inductively Coupled Plasma Mass Spectrometry.....	43
5.6	Powder X-ray Diffraction	44
5.7	Scanning Electron Microscopy	44
5.8	DNA Extraction and Computational Biology.....	45
5.9	X-ray Absorption Near-Edge Spectroscopy - VESPERS.....	46
5.10	Statistical Analysis.....	47
6	Results.....	48
6.1	Bulk Chemical Compositional Changes versus the Abundance of (sulf-)arsenides.....	49
6.1.1	Arsenate and (sulf-)arsenides in the tailings material.....	53
6.2	Tailings microbiological composition	55
6.2.1	Bulk microbial community composition	55
6.2.2	Metal-cycling microbial populations	56
6.2.3	Iron and/or sulfur-cycling community composition	57
6.2.4	Identification of potential As-cycling and/or As-resistant communities	60
6.2.5	Microorganisms common to metal-contaminated environments.....	61
6.2.6	Nitrogen-cycling community composition	61
6.2.7	Methanotrophic and methylotrophic populations	62

6.2.8	Identified species in the tailings sites.....	63
6.3	Multivariate Statistical Analysis.....	63
6.3.1	Analysis of Similarities.....	63
6.3.2	Non-metric multidimensional scaling analysis.....	64
6.3.2.1	Bulk microbial community relationships with environmental and geochemical variables	64
6.3.2.2	Microbial community site-specific relationships with environmental and geochemical variables.....	66
6.3.2.3	Site-specific overall trends relating the environmental and geochemical variables to microbial structures.....	70
7	Discussion.....	73
7.1	Geochemical and mineralogical features of the tailings material at sites A, B and C..	73
7.2	Main environmental and/or geochemical drivers in microbial diversity across each tailings site	75
7.2.1	Contact pH as related to microbial communities.....	76
7.2.2	Variation of microbial communities with depth in each tailings profile	77
7.2.2.1	The abundance of S and C-oxidizing and -reducing bacteria with depth.....	78
7.2.3	Microbial community shift due to changes in total carbon content.....	78
7.2.4	Iron and sulfur-cycling bacteria in neutral-to-alkaline pH conditions.....	79
7.2.5	Microbial community composition versus the average valence of As	81
7.2.5.1	The role of nitrogen-cycling “group 1” bacteria with respect to the valence of arsenic	83
7.2.5.2	The role of bacteria capable of S, Fe and As cycling with respect to As valence	84
7.2.5.3	Relation of methanotrophic bacteria to As-reduction.....	86
7.2.6	Silver relation to microbial communities.....	88
7.3	Iron mobilization in alkaline tailings	89
7.4	Summary of microbes potentially involved in As-cycling for use in bioleaching of As-rich neutral-pH tailings	91
	Mineralogical effects on the microbial community: a summary	92
8	Conclusions.....	93
	Chapter Four: The bioleaching potential of Co from selected alkaline legacy mine tailings sites from the Cobalt Mining Camp, Ontario.....	94
9	Introduction.....	94
9.1	Background Information.....	96
9.1.1	Past Microbial Studies on the Farr and Mill Creek Wetlands in Cobalt, ON.....	96

9.1.2	Microbial Communities Involved in As-cycling	97
9.1.3	Bioleaching of Arsenide or Arsenate-ores	99
10	Materials and Methods.....	100
10.1	Study Area, Sampling Methods and Storage	100
10.2	Bioleaching Experiment Setup	100
10.2.1	Initial Preparation.....	100
10.2.2	Aerobic and Anaerobic Experiment Setup and Incubation.....	101
10.3	Bi-weekly Analyses	103
10.3.1	Contact pH and ORP Measurements	103
10.3.2	Chemical Analysis	103
10.4	Experiment Shutdown and Sample Preservation.....	104
10.5	DNA Extraction and Computational Biology.....	104
10.6	Statistical Analysis.....	104
11	Results.....	105
11.1	Trends of Contact pH.....	105
11.2	Total and Dissolved Cobalt and Arsenic Concentration.....	106
11.3	Percent Metal Recovery from Bioleaching Enrichment Experiments.....	109
11.3.1	Cobalt and Arsenic Recovery	109
11.4	Relation of As and Co concentrations to pH	112
11.5	Microbial Community Composition.....	112
11.5.1	Phylum-level Bulk Microbial Composition.....	114
11.5.2	Order-level Bulk Microbial Composition.....	115
11.5.3	Control Experiment Microbial Community Composition	116
11.5.4	Chemolithotroph-enrichment Experiment Microbial Community Composition	118
11.5.5	Heterotroph-enrichment Experiment Microbial Community Composition.....	120
11.5.6	Diversity of As, S, Fe and N-cycling Microbial Communities Between Enrichments	120
11.5.6.1	Control Experiments	121
11.5.6.2	Chemolithotroph-enrichments	121
11.5.6.3	Heterotroph-enrichments	122
11.5.6.4	Arsenic-cycling Populations	123
11.5.7	Identified Species in the Bioleaching Experiments	124
11.5.8	Comparison of the Background Microbial Community to the Enriched Microbial Communities.....	125
11.6	Multivariate Statistical Analysis.....	127

11.6.1	Non-metric Multidimensional Scaling Analysis.....	127
12	Discussion.....	129
12.1	Contact pH as Related to the Concentration Fluctuations of As and Co.....	129
12.2	Potential Precipitation as a Solid Phase.....	129
12.3	Microbial Communities in Treatments versus the Tailings Background Microbial Community.....	131
12.4	Microbial Community Structure as Related to High Concentrations of Co and As in Solution.....	132
12.4.1	Leaching Patterns in the Control Experiments.....	133
12.4.2	Leaching Patterns in Chemolithotroph-enrichments.....	133
12.4.3	Leaching Patterns in Heterotroph-enrichments.....	134
12.5	Mechanisms of Microbial Leaching.....	134
12.6	Suggestions for Future Bioleaching of the Cobalt Mining Camp Tailings.....	136
13	Conclusions.....	136
Chapter Five: General Conclusions and Project Implications.....		137
14	Conclusions.....	137
14.1	General Conclusions.....	137
15	Future Work.....	138
16	Project Implications and Potential Applications.....	139
17	References.....	140
Appendix A: The mineralogy and geochemistry of Cobalt-bearing mine tailings in North-Eastern Ontario, Canada (Courchesne et al., 2020).....		189
Appendix B: Mineralogy of the Cobalt Mining Camp.....		270
Appendix C: X-ray Diffractograms.....		271
Appendix D: Raw Sequence Data and Rarefaction Curve.....		274
Appendix E: XANES Spectra.....		276
Appendix F: Analysis of Similarities (ANOSIM).....		279
Appendix G: Bulk Chemical Data.....		280
Appendix H: Additional SEM results from sites B and C.....		282
Appendix I: Additional Taxonomic Plots.....		284
Appendix J: Correlation Matrices.....		288
Appendix K: Output Tables from NMDS Plots.....		291
Appendix L: Silver Concentration versus Depth.....		295
Appendix M: Eh Measurements.....		296
Appendix N: Raw Sequence Data and Rarefaction Curve.....		297

Appendix O: Concentrations of Total and Dissolved Cobalt and Arsenic Released Over Time	300
Appendix P: Total and Dissolved Metal Concentrations from Enrichment Experiments	303
Appendix Q: Additional Taxonomic Plots after Bioleaching Experiments.....	309

List of Figures

Figure 1. a) Photo showing the location of Cobalt in Ontario, relative to Sudbury and Toronto; b) A photo showing the mines, mills, and tailings deposits in the Cobalt Mining Camp.	41
Figure 2. Photographs of the three tailings sites with their 30-cm depth profiles, showing site A (a, d), B (b, e) and C (c, f) at the day of sampling.	43
Figure 3. Depth profile plots of pH (a), Eh (b), total sulfur (c) and total CO ₂ (d) versus depth [cm].	50
Figure 4. Depth profile plots of sites A to C (rows a – c)) with the concentrations of (1) As, (2) Co and (3) Fe, and (4) the average As valence versus depth [cm].	51
Figure 5. Depth profiles of sites A to C (rows a – c)) with columns as (1) Co#, (2), Fe# and (3) S# versus depth [cm].	52
Figure 6. Two XY-plots of Co# versus (a) S# and (b) Fe#.	53
Figure 7. SEM photomicrographs and EDS-chemical maps for representative grains from each tailings site. A silver-sulfide (a, b), Ni, Co-arsenate coating on silicates (c, d), Ni, Co-arsenate coating on carbonates (e, f), and a Co-arsenate coating on silicates and an Fe, Co-arsenide (g, h).	55
Figure 8. Normalized relative abundance taxonomic bar plot of the background tailings microbial communities at the Phylum level.	57
Figure 9. Normalized relative abundance taxonomic bar plot of the background tailings microbial communities at the Order level.	58
Figure 10. Normalized relative abundance taxonomic bar plot of the background tailings microbial community at the Genus level.	59
Figure 11. NMDS plot of microbial communities showing distinct groupings per site, coloured by pH, with insets of Co# vs (b) S# and (c) Fe#.	65
Figure 12. NMDS plot showing the variation in environmental and geochemical variables with site, and their effect on the microbial communities of sites A, B and C.	67
Figure 13. Site-specific NMDS plots showing how the environmental and geochemical parameters effect the microbial community within the tailings samples of site A (a), site B (b), and site C (c). The equation for the average As valence ratio (AVR) is given in Eq. 5.	69
Figure 14. An annotated NMDS plot showing the variation in important environmental and geochemical parameters on the microbial community composition of tailings from site A.	71
Figure 15. An annotated NMDS plot showing the variation in important environmental and geochemical parameters on the microbial community composition of tailings from site B, with an additional inlet showing the average of As and the percent of As that is As ⁵⁺ at D = 25 and 30 cm.	72
Figure 16. An annotated NMDS plot showing the variation in important environmental and geochemical parameters on the microbial community composition of tailings from site C.	73

Figure 17. The bioleaching experiment schematic, showing two methods of leaching (aerobic or anaerobic) each of which in three growth conditions (control, heterotroph-enrichment, and chemolithotroph-enrichment).	102
Figure 18. XY-plots showing the variation of pH within the 18-week experiments. The aerobic experiments are observed in a) – c) and the anaerobic experiments in d) – f).	107
Figure 19. Six double-bar graphs illustrating the cumulative percent of total and dissolved Co and As released during the 18-week control bioleaching experiments. The aerobic experiments are shown in a) to c) and the anaerobic in d) to f).	110
Figure 20. Six double-bar graphs showing the cumulative percent of total and dissolved Co and As released during the 18-week chemolithotroph-enrichment experiments. The aerobic experiments are shown in a) to c) and the anaerobic in d) to f).	111
Figure 21. Six double-bar graphs showing the cumulative percent of total and dissolved Co and As released during the 18-week heterotroph-enrichment experiments. The aerobic experiments are shown in a) to c) and the anaerobic in d) to f).	113
Figure 22. Normalized relative abundance taxonomic bar plot of the microbial communities after bioleaching experiments on the Phylum level.	115
Figure 23. Normalized relative abundance taxonomic bar plot of the microbial communities after bioleaching experiments on the Order level.	117
Figure 24. Normalized relative abundance taxonomic bar plot of the microbial communities after bioleaching experiments on the Genus level.	119
Figure 25. NMDS plot showing the similarities and differences in the microbial communities per six bioleaching experiments.....	128

List of Tables

Table 1. The naming scheme for each sample, used in the taxonomic plots.....	42
Table 2. The variation in groups of microbes as related to the average As valence and depth of site C's tailings profile.....	82

Abbreviations

Average	<i>A</i>
Anaerobic control experiment	<i>AC</i>
Anaerobic chemolithotroph-enrichment	<i>ACh</i>
Anaerobic heterotroph-enrichment	<i>AH</i>
Anaerobic glove box	AGB
Silver nanoparticles	AgNPs
Acid mine drainage	AMD
Analysis of similarities	ANOSIM
Ammonia-oxidizing bacteria	AOB
Acid-producing bacteria	APB
Arsenic-oxidizing bacteria	AsOB
Arsenic-reducing bacteria	AsRB
Average arsenic valence ratio	AVR
Biologically-controlled mineralization	BCM
Biologically-induced mineralization	BIM
Back-scattered electrons	BSE
Aerobic control experiment	<i>C</i>
Canadian Council of Ministers of the Environment	CCME
Aerobic chemolithotroph-enrichment	<i>Ch</i>
Cobalt Mining Camp	CMC
Depth	D
Deionized	DI

Energy dispersive X-ray spectrometry	EDS
Environmental Protection Agency	EPA
Extracellular polysaccharides	EPS
Iron-oxidizing bacteria	FeOB
Iron-reducing bacteria	FeRB
Gram per ton	g/t
Group 1	G1
Group 2	G2
Group 3	G3
Group 4	G4
Group 5	G5
Aerobic heterotroph-enrichment	<i>H</i>
Inductively coupled plasma mass spectrometer	ICP-MS
Milligram per kilogram	Mg/kg
Methane monooxygenase enzyme	MMO
Methane-oxidizing bacteria	MOB
Most probable number	MPN
Minimal salts media	MSM
Non-metric multidimensional scaling	NMDS
Nanoparticles	NPs
Nitrate-reducing bacteria	NRB
Oxidative reductive potential	ORP
Operational taxonomic unit	OTU

Ounces	oz
Polymerase chain reaction	PCR
Platinum-group elements	PGE
Parts per million	ppm
Parts per billion	ppb
Powder X-ray diffraction	pXRD
Point of zero charge	PZC
Reps per minute	RPM
Secondary electrons	SE
Scanning electron microscopy	SEM
Sulfur-oxidizing bacteria	SOB
Sulfate-reducing bacteria	SRB
Transmission electron microscopy	TEM
Trivalent methylated arsenic	TMA
Tailing management facility	TMF
Total organic carbon	TOC
United States Environmental Protection Agency	USEPA
Very Sensitive Element and Structural Probe Employing Radiation from a Synchrotron	VESPERS
Weight percent	wt %
X-ray absorption near edge spectroscopy	XANES
Yellow Springs Instrument	YSI

Chapter One: Introduction

1 General Introduction

1.1 Arsenic-bearing Mine Tailings in Canada

Arsenic-bearing mine tailings in Canada are often associated with gold (Au) and uranium (U) mining activities and occur in the Northwest Territories, the Yukon, Nova Scotia and Saskatchewan. In tailings, arsenic (As) can occur in a variety of forms, with the most common being arsenopyrite, arsenical pyrite, arsenates, and As-bearing Fe-oxyhydroxides (Paktunc et al., 2003).

There exists a significant As contamination legacy due to mining activities around Yellowknife, Northwest Territories. The Giant Mine, located on the shore of Great Slave Lake, is considered to be the largest anthropogenic source of bioaccessible As in the region (MVRB, 2013). Over 7 million troy ounces (oz) of refractory Au was recovered from primarily arsenopyrite and (arsenical-)pyrite between 1948 and 1999 (Andrade et al., 2010; Jamieson, 2014; Fawcett et al., 2015). Due to the refractory nature of the Au-deposit, roasting of the As-rich Au-ore was implemented as a pre-treatment prior to cyanidation (Jamieson, 2014; Walker et al., 2015). As a consequence of the roasting, As became more toxic, soluble, and bioaccessible, due to the conversion from an As-hosted sulfide to an As-hosted oxide (Jamieson, 2014). The abundance of neutralizing carbonate minerals within the gangue material produced a neutral-to-alkaline pH leachate from the tailings and waste rock (Jamieson, 2014; Fawcett et al., 2015; Walker et al., 2015). Jamieson (2014) argued that the concentration of As into nearby water sources was potentially enhanced by a higher pH leachate. During Giant Mine's fifty-year mine life, As contamination occurred in various ways: air contamination by As_2O_3 -bearing dust in the mine itself; smelter emission of As_2O_3 particulate matter and their deposition on lakes, rivers,

soils and sediments, and drainage of As from roasting products deposited within tailings impoundments into surface- and groundwaters (Andrade et al., 2010; Jamieson, 2014; Fawcett et al., 2015; Walker et al., 2015). The latter two types of contaminations resulted in As concentrations in nearby drinking water sources above the Canadian Council of Ministers of the Environment (CCME) water quality guidelines (5 µg/L) (CCME, 2001). The Giant Mine is now classified as an abandoned mine, with the costs for its remediation estimated at \$1 Billion Canadian (AANDC, 2012; Jamieson, 2014).

Similarly to the Giant Mine in NWT, the Nova Scotia gold mining district in Nova Scotia, Canada has also left behind a large environmental legacy of As contamination (Walker et al., 2009). During over 80 years (1861-1942) of mining activities in the 64 gold mining districts of Nova Scotia, 1.2 million oz of Au (34020 kg of Au) was recovered from arsenopyrite-bearing ore which led to the deposition of over 3 million tonnes of tailings material (Walker et al., 2009; DeSisto et al., 2016). Orogenic Au-deposits exist in the Meguma Terrane of Nova Scotia with an analogous ore vein gangue mineralogy to that of the Giant Mine, with the exception of slightly less carbonate mineral component (< 5-15 % carbonate minerals) and higher sulfide content (Groves et al., 1998; Kontak and Smith, 1998; Ryan and Smith, 1998). Contrary to the Giant Mine, the tailings within the Nova Scotia gold mining district have a wide range of As concentrations (10 mg/kg to 31 weight percent (wt %), median: 2550 mg/kg) and the As content is associated with the arsenopyrite-rich waste from gravity concentrates (Corriveau et al., 2011a, 2011b; Parsons et al., 2004, 2015; Jamieson, 2014). There are four different types of tailings deposits within the Nova Scotia gold mining district, 1) hard-pan bearing; 2) oxic; 3) high calcium; and 4) wetland-type. In these tailings, As occurs in different geochemical and mineralogical environments and thus different remediation techniques will be required to contain

the As contamination (DeSisto et al., 2016). The Nova Scotia gold mining districts are affected by the drainage of As-bearing effluents with acidic-to-neutral pH values (Walker et al., 2009), as well as by aeolian transport of As-bearing particulate matter from tailings into nearby residential areas (Corriveau et al., 2011a and b).

The Ketz River Mine is located in south-central Yukon, Canada, and hosts Au-bearing ore bodies composed of either sulfide (11.3 g/t Au) or oxide ore (18 g/t Au) (Paktunc et al., 2004). Here, the Au occurs as invisible gold in arsenopyrite and pyrite and as coarse gold (grains up to 25 microns in diameter) within goethite and hisingerite ($\text{Fe}^{3+}_2(\text{Si}_2\text{O}_5(\text{OH})_4 \cdot 2\text{H}_2\text{O})$) (Abercrombie, 1991). From 1988 to 1990, 2.8 tonnes of Au were produced through conventional carbon-in-pulp leaching (Paktunc et al., 2004, 2015) and 310,000 tonnes of waste material were deposited into a tailings impoundment under partial water cover (Paktunc et al., 2004). As of 2003, an average of 4 - 7 wt % As occurs in the tailings, with As concentrations reaching 34 wt % As_2O_5 in Fe(III)-oxyhydroxides (Paktunc et al., 2004). The Fe(III)-oxyhydroxides occur as both discrete particles as well as secondary reaction rims on pyrite and arsenopyrite (Paktunc et al., 2015). Soprovich (2000) showed that the mobilization of As from the tailings impoundments were above the environmentally acceptable limits for mine effluents (0.5 mg/L), due to numerous (geochemical) factors, such as: 1) the presence of highly soluble Fe \pm Ca-arsenate minerals; 2) the instability of Fe(III)-oxyhydroxides having Fe/As molar ratios less than 4; and 3) As mobilization from natural sources, such as unmined ore and the surrounding mineralized rocks (Paktunc et al., 2003, 2004, 2015). Considering the instabilities of both Fe \pm Ca-arsenate minerals at neutral pH conditions, As will continue to leach in concentrations above the acceptable limits from the Ketz River Mine tailings site (Paktunc et al., 2003, 2004, 2015).

The high-grade, unconformity-type uranium deposits in the Athabasca basin, Saskatchewan, Canada has on average 1.2 wt % As (Canada, 1998), but can contain locally up to 10 wt % As (Langmuir, 1999). The U-deposits in the basin vary from mono-minerallic to polymetallic, with the polymetallic deposits having the highest concentration of As (Schindler et al., 2013). Mining in the Athabasca basin began in 1953, and has continued since (Donahue et al., 2000; Jefferson et al., 2007; Shaw et al., 2011). Nickel and cobalt (Co)-bearing arsenide and sulfarsenide minerals (e.g. nickeline, cobaltite, and gersdorffite) are the primary As-mineral phases in the U-ore of the Athabasca basin (von Pechmann, 1981, Schindler et al., 2013 and references therein). The high-grade ore was processed using sulfuric acid (H₂SO₄) digestion under strong oxidizing conditions, leading to the liberation of As from the As-bearing minerals (Essilfie-Dughan et al., 2013). During early U-mining (pre-1975) in the area, the tailings were disposed into topographic lows and lakes (Donahue et al., 2000). After 1975, tailings management facilities (TMFs) were built, followed by engineered in-pit TMFs in 1984 (Donahue et al., 2000). In the tailings, As mainly occurs as pentavalent (As⁵⁺) adsorbed to ferrihydrite, through inner-sphere bidentate complexes (Essilfie-Dughan et al., 2013). The long-term stability of the As sorbed ferrihydrite is of great concern, since ferrihydrite is metastable and can transform over time into goethite and hematite. During this phase transformation the surface area of the Fe-(hydr)oxide polymorphs decreases which subsequently results in the desorption and release of As into solution (Schwertmann and Murad, 1983; Manceau and Drits, 1993; Essilfie-Dughan et al., 2013). However, Das et al. (2011), suggested that if the environmental conditions remain stable within the TMFs, the As-bearing ferrihydrite should remain stable for thousands of years. Due to pH buffering, and neutralization and evaporation processes, a number of secondary As-bearing minerals such as troegerite ((H₃O)[(UO₂)(AsO₄O)(H₂O)₃], and gypsum form during

the interaction of mill-process solutions with limed-treated tailings material (Schindler et al., 2013). Laird et al. (2014) showed that within the surrounding lakes of the Saskatchewan uranium mines, the As concentrations are 1.3 to 110 times than that of background and reference lakes. Additionally, Laird et al. (2014) concluded that: 1) more research is needed to further understand the mechanism of metal transport into the lakes and the environmental and ecological health risks of the lakes within a close proximity to the uranium mines and TMFs and 2) that the treated effluent management system, TMFs, and waste-rock piles are most likely the source of As contamination within the lakes, as they are connected through aquatic systems.

1.2 Thesis Objectives

The interaction between minerals and microorganisms is of great importance in the interdisciplinary field of geomicrobiology, which integrates the geology, chemistry and biology fields (Gadd, 2010). Geomicrobiology is defined as the roles that microorganisms play in geological processes (Parkes, 1998; Canuel, 2007; Konhauser, 2007; Ehrlich and Newman, 2009). Our understanding of these roles can, for example, enhance our understanding of the biogeochemical cycling of elements, the formation of minerals, mineral dissolution and chemical transformations of elements, while thereby linking these roles for their potential exploitation in bioremediation or biotechnological processes (Gadd, 2010).

This thesis will be presented in five chapters: Chapter 1) a general introduction and objectives for the thesis; Chapter 2) a literature review of the biogeochemistry of arsenic, cobalt and silver, and mineral-microbial interactions; Chapter 3) the first research chapter entitled *The geochemistry, mineralogy and microbiology of selected alkaline legacy mine tailings sites from the Cobalt Mining Camp, Ontario*; Chapter 4) the second research chapter entitled *The*

bioleaching potential of Co from selected alkaline legacy mine tailings sites from the Cobalt Mining Camp, Ontario; and Chapter 5) on project conclusions and implications. Chapter 3 is based on earlier work from my undergraduate thesis, which addressed the geochemical and mineralogical composition and relationships therein of two tailings sites. The work of which is appended in this thesis (Appendix A). Chapter 4 focuses on results and implications of a bench-scale bioleaching study. More specifically, the key objectives of this study include to:

- (1) Characterize the geochemical, microbial and mineralogical composition of each site, while identifying site-specific similarities and differences;
- (2) Identify the biogeochemical relationships occurring at each site, in order to determine how variations in geochemical and mineralogical character of the tailings affect the composition of the microbial communities, including whether changing As valence has an effect on the microbial community composition;
- (3) Design and conduct bench-scale oxidative and reductive bioleaching experiments to determine the bioleaching potential of the tailings; and
- (4) To compare and contrast the microbial community composition occurring both before and after bioleaching experiments.

1.3 Original Contributions

This study will aid in the current lack of knowledge and understanding of the biogeochemical composition and relationships in arsenic-bearing tailings material of neutral contact pH. The results of this study may also improve the current understanding of how As-bearing tailings characterized by neutral contact pH drainage can be effectively remediated in order to prevent any long-term environmental impacts.

Chapter Two: Literature Review

2 Biogeochemistry of Arsenic, Cobalt and Silver

2.1 Arsenic

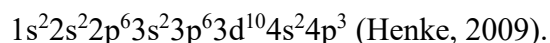
2.1.1 Occurrence, Abundance and Use

Arsenic is the 47th most abundant, naturally occurring, ubiquitous element that exhibits both metallic and non-metallic properties (Essilfie-Dughan et al., 2013, and references therein). Arsenic has an average crustal and upper continental crust abundance of 2.5 ppm, and 5.7 ppm, respectively (Hu and Gao, 2008; Essilfie-Dughan et al., 2013). The concentration of As is commonly more abundant in marine shales and mudstones (Tourtelot, 1964), and when concentrated by magmatic and hydrothermal processes (Boyle and Jonasson, 1973; Essilfie-Dughan et al., 2013; Howell et al., 2014). Arsenic is known worldwide for its toxicity to all forms of life; however, it is a useful element in metallurgical applications as well as in the manufacture of wood preservatives (Wang and Mulligan, 2006), pesticides, herbicides, crop desiccants, and as an additive to livestock feed (Howell et al., 2014). Arsenic can also be used as a “pathfinder” element for (poly)metallic ore deposits, especially Au, Cu, Sn and W-deposits (Boyle and Jonasson, 1973; Howell et al., 2014). Globally, As can occur in the environment due to the natural weathering of As-bearing sediments, biological activity, and volcanic emissions (Weisener et al., 2011), however, industrial activities (e.g. mining and fossil fuel combustion) are the most important environmental sources (Duker et al., 2005; Howell et al., 2014). During common pyrometallurgical mining operations such as roasting and smelting, As is volatilized as arsenic trioxide ($As_2O_3(g)$) and/or arsenic trisulfide ($As_2S_3(g)$) (Valenzuela, 2000; Weeks and Wan, 2000). In the past, these phases are then collected and stored in underground chambers

(Piret, 1999) or if storage containment is poor, they are left on surface (Walker et al., 2009.). The high solubility and toxicity of As_2O_3 , in particular, is of great environmental concern, as there is the potential for leaching into nearby groundwater (Filippou and Demopoulos, 1997). In the environment, the toxicity, mobility and fate of As is dependent on chemical speciation, mineralogy, pH, redox potential and biological processes (Mulligan and Yong, 2004; Bowell et al., 2014).

2.1.2 Chemistry and Geochemistry of Arsenic

Arsenic can exist in nature in four different oxidation states, -3, 0, +3 and +5, and as organic and inorganic species (Essilfie-Dughan et al., 2013, and references therein). The most abundant oxidation states of arsenic in the environment are trivalent (As^{3+}) and pentavalent (As^{5+}) arsenic, of which As^{3+} is 25 – 60 times more toxic than As^{5+} and several hundred times more toxic than organic As-species (Smedley and Kinniburgh, 2002; Essilfie-Dughan et al., 2013). The higher toxicity of As^{3+} relative to the other oxidation states is directly related to its coordination geometry (Zampella et al., 2012). Trivalent As, as well as Pb^{2+} (for example) both have a stereochemically active (or stereoactive) lone pair of electrons, resulting in a distorted molecular structure (Walsh and Watson, 2005; Walsh et al., 2011; Zampella et al., 2012). The electron configuration of As^0 is written as:



Trivalent As has the formal electron configuration: $3d^{10} 4s^2 4p^0$ (Henke, 2009). Hybridization of the *s*- (spherical) and *p*- (a defined direction) orbitals results in the movement of the $4s^2$ electrons into a *p*-orbital with a defined direction, resulting in a stereoactive lone pair of electrons. This pair of electrons has a higher affinity and selectivity to proteins in a cell, potentially leading to

metal toxicity in humans and ecological receptors (Zampella et al., 2012). Trivalent methylated arsenic (TMA) species have been identified as being more toxic than inorganic As^{3+} , as TMA species are more capable of causing DNA breakdown in all life forms (Styblo et al., 2000; Dopp et al., 2004). In general, As^{3+} is known to be more mobile than As^{5+} (Korte and Fernando, 1991), however, this varies with As-species and Eh-pH conditions. The most thermodynamically stable As-species are: 1) $(\text{H}_2\text{AsO}_4)^-$ and $(\text{HAsO}_4)^{2-}$ within the natural range of groundwater redox conditions (150 - 500 mV and pH of 4 - 7); 2) $(\text{H}_2\text{AsO}_4)^-$, in acid-mine drainage waters (pH < 5); and 3) $\text{As}(\text{OH})_3$ within very reduced waters (Eh < 200 mV) (Wilson et al., 2010; Bowell and Craw, 2014).

Arsenic behaves similar to other chalcophile elements, in that it can be: 1) released by sulfide oxidation; 2) altered by various biogeochemical processes, and 3) sequestered through adsorption and co-precipitation with Fe-minerals, clay minerals, and organic matter (Bowell et al., 2014). In the presence of sulfur, low pH, and reducing conditions, sulfides and arsenides such as arsenopyrite (FeAsS), löllingite (FeAs_2), orpiment (As_2S_3) and realgar (AsS) are the most stable As-bearing phases (Bowen, 1979; Vink, 1996; Wilson et al., 2010; Bowell et al., 2014). Under oxidizing conditions, scorodite ($\text{FeAsO}_4 \cdot 2\text{H}_2\text{O}$) and amorphous hydrous ferric arsenate are among the common As^{5+} -bearing phases in mine tailings (Walker et al., 2009; Wilson et al., 2010). The sorption rate of arsenate (AsO_4^{3-}) is high on nanocrystalline Fe-(oxy)hydroxide particles and on clay minerals (Fordham and Norrish, 1979; Wilson et al., 2010). Specifically, the sorption of arsenate on the clay minerals kaolinite and montmorillonite increases as pH decreases, with a maximum adsorption at circa pH = 4 to 6 (Wilson et al., 2010). Conversely, arsenite (AsO_3^{3-}) sorption on select clay minerals increases as pH approaches a neutral value with a maximum adsorption at circa pH = 7 (Elkhatib et al., 1984; Wilson et al., 2010). Highly

porous surface coatings on Fe-oxides can increase the amount of adsorbed arsenate species on the surface of the minerals (Wilson et al., 2010). Elkhatib et al. (1984) stated that As^{3+} adsorption is irreversible and governed by the presence of Fe-oxides (i.e. amorphous Fe-oxides and magnetite) and Eh. Arsenate and arsenite species both adsorb to Fe-hydroxides (i.e. goethite), with a maximum sorption at pH of 7 and 4, respectively (Wilson et al., 2010). Acero et al. (2006) have identified jarosite, schwertmannite and goethite as major hosts of As in acid mine drainage. The authors showed that more As can be sequestered by schwertmannite and H_3O -jarosite than by goethite and that As is released during the transformation of schwertmannite and jarosite into goethite with increasing pH.

2.1.3 Primary and Secondary Arsenic Minerals

In terms of mineral phases, As can occur as native As and in arsenides, sulfides, oxides, arsenates, mixed-anion arsenates, and, in rare cases, arsenites, for a total of 586 As-bearing minerals as of 2014 (Bowell et al., 2014). Arsenic is present in many rock-forming minerals as it can substitute for P^{5+} , Si^{4+} , Al^{3+} , Fe^{3+} and Ti^{4+} (Bowell et al., 2014). However, pyrite is known as the largest reservoir of As in crustal rocks (Nordstrom, 2000), with As concentrations up to 16.5 wt % in synthetic marcasite and 10 wt % in natural pyrite (Reich et al., 2005; Neumann et al., 2013; Simon et al., 2013). Several of the most common primary As-bearing minerals consist of: arsenopyrite, cobaltite, enargite, gersdorffite, löllingite, and pyrite (Drahota and Filippi, 2009). Secondary As minerals, such as As oxides, Ca, Mg, Fe-arsenates, sulfoarsenates and -ites, and other metal arsenates (e.g. Co, Ni, Zn, Pb) are formed when primary As minerals are subjected to weathering processes (e.g. exposure to the atmosphere and surface or ground waters; Drahota and Filippi, 2009). Scorodite is the most common secondary As mineral under oxidizing and

acidic conditions, forming from the oxidation of arsenopyrite or As-bearing pyrite (Drahota and Filippi, 2009). In near-neutral pH, high As^{5+} and low Fe^{3+} conditions, minerals of the pharmacosiderite group such as arseniosiderite, a Ca-Fe arsenate are more common (Krause and Ettl, 1989; Swash and Monhemius, 1995; Drahota and Filippi, 2009). Other metal arsenates are rare in nature, with their occurrence restricted to specific chemical systems in natural environments, such as in tailings from five-element (Ni-Co-As-Ag-Bi±U) vein deposits and environments polluted by As pesticides (Drahota and Filippi, 2009).

2.1.4 Microbial-driven Arsenic Processes

Within the Earth's environmental systems, biogeochemical cycles are largely driven by electron transfer among microorganisms (microbes; Huang, 2014). The release of As into the environment is influenced by a combination of mobilisation, sequestration and transformation processes, most of which are either directly or indirectly induced by the activity of microbes (Huang, 2014). Abiotic As transformation can also take place but at a much slower rate and of lesser importance to microbially-mediated As transformation (Ahmann et al., 1997; Newman et al., 1997; Jones et al., 2000). The behaviour of As in the environment is influenced by a number of naturally-occurring redox reactions, resulting in changes to As mobility through a change in oxidation state (i.e. $\text{As}^0 / \text{As}^{3+} / \text{As}^{5+}$) and dissolution and precipitation of As-bearing minerals (Huang, 2014).

The reduction and oxidation of Fe and S are among a few of the most studied natural redox reactions. Corsini et al. (2010) showed that the mobilization of As can be attributed to the microbial Fe-reductive dissolution, when As and Fe occur together in solid phases (Cummings et al., 1999). *Shewanella* strains can immobilize As through microbial Fe-reduction via the

formation of Fe³⁺-arsenate precipitates (Jiang et al., 2013). Microbial-induced Fe³⁺-hydroxide formation (through Fe-oxidation) can result in the sequestration of As, and its immobilization in acid mine drainage environments (Duquesne et al., 2003; Ma and Lin, 2012). This process has been applied for remediation of As contaminated sites in anoxic environments (Huang, 2014). During sulfidation, As has the potential to be mobilized or immobilized. Arsenic can be sequestered by ferrihydrite and secondary Fe²⁺-minerals, such as magnetite (Saalfield and Bostick, 2009; Kocar et al., 2010), and also mobilized through S-reductive dissolution of ferrihydrite, resulting in the release of As-S complexes into pore waters (Burton et al., 2011). By exploiting microbial-mediated redox processes, As can be bioleached from sulfide minerals by using acidophilic Fe-oxidizing microbes such as *Acidithiobacillus (At.) ferrooxidans* (Marquez et al., 2012). *At. ferrooxidans*, among others, is also capable of oxidizing As³⁺ to As⁵⁺, decreasing As mobility (Zhang et al., 2007). Microorganisms that are able to oxidize or reduce As (e.g. the oxidation of arsenite (As³⁺)) do so heterotrophically as a mode of detoxification, whereas those that gain energy from this oxidation or reduction process are chemolithotrophic organisms (Oremland and Stolz, 2005). These chemolithotrophic organisms use As as a terminal electron acceptor in anaerobic respiration (Langner and Inskeep, 2000; Stolz et al., 2002; Corsini et al., 2010). Through the reductive dissolution of both Mn and Fe-(hydr)oxides by microbes such as *Geobacter* spp., As⁵⁺ can be liberated (Corsini et al., 2010). Solid-associated As⁵⁺ (adsorbed and structurally incorporated) has the potential to be mobilized through respiratory As⁵⁺-reduction (Zobrist et al., 2000; Babechuk et al., 2009; Huang et al., 2011). In addition to As⁵⁺, As³⁺ can serve as an electron donor for microbial respiration in combination with O₂ or nitrate, for oxic and anoxic conditions, respectively (Paez-Espino et al., 2009). *Thermus aquaticus*, *Thermus thermophilus* (Gihring et al., 2001) and *Sinorhizobium* sp. M14 (Drewniak et al., 2008b), as well

as species within the genera *Pseudomonas* (Drewniak et al., 2010), *Alcaligenes*, *Thiomonas*, *Herminiimonas*, and *Agrobacterium*, have all been identified as being able to oxidize As^{3+} to As^{5+} in As-contaminated soils or tailings (Cai et al., 2009). Additionally, known dissimilatory As^{5+} -reducing microbes, in anoxic, limed mine tailings environments, consist of, for example: *Sulfurospirillum barnesii*, *Bacillus arsenicoselenatis*, *B. selenitireducens*, *S. arsenophilum*, *Desulfotomaculum auripigmentum*, *Chrysiogenes arsenatis*, and *Desulfomicrobial strain Ben-RB*, as well as the archaea *Pyrobaculum arsenaticum* and *P. aerophilum* (Macur et al., 2001). While in acidic mine tailings conditions, *Sinorhizobium* sp. M14, *Shewanella* sp. O23S and *Aeromonas* sp. O23A have been identified as species that can either reduce arsenate through detoxification (*Sinorhizobium* sp. M14; Drewniak et al., 2008b) or through anaerobic respiration (*Shewanella* and *Aeromonas* spp.; Drewniak et al., 2010).

Drewniak et al. (2008a) also identified 22 As-tolerant bacterial isolates within biofilms from the Zloty Stok gold mine site within the genera *Arthrobacter*, *Bacillus*, *Brevundimonas*, *Chryseobacterium*, *Desemzia*, *Microbacterium*, *Micrococcus*, *Paracoccus*, *Pseudomonas*, *Rhodococcus*, *Serratia*, *Sphingomonas*, *Strentrophomonas*, and *Streptomyces*. Numerous species within the *Acidithiobacillus* genus are capable of As-resistance as well, e.g. *At. caldus* and *At. ferrooxidans*, as well as *Leptospirillum ferriphilum* and *Corynebacterium glutamicum* (Dopson et al., 2003; Ordóñez et al., 2005; Mateos et al., 2006). As of 2006, the latter species was identified as being the most As^{3+} and As^{5+} -resistant species (Mateos et al., 2006).

The production of siderophores by microbes, can aid in enhancing the dissolution of insoluble minerals while providing the microbes with a nutrient source (Gadd, 2004). Siderophores can inhibit the formation of Fe, As-bearing secondary minerals through their complexation of Fe^{3+} , leaving As in the soluble phase (Huang, 2014). This is important in mine waste environments, as

siderophores produced by *Pseudomonads* strains, such as *Pseudomonas azotoformans*, can promote mineral dissolution and As mobilization in mine waste (Matlakowska et al., 2008).

The occurrence of most biogenic As-minerals formed by microbes are to this day unclear, however, the production of these minerals can immobilize As in solution. For example, microbes can form diagenetic Ca-arsenates (Martinez-Villegas et al., 2013), scorodite and As-bearing sulfides, and calcite by As³⁺-tolerant *Sporosarcina ginsengisoli* (Huang, 2014). Certain bacterial species, such as *Bacillus cereus* (Giri et al., 2013) and *Acidithiobacillus ferrooxidans* (Chandraprabha and Natarajan, 2011; Yan et al., 2010), can have As³⁺ and As⁵⁺ sorb to their surface through electrostatic interactions (Huang, 2014). The sorption of As to a microbial surface is dependent on the point of zero charge, for example, the maximum As³⁺ adsorption for *Bacillus cereus* is at a pH of 7.5 (Giri et al., 2013).

2.1.5 Remediation and Disposal of Arsenic

Arsenic contamination has been long recognized as a global problem, with the largest contributors to contamination being from the oxidation of As-bearing sulfide minerals and the reductive dissolution of As-bearing Fe³⁺-oxyhydroxides (Bowell and Craw, 2014). These forms of contamination can occur through either natural processes or a result of industrial activity, like mining (Bowell and Craw, 2014). Therefore, as of 2001, the United States Environmental Protection Agency (USEPA) has put in place a maximum allowable concentration of As in drinking water, as 10 mg/L (Bowell and Craw, 2014). Due to the potential toxicity of As to humans and ecological receptors, there has been an increasing effort to lessen the potential impact of As contamination by monitoring both legacy and existing sites, as well as creating guidelines for future operational sites (Bowell and Craw, 2014).

The remediation of As contaminated sites is a relatively new and technologically innovative field involving bioremediation and hyperaccumulation methods (Wang and Mulligan, 2006), and exploiting the geochemical affinities existing between As and low-temperature phases in order to reduce As bioavailability in the environment (Morin and Calas, 2006). There are numerous As-bearing compounds that have been widely researched for safe and long-term disposal, due to the potentially toxic effects of As in the environment. The long-term stability of such compounds depends on the: site characteristics, particle crystallinity, size distribution, effects of bacterial activity, and whether complexing agents are present (Riveros et al., 2011). Currently, the most favoured As disposal method is the formation of a compound containing Fe^{3+} and As^{5+} , either as a poorly crystalline As-bearing ferrihydrite or as crystalline ferric-arsenate (e.g. scorodite) (Riveros et al., 2011; Bowell and Craw, 2014). The formation of As-bearing ferrihydrite, where arsenate oxyanions are strongly adsorbed to the surface of the mineral, is a stable low-temperature disposal method under oxidizing conditions in a pH environment of 4 – 7 (Riveros et al., 2011). Here, the highest stability occurs at a high Fe / As ratio (> 3), and in the presence of base metals such as Cd, Cu and Zn (Riveros et al., 2011). Crystalline ferric arsenate minerals, such as scorodite, is the high-temperature As disposal method (Riveros et al., 2011). Scorodite has been observed to be more stable than As-bearing ferrihydrite, however, it has also been observed to dissolve above pH 4 under reducing conditions (Riveros et al., 2011). Additionally, scorodite may undergo reductive dissolution in the presence of Fe-reducing bacteria (e.g. *Shewanella putrefaciens* CN32 and ANA-3) after the formation of Fe^{2+} -carbonate minerals, by the aforementioned Fe-reducing bacteria (Revesz et al., 2015). Nevertheless, the formation of an insoluble ferric arsenate compound is presently being used in the bioleaching of

As-bearing Au ores as the USEPA has deemed it stable for long-term disposal (Acevedo et al., 1998; Nyombolo et al., 2000; Duquesne et al., 2003; Corkhill et al., 2008).

2.2 Cobalt

2.2.1 Occurrence, Abundance and Use

Cobalt is classified as a siderophile and ferromagnetic element, with diverse uses based on its hardness, low thermal and electrical conductivity, high melting point, multiple valences, and its resistance to wear when alloyed with other metals (Hamilton, 1994; Slack et al., 2017). The demand for Co has increased significantly in recent years due to the growing electric and solar-powered car industry (The Cobalt Institute, 2019). Cobalt is also used for producing permanent magnets in wind turbines, increasing the strength and resistance of superalloys, and in healthcare, pigments, electronics and catalysts (The Cobalt Institute, 2019).

The bulk average Co concentration in the Earth's crust is 29 ppm (Slack et al., 2017), with ultramafic igneous rocks, such as dunite and serpentinite, having the highest averages of 109 and 115 ppm Co, respectively (Slack et al., 2017). The presence of Co in minerals can range from less than 10 ppm to greater than 8 %, the latter of which in Co-rich ores (Young, 1957). Cobalt can become enriched to form ore deposits through the following processes: 1) magmatic differentiation, where basic or ultrabasic rocks become more concentrated in Co, Ni, Cr, etc. (e.g. Sudbury norite, a unit within the Sudbury Igneous Complex, Ontario; Stonehouse, 1954); 2) hydrothermal activity, which may form the largest number of deposits (e.g. Cobalt, Ontario; Kissin, 1992); 3) chemical weathering, leading to the formation of Co-laterite deposits (Vhay, 1952); and 4) concentration of Co in organic matter, forming Co-rich coal deposits (Young, 1957). Worldwide, Co is most commonly mined from stratiform sediment-hosted Cu-Co

deposits, Ni-Co laterite deposits, and magmatic Ni-Cu(-Co-PGE) sulfide deposits (Slack et al., 2017). Lesser amounts of Co are also produced from: black-shale-hosted Ni-Cu-Zn-Co deposits, skarn deposits, iron-oxide deposits, Mississippi Valley-type Zn-Pb deposits, volcanogenic massive sulfide deposits, and polymetallic vein (or five-element vein) deposits (Kissin, 1992; Slack et al., 2017).

2.2.2 Primary and Secondary Co-bearing Minerals

Cobalt occurs in primary (hypogene) and secondary (supergene) minerals. Primary Co-core minerals include sulfides and (sulf-)arsenides, such as carrollite ($\text{Cu}(\text{Co},\text{Ni})_2\text{S}_4$), pentlandite ($(\text{Fe},\text{Ni},\text{Co})_9\text{S}_8$), safflorite ($(\text{Co},\text{Fe})\text{As}_2$), skutterudite ($(\text{Co},\text{Fe},\text{Ni})\text{As}_{2-3}$), cobaltite (CoAsS), cobaltiferous pyrite ($(\text{Fe},\text{Co})\text{S}_2$), and pyrrhotite ($(\text{Fe},\text{Co})_{1-x}\text{S}$) (Young, 1957; Slack et al., 2017). Secondary Co-bearing mineral phases are those that form during weathering, such as erythrite ($\text{Co}_3(\text{AsO}_4)_2 \cdot 8\text{H}_2\text{O}$), also known as “cobalt bloom”, and oxyhydroxides (e.g. heterogenite ($\text{CoO}(\text{OH})$); Slack et al., 2017). Although the former Co-arsenate is an important secondary Co-mineral in the mine tailings around Cobalt, ON, it is a relatively rare mineral in As-bearing mine tailings (Drahota and Filippi, 2009; Nordstrom et al., 2014; Mayzlan et al., 2014). The formation of cobalt phosphates (e.g. pakhomovskyite ($\text{Co}_3(\text{PO}_4)_2 \cdot 8\text{H}_2\text{O}$)), may play an important factor during bioleaching of Co-bearing alkaline mine waste as phosphate-bearing salt solutions are often used to enhance microbial activities in the waste rock material. Cobalt phosphates are sparingly soluble salts with $\text{Co}_3(\text{PO}_4)_2$ being the compound with the lowest solubility [$\text{Co} = 2.56 \cdot 10^{-13}$ mg/kg, at equilibrium], as determined via the geochemical speciation program Visual Minteq (Gustafsson, 2019). Erythrite and pakhomovskyite are both members of the vivianite-mineral group ($\text{A}_3(\text{XO}_4)_2 \cdot 8\text{H}_2\text{O}$, where A = divalent, Mg, Fe, Co, Ni, Zn, and X = As, P), hence, it is not

uncommon for P to substitute for As inside the crystal lattice of erythrite during incubated bioleaching experiments (Frost et al., 2003).

Cobaltiferous oxyhydroxides are also common in secondary Co-deposits (e.g. goethite (FeO(OH))), however, whether Co is structurally incorporated into the mineral's crystal lattice or adsorbed onto the surface remains unclear (Slack et al., 2017). With an ionic radius of 0.58 Å, Co²⁺ can to a certain degree substitute for Mg, Cu, Fe²⁺, Fe³⁺, Mn³⁺, Ni²⁺ and Sn⁴⁺ in a mineral's crystal lattice, due to a similar ionic radii, ranging from 0.49 to 0.63 Å (Shannon, 1976; Hamilton, 1994, Slack et al., 2017). Cobalt can occur in two oxidation states (divalent and trivalent), with divalent Co (Co²⁺) being the most thermodynamically stable within most environmental conditions (Hem, 1985). Trivalent cobalt (Co³⁺) occurs when Co²⁺ is oxidized by manganese (Mn³⁺, Mn⁴⁺, Mn⁷⁺), and is subsequently sorbed to, and structurally incorporated into, Mn-oxides (Murray and Dillard, 1979; Tanaka et al., 2013; Simanova and Pēna, 2015).

2.2.3 Cobalt in Soils

In soils, the total content of Co present is within the range of 0.1 to 50 ppm, of which only 0.1 - 2 ppm is bioavailable (Young, 1979; Hamilton, 1994). Through weathering, Co can be leached from its original material(s) and enter soils and sediments, whereby it can be partially taken up by plants, animals, and eventually humans (Hamilton, 1994). Cobalt is an essential element to most forms of life; the lack of bioavailable Co in soils (< 0.08 ppm) can lead to a vitamin B12 deficiency in ruminants (Patterson, 1938; Young, 1957; Hamilton, 1994). With the addition of lime to soils, the availability of Co decreases, therefore in most countries, Co-salts or -chelated compounds are added to fertilizers, lime, and sewage sludge (Hamilton, 1994). The amount and composition of organic matter, clay mineralogy, pH, redox potential, adsorption, co-

precipitation, and organic complexation processes all have a role in controlling the availability of Co for plant translocation via root system and foliage (Hamilton, 1994). The concentration of Co in soils and/or sediment is a function of its proximity to a Co-source, i.e. industrial activity, and whether the surrounding rocks are enriched in Co (Hamilton, 1994). However, Hamilton (1994) stated that, in general, the concentration of Co within soils and sediments is directly proportional to that of Fe.

2.2.4 Bioleaching of Cobalt-ores

Newsome et al. (2020) completed metal-reducing leaching experiments with laterite sediments, where Co occurred with Mn as Co-Mn-oxides. The authors identified: 1) the recoverable concentrations of Co and Mn both increased proportionally to each other; 2) recoverable Fe only slightly increased; and 3) the growth of Mn- and Fe-reducing bacteria (e.g. *Clostridiales*) and the *Penicillium* fungi within the leached materials. Newsome et al. (2020) concluded that the leaching of Co in laterites is controlled by Mn-reducing and -oxidizing bacteria, and therefore by the Mn biogeochemical cycling of microbes. An Fe-reducing bacterium, *Shewanella putrefaciens*, was identified by Crowe et al. (2007) to release both Co and Ni into an aqueous phase, through the dissolution of Mn-minerals.

In order to bioleach sulfidic, polymetallic mine tailings and tailings flotation concentrate, Zhang et al. (2020) employed a consortium of mesophilic and acidophilic microorganisms, consisting mainly of *Acidithiobacillus (At.) ferrooxidans* and *At. thiooxidans*. In these tailings, Co mainly occurred attached to the surface of framboidal pyrite, with direct, oxidative microbial attack being the predominant mode of leaching (Zhang et al., 2020). The use of this mesophilic and acidophilic consortium proved efficient for the bioleaching of Co, with 91 and 66 %

extraction of Co from the bulk tailings (within 13 days) and the tailings flotation concentrate, respectively (Zhang et al., 2020). Marrero et al. (2015) showed that the same mesophilic and acidophilic organisms as used by Zhang et al. (2020) can also be employed for bioleaching Co and Ni from oxidized, laterite tailings through aerobic and anaerobic reductive dissolution. Similar amounts of Co (55 – 60 %) and Ni (53 – 57 %) were recovered after only 7 days in the aerobic and anaerobic bioleaching experiments (Marrero et al., 2015). Cui et al. (2015, 2018) also identified heterotrophic bacteria, rather than acidophilic bacteria, that are capable of bioleaching Ni and Co from a sulfidic concentrate at a neutral pH, with an added secondary sulfuric acid step, resulting in a total of 76.3 % Ni and 60.7 % Co recovery. Comparatively, in a study by Yang et al. (2019), the authors tested the bioleaching efficiency of fungi, namely *Aspergillus niger*, on both Co-bearing lateritic and pyritic ores. Yang et al. (2019) concluded that (1) bioleaching Co from lateritic versus pyritic ore using fungal biomass had much higher recovery rates, 65.9 ± 1.8 % versus 4.9 ± 2.7 %, for lateritic and pyritic ores, respectively, and (2) in the lateritic ores, the Co (occurring as Co-bearing goethite) was bioleached via direct interaction between the fungus and minerals, with *A. niger* releasing metabolites to dissolve the Co-phases.

Bioleaching of Co from an arsenide ore was conducted using Fe-oxidizing acidophilic microorganisms (*Acidithiobacillus ferrooxidans* and *Leptospirillum ferriphilum*; Giebner et al., 2019a). These microorganisms were not able to grow efficiently in the presence of arsenides, however, Giebner et al. (2019a) concluded that with the addition of citrate, Co was more effectively liberated and the bacterial activity was stabilized. Giebner et al. (2019b) also conducted the first bioleaching study on safflorite (CoAs_2)-bearing ore, with an acidophilic Fe-

oxidizing consortium, resulting in an 80 % recovery of both Co and Ni, however only 50 % of the As being liberated, due to ferric-arsenate precipitates.

The biogeochemistry of Co is, to this day, poorly understood (Newsome, 2020). More extensive studies on how the biogeochemical cycling of Co affects its behaviour in the environment is warranted, so as to aid in developing new recovery techniques from Co-ores, such as the bioleaching potential of Co at an exclusively neutral pH.

2.3 Silver

2.3.1 Occurrence, Abundance and Use

Silver (Ag) is a precious and transition metal, with a white to gray-metallic appearance that is valued for its use as currency as well as in jewelry, photoprocessing, electronics, and healthcare (Purcell and Peters, 1998; VandeVoort and Arai, 2012). Per year, approximately 140 million troy oz of Ag are consumed, with between 2.4 and 2.5 million kg being lost to the environment (Scow et al., 1981).

The range of Ag contained within the Earth's crust is between 0.04 to 50 ppm, with an average of 0.07 ppm (Purcell and Peters, 1998; Luoma and Rainbow, 2008). In nature, Ag can occur as one of four forms: 1) as a native element; 2) as a primary component of Ag-minerals; 3) as a trace to minor component in associated ore minerals; and 4) as a natural alloy with other metals (i.e. Au and Cu) (King, 2020). Unlike Co, Ag has four oxidation states, native (Ag^0), monovalent (Ag^+), divalent (Ag^{2+}), and trivalent (Ag^{3+}) (VandeVoort and Arai, 2012). However, due to the very high ionization energies of Ag^{2+} and Ag^{3+} , Ag^0 and Ag^+ are the most common in the environment (VandeVoort, 2012).

Silver often occurs in association with quartz, Au, Cu, sulfides and arsenides (King, 2020). Native Ag is uncommon within oxidized zones and above other mineralized zones, such as in zones of Pb-Zn mineralization (King, 2020). Silver deposits are normally associated with hydrothermal activity, with Ag occurring within veins and cavity fillings (e.g. Cobalt, Ontario) (Joyce et al., 2012; King, 2020). A majority of the mined silver is produced as a by-product of Pb-Zn mining (40 %), Cu mining (22 %) and Au mining (13 %) (Emsley, 2001). Silver is conventionally extracted from Pb and Zn-sulfide ore by high-pH preferential flotation technology (Hu et al., 1983), with a newer low-alkalinity method having been developed in 2012 in China by Sun et al. (2012). Comparatively, cyanidation is the common practice for Ag and Au recovery from arsenopyrite-bearing ore (Espieill et al., 1986). Silver can also occur in five-element vein deposits, such as that observed in Cobalt, ON (Kissin, 1992). The Ag-bearing ore within the Cobalt camp was processed using methods such as flotation separation, cyanide dissolution and Hg pan amalgamation to extract silver (Percival et al., 2004).

2.3.2 Silver Mineralogy

Silver is associated with different mineral groups, such as: sulfides, (sulf-)arsenides, sulfates, antimonides, carbonates, silicates, oxides, hydroxides, tellurides, and halides (Joyce et al., 2012; King, 2020). Monovalent Ag occurs as: 1) the substitution of Ag for metal cations within an ore mineral (for example, Pb in galena; Bell and Kramer, 1999); 2) native Ag or Ag-mineral inclusions within an ore mineral (King, 2020); or 3) it can be replaced by other divalent or trivalent metal cations, such as: Fe^{2+} , Zn^{2+} , Pb^{2+} , Cd^{2+} , and As^{3+} (Bell and Kramer, 1999), shown in Equation 1 (Cloke, 1963).



The most common Ag-ore minerals include: argentiferous galena (PbS), the low and high temperature polymorphs acanthite and argentite (Ag_2S), proustite (Ag_3AsS_3), stephanite (Ag_5SbS_4), and tetrahedrite-group minerals ($(Cu,Fe,Ag)Sb_4S_3$; (Bell and Kramer, 1999; King, 2020). Monovalent Ag can sorb rapidly onto amorphous FeS (Adams and Kramer, 1998) and other colloidal or particulate sulfides at low nanomolar concentrations (Bell and Kramer, 1999). At higher concentrations of Ag, Ag will replace metal cations, yielding $Ag_2S_{(s)}$ (Bell and Kramer, 1999).

2.3.3 Silver in the Soil Environment

In soils, the average Ag concentration is 3 ppm (Kramer, 1996). The concentration of Ag in soils and pore waters is controlled mainly by chemical weathering, through the dissolution of Ag-bearing minerals (VandeVoort and Arai, 2012). In both organic and inorganic species, Ag^+ has a strong covalent bond with sulfur ($2-$; S^{2-}) and forms a linear di-coordinate arrangement ($-S-Ag-S-$), resulting in zig-zag chains in minerals and organic complexes (VandeVoort and Arai, 2012). These zig-zag chains can also be formed in solution and aggregate to form colloids (VandeVoort and Arai, 2012). In anoxic sediment, thiols (an organosulfur compound) can act as ligands for Ag^+ , resulting in the formation of acanthite or argentite (below or above $173\text{ }^\circ\text{C}$, respectively) (Frueh, 1958; Bell and Kramer, 1999). Thiol compounds have also been shown to mobilize a portion of Ag^+ by forming strong soluble complexes (Adams and Kramer, 1998), however the importance of these complexes in nature is yet to be determined (Bell and Kramer, 1999). The sorption of Ag^+ can occur both above and below the point of zero charge (PZC) on

clay minerals at the soil mineral-water interface, through either outer-sphere or inner-sphere complexes, respectively (Vandervoort and Arai, 2012). For example, Ag^+ can sorb to: ferrihydrite below its PZC of 6, and to iron oxides (PZC \sim 6.5) and birnessite (PZC \sim 2.8) above a pH of 4 (Dyck, 1968; Smith and Carson, 1997; Jacobson et al., 2005).

2.3.4 Microbial Interaction with Silver

Silver does not appear to play an essential role in cell metabolism (Stiefel, 1996; Fisher and Wang, 1998), however Ag^+ has been included in the formation of $\text{Fe}^{2+}\text{-S}^{2-}$ clusters in proteins (Beinert et al., 1997). Monovalent Ag has become a concern in marine and freshwater environments as benthic organisms show a strong bioaccumulation to silver (Crececius, 1993; Luoma, 1993), due to Ag's strong affinity to sulfur (Smith and Martell, 1977). Russell and Hugo (1994) illustrated that some bacteria are able to gain Ag^+ -resistance in the environment, for example *E. coli* was able to decrease its uptake of Ag^+ , reducing its exposure. However, Ag can also be very toxic to microbes and viruses (Emsley, 2001) due to the preferential binding of S-containing ligands within microbial cells, such as the thiol group on the amino acid cysteine (Liau et al., 1997). Therefore, the USEPA has placed a maximum concentration level of 0.1 mg/L Ag in drinking water (EPA, 2011).

Huerta-Rosas et al. (2020) identified a chemoorganotrophic microbial consortium that were capable of aerobic bioleaching of Mn and Ag from mine tailings located in Mexico using bacterial and fungal strains isolated from the tailings. The bacterial strains consisted of *Roseospira* sp. and *Sphingomonas* sp., and together with the fungal strains, there was a total recovery of 40 – 67 % Ag. A culture of moderately thermophilic acidophiles (*At. caldus* and *Leptospirillum ferriphilum*) have also been identified as being capable of cooperative

bioleaching of chalcopyrite and Ag-bearing mine tailings, with Ag mainly occurring as Ag-sulfate (Zhao et al., 2015).

2.3.5 Silver Nanoparticles

Silver can also occur in the environment as manufactured silver nanoparticles (AgNPs), composed of Ag⁰, and a diameter range between 1 and 100 nm (Oberdorster et al., 2005). These metallic NPs are being biosynthesized in an emerging field call bionanomining, an agglomeration of mining and bionanotechnology (Wong-Pinto et al., 2020). The biosynthesis of NPs can be achieved through the use of bacteria, fungi, yeast, plants and/or algae (Wong-Pinto et al., 2020). Silver NPs have been biosynthesized using an EPS (extracellular polysaccharides) layer secreted by *Lactobacillus brevis*, of which showed antimicrobial activity against *Staphylococcus aureus* and *E. coli*, antioxidant activity against free radicals, and potential anticarcinogenic applications (Rajoka et al., 2020). Due to the small particle size of AgNPs, they have a large surface area and therefore large and potentially reactive surface, making their fate in soil-water environments unpredictable and of a serious environmental concern (Oberdorster et al., 2005; VandeVoort and Arai, 2012). Silver NPs have the potential to also be toxic to bacterial membranes, causing protein denaturation and apoptosis (VandeVoort and Arai, 2012; and references therein), due to their possible preferential binding to S-ligands once inside the cell (Wigginton et al., 2010). However, the toxicity mechanism of AgNPs, in terms of bacterial cells, is not fully understood.

Geological processes have also been identified as a culprit of AgNPs in the environment, such as those seen in association with nickel-laterite ore deposits in New Caledonia (Cymes et al., 2017) and in epithermal Au-deposits (*cf.* Burke et al., 2017). In New Caledonia, the

occurrence of AgNPs in untreated mine effluents is causing serious negative impacts on the organisms residing in the New Caledonian reef ecosystem (Cymes et al., 2017).

2.3.6 Silver-bearing Waste

Silver released is in the form of solid waste, with 66 % coming mainly from households, and the remaining 34 % from anthropogenic activities such as smelting and mining (Purcell and Peters, 1998). In sulfide-bearing tailings from Ag-Cu-Pb-Zn-producing mines in Taxco, Mexico, primary Ag occurs as Ag-sulfosalts and arsenides, with its release primarily driven by pH and naturally occurring oxidation-neutralization processes (Talavera Mendoza et al., 2005).

Additionally, due to Au cyanidation processes, the resulting waste can contain residual Au and Ag, such as at a tailings site from the Novo-Ursk auriferous pyritic deposit in the Kemerovo region of Russia, where Ag primarily occurs as isomorphic impurities in alunite-jarosite minerals (Myagkaya et al., 2016). During oxidation of the waste, AMD (acid mine drainage) water is produced containing high concentrations of potentially toxic metal(loid)s, as well as Au and Ag existing in “*dissolved+colloidal*” and particulate forms, which then flows into the Ur River (Myagkaya et al., 2016). The reclamation and recycling of Ag should be encouraged as to minimize the amount of Ag-bearing minerals and materials at waste sites, in outfalls, and in biosolids (Purcell and Peters, 1998).

3 Mineral-Microbe Interactions

3.1 Overview

Microorganisms including different bacteria and archaea have been identified in a wide range of Earth’s extreme environments, from crystalline rocks of the deep surface, within frozen

ice from thousands of metres under Antarctic ice sheets, acid mine drainage, hot springs, to deep ocean hydrothermal vent systems (Dong, 2010). Microbes are responsible for playing key active roles in the biosphere, with biotransformations, biogeochemical cycling, metal and mineral transformations, decomposition, bioweathering, and soil and sediment formation being the most environmentally vital (Gadd, 2010). Comparatively, metals and minerals are also able to affect the growth, activity, and survival of microbes (Gadd, 2010). In environments where oxygen is abundant, aerobic microbes can interact with oxide and silicate minerals in order to gain essential nutrients. In order to avoid exposure to sunlight, aerobic microbes commonly interact with minerals in a near-surface environment or in pore spaces below the mineral surface (Dong, 2010). Conversely, in environments where oxygen is limited, anaerobic microbes utilize oxidized forms of metals as terminal electron acceptors (Lovely, 2000; Newman, 2001; Lloyd, 2002; Konhauser, 2007; Dockrey et al., 2014) through the simultaneous conversion of reduced to oxidized carbon (C)-, sulfur (S)-, or nitrogen (N)- species (e.g. organic C and S⁰; Konhauser, 2007). Gorby et al. (2006) and Lu et al. (2012) have suggested that electron transport does not only occur between bacteria and minerals, but also within different microbial communities, creating a network of interaction and resource sharing (Nielsen et al., 2010).

Mineral-microbe interactions are often energetically favourable, as microbes seek nutrients for their growth and cellular metabolism from minerals, whereas the chemical system along a mineral surface seeks to achieve a minimal Gibbs free energy through the charge satisfaction of underbonded atoms (Konhauser, 2007; Dong, 2010; Dong and Lu, 2012). The charge, the hydrophilicity/hydrophobicity of the microbial cell surface, and the chemical properties of a mineral surface are key properties that directly facilitate mineral-microbe interactions (Caccavo et al., 1997; Korenevsky and Beveridge, 2007). Due to microbes' small

size, high surface area-to-volume ratio, and metabolic diversity, microbes are also able to interact with metals (Dockrey et al., 2014) and regulate their fate in the environment, thus influencing their sequestration, mobility, bioavailability, and toxicity (Barkay and Schaefar, 2001; Gadd, 2004; Gadd, 2010).

3.2 Microbe-mineral Contact Mechanisms

Microorganisms have three modes of contact with a mineral surface: contact, non-contact, and a combination of the two (Rohwerder et al., 2003; Singh, 2016). The interaction between a mineral and a microbe occurs through the secretion of an extracellular polysaccharide (EPS) layer, with each EPS layer being highly variable in physicochemical properties (Konhauser, 2007). Other surface appendages may also play a role in microbial attachment to mineral surfaces since they serve as anchors, enhancing mineral dissolution (Barker et al., 1998; Welch et al., 1999). As microbes attach to a mineral (or rock) surface, they produce signal molecules to attract other organisms and gradually buildup a community called a biofilm (Harrison et al., 2005). A biofilm can be tens to hundreds of microns in diameter (Singh, 2016). Throughout the stages of biofilm formation, the secreted EPS has several functions: 1) it assists during the attachment of bacteria to a mineral surface; 2) it serves as a protective matrix from external stressors; 3) it provides a glue for cells within an established biofilm; and 4) it can create favourable microenvironments around the bacteria for further biofilm development, including the colonization of different bacterial species (Konhauser, 2007; Singh, 2016). Once a biofilm has been established, the minerals and rocks can experience weathering processes, including precipitation, dissolution, and transformation (Dong, 2010). These microbial-mediated processes are either directly controlled by the microbe or stimulated by extracellular biochemical reactions

(Dong and Lu, 2012), and have the possibility to impact elemental gradients within the surrounding environment (Gadd, 2010).

3.3 Microbial-mediated Mineral Precipitation

Microbe-mineral interaction can result in biologically-controlled mineralization, biologically-induced mineralization (Frankel and Bazylinski, 2003), and the formation of biogenic minerals (Konhauser, 2007; Dong et al., 2009; Lu and Wang, 2012). Biologically-controlled mineralization (BCM) occurs when the nucleation and growth of the biogenic minerals are physically controlled by the metabolic activities of microbes (Dove, 2010). Biologically-induced mineralization (BIM) occurs when the mineralization is not directly controlled by microbes but occurs as a result of changes in microenvironments resulting from microbial metabolism (Frankel and Bazylinski, 2003; Konhauser, 2007). Biogenic minerals can include carbonates, silicates, phosphates, and sulfides, that can be precipitated by microbes under favourable conditions (Frankel and Bazylinski, 2003; Konhauser, 2007; Dong et al., 2009; Lu and Wang, 2012). Biogenic minerals may also form through redox transformation of metals, sorption phenomena, or through interaction with metabolic byproducts, in which organic and inorganic metabolites may either cause metal precipitation in the cellular microenvironment, or lead to secondary mineral formation caused by chemical changes in the substrate (Ehrlich, 1996; Hamilton, 2003; Glasauer et al., 2004; Konhauser, 2007; Ehrlich and Newman, 2009). When rapid, both biotic and abiotic mineral formation has the potential to be detrimental for surrounding microbes, as the formation of these new minerals can completely encrust the cell, obstructing nutrient uptake and waste output (Saini and Chan, 2013). Cells, however, have the ability to avoid this by several mechanisms including promoting localized precipitation on

extracellular surfaces or discouraging mineral formations through acidification of the extracellular environment (Hegler et al., 2010; Chan et al., 2011).

3.4 Microbial-mediated Mineral Dissolution and Transformation

Microbial dissolution of minerals can occur through, 1) the production of siderophores, highly-specific Fe^{3+} -ligands that can bind and shuttle Fe (Gadd, 2010); 2) microbial oxidation of reduced minerals (e.g. acid mine drainage, *Acidithiobacillus* sp.); and 3) microbial reduction of oxidized minerals (Konhauser, 2007; Dong, 2010). Siderophores as well as the production of surface polymers, aid in microbe attachment to dissolve minerals and gain essential nutrients (Liermann et al., 2000; Maurice et al., 2000; Hersman et al., 2001; Ams et al., 2002; Roberts et al., 2006; Maurice et al., 2009). The microbial oxidation and reduction of minerals can result in metal(loid) mobilization or immobilization (Gadd, 1993; Gharieb et al., 1999; Lovley, 2000; Holden and Adams, 2003; Schröder et al., 2003; Lloyd et al., 2003). For example, certain higher valency species such as Mn^{4+} and Cr^{6+} become mobile and immobile, respectively, when they are reduced to Mn^{2+} and Cr^{3+} , respectively (Gadd, 2004). Redox studies have been primarily focused on minerals with redox-sensitive elements, such as Fe (e.g. Lovley, 2000; Konhauser et al., 2011) and S (Dahl and Friedrich, 2008). Many organisms, such as Fe and S-cycling bacteria (e.g. *Acidithiobacillus* and *Thermodesulfobacterium*, respectively; Konhauser, 2007), can utilize the energy provided from the redox transformation of Fe and/or S for energetic and metabolic processes (Dong and Lu, 2012). Other important bacterial genera in Fe-cycling bacteria include, for example, *Geobacter*, *Shewanella* (Konhauser, 2007) and *Thiobacillus* (Dockrey et al., 2014). However, bacterial and archaeal genera involved in S-cycling include *Thermodesulfovibrio* and

Thermodesulfobium, and *Archaeoglobus* and *Caldivirga* (Konhauser, 2007). In Chapters 3 and 4, important Fe, S, and As-cycling bacteria will be discussed.

3.5 Metal(loid) Mobilization and Immobilization

Understanding mineral-microbe reactions provides insight into understanding the biogeochemistry of metal(loid)s, their cycling in the environment, and how microorganisms affect metal bioavailability, mobility, and transfer between biotic and abiotic pools (Gadd, 2004, 2010). Whether metals are mobile or immobile depends on the microorganisms involved, the environment, and physicochemical conditions (Gadd, 2004, 2010). Microbial mobilization of metals can be accomplished by, for example, protonation, chelation, and chemical transformation (Gadd, 2010), whereas immobilization can be achieved by processes such as precipitation or crystallization of insoluble organic or inorganic compounds, or by sorption via electronic attractions (Dong and Lu, 2012), uptake and intracellular sequestration (Gadd, 2004). Burford et al. (2003) stated that the bioavailability of a metal is primarily influenced by sorption. Metal(loid)s also have the capability to be mobilized or immobilized indirectly as a result of other reductive mechanisms such as the reduction of Cr^{6+} to Cr^{3+} by Fe^{2+} , which was produced through biogenic reduction of Fe^{3+} (Gadd, 2004). There are taxonomically diverse microbial species that are capable of performing dissimilatory metal reduction that have been isolated from metal-contaminated environments (Lloyd, 2003; Gadd, 2010; Satyanarayan et al., 2013). In anaerobic conditions, bacteria and archaea commonly employ dissimilatory metal reduction in order to gain energy for growth support (Lovely, 1993; Nies, 1999; Lloyd, 2003; Gadd, 2010; Lovely, 2013).

3.6 Applications for Bioremediation

Despite the potential metal toxicity on microbes, different species are able to grow and thrive in metal-contaminated environments (Gadd, 2010). Therefore, knowledge of mineral-microbe interactions can be exploited for their use in bioleaching or bioremediation processes (Gadd, 2004, and references therein; Dong and Lu, 2012). Bioleaching is defined as the dissolution of metal-bearing phases from their mineral resources through biological oxidation, reduction, and/or complexation processes (Bosecker, 1997; Rohwerder et al., 2003; Rawlings and Johnson, 2007; Konhauser, 2007; Mammadov et al., 2016). Microbes have the ability to mobilize metal(loid)s through a variety of metabolisms including autotrophic- and heterotrophic–induced leaching, thus resulting in the dissolution of otherwise insoluble metal compounds and minerals, including sulfides and more complex ores (Gadd, 2004). Organisms that are commonly employed in biomining commonly include: 1) thermophilic bacteria, which can survive and thrive at high temperatures; 2) chemophilic bacteria, which can tolerate both strong acid and alkalis; 3) autotrophic bacteria, which have the capabilities to gain energy from inorganic compounds through photosynthesis or chemosynthesis; and 4) those that can produce biofilms (Singh, 2016). *Acidithiobacillus ferrooxidans*, *Leptospirillum* sp., *Thiobacillus ferrooxidans*, *Sulfolobus acidocaldarius*, Sulfobacilli, and *Thermothrixthiopara* sp. are a few examples of bacteria commonly used within the biomining industry (Singh, 2016). In leaching systems, microbes interact with minerals through a combination of contact and non-contact interactions, stimulating more efficient leaching of ore minerals through biofilm production (Singh, 2016). Mineral-microbe interactions have been extensively studied in acidic mine waste environments, especially with respect to the microbial oxidation of sulfide minerals such as pyrite (*cf.* Bigham et al., 1990; Karavaiko et al., 1994; Brandl, 2001). However, there have been fewer studies on

the environmental impact of mine drainage systems containing an abundance of carbonate minerals (Jurjovec et al., 2002). Although certain metal(loid)s (e.g. As, Cu⁺, Cr, Fe²⁺, Mo, Ni, Se and Zn) can pose a threat to water quality under circumneutral pH conditions (Heikkinen et al., 2009; Lindsay et al., 2009); the roles of bacteria in dissolution-reprecipitation processes under circumneutral-to-alkaline pH environments are not well understood.

Studies have for example shown that acidophilic bacteria are able to overcome pH-limiting growth conditions through the formation of acidic microenvironments at sulfide-mineral surfaces (Southam and Beveridge, 1992; Mielke et al., 2003). However, it is unclear whether microbial activities in microenvironments can affect mineral assemblages that are common in soils, tailings, ore deposits, regoliths, micro- and even nano-environments (Schindler and Hochella, 2016) or the mobility and sequestration of metal(loid)s on a larger scale within circumneutral mine drainage systems on a larger scale. There are also gaps in the literature pertaining to neutral-pH tailings in a sulfur and/or Fe-poor environment as well as the metal-cycling neutrophilic microorganisms that participate in weathering in these systems, as most studies discuss acidophilic Fe- and S- cycling bacteria in both acidic and near-neutral environments (e.g. Bigham et al., 1990; Southam and Beveridge, 1992; Karavaiko et al., 1994; Brandl, 2001; Heikkinen et al., 2009; Dockery et al., 2014).

Chapter Three: The geochemistry, mineralogy and microbiology of selected alkaline, legacy mine tailings sites from Cobalt, Ontario

4 Introduction

Knowledge and understanding of the interactions between minerals and microorganisms are essential in the interdisciplinary and growing field of geomicrobiology, an integration of geology, chemistry and biology (Parkes, 1998; Canuel, 2007; Konhauser, 2007; Ehrlich and Newman, 2009, Gadd, 2010). Studying mineral-microbial relationships can enhance our knowledge of the biogeochemical cycling of elements, the formation of new and/or biogenic minerals, mineral dissolution, and chemical transformation of elements (Gadd, 2010).

This knowledge can be also used to potentially exploit microbial communities in bioremediation or biotechnological processes such as bioleaching, where the biological oxidation, reduction and/or complexation processes results in the dissolution of metal-bearing phases from their mineral resources (Bosecker, 1997; Rohwerder et al., 2003; Rawlings and Johnson, 2007; Konhauser, 2007; Mammadov et al., 2016). Bioleaching is known as an effective strategy as a method of green mining and bioremediation of low-grade ore and/or mine tailings (Dong, 2010; Singh, 2016). Most bioleaching studies to date have been focused on sulfidic mine tailings and low-grade ore bodies rich in Cu and Au-sulfides (Rohwerder, 2003; Singh, 2016), with minor focus on bioleaching neutral-pH tailings material under strong acidic conditions (Lombardi and Garcia, 2002).

The potential exploitation of microorganisms for the bioleaching of metalloid-rich, neutral-to-alkaline pH material in neutral conditions has not been considered in greater detail due to the fact that:

- (1) The common bioleaching microbes are classified as acidophiles, and therefore thrive in acidic conditions and have the capability to tolerate high concentrations of metals (Singh, 2016) and

- (2) Mineral-microbe interactions for neutrophilic, metal-cycling microbial communities are less understood (Pettit et al., 1999; Kirby and Cravotta, 2005).

The current mining and exploration activities in and around the Cobalt mining camp (CMC) in Northeastern, Ontario, Canada, do not consider the potential bioleaching of the near-neutral mine tailings at the CMC. This study will thus continue our efforts to elaborate the potential bioleaching of the tailings material at the CMC (Appendix A). For this purpose, we will focus in this study on mineral-microbial relationships in the tailings, a prerequisite for any potential bioleaching study. Hence, the objectives of this study are to:

- (1) Characterize the microbial communities within the tailings material;
- (2) Identify site-specific differences within the microbial communities;
- (3) Characterize the microbial, geochemical and mineralogical relationships in order to identify how variations in geochemical and mineralogical character of the tailings affect the composition of the microbial communities; and
- (4) Investigate whether the average valence of As has an effect on the composition of the microbial community.

These objectives will be accomplished through utilizing a variety of analytical methods (i.e., inductively coupled plasma mass spectrometry, X-ray diffraction, scanning electron microscopy, X-ray absorption spectroscopy, Illumina MiSeq 16S rRNA gene sequencing), with subsequent multi-variate analyses using statistical methods (e.g. non-metric multidimensional scaling (NMDS)).

In the precursor undergraduate thesis study, we identified important mineralogical-geochemical relationships within two tailings profiles. The authors showed that tailings material became depleted in Fe and enriched in Co and As with an increasing degree of alteration of the

original tailings material (enriched in (sulf-)arsenides). The trend was visualized in plots with the Co-As-Sb-Zn number (Co#) versus the Fe number (Fe#), and were defined as:

$$\text{Co} - \text{As} - \text{Sb} - \text{Zn number (Co\#)} = \left(\frac{\text{Co} + \text{As} + \text{Sb} + \text{Zn}}{\text{Co} + \text{As} + \text{Sb} + \text{Zn} + \text{Al}} \right) \times 100 \% \quad (2)$$

and

$$\text{Fe number (Fe\#)} = \left(\frac{\text{Fe}}{\text{Fe} + \text{Al}} \right) \times 100 \% \quad (3)$$

The authors proposed that abiotic processes such as mineral replacement reactions and the complexation of Fe by carbonate species could have resulted in the mobilization and thus depletion in Fe with increasing degree of alteration. As the role of microbes during this process were not addressed by Courchesne et al. (2020), this study will specifically investigate whether enrichments in Co and As and depletion in Fe at certain depths within each tailings site are products of microbial activities, or whether the enrichments or depletions in Co, As and Fe are an abiotic process, of which control the microbial composition.

4.1 Background information

4.1.1 Past studies on the relationships between microbial communities and geochemical-mineralogical parameters

Numerous studies characterized the relation between the microbial communities composition and the variation of geochemical and mineralogical parameters in tailings material. For example, Diaby et al. (2007), Bruneel et al. (2007), Kock and Schippers, (2008), and Wakelin et al. (2012) showed that: (1) Fe- and S-oxidizing acidophiles are dominant in sulfidic mine tailings, especially in the oxidation zone (Diaby et al. 2007); (2) accelerated dissolution of Fe³⁺-containing minerals (e.g., jarosite and goethite) is accomplished by Fe-reducing bacteria (Bruneel et al. 2003); (3) the genera *Thiomonas* was identified as being able to actively oxidize

As (Bruneel et al. 2003); (4) the acidophilic Fe^{2+} - and S-oxidizing bacteria communities are controlled by the pH, redox potential and Fe concentration (Kock and Schippers, 2008); and (5) lithotrophic bacteria and abiotic processes played a prominent role in primary sulfide-mineral weathering, whereas heterotrophic bacteria controlled secondary mineral weathering (Wakelin et al., 2012).

The composition of microbial communities and their relation to geochemical and mineralogical factors in As-rich mine tailings of near neutral-pH are less commonly studied although As-cycling is known to play an important role on the bacterial community structure and composition (Guan et al., 2017). For example, Majzlan et al. (2011) characterized the mineralogical, geochemical and microbiological composition of the As- and Sb-rich mine tailings of near-neutral pH in Slovakia, near Pezinok. The authors showed that a few of the most predominant bacterial genera in the tailings were aerobic heterotrophic bacteria, for example, *Sphingomonas*, *Caulobacter* and *Janthinobacterium*, and that these genera are also common in As-contaminated soils (Macur et al., 2001; Ellis et al., 2003; Cai et al., 2009); (2) the formation of siderite (FeCO_3) was the result of the activity of Fe-reducing bacteria such as *Geobacter* and *Rhodoferax* genera; (3) acidophilic organisms such as *Acidithiobacillus* strains are able to thrive in neutral-pH tailings environments within microenvironments around altered and/or decomposing sulfide grains.

Additionally, Guan et al. (2017) showed that within As-rich soils and sediments contaminated by gold mining activities, the concentration of As was the most important factor controlling the microbial composition (e.g. *Clostridium* was the dominant bacterial genera within high As samples), with total organic carbon (TOC) and the concentrations of Fe and Mn having a secondary controlling effect. The former was also observed by Sheik et al. (2012) in Cr- and As-

contaminated soil by the leather tanning industry in Pakistan. Guan et al. (2017) also showed that the bacterial communities built up an As-tolerance through phylum-level horizontal gene transfer, mainly within the Proteobacteria phylum.

This study will examine in greater detail how the physicochemical properties and the mineralogy of the tailings material at the Cobalt mining camp affect the microbial community assemblage and whether certain groups of taxa are preferred over others within different environmental and physicochemical conditions.

4.1.2 Previous microbial studies on sediments around the Cobalt mining camp

There has not been a bulk microbiological study on the tailings material in the Cobalt mining camp. However, Little et al. (2020) conducted a paleolimnological-microbiology study on several lakes in the mining camp. They identified As-tolerant diatoms such as *Achnantheidium minutissimum* and populations that had statistically significant relationships with As such as *Tabellaria flocculosa*. The authors concluded that lake depth and pH were the significant drivers in community compositional changes and that the concentrations of As in the studied organisms had only minor effects on the compositions of the microbial communities.

Kelly et al. (2007) and Kwong et al. (2007) calculated the abundance of sulfate-reducing bacteria (SRB), iron-reducing bacteria (FeRB), \pm acid-producing bacteria (APB) in wetland sediments of the Cobalt mining camp through most probable number (MPN) methods. Kelly et al. (2007) analyzed sediment samples from the Farr Creek drainage area and determined that: (1) bacteria populations were constant within the upper 50 cm of the sediments; (2) acid-producing oxidizing bacteria occurred in similar abundance as reducing bacteria and that therefore oxic and

anoxic conditions existed throughout the wetland; and (3) the abundance of SRB, FeRB and APB in numerous core samples depicted different trends with respect to depth.

Kwong et al. (2007) analyzed sediment samples from the Farr and Mill Creek wetlands to assess the roles of sulfate- and Fe-reducing bacteria in the mobilization and deposition of metals within the sediment columns. The authors also studied changes in As speciation with the redox conditions in the surface sediments using X-ray absorption spectroscopy. These studies showed that:

- (a) microbial sulfate reduction occurs locally in the wetland, potentially leading to As co-precipitation with sulfides such as framboidal pyrite;
- (b) the dissolution of As-bearing minerals is the main source of As release in the wetlands;
- (c) changes in redox conditions within the surface sediments (from reduced to oxidizing conditions) results in the remobilization of As.

4.1.3 Past studies on the speciation of As in natural waters and sediments around the Cobalt mining camp

Chen et al. (2019) and Beauchemin and Kwong (2007) characterized the speciation of As in lake sediments near Cobalt and Crosswise Lake, near the exit of Little Cobalt Lake close to Mill Creek and in submerged tailings underneath the Farr and Mill Creek streams. Chen et al. (2019) showed that As^{5+} was the dominate As valence in the lakes and streams that were affected by the As-contaminated tailings, and that pH, temperature, light and the presence of nitrate and chloride strongly affected the stability of As^{3+} in these waters. Beauchemin and Kwong (2007) conducted redox experiments in order to examine the remobilization of As under anaerobic and

reducing conditions. The authors showed that (1) Al-(hydr)oxides were the primary sorption phases as opposed to Fe-(hydr)oxides, which occurred in minor to trace amounts; (2) in the absence of soluble C species, As^{5+} species were only reduced to the more soluble As^{3+} species, which resulted in the competitive binding of arsenate and phosphate groups to adsorption sites on the Al-hydroxides, in an increasing mobilization of As; and (3) in the presence of soluble C, As^{5+} is reduced to As^{1-} -species which subsequently precipitates in the form of arsenides. The authors concluded that both, prolonged flooding periods and the addition of sufficient soluble C, could stimulate microbial As-reduction and favour the stabilization of arsenide-bearing minerals.

5 Materials and Methods

5.1 Study Area

The Cobalt Mining Camp is in Northeastern Ontario and contains 16 tailings sites (Fig. 1). Three tailings sites within the Farr Creek drainage basin were chosen on the basis of their previously reported As, Co, and Ag content (Ontario Ministry of the Environment, 2011). These tailings sites are referred hereafter to as sites A, B and C. Appendix A describes in detail the historical background, geographical settings and the chemical and mineralogical compositions of the tailings sites A and B. Site A occupies an area around a lake within the town of Cobalt and its tailings material originated from five different mines. Site B is located immediately down-hill of a former processing mill at which its tailings material was derived and is covered with a patchy clay topsoil due to remediation efforts in the 1990's (Dumaresq, 1993, Percival et al., 2004). Site C occurs in a low-lying wetland, with a majority of its tailings having been flushed into a nearby creek as well as Cobalt Lake, due to erosion and/or dam failure. Its tailings material originated

from a mill which processed high-grade ore using a cyanide-mercury amalgamation technique (Anderson, 1993).

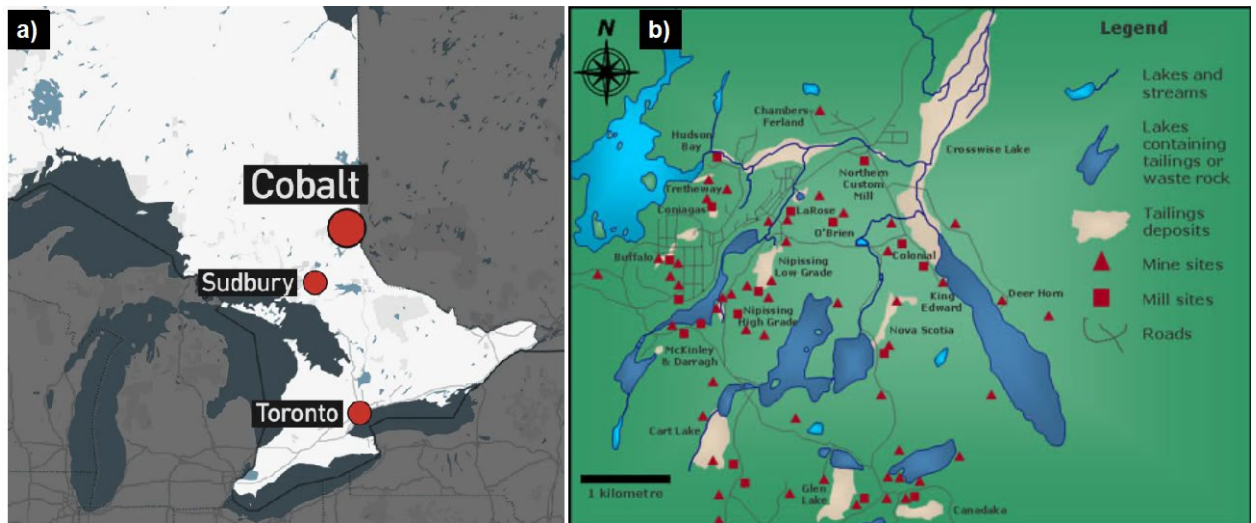


Figure 1. a) Photo showing the location of Cobalt in Ontario, relative to Sudbury and Toronto; b) A photo showing the mines, mills, and tailings deposits in the Cobalt Mining Camp.

5.2 Sampling methods and storage

Three tailings profiles were sampled in September 2019 (sites A and B) and October 2019 (site C) (Fig. 2). The profiles at sites A and B were sampled in close proximity to those by Courchesne et al. (2020). The profile at site C was taken directly beside a former tailings dam. Each of the three tailings profiles was sampled in 5-centimetre (cm) increments to a depth of 30 cm. These 5-cm layers were labelled with the following scheme: site identifier (A, B or C), followed by the lower depth, thus A-5 (site A, 0 – 5 cm), A-10 (site A, 6 – 10 cm), A-15 (site A, 11 – 15 cm), A-20 (site A, 16 – 20 cm), A-25 (site A, 21 – 25 cm), A-30 (site A, 26 – 30 cm). The naming scheme can also be found in Table 1 and is used in the microbial taxonomic plots and in tables and figures found in the Appendices. The 18 samples were sealed in plastic bags, placed into a cooler with freezer packs in order to maintain a temperature of 4 °C, and stored in a

fridge at the Vale Living with Lakes Centre, Laurentian University. A subset of each sample was placed into separate plastic bags for 16S rRNA extractions and stored in a freezer at -20 °C. A second subset was dried in an oven at 80 °C for 2 days and then stored at room temperature for geochemical and mineralogical analysis.

5.3 Field measurements

During sampling, contact pH and ORP measurements were taken using a handheld field instrument, YSI Quatro. A 4-point pH standardization was completed before sampling using standardized solutions of pH 2, 4, 7, and 10. ORP standardization was done using Zobell’s ORP solution (228 mV). Both pH and ORP were completed with a 1:2 tailings to deionized (DI) water ratio. The ORP mV value was then converted to an Eh value simply by adding 200 mV to the ORP voltage (YSI Environmental, 2005).

Table 1. The naming scheme for each sample, used in the taxonomic plots.

Sample ID	Site	Depth range (cm)
A-05	A	0 - 5
A-10	A	6 - 10
A-15	A	11 - 15
A-20	A	16 - 20
A-25	A	21 - 25
A-30	A	26 - 30
B-05	B	0 - 5
B-10	B	6 - 10
B-15	B	11 - 15
B-20	B	16 - 20
B-25	B	21 - 25
B-30	B	26 - 30
C-05	C	0 - 5
C-10	C	6 - 10
C-15	C	11 - 15
C-20	C	16 - 20
C-25	C	21 - 25
C-30	C	26 - 30

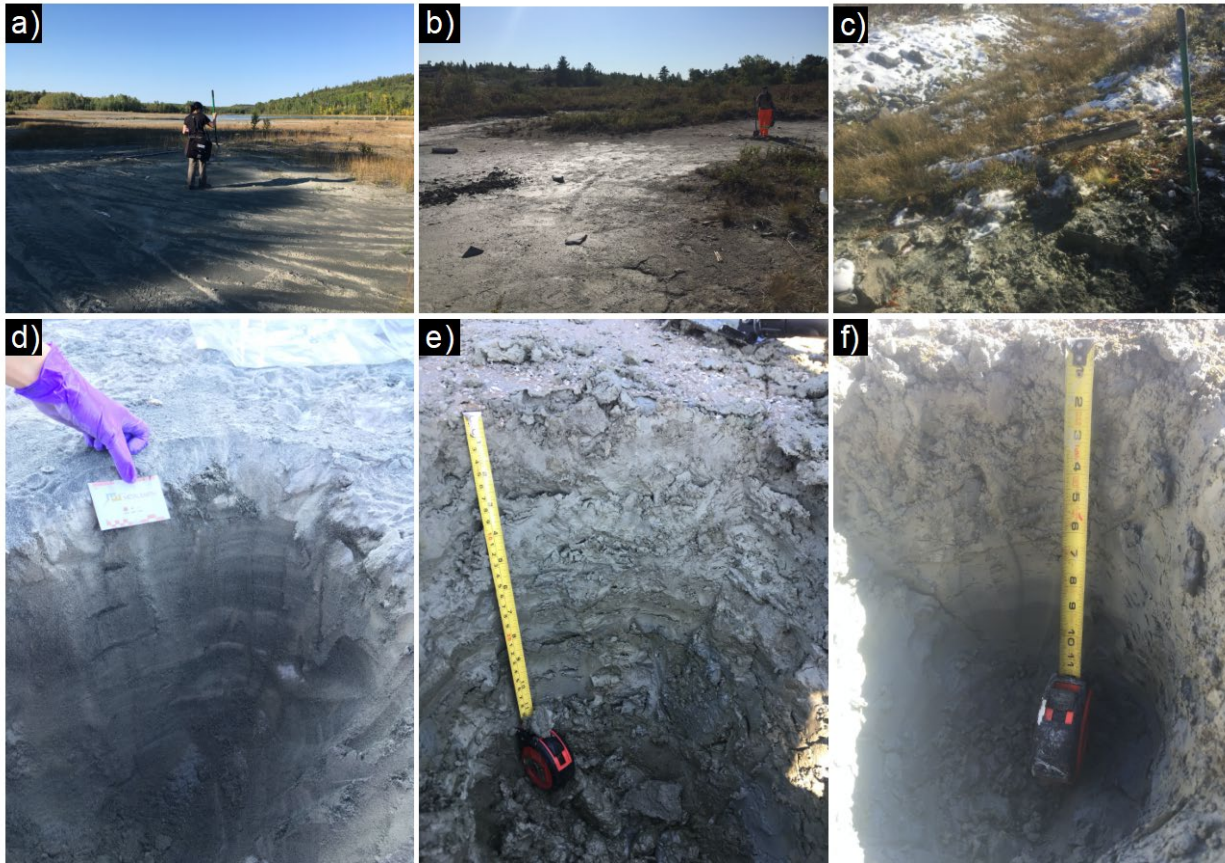


Figure 2. Photographs of the three tailings sites with their 30-cm depth profiles, showing site A (a, d), B (b, e) and C (c, f) at the day of sampling.

5.4 Total Carbon and Sulfur Analysis

The 18 tailings samples were analyzed for total carbon ($\text{CO}_{2(\text{T})}$) and total sulfur ($\text{S}_{(\text{T})}$) at the Geoscience Laboratories, Sudbury, Ontario. The samples were analyzed following their standard laboratory procedures, involving sample combustion and subsequent measurement by infrared absorption.

5.5 Chemical analysis - Inductively Coupled Plasma Mass Spectrometry

Chemical analysis of all 18 samples was carried out at the Perdue Central Analytical Facility, Sudbury, Ontario following the Environmental Protection Agency (EPA) method 3052

(EPA, 1996). A single digest was obtained through mixing 0.5 g (± 0.002) sample, 9 mL HNO₃, 2 mL HCl, 3 mL HF and 2 g of H₃BO₃ following the procedure of Wilson et al. (2006). The digests were diluted by factors of 1000 or 10000 and analyzed on a NexION[®] 1000 ICP-MS using a 7-point calibration curve. The internal standards Ru-101 and Re-185 were used for the corrections of drifts for the low to medium and heavy mass isotopes, respectively. For quality assurances, a method blank, duplicate and certified reference material (TILL-1; Lynch, 1990) was analyzed after every 9th sample. The certification report for TILL-1 is available upon request to Canmet MINING.

5.6 Powder X-ray Diffraction

Three samples from each depth profile were prepared for X-ray powder diffraction. These samples were chosen based on their Co, As and Fe concentrations or their average valence of As. Nine X-ray diffraction patterns were recorded with either a Philips 159 PW 1729 or a Bruker D 5000 X-ray diffractometer using Cu-K α radiation ($\lambda = 1.5418 \text{ \AA}$) at 40 kV and 30 mA. Diffraction patterns were collected over a range of 5-75° and 5-65° 2 θ with a step size of 0.02° and a counting time of 2 s step⁻¹. All minerals identified both previous to this study and within this study, as well as their chemical formula, are listed in Appendix B. Additionally, all recorded X-ray diffraction patterns are listed in Appendix C.

5.7 Scanning Electron Microscopy

A total of seven samples were prepared for SEM, two from sites A and B, and three from site C. The samples were embedded into epoxy pucks and polished using MicroPolish Alumina powder on 8-inch Nylon PSA Buehler discs. Six of the carbon coated epoxy pucks were

analyzed using a JEOL 6400 SEM operating at 20 kV, equipped with both backscattered (BSE) and secondary (SE) electron detectors and an Energy Dispersive X-ray Spectrometer (EDS). Additional SEM work was carried out on one sample from site C with a FEI Quanta 650 FEG field emission scanning electron microscope at the Manitoba Institute of Materials, University of Manitoba.

5.8 DNA Extraction and Computational Biology

Genomic DNA from the total microbial community within each of the 18 samples were extracted from 0.25 g of tailings material using the Metagenom Bio Inc. Sox DNA Isolation Kit (Metagenom Bio Inc., Toronto, ON, Canada). A method blank extraction (DNA extraction column loaded with sterile deionized water) was also completed to determine whether background contaminants were present. Manufacture protocols were followed, including the optional 10-minute heating step at 70 °C, after the addition of Solution Sox 1, to enhance DNA yields. The extracted DNA was quantified using a Take3 spectrophotometry system on a Synergy HI microplate reader (BioTek, Winooski VT, USA). DNA amplification was then tested by polymerase chain reactions (PCR) in 10 µL reactions. Each reaction had: 5 µL of Phire Green Hot Start Master Mix, 0.3 µL of both forward (F) and reverse (R) primers (27F, 1492R) (10 µmol), 0.8 µL of extracted DNA, and 3.6 µL of sterile Milli-Q water. The following parameters were implemented to conduct PCR reactions: initial denaturation at 98 °C for 30 seconds, 30 cycles of denaturation at 98 °C for 5 seconds, 30 cycles of annealing at 55 °C for 5 seconds, 30 cycles of extension at 72 °C for 25 second, and a final extension step at 72 °C for 60 seconds. Verification of the PCR products was accomplished by gel electrophoresis on a 1 % agarose gel.

The extracted DNA was sent for 16S rRNA sequencing on the Illumina MiSeq platform at Metagenom Bio Inc. (Toronto, ON). The V4 region of the 16S rRNA gene was targeted using the following primers, 515F (Parada et al., 2016) and 806R (Apprill et al., 2015). With the use of the BBDuk tool (<https://jgi.doe.gov/data-and-tools/bbtools/bb-tools-user-guide/bbduk-guide/>), the primers were trimmed from the forward and reverse reads. Using the DADA2 pipeline (version 1.8), the trimmed reads were processed, using the default filtering and merging parameters, with the sample interference being conducted using the pseudo-pooling method (Callahan et al., 2016). To assign taxonomy, the Silva132 database was used (Quast et al., 2012). Post taxonomy assignment, a rarefaction curve graph of all samples was generated, using the vegan package (Oksanen et al., 2019; Figure 1 of Appendix D). Contaminants in the data were determined using the BiocManager package decontam (Davis et al., 2018), using both frequency and prevalence methods, in order to (a) remove common contaminants and (b) to remove identified organisms in the method blank. Table 1 in Appendix D shows the raw sequence data information of all samples, including the total number of sequences, the percent of sequences that were filtered out, and the percent of sequences recovered, per sample.

5.9 X-ray Absorption Near-Edge Spectroscopy - VESPERS

X-ray absorption near-edge spectroscopy (XANES) spectra were characterized at the Very Sensitive Element and Structural Probe Employing Radiation from a Synchrotron (VESPERS) beamline at the Canadian Light Source in Saskatoon, Saskatchewan, in order to determine the average valence of As in the collected tailings material. XANES scans were collected on powdered samples in fluorescence mode using a Canberra 13-element Ge detector. The energy position was calibrated to the gold L3 edge ($E_0 = 11919$ eV) using the maximum first

derivative of the XANES spectrum of a gold foil standard. Samples were mounted at a 45° angle to the X-ray beam and the detector was positioned at a 90° angle to the X-ray beam. Three different spots on each sample were selected and each spot was scanned three times. The scan parameters of the XANES spectra with respect to E_0 were from 11667 to 12166 eV with a step-size of 10 eV, 0.3 eV or 0.1k for the pre-, near-, or post-edge region (respectively) per step and with a dwell time of 2 to 2.5s per step. Arsenic standards for As^{5+} , As^{3+} , As^{1-} and As^{3-} were a Na-arsenate ($Na_2AsO_4 \cdot 7H_2O$), arsenic trioxide, arsenopyrite and gallium arsenide, respectively, and were scanned with a 1s dwell time (Fig. 1 of Appendix E). An accurate edge position for As could not be unequivocally determined in the X-ray absorption spectra of the samples from site A as they had a very low signal to noise ratio. A summary of the spectral results from the XANES analysis can be found in Figures 2 and 3 of Appendix E.

5.10 Statistical Analysis

Data and multivariate statistical analyses were conducted using R (R Core Team, 2018), dplyr (Wickham et al., 2018), phyloseq (McMurdie and Holmes, 2013), and vegan packages. Graphs were generated using ggplot2 (Wickham, 2016).

Non-metric multidimensional scaling (NMDS) was implemented using the environmental fit function of the vegan package in R software (version 1.3.959). The relative abundance of microbial data (operational taxonomic units; OTUs) was log transformed and subjected to the Bray-Curtis dissimilarity calculation, using the betapart package in R software. Each point of an NMDS plot represents the microbial community composition of a sample within a reduced multidimensional space, with the distance between two points (i.e. two samples) representing the

difference between the two samples microbial community composition. Hence, the closer two points are together, the more similar is there microbial community composition.

An Analysis of Similarities (ANOSIM) is a statistical test that was conducted using the `anosim` function in the `vegan` package in R software. The use of an ANOSIM is to identify whether similarities (or differences) exist between two or more groups of samples. An ANOSIM provides an R-value associated with the similarities between the tested groups (Clarke, 1993). An R-value closer to 1.0 suggests that there are dissimilarities between groupings, while an R-value closer to 0.0 suggests dissimilarities within groups (Clarke, 1993). The ANOSIM groupings here were selected based on site. The ANOSIM results can be found in Figure 1 of Appendix F.

6 Results

The geochemistry and mineralogy of the tailings material at sites A and B are very similar to those previously studied in Appendix A by Courchesne et al. (2020) and thus will only be briefly addressed. Additional information of the mineralogical and chemical composition of the tailings materials at the sites A, B and C is given in Appendices C, E, G, and H.

The tailings material at sites A and B depict a grey tone (Fig. 2d, 2e), whereas the material at site C has a brown tone (Fig. 2f). The occurrence of dark and/or light-coloured laminations occur in all three tailings profiles with reddish-brown oxidized material at depth (D) = 25 cm at site B and at D = 11 cm at site C, and a thick dark-colouration at D = 25 to 30 at site C. The average contact pH and Eh values for the materials at the sites A, B and C are pH = 8.4 (\pm 0.2) and Eh = 0.28 V (\pm 0.01), pH = 8.0 (\pm 0.3) and Eh = 0.26 V (\pm 5.7E-03), and pH = 7.6 (\pm 0.2) and Eh = 0.36 V (\pm 8.87E-03), respectively (Fig. 3a, 3b). However, pH and Eh can slightly

vary with depth for each profile. For example, material at $D = 15$ and 20 cm at site A has a higher contact pH and lower Eh than those at other depths within the profile. Similarly, material at $D = 20$ cm at site B has also a lower contact pH than the material above or below.

The tailings material at the sites A and B have similar amounts of sulfur ($S_{(T)}$) whereas the material at site C has a higher concentration of $S_{(T)}$ (Fig. 3c). The total carbon ($C_{(T)}$) content in the tailings material differs between the sites with the lowest and highest content at sites A and C, respectively (Fig. 3d). The concentrations of $S_{(T)}$ and $C_{(T)}$ vary, similar to Eh and contact pH, with depth. For example, material with the lowest contact pH at site B ($D = 20$ cm) also has the highest amount of $S_{(T)}$ and $C_{(T)}$ (Fig. 3). The highest amount of $S_{(T)}$ for all characterized tailings material occurs at $D = 30$ cm at site C with 0.56 wt % $S_{(T)}$ (Fig. 3c).

6.1 Bulk Chemical Compositional Changes versus the Abundance of (sulf-)arsenides

The concentrations of metal(loid)s of interest such as As, Co, Fe and the average valence of As also vary with depth (Fig. 4). A common feature at all three sites is the occurrence of tailings material which is depleted in Fe and/or enriched in As and Co (at $D = 25$ cm at site A, at $D = 20$ cm at site B, and $D = 30$ cm at site C) (Fig. 4). This depletion in Fe in the materials from sites B and C also coincides with a higher average As valence (Fig. 4). Tailings material enriched in Fe also occur at all three sites and coincides here with elevated concentrations of Co and/or As ($D = 5$ and 20 cm at site A, $D = 15$ cm at site B, and $D = 15$ cm at site C) (Fig. 4). The material at site B depicts a higher average valence of As ($+4.30$) than site C with an As valence of $+3.28$ (Fig. 3). A notable feature is the decrease in the average valence of As with depth at site C resulting in the lowest observed average valence of As with $+0.25$ at $D = 30$ cm (Fig. 4). The

percent range of As^{5+} in materials from site B is 43 – 88 % and 12 – 73 % in materials from site C (Table 2 in Appendix G).

Similar to the Co – Zn – Sb – As number (Co#) (Equation 2) and Fe number (Fe#) (Equation 3) (Appendix A; Courchesne et al. 2020), we define here the S number (S#) (Equation 4) as

$$S\ number\ (S\#) = \frac{S}{Al+S} \times 100\ \% \quad (4)$$

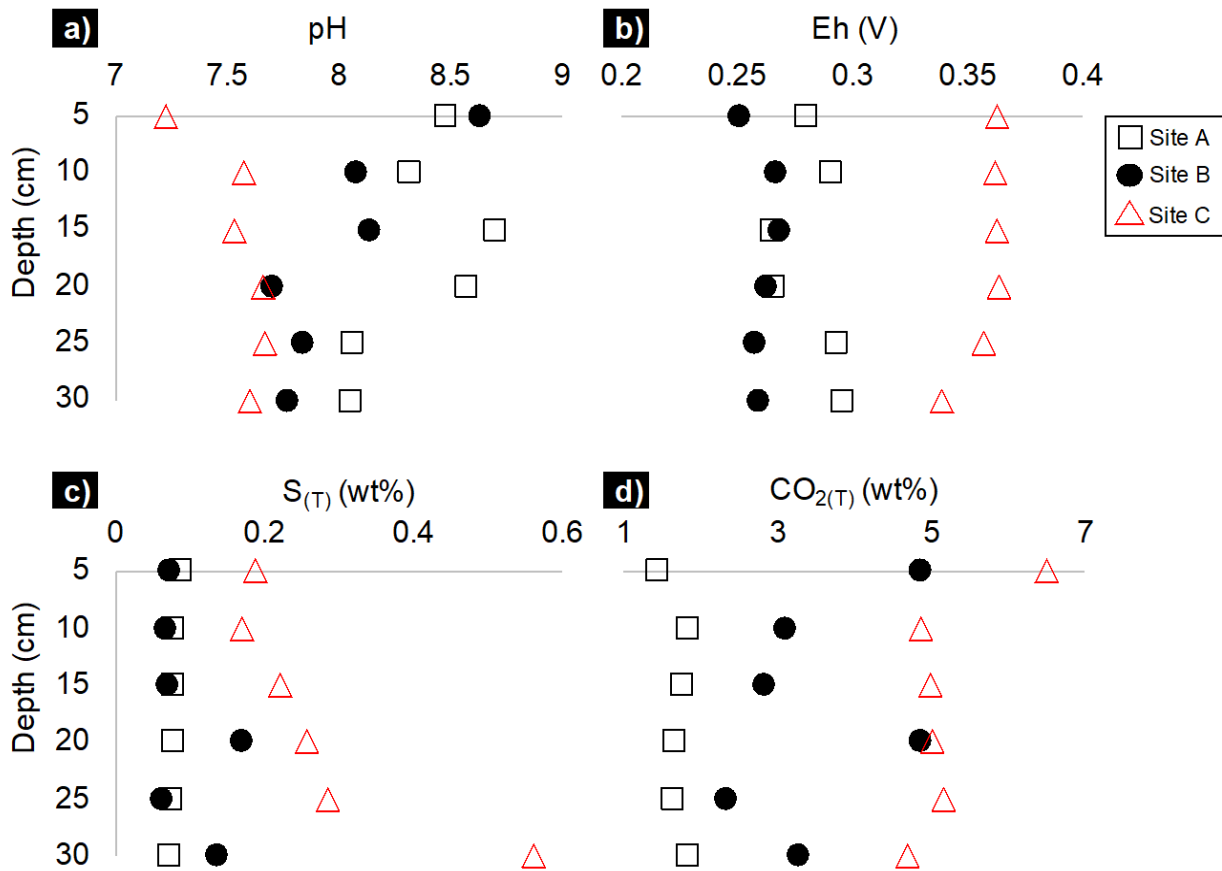


Figure 3. Depth profile plots of pH (a), Eh (b), total sulfur (c) and total CO2 (d) versus depth [cm].

The tailings material from site A has a higher Fe# and much lower Co# than the materials at sites B and C (Fig. 5, Fig. 6). At greater depths of sites B and C, the S# and Fe# increases and

decrease between D = 20 cm and D = 30 cm, respectively (Fig. 5). In the same depth interval, the change in Co# with depth is not uniform as it decreases and increases with depth at sites B and C, respectively (Fig. 5). The S# in the tailings material at site A is relatively constant ($\pm 2\%$), whereas distinct maxima in material at site B and C coincide with maxima in Fe# and Co#, respectively (Fig. 5, Fig. 6).

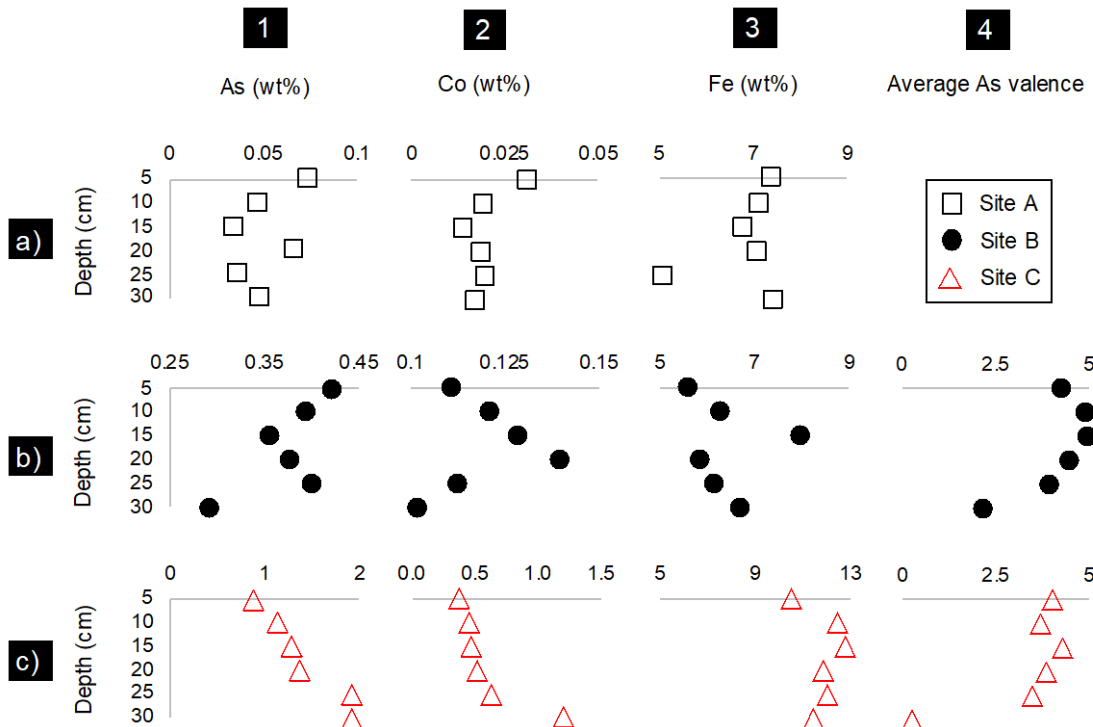


Figure 4. Depth profile plots of sites A to C (rows a) – c)) with the concentrations of (1) As, (2) Co and (3) Fe, and (4) the average As valence versus depth [cm].

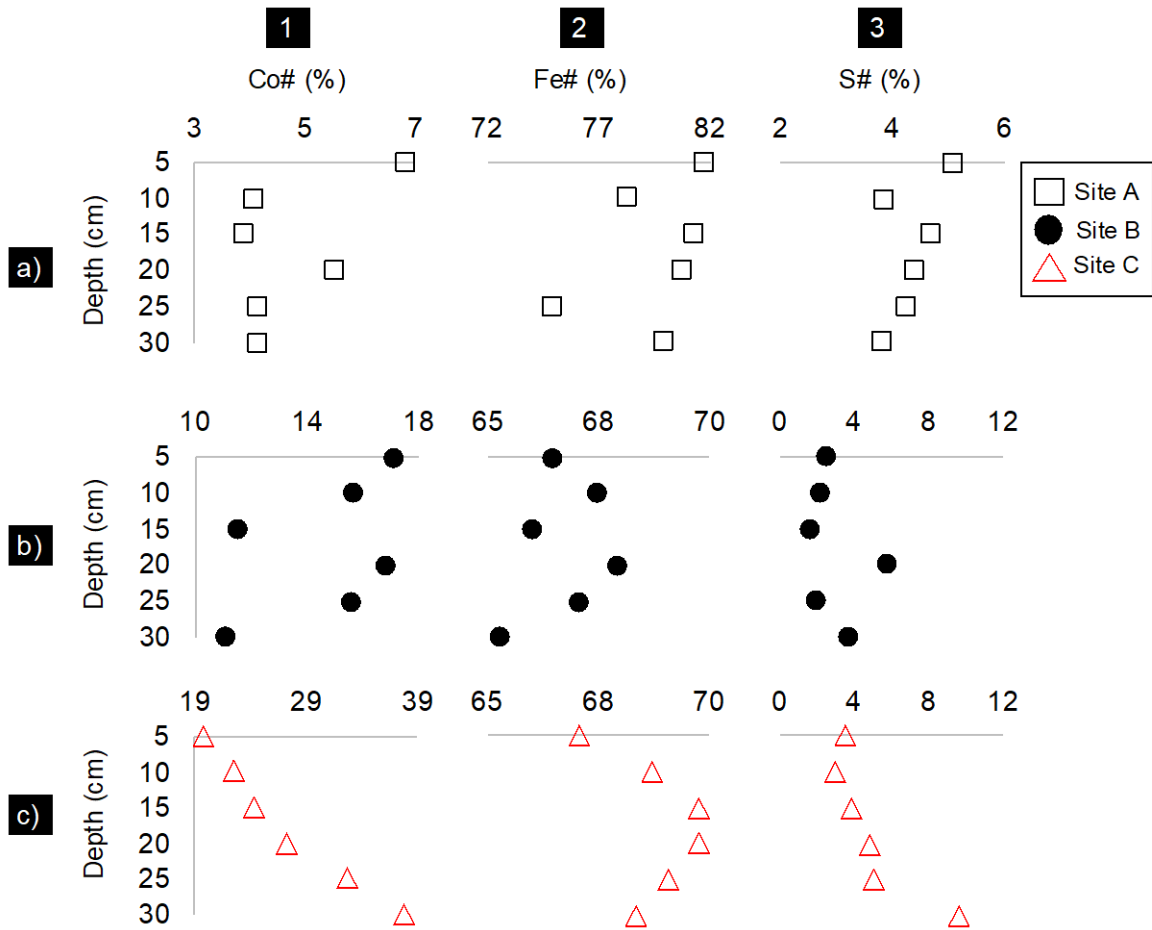


Figure 5. Depth profiles of sites A to C (rows a) – c)) with columns as (1) Co#, (2), Fe# and (3) S# versus depth [cm].

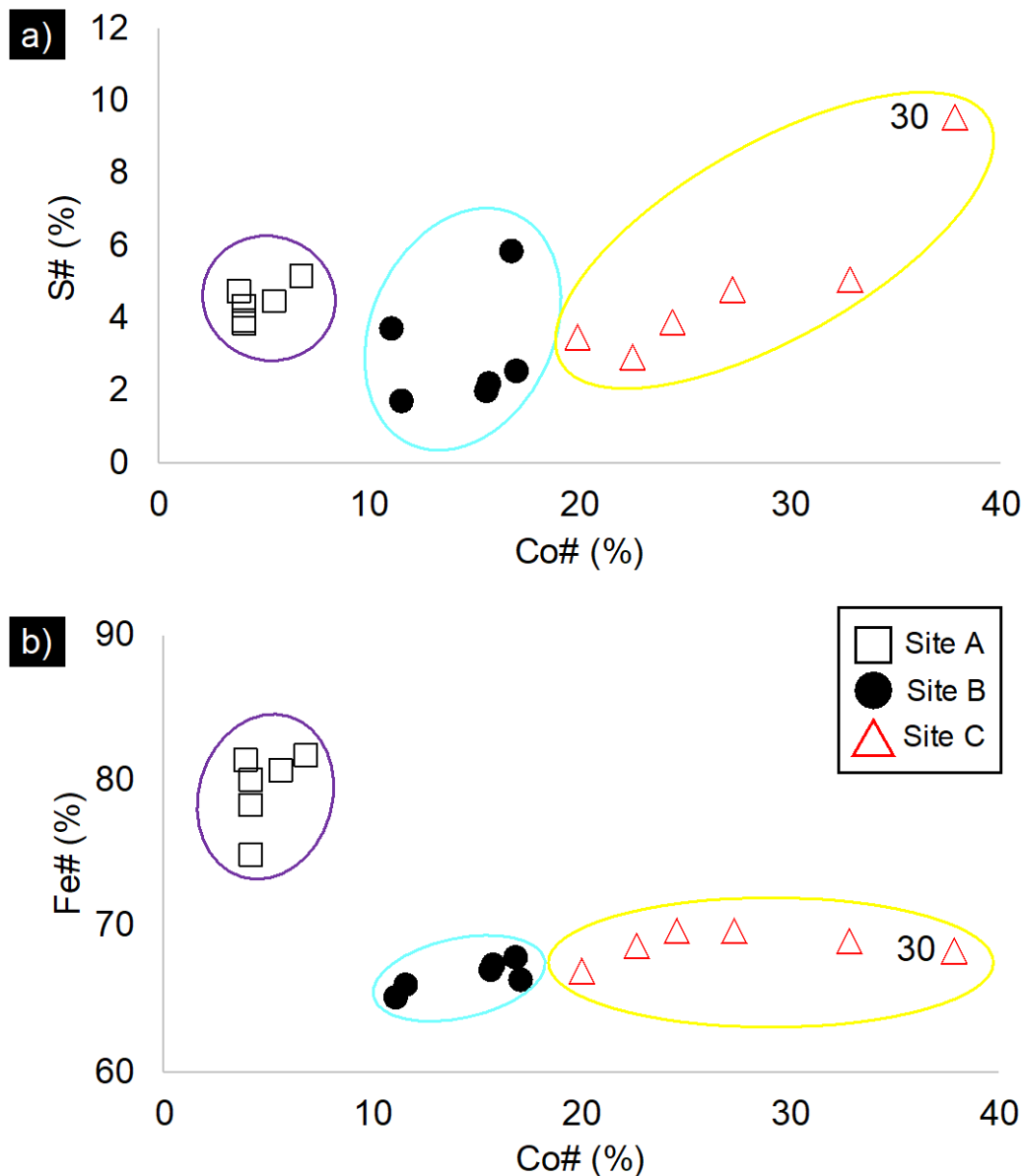


Figure 6. Two XY-plots of Co# versus (a) S# and (b) Fe#.

6.1.1 Arsenate and (sulf-)arsenides in the tailings material

Material from D = 15 and 25 cm at site A was chosen for SEM characterization as we were interested in mineralogical changes between material of high and low Fe# (Fig. 5). At site B, tailings material at D = 10 and 25 cm were selected in order to examine the mineralogical composition of samples with similar Fe# and Co# (Fig. 5). Tailings material from D = 20 to 30

cm at site C was chosen in order to characterize changes in the mineralogical composition with an increase in Co# and As valence and decrease in Fe# and S# (Fig. 4, Fig. 5).

SEM characterization of material from the seven chosen samples suggests that (sulf-)arsenide-bearing grains consist primarily of arsenopyrite, with minor amounts of chalcopyrite, safflorite, cobaltite \pm skutterudite, cobaltoan arsenopyrite, roselite, cobaltoan olivenite, argentobismutite and argentopyrite (on the basis of the stoichiometry of the elements; Fig. 7). Secondary arsenate minerals occur predominantly in mineral surface coatings on silicates and carbonates as Co-Ni-Zn-Fe-arsenates. Additionally, within samples of sites A and C, there are the minor occurrences of Fe (\pm Ti)-(hydr)oxides, that are absent in site B.

At site A, (sulf-)arsenides are the dominant As-bearing phase at D = 15 cm, whereas the proportion of arsenates to arsenides is approximately equal at D = 25 cm (on the basis of 25 observed As-bearing mineral grains and surface coatings). At site B, arsenates are the dominant As phase over (sulf-)arsenides at both depths (on the basis of 39 As-bearing mineral grains and surface coatings) (Fig. 7). Additionally, in site B at D = 25 cm, Ag occurs as Ca-Fe-Ag arsenates (Figure 1a, 1b in Appendix H), unidentified As-Fe-S-Ag-O phases (Figure 1c, 1d in Appendix H), and as an unidentified Fe-Sb-S-Ag-O phase.

At D = 20 and 25 cm at site C, arsenates are also predominant over (sulf-)arsenides, but the ratio of arsenate to (sulf-)arsenide is smaller than at site B (on the basis of 69 As-bearing mineral grains and surface coatings) (Fig. 7). Material at D = 30 cm of site C contains three distinct groups of: (1) sulf-arsenides, (2) arsenides, and (3) sulfides (Figure 2 in Appendix H). The former two groups are a mixture of Co-Fe-Ni-Zn rich arsenides and sulfarsenides, whereas the latter sulfide group consists of Fe-sulfides and minor Zn-sulfides. The majority of the examined grains (33 out of 47) correspond to (sulf-)arsenides, with the remainder being Fe (\pm

Zn) sulfides. Although Fe-sulfide grains can be slightly altered, none of the observed (sulf-)
)arsenide grains depict visible (micrometer-size) mineral surface coatings (Figure 2 in Appendix
 H). Additionally, none of the sulfide grains depict textures or crystal forms which would point
 towards their biogenic origin (e.g. framboidal textures).

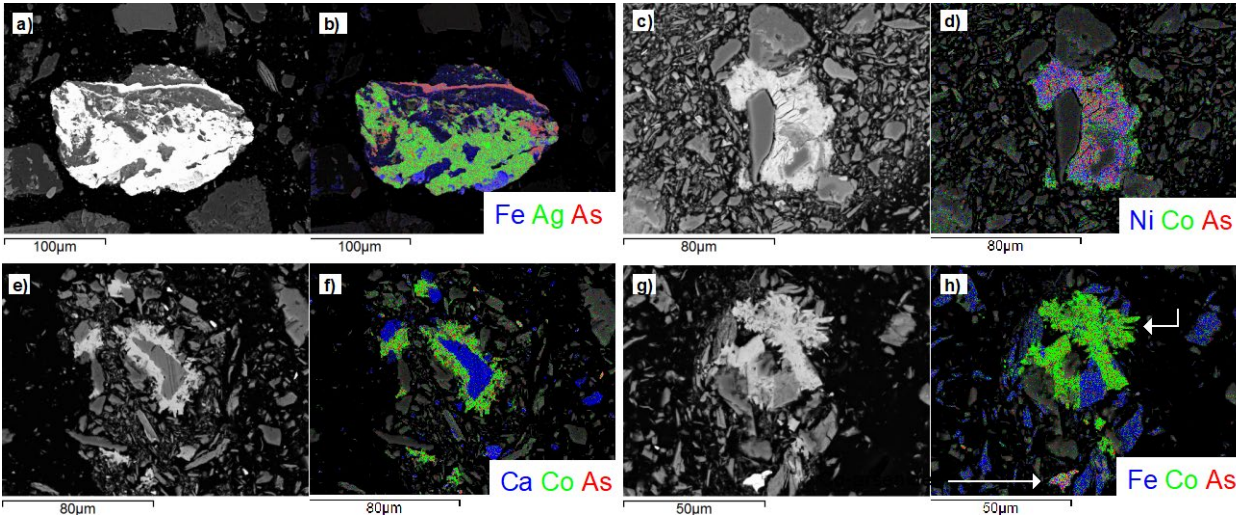


Figure 7. SEM photomicrographs and EDS-chemical maps for representative grains from each tailings site. A silver-sulfide (a, b), Ni, Co-arsenate coating on silicates (c, d), Ni, Co-arsenate coating on carbonates (e, f), and a Co-arsenate coating on silicates and an Fe, Co-arsenide (g, h).

6.2 Tailings microbiological composition

In order to better characterize trends in the microbial data, taxa with a relative abundance below 2 % (or 0.5 % for Species-level description) are grouped together into a single category, and only taxa with a relative abundance > 2 % will be described here. Additional taxonomic abundance graphs (Kingdom, Class, Family and Species) can be found in Appendix I.

6.2.1 Bulk microbial community composition

Within materials from all three tailings sites, the bulk microbial community composition consists mainly of the Proteobacteria (14 – 75 %) and Actinobacteria (5 – 48 %) phyla, with lesser amounts of Chloroflexi (5 – 21 %), and Acidobacteria (3 – 9 %) (Fig. 8). Tailings material at site B contains more Proteobacteria (49 – 75 %) than materials from sites A (14 – 50 %) and C (38 – 54 %). Acidobacteria occur within all samples at site A, whereas material only in the bottom 10 or top 15 centimetres at site B and C contain Acidobacteria, respectively. At the phylum level, a few minor differences exist between each tailings site: 1) tailings material at site A depict the only occurrences of Firmicutes (4 - 13 %) and Euryarchaeota, as well as a comparatively higher relative abundance of Gemmatimonadetes (3 - 12 %); and 2) there are less Actinobacteria (8 – 28 %) and a higher abundance of Nitrospirae (41 % at D = 30 cm) in the material at site C relative to those at sites A and B.

6.2.2 Metal-cycling microbial populations

In a tailings system, lithotrophic organisms commonly occur. These microorganisms can couple the oxidation of reduced inorganic compounds such as hydrogen sulfide (HS^-) and Fe^{2+} to the reduction of a terminal electron acceptor such as oxygen (O_2) and sulfate (SO_4^{2-}) under aerobic and anaerobic conditions. With inputs of organic matter, in legacy tailings sites, a mix of metal-cycling and soil nutrient-cycling organisms (e.g. N and C) can appear. Given that the studied tailings system is neutral-to-alkaline, we are interested in metal-mobilizing organisms under these pH conditions.

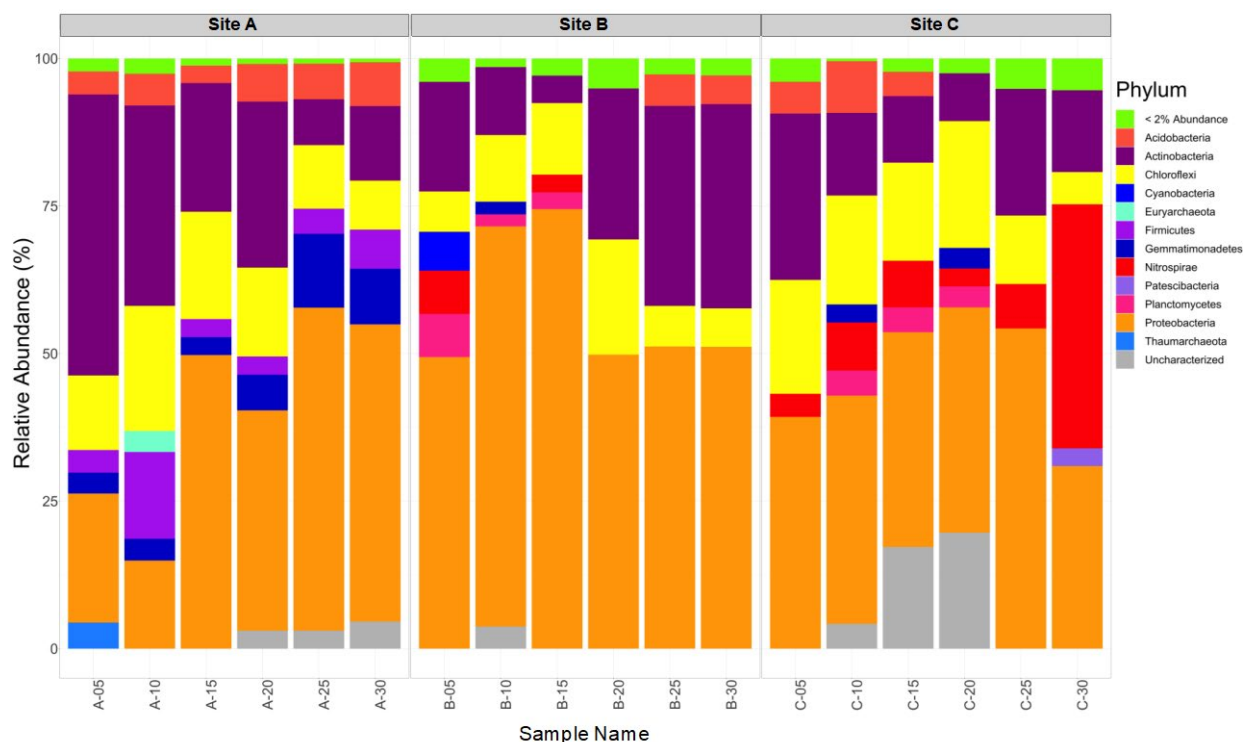


Figure 8. Normalized relative abundance taxonomic bar plot of the background tailings microbial communities at the Phylum level.

6.2.3 Iron and/or sulfur-cycling community composition

The identified Fe- and S-oxidizers occur within the Betaproteobacteriales and Acidiferrobacteriales orders (Fig. 9). Microorganisms identified as known Fe-oxidizing bacteria (FeOB) are within the genus *Sideroxydans* (Fig. 10), with known S-oxidizing bacteria (SOB) within the genera *GOUTA6* (isolated from contaminated groundwater), *Limnobacter*, and *Sulfuricella* (Fig. 10). The three identified genera *Gallionella*, *Sulfurifustis* and *Thiobacillus* have the capability to oxidize both reduced Fe- and S-species, with oxidation being coupled to nitrate-reduction.

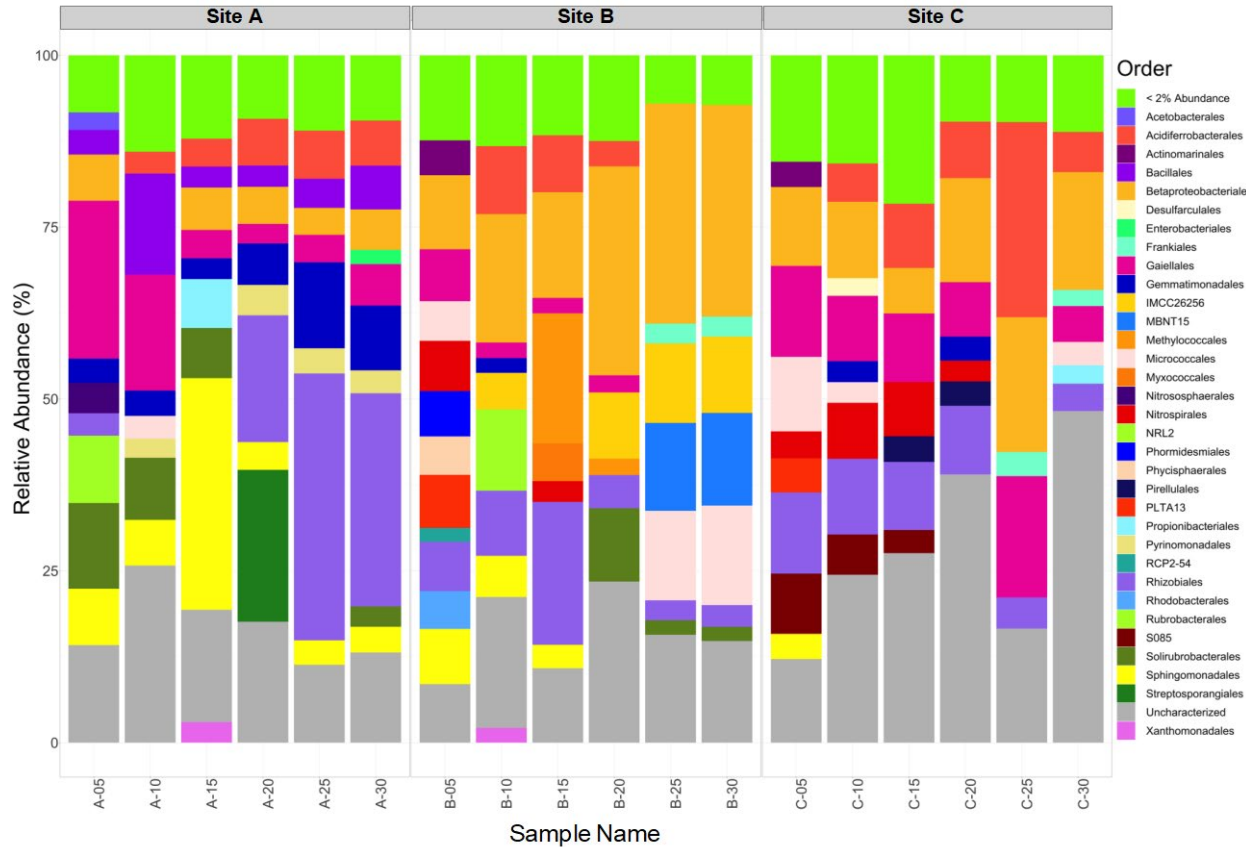


Figure 9. Normalized relative abundance taxonomic bar plot of the background tailings microbial communities at the Order level.

The tailings material within site B has the largest population of Fe- and S-oxidizers, with a percent relative abundance ranging from 6 – 28.5 % (Fig. 10). The material at site B has a large occurrence of bacteria that can oxidize Fe or S at D = 25 and 30 cm, with 28.5 and 28 % abundance, respectively for either sample, including the SOB *Sulfuricella denitrificans* (see Fig. 4 in Appendix I). The abundance of Fe- and S-cycling bacteria within the material at site C is close to that of site B, ranging from 2 to 28% (Fig. 10). Similar to the material at site B, the highest occurrence of SOB at site C occurs at D = 25 cm, with 28 % abundance being allocated to only the SOB genus *Sulfurifustis*. *Limnobacter* only occurs in the top 5 centimetres (D = 5 cm at an abundance of 3 %) at site A, whereas *Sulfurifustis* occurs at greater depths at site A (D = 10 to 30 cm) and depicts here an increasing abundance with depth (3 – 7 %; Fig. 10). Hence,

material at site A has the lowest population of Fe- and S-oxidizers. Overall, the tailings material have a higher proportion of bacteria that are capable of oxidizing both Fe and S, when compared to those that can only oxidize Fe or S.

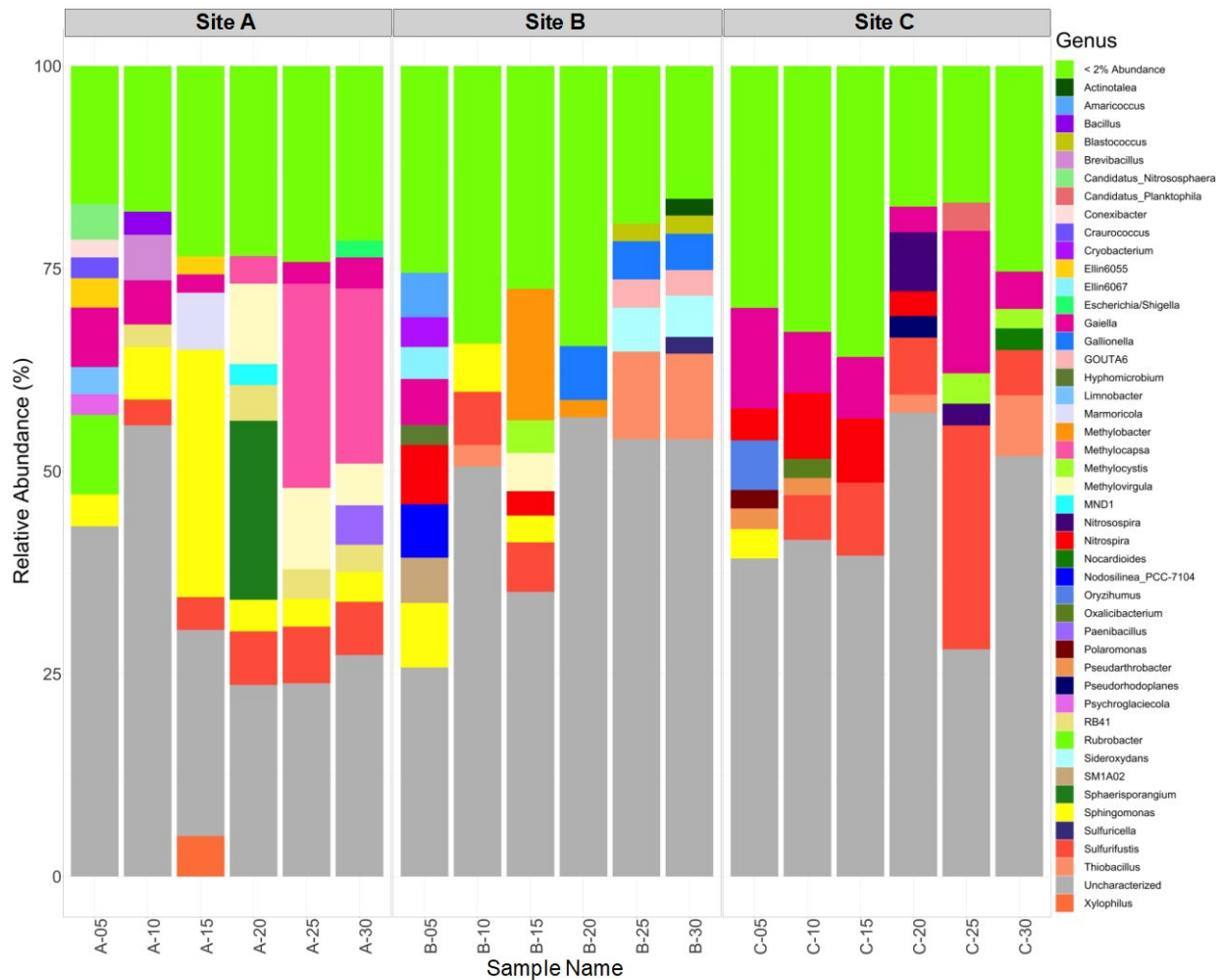


Figure 10. Normalized relative abundance taxonomic bar plot of the background tailings microbial community at the Genus level.

In addition to SOB and FeOB, there are also sulfate-reducing bacteria (SRB) of the class Thermodesulfovibrionia (Uncharacterized genera) and minor occurrences of known Fe-reducing bacteria (FeRB). The class Thermodesulfovibrionia occurs in material at site C, at D = 25 and 30 cm with a relative abundance of 5 and 41 % (Fig. 2 in Appendix E). The FeRB include those

within the *Bacillus* and *Paenibacillus* genera, of the Bacillales order, and one FeRB identified as *Rhodoferrax ferrireducens* (Fig. 4 in Appendix E), of the Burkholderiales order (Fig. 9). Both the *Bacillus* (2.85 %) and *Paenibacillus* (4.9 %) genera only occur within site A, at depths of 10 and 30 cm, respectively (Fig. 10). *Rhodoferrax ferrireducens* occurs only within materials from site C, at D = 30 cm with an abundance of 1.32 %.

6.2.4 Identification of potential As-cycling and/or As-resistant communities

The identified genera which include species that have As-cycling capabilities belong to the orders: Bacillales, Nitrososphaerales, Enterobacteriales, Rhizobiales, Betaproteobacteriales, Rubrobacteriales and Sphingomonadales (Fig. 9), and consist of: *Bacillus*, *Candidatus Nitrososphaera*, *Escherichia*, *Methylocystis*, *Polaromonas*, *Rubrobacter* and *Sphingomonas* (Fig. 10). There were also a number of As-resistant microorganisms identified within the *Blastococcus*, *Brevibacillus*, *Cryobacterium*, *Pseudarthrobacter*, *Sphingomonas*, and *Xylophilus* genera (Fig. 10), belonging to the following orders: Frankiales, Bacillales, Micrococcales, Sphingomonadales and Betaproteobacteriales (Fig. 9). Most of the As-cycling and/or -resistant genera identified are site-specific, with the exception of, 1) *Sphingomonas* identified throughout the tailings profile at site A, the top 15 cm at site B and within the first 5 cm of the tailings material at site C; and 2) *Methylocystis* occurring in materials at D = 15 cm of site B and D = 25 and 30 cm at site C. The tailings material at site A has the highest proportion of potentially As-cycling and/or -resistant microbes (3.5 – 36 %), with the highest abundance (36 %) occurring at D = 15 cm identified as *Sphingomonas* (31 %) and *Xylophilus* (5 %). A majority of the As-cycling and/or -resistant population at site B occurs within the top 15 cm (6 – 12%), with a total of 4 % *Blastococcus* in the bottom 10 cm. Comparatively, the As-cycling and/or -resistant

community within the tailings material of site C ranges from 2 – 9 %, with the highest abundance of, for example, *Polaromonas*, *Pseudarthrobacter* and *Sphingomonas*, at D = 5 cm.

6.2.5 Microorganisms common to metal-contaminated environments

The identified genera *Gaiella*, *Gallionella*, *Methylobacter*, *MND1*, *Sphingomonas*, *Sulfuricella*, *Sulfurifustis*, and *Thiobacillus* (Fig. 10) are common to metal-contaminated environments. Additionally, within the identified genera *Blastococcus*, *Hypomicrobium*, and *Methylocystis*, there are species which are tolerant to metal(loid)s in metalliferous environments (Fig. 10). Within the tailings material of site A, 11 to 37 % of the identified genera are common in metal-contaminated environments, with 10 to 30 % in the material of site B, and 10 to 50 % in the material of site C. *Gaiella*, *Sphingomonas* and *Sulfurifustis* are abundant throughout site A, with a noteworthy 30.5 % abundance of *Sphingomonas* at D = 15 cm. The characterized genera at site B that are common to metalliferous environments are more diverse and widespread when compared to site A and C tailings. Here, *Methylobacter* (average (A) = 9 %), *Sphingomonas* (A = 5.8 %) and *Thiobacillus* (A = 7.8 %) have the highest % abundance, of the specified genera. The tailings material at site C are slightly less diverse than site B, with *Gaiella* (A = 9 %) and *Sulfurifustis* (A = 11 %) being the most common. *Gaiella* and *Sulfurifustis* are predominant at D = 25 cm of site C, with highest % abundances of 18 and 28 %, respectively (Fig. 10).

6.2.6 Nitrogen-cycling community composition

Known N-cycling genera were identified from the orders Nitrososphaerales, Acetobacterales, Gaiellales, Propionibacteriales, Rhizobiales, Nitrospirales, Micrococcales, Bacillales, Rubrobacterales, and Betaproteobacteriales (Fig. 9). From these orders, the genera

Craurococcus, *Gaiella*, *Marmoricola*, *Nitrosospira*, *Oryzihumus*, *Rubrobacter*, *Sideroxydans*, *Sulfuricella*, and *Thiobacillus* are nitrate-reducers (involved in denitrification), while *Candidatus Nitrosphaera* and *Nitrospira* are ammonia oxidizers (involved in nitrification). Additionally, the genera *Methylocapsa*, *Methylovirgula*, *Paenibacillus* and *Thiobacillus* are involved in nitrogen fixation (Fig. 10).

At site A, the most prominent genera include *Gaiella* (2 - 7 %), *Methylocapsa* (3 - 25 %) and *Methylovirgula* (5 - 10 %), with the latter two denitrifying bacteria being more abundant in the lower half of the tailings profile (D = 16 to 30 cm) (Fig. 10). The tailings material at site B include the genera *Gaiella*, *Nitrospira*, *Sideroxydans*, *Sulfuricella* and *Thiobacillus*, with *Nitrospira* and *Thiobacillus* being the most abundance genera at D = 5 cm (7 %), at D = 25 and 30 cm (10.5 – 11 %), respectively (Fig. 10). Additionally, the denitrifying bacteria *Sideroxydans* and *Sulfuricella* occur in tailings from site B at D = 20 and/or 25 cm (2 – 5 %). Comparatively, materials of site C are characterized by abundant *Gaiella* throughout the tailings profile (3 – 18 %), *Nitrospira* within the top 20 cm's (3 – 8 %), *Oryzihumus* in the top 5 cm (12.6 %), *Nitrosospira* at D = 20 and 25 (~ 3 and 7 %) and *Thiobacillus* at D = 20 and 30 cm (2 – 7.5 %; Fig. 10). Therefore, bacteria capable of denitrification are more abundant at greater depths, while nitrifying bacteria are more abundant at shallower depths in all three sites.

6.2.7 Methanotrophic and methylotrophic populations

Identified methanotrophic and methylotrophic microbial communities occur within the Rhizobiales, and Methylococcales orders (Fig. 9), and include the identified genera *Hyphomicrobium*, *Methylobacter*, *Methylocapsa*, *Methylocystis*, *Methylovirgula*, and *Psychroglaciecola* (Fig. 10). The highest occurrence of methano- and methylotrophic

microorganisms occur at D = 5, 20, 25 and 30 cm of site A which include *Methylocapsa* (3 - 25 %), *Methylovirgula* (5.5 – 10 %) and *Psychroglaciececola* (2.5 %; Fig. 10). At site B, *Hyphomicrobium* (2.5 %), *Methylobacter* (2 – 16 %), *Methylocystis* (4 %), and *Methylovirgula* (5 %) occur within the top 20 cm (Fig. 10). The characterized methano- and methylotrophic microorganisms only occur within the bottom 10 cm of site C and are composed exclusively of *Methylocystis* (2 – 4 %; Fig. 10).

6.2.8 Identified species in the tailings sites

The species that were confidently identified in the tailings above an abundance of 0.5%, are: *Sulfuricella denitrificans*, *Nodosilinea_PCC-7104 epilithica*, *Rhodoferax ferrireducens*, *Sphingomonas flava* and *jaspsi*, *Aneurinibacillus migulanus*, *Sediminibacterium salmoneum*, and *Methylobacter tundripaludum* (Fig. 4 of Appendix I). Most of these species identified are either common to metal-contaminated sites or have been found in metalliferous environments as described above. Of the characterized species, *Sulfuricella denitrificans*, *Rhododerax ferrireducens*, *Sediminibacterium salmoneum*, and *Methylobacter tundripaludum* can play a role in S, Fe, and/or As-cycling.

6.3 Multivariate Statistical Analysis

6.3.1 Analysis of Similarities

An analysis of similarities (ANOSIM) test was implemented in order to evaluate the relationships between the microbial community compositions and the environmental (or field parameters) and geochemical variables between each site, the data for which can be found in Figure 1 of Appendix F. The ANOSIM test resulted in an R-value of 0.742 with a p-value of

0.001. An R-value closer to 1 implies a high dissimilarity between tested groupings, while a p-value < 0.05 implies a high statistical significance. This indicates a strong, statistically significant difference in the microbial communities based on the site grouping (data for this test can be found in Table 1 of Appendix G).

6.3.2 Non-metric multidimensional scaling analysis

In the following sections, environmental and geochemical variables \pm mineralogical compositions and As valences will be related to the bulk (Fig. 11 and Fig. 12) and site-specific (Fig. 13 – Fig. 16) microbial community composition, using non-metric multidimensional scaling (NMDS) plots. The r^2 values for the correlations relating the environmental and geochemical variables to each other are listed in Appendix J. The vectors for an NMDS plot point in the direction of the most rapid change of each (or each group) of variables, with the length of each arrow being proportional to the correlation between the ordination and said (group of) environmental variable(s). Variables were grouped based on overlapping arrows, hence signifying their close correlation and relationship. A stress value produced for an NMDS plot which is less than 0.2 is considered good as it means that the ordination distances (and therefore the axes from which they are derived) explains 80 % of the variability in the data. Hence, the lower the stress value, the higher our confidence in capturing the major patterns in the data. The circles on Figures 11, 12 and 13 correspond to a 95 % confidence interval.

6.3.2.1 Bulk microbial community relationships with environmental and geochemical variables

The microbial community composition at site A compared to that of sites B and C are less diverse (indicated by the smaller versus larger-sized confidence intervals), with the bottom 15 centimetres of site A (D = 20, 25 and 30 cm) being very similar (Fig. 10, Fig. 11a). The

microbial community composition for site C has a sizeable overlap with site B and small overlap with site A, shown by the 95 % confidence interval ellipses (Fig. 11a). Nevertheless, there are three distinct site groupings. These groupings are also evident in the plots with the Co# versus Fe# and S# (Fig. 5, Fig. 11b and c).

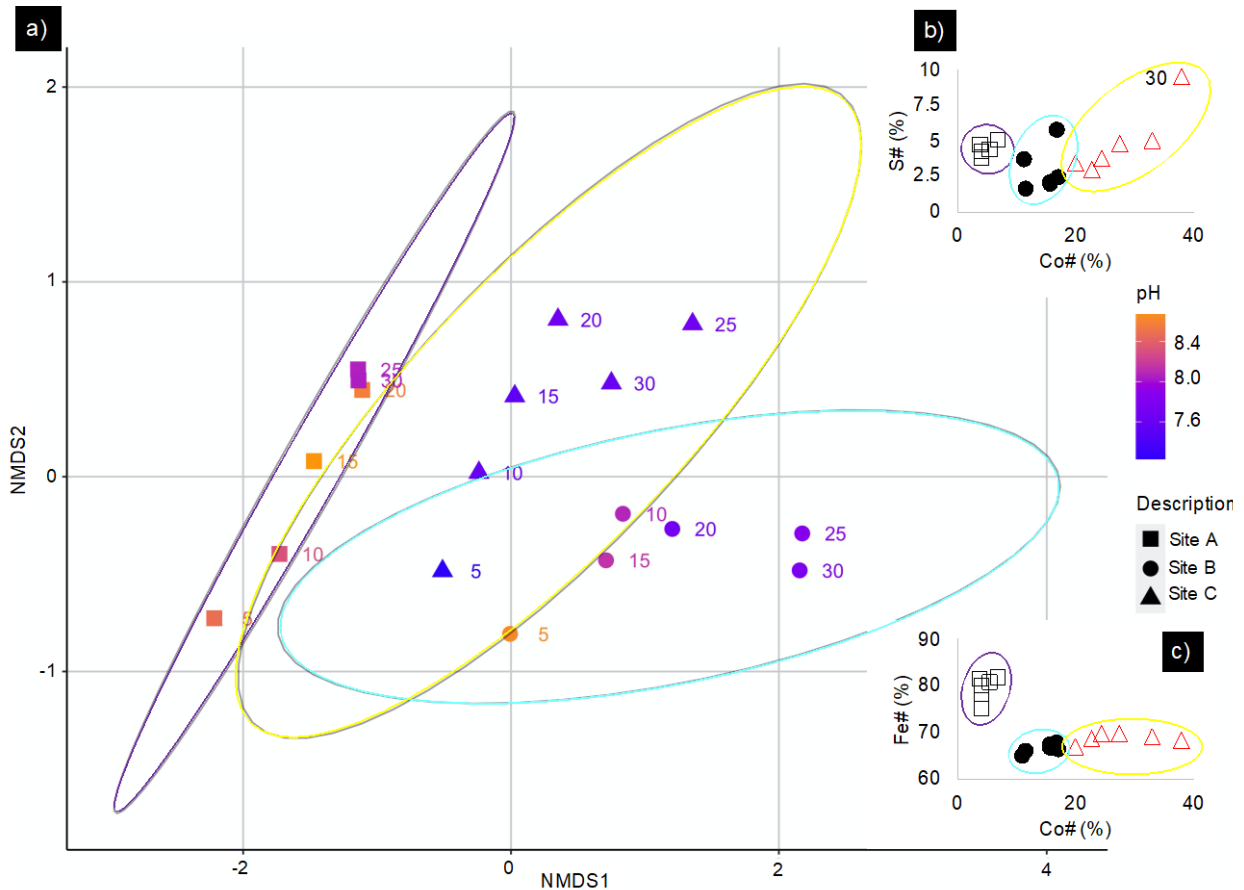


Figure 11. NMDS plot of microbial communities showing distinct groupings per site, coloured by pH, with insets of Co# vs (b) S# and (c) Fe#.

Well-defined relationships are observed when incorporating the environmental and geochemical variables into the bulk microbial community NMDS plot (Fig. 12). The controlling variables on the bulk microbial community composition can be divided into two groupings, the first group being those with significant r^2 and p-values (> 0.5 and < 0.05 , respectively) and the second including those with slightly less significant r^2 and p-values (< 0.5 and between 0.05 and

0.1, respectively). The first grouping includes the concentration of Fe#, depth and the concentration of Ag, while the less important grouping consists of pH, Eh, the concentrations of As, Ca, Co and S_(T) and the Co# (see Table 1 in Appendix K). The following observations from Figure 12 can be made:

1. The Fe# is highest in tailings of site A (specifically in the bottom 15 cm's) and lowest in tailings from site B; this observation is directly opposite to the concentration of Ag;
2. The group 1 (G1; S#, Eh, Fe concentration), group 2 (G2; S_(T), concentrations of As and Co), the concentration of Ca, the Co# and the amount of CO_{2(T)} are highest at greater depths ($D \geq 15$ cm) in the tailings from site C; and
3. Tailings from site C have the lowest pH values (lowest in $D = 5$ cm)

6.3.2.2 Microbial community site-specific relationships with environmental and geochemical variables

The relationships between the microbial community composition of sites A to C with environmental and geochemical variables are shown in Figure 13-c for sites A to C.

The composition of the microbial communities at site A is primarily controlled by depth ($r^2 = 0.96$), the concentration of Ag ($r^2 = 0.88$) and S_(T) ($r^2 = 0.77$), all of which have p-values < 0.05 (Table 2 in Appendix K). The relationship between the changes in these, other environmental variables and microbial community composition at site A is depicted in Figure 13a. Material at $D = 30$ cm of site A has the highest Eh value which is inversely proportional to the contact pH ($r^2 = -0.94$). The contact pH values are within group two (G2) (Fig. 12) along with the concentrations of As and Ca. Variables of G1 are the concentrations of Ag and CO_{2(T)}, both of which have a strong inverse correlation with group 5 variables, S# ($r^2 = -0.86$ and -0.84 , respectively) and

Fe# only with Ag ($r^2 = -0.71$). The Fe# and S# vary throughout the profile (e.g. both have maximas at D = 5 and 15 cm). At D = 5 cm, the highest concentration of group 3 (G3, Fe and S_(T)) and group 4 (G4, Co# and the concentration of Co) variables occur.

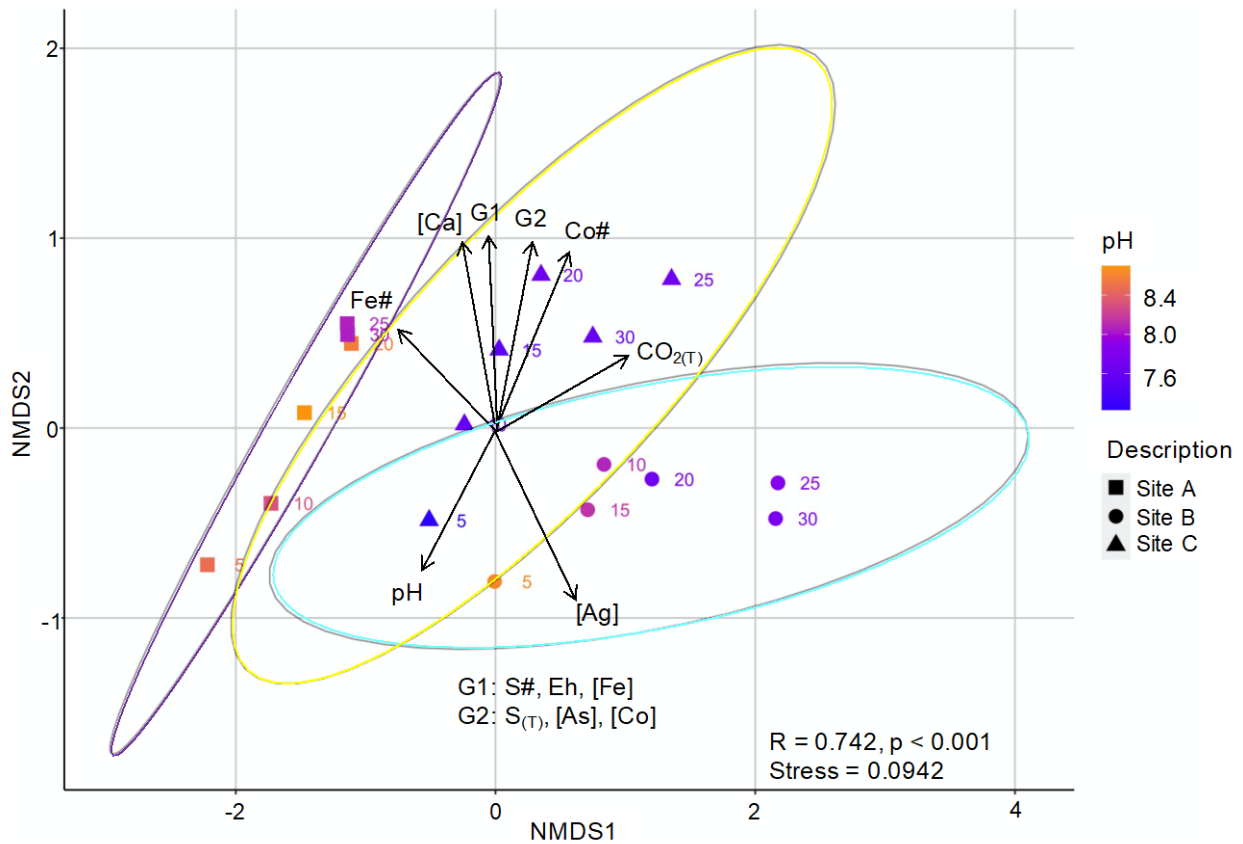


Figure 12. NMDS plot showing the variation in environmental and geochemical variables with site, and their effect on the microbial communities of sites A, B and C.

In comparison to the microbial communities at site A, the composition of the microbial community at site B are primarily controlled by depth, Eh, pH and the concentration of Ca (r^2 values > 0.75 and p-values between 0.005 and 0.08) (Table 3 in Appendix K).

Within tailings from site B, pH, the concentrations of Ag and As, the average valence of As, and the percent abundances of As⁵⁺ and As¹⁻-species are highly correlated to depth ($r^2 > 0.65$). The highest contact pH increase occurs within the first 15 cm's of tailings from site B, with the lowest pH values at D = 25 and 30 (Fig. 3). The concentration of Fe and the percent abundance

of As^{3+} -species are within G2, both of which have very high values at $D = 10$ and 15 cm, and are positively correlated ($r^2 = 0.72$) (Fig. 13b). The largest decrease in Eh is from $D = 10$ to 15 cm in material from site B. The group 4 (G4) variables (average As valence and the percent abundance of As^{5+} -species) are inversely correlated to As^{1-} ($r^2 > 0.9$), and have the highest values at $D = 10$ and 15 cm (Fig. 13b). The concentrations of As and Co are very low at $D = 30$ cm and $D = 25$ and 30 cm respectively. Within group 5 (G5), there is a maxima for the Co# and the concentration of $\text{CO}_{2(\text{T})}$ at $D = 5$ and 20 cm (Fig. 13b).

The microbial community composition at site C is controlled dominantly by: pH, depth, Eh, concentrations of As and Co, Co#, S#, $\text{S}_{(\text{T})}$, and the percent abundances of As^{5+} , As^{3+} , and As^{1-} -species, all of which have $r^2 \geq 0.75$ and p-values ≤ 0.06 (Table 4 in Appendix K). Similar to site B, these above-mentioned variables are significantly positively or negatively correlated with depth ($r^2 > 0.8$ or $r^2 < -0.8$). The Co#, along with the G1 and G2 variables, all increase with depth, with maxima for each variable or group of variables at $D = 30$ cm or $D = 25$ and 30 cm (Fig. 13c). The G4 variables (with the exception of the average As valence ratio of positive to negative valences (AVR; Equation 5) have a strong negative correlation with the G1 variables ($r^2 \leq -0.65$). The contact pH values are inversely proportional to the $\text{CO}_{2(\text{T})}$ concentrations ($r^2 = -$

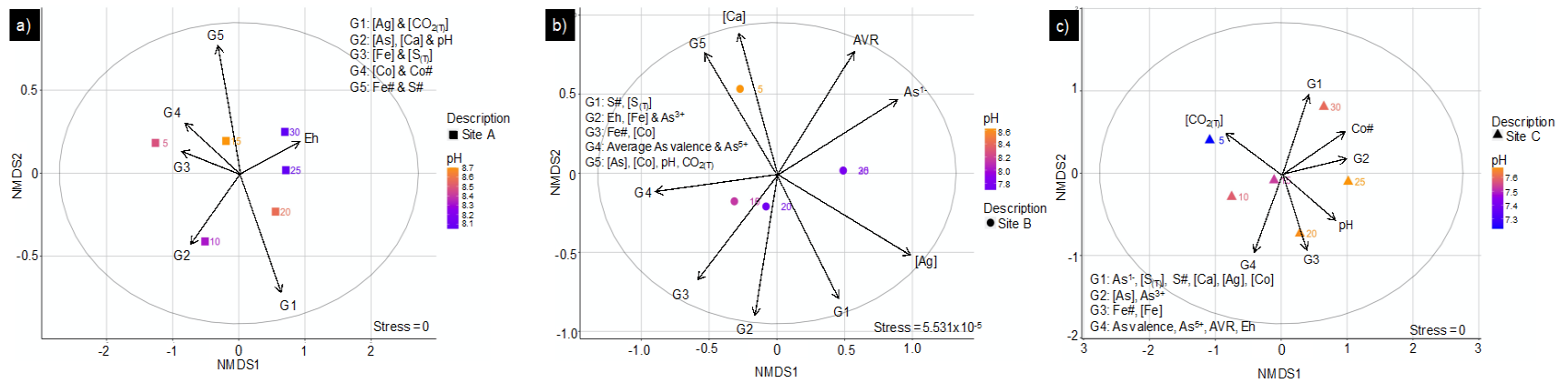


Figure 13. Site-specific NMDS plots showing how the environmental and geochemical parameters effect the microbial community within the tailings samples of site A (a), site B (b), and site C (c). The equation for the average As valence ratio (AVR) is given in Eq. 5.

0.9), with the highest and lowest values respectively at D = 5 cm. Maxima of the average As valence, percent abundance of As⁵⁺-species and the AVR occur at D = 15 cm.

$$\text{Average As valence ratio (AVR)} = \left[\frac{(\text{As}^{5+} + \text{As}^{3+})}{(\text{As}^{1-})} \right] \times 100 \% \quad (5)$$

The most important observations from all three tailings sites are that: (1) the tailings microbial community composition of site A is very different from that of sites B and C; (2) the tailings from each site is controlled by different variables, with only depth being the significant variable affecting each sites microbial community composition; and (3) the percent abundances of different As-species are one of the main variables in controlling the tailings microbial community composition at site C.

6.3.2.3 Site-specific overall trends relating the environmental and geochemical variables to microbial structures

The significance of the variable depth on the microbial community composition at site A can be also recognized in a site-specific NDMS plot for site A (Fig. 14). This plot also indicates that other variables such as Eh, CO_{2(T)}, pH, Fe#, Co#, S# and S_(T), are of much lower significance than depth.

The microbial community composition at site B is predominantly controlled by depth and the proportion of As⁵⁺ with respect to total As (i.e. the proportion of arsenates to arsenides; Fig. 15). The latter value decreases from 87 – 98 % at D = 10 - 20 cm to 78 % at D = 25 and 43 % at D = 30 cm. Furthermore, a large increase in the Co# between D = 15 and 20 cm and its decrease towards D = 30 cm coincides with a change in the microbial community composition (Fig. 6, Fig. 15).

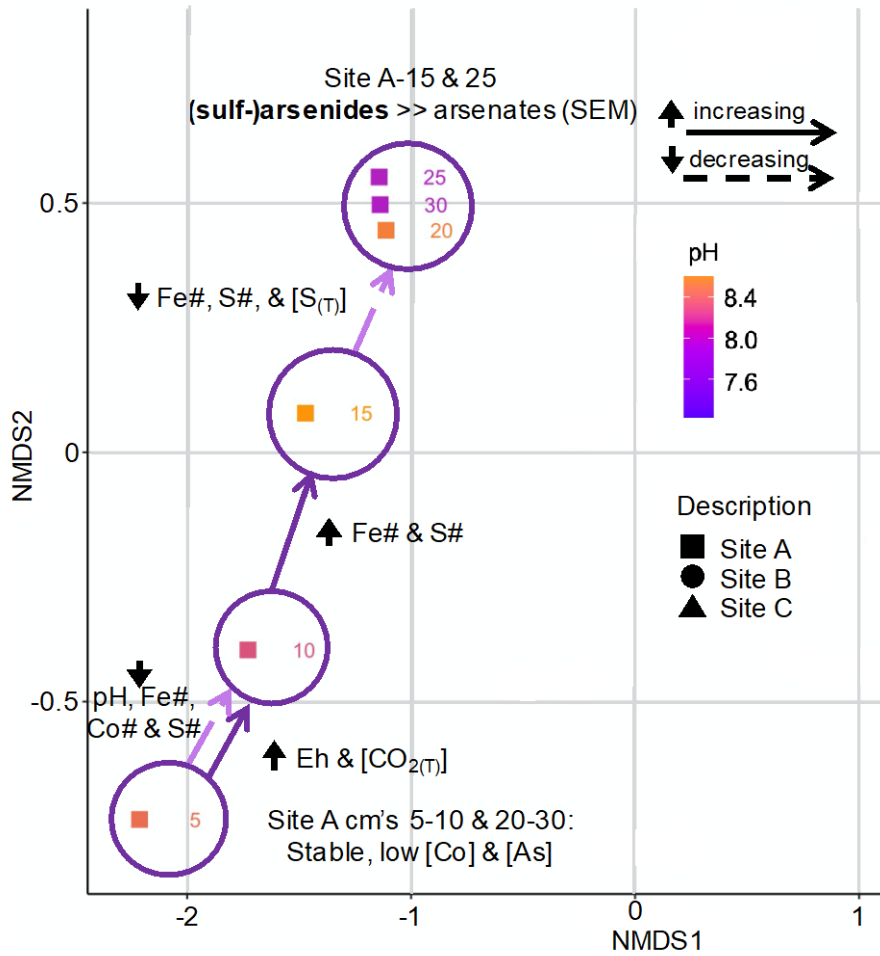


Figure 14. An annotated NMDS plot showing the variation in important environmental and geochemical parameters on the microbial community composition of tailings from site A.

The microbial community composition at site C follows a continuous increase in the concentration of As, Co#, S# and the amount of As⁵⁺ (70 – 85 % of As is As⁵⁺) when transitioning from D = 5 cm to D = 25 cm (Fig. 16), therefore correlating strongly with the proportion of arsenates. A sharp decrease in the As valence, the proportion of As⁵⁺ (5 %) and the Fe# between D = 25 and 30 cm coincides not only with an increase in the S and Co# but also with a change in the microbial community composition.

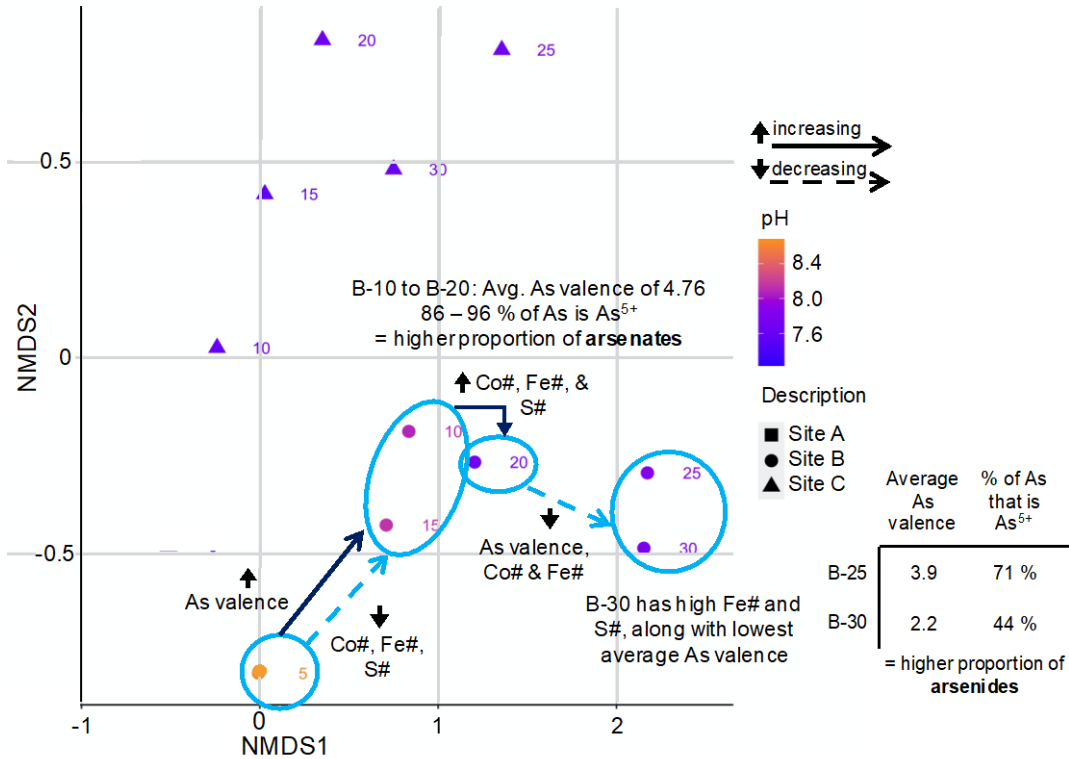


Figure 15. An annotated NMDS plot showing the variation in important environmental and geochemical parameters on the microbial community composition of tailings from site B, with an additional inlet showing the average of As and the percent of As that is As⁵⁺ at D = 25 and 30 cm.

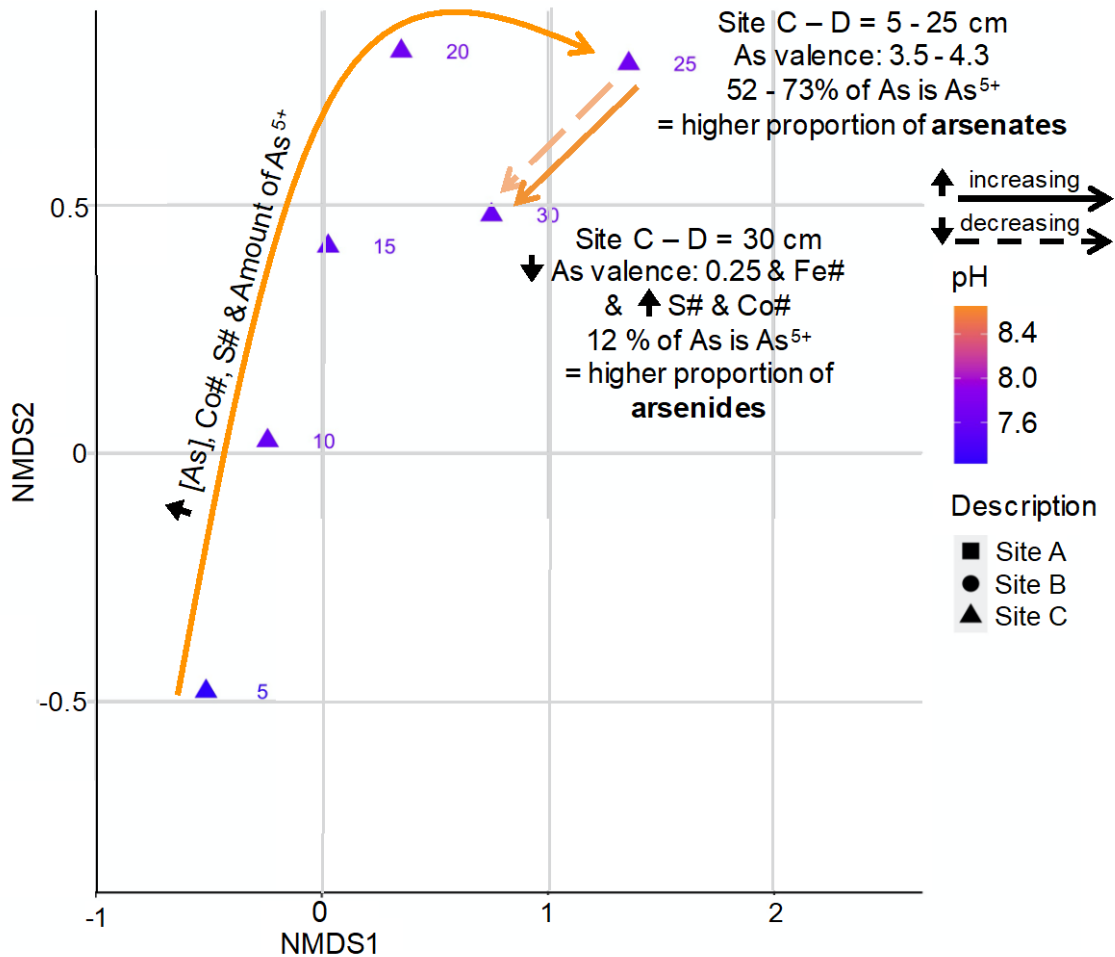


Figure 16. An annotated NMDS plot showing the variation in important environmental and geochemical parameters on the microbial community composition of tailings from site C.

7 Discussion

We will first address common and different geochemical and mineralogical features in the tailings material examined in this study versus those studied by Courchesne et al. (2020) (Appendix A) before addressing the composition of the microbial communities in the tailings materials at sites A, B and C and their relationships with the corresponding geochemical and mineralogical features.

7.1 Geochemical and mineralogical features of the tailings material at sites A, B and C

Although the sampling in this study was at a lower resolution than the study by Courchesne et al. (2020) (samples from every 5 cm versus every 1 cm), the tailings profiles recorded at the sites A and B show similar chemical and mineralogical features and trends:

- (1) Tailings material at site B has higher Co#, lower concentrations of Fe and higher proportions of secondary arsenate phases in the form of mineral surface coatings than the material at site A (Fig. 4, Fig. 6);
- (2) Tailings material at all sites has only minor amounts of Fe-(hydr)oxides
- (3) At sites A, B and C, tailings material with higher Co#'s have lower amounts of Fe than those with lower Co#' (Fig. 4, Fig. 6); and
- (4) At sites B and C, material with a high S# value generally coincides with a lower As valence (e.g. D = 20 and 30 cm in sites B and C) (Fig. 4, Fig. 6).

The tailings material at site C was not characterized by Courchesne et al. (2020) and shows different geochemical and mineralogical trends. Material from site C contains much higher concentrations of Fe, As, S, Co and other metals. The tailings material at sites B and C follow a similar trend with respect to the average valence of As. Tailings materials at lower depths at both sites are characterized by higher valences of As (approaching +5.0), whereas material at greater depths (D = 30 cm) has a lower average valence for As with +2.2 (site B) and +0.25 (site C) (Fig. 4). The lowest measured valence of As in the bottom layer of site C coincides with a high number of Fe-sulfides, and Co-Zn-Ni-Fe (sulf-)arsenides and the absence of any arsenate-bearing mineral surface coatings (Figure 2 in Appendix H). Furthermore, the material at site C exhibits similar zonations as observed in acidic tailings depth profiles, such that there is a reduced zone at greater depth, a transition and a surficial oxidized zone (Lottermoser, 2007). This zonation is not sharp on the cm-scale and can be recognized by a gradual decrease in Eh, CO_{2(T)} content, Co#,

S# and concentrations of As and Co, and an increase in Fe#, S_(T). Additionally, as the average valence decrease with depth, there is a gradual oxidation of (sulf-)arsenides, leaching of metal(loid)s and increasing acidity towards the surface. Additionally, a higher abundance of darker material at greater depth suggests an increase in organic matter and perhaps higher activity of microbial communities. Hence, a high Co# at the bottom of site C does not correspond to a high ratio of arsenates versus (sulf-)arsenides (as observed at site A and B) as the latter minerals are minor rather than trace phases.

7.2 Main environmental and/or geochemical drivers in microbial diversity across each tailings site

Microbial diversity in mine waste environments can be shaped by various environmental factors and geochemical variables. The characterization of their diversity is important in understanding the biological response to the environmental and geochemical conditions. The variables associated with governing the microbial structure in the tailings are different and more complex than those associated with trends in the mineralogical data (i.e. Co, Fe and S#'s). The following is a short overview of the relationships of the bulk and site-specific microbial communities with the environmental and geochemical variables that have been previously discussed. The most statistically significant environmental and geochemical variables controlling the bulk tailings samples of the CMC are depth, the Fe# and the concentration of Ag. The most significant factors governing the composition of the microbial communities within each site consist of: depth and the concentrations of Ag and S_(T) at site A, depth, Eh, pH, and the concentration of Ca at site B, and pH, depth, concentrations of As and Co, the Co and S#'s, and

the percent abundances of As⁵⁺, As³⁺ and As¹⁻-species at site C. On the basis of these observations, the following conclusions can be made:

- 1) depth is a primary explanatory variable in shaping the microbial community structure within bulk microbial community and the tailings of each site,
- 2) the concentration of various elements, including Ca, Fe and the metal(loid)s Ag, As, Co, Zn, Ni and Sb, play a major role in determining the microbial communities present at specific sites,
- 3) the different abundances of As mineral species present strongly correlate with different microbes present in material from site C, and
- 4) the Fe# does not play a site-specific role in the abundance of microbial communities but it is important parameter to differentiate the microbial community structures between the different sites.

7.2.1 Contact pH as related to microbial communities

Within the tailings of the CMC, the pH values per site occur within 1 to 2 pH units of each other, with material from site B having the largest diversity in pH (Fig. 3). Contact pH has been shown by several studies as being a primary controller in microbial diversity (e.g. Li, J et al., 2014a; Sun et al., 2016). This is due to the fact that most microbes have a low adaptability to a large window of pH values (e.g. *Rhodoferrax ferrireducens* has an optimal growth pH of 6.7 – 7.1; Finneran et al., 2003). Hence, beyond this small window the microbes either cannot survive or adapt, and are therefore outcompeted by those that can. For example, Rousk et al. (2010) showed that an increase in soil pH shifted the communities from Acidobacteria subgroups 1-3 to subgroups 5-7. The results of this study do not exactly share the same observation as in Rousk et

al. (2010), as there are no large pH fluctuations at sites A, B and C with depth. However, shifts in pH influence environmental and/or geochemical properties and features, such as the solubility of minerals (Kelley and Tuovinen, 1988; Bigham et al., 1996) and the availability of nutrients such as organic carbon (Kemmitt et al., 2006). Therefore, the tailings remediation of site B (Percival et al., 2004; Dumaresq, 2009; Courchesne et al., 2020) could have influenced the decreasing pH trend observed in the depth profile, and thereby indirectly influence the microbial composition.

7.2.2 Variation of microbial communities with depth in each tailings profile

It has been widely shown that the microbial composition changes with depth (e.g. Koizumi et al., 2003a; Eilers et al., 2012; Xiao et al., 2017; Ji et al., 2018), with the metalloid-rich, neutral-pH mine tailings of the CMC being no exception. The R^2 statistics indicate that depth is an important controlling factor for the microbial community compositions at all three tailings sites. For example, the diversity at site B changes mostly across the NMDS1 axes with depth, whereas a greater diversity across both NMDS1 and NMDS2 axes occurs for sites A and C (Fig. 11). There are also, similarities in the microbial composition between samples at similar depths but different sites. For example, surface samples at sites B and C have similar microbial compositions on the order and family-level taxa (Fig. 8 and Figure 3 in Appendix I). Hence, depth strongly controls the diversity in the microbial community structure for each site and sometimes in samples from different sites but similar depths. Additionally, similar to the change in the structure of the microbes, there is also a clear mineralogical change with depth, specifically at site C, which will be discussed in the following sections.

The most pronounced depth-related diversity observed in the microbial communities are: (1) a relative high proportion of FeOB and SOB at greater depths at sites A and B; (2) a relative high

abundance of methanotrophs at greater depths at sites A and C; and (3) conversely to site B, a relative high abundance of SRB in the bottom 10 cm of site C.

7.2.2.1 The abundance of S and C-oxidizing and -reducing bacteria with depth

The S-reducing class of bacteria, Thermodesulfovibrionia within the phylum Nitrospirae, occurs at a 46 % relative abundance within the bottom 10 centimetres of site C (Figure 2 in Appendix I). Similarly, Koizumi et al. (2003a, b), Sahm et al. (1999), and Ravensschlag et al. (2000) showed that the proportions of Nitrospira-like genus (nitrite-oxidizing bacteria of the phylum Nitrospirae), SRB, and methanogens increase with soil depth. The proportion of SOB can also increase with depth, as seen at pyrite-bearing mine tailings (Elberling et al. 2000).

At site A and C, the abundance of bacteria capable of 1) using methane as a C and energy source (i.e. methanotrophs; Finn et al., 2020) and 2) nitrogen (i.e. *Gaiella*) increases with depth. This is in contrast to the observations by Koizumi et al. (2003a) who showed that the abundance of methane-producing methanogens (microorganisms (mainly archaea); Finn et al., 2020) increases with depth. This feature is also observed for the facultatively anaerobic and methanotrophic *Methylobacter* genera which occur in oxygen-limited environments (such as at greater depths), with their abundance in this environment being attributed to the coupled methane oxidation to nitrate or nitrite reduction (van Grinsven et al., 2020). Van Grinsven et al. (2020) suggest that the abundance of *Methylobacter* at greater lake water depths is attributed to nitrate-reducing microorganisms providing *Methylobacter* with a source of nitrite, which enables this genus to thrive in such an environment.

7.2.3 Microbial community shift due to changes in total carbon content

Mendez et al. (2007) and Chen et al. (2013) show that TOC plays a role in the structure of the microbial communities within tailings sites. In the CMC tailings, the $\text{CO}_{2(\text{T})}$ seems to affect the microbial community composition at site B, due to the previously mentioned revegetation in the late 1990's (Percival et al., 2004; Dumaresq, 2009). It should also be noted that the Ag-veins in the CMC were lined with carbonate minerals, such as calcite and dolomite (Andrews, 1986), and were therefore not a product of remediation. Here, the $\text{CO}_{2(\text{T})}$ content decreases from 5 wt % at the top to 3 % at the bottom (Fig. 3d) and resulted most likely in a much higher diversity of common soil microorganisms at the top sample (B-05) such as the occurrence of the Rhizobiales, Rhodobacterales and Sphingomonadales orders, of which are all capable of fixing carbon and nitrogen (Garris et al., 2018). These bacterial orders are also considered drivers in contaminated soil bioremediation (Garris et al., 2018).

7.2.4 Iron and sulfur-cycling bacteria in neutral-to-alkaline pH conditions

In the neutral-pH tailings of the CMC, the abundance (or lack of abundance) of Fe- and S-bearing minerals strongly affected the structure of the bulk microbial diversity. This relationship can be perceived by the groupings of samples based on site in the plots of Co# vs Fe# and S#, and NDMS plots. Additionally, the occurrence of Fe and S-bearing minerals can be attributed to 1) pH, 2) the concentration and average valence of As, and 3) depth and/or Eh, due to their high correlation values to the Fe and/or S#'s (Appendix J). In acidic pH environments and/or those characterized by AMD, Fe and S-cycling bacteria are well-characterized (e.g. Kock and Schippers, 2008; Guan et al., 2017). However, in metal(loid)-rich, Fe- and S-poor tailings environments with a neutral-to-alkaline pH, the role of these microbes are not as well understood.

In general, the CMC tailings have a higher abundance of FeOB and SOB relative to FeRB and SRB, presumably due to the oxidizing conditions of the tailings (Fig. 3). However, there are site-specific inverse correlations with depth between these two Fe and S-cycling groupings, i.e. at site B FeOB and SOB increase with depth, and at site C FeRB and SRB increase with depth. At greater depths of site C, the known SRB order Thermodesulfobionia occurs (Rabus et al., 2006; Gao et al., 2015) along with *Rhodoferax ferrireducens*, a dissimilatory Fe³⁺-reducing bacterium (Finneran et al., 2003). The occurrence of the FeRB and SRB in the bottom layer of material from site C coincides with a drop in the average valence of As (Fig. 4) and high S# (Fig. 6), and a high ratio of primary (sulf-)arsenides to secondary arsenates (as observed on the SEM, Figure 2 in Appendix H).

There are also high abundances of FeOB and/or SOB (most of which are nitrate-dependent) at greater depths of sites A and B, with highest occurrences consisting of *Gallionella* sp., *Sideroxydans* sp., *Thiobacillus* sp., and *Sulfuricella denitrificans* (Fig. 10 and Figure 4 in Appendix I). The existence of these bacteria at greater depths in the tailings profile (bottom 10 cm of sites A and B) could be attributed to potentially less oxic or anoxic conditions (observed by the lower average As valence (Table 2 in Appendix G). This could also be due to the possible occurrence of more (sulf-)arsenides in the bottom layer of site B, however, further SEM characterization is necessary in order to see whether there is indeed a higher abundance of primary arsenides versus secondary arsenate coatings.

As nitrate is considered a chemical oxidant under anoxic conditions, oxidation of Fe or S species through nitrate-reduction is possible under reducing conditions (Haaijer et al., 2012). For example, *Thiobacillus* and *Sulfuricella denitrificans* are capable of coupling the oxidation of Fe or S-species to nitrate-reduction under reducing conditions (Haaijer et al., 2012). Additionally,

FeOB communities composed of, for example, *Sideroxydans*, can thrive in environments with high concentrations of nitrate and in the presence of FeOB capable of coupling Fe-oxidation to nitrate-reduction (Bryce et al., 2018).

7.2.5 Microbial community composition versus the average valence of As

The following sections discuss the relationship between Fe and S-oxidizing and -reducing bacteria and the average valence of As representing the ratio of arsenides versus arsenates. Although the SEM studies did not provide any direct evidence for the biologically-controlled mineralization (BCM) and dissolution of Fe or As-minerals, biologically-induced formation (BIM) and dissolution of Fe, S, and As-bearing minerals occurred most likely throughout the tailings, i.e. nucleation and dissolution were not physically controlled by the metabolic activities of microbes (BCM; Dove, 2010), but were products of changes in bacteria-induced microenvironments (BIM; Konhauser, 2007).

The biogeochemical cycling of As is important in terms of ecological toxicity and bioremediation processes. Microbes have a variety of roles in As-cycling, such as the biomethylation of As (e.g. arsenite to trimethylarsine), the reduction of arsenates, and the oxidation of arsenides or arsenites (Gadd, 2010). An understanding of the role of microbes on the cycling of As is a prerequisite for a bioleaching study (Chapter 4) and can be gained through exploring the relationship between the average valence of As and the microbial community composition at the sites A, B and C.

Material with a comparatively low average valence of As (+2.18) at D = 30 cm of site B (Fig. 3) contains a large proportion of FeOB and SOB, as well as microbes that are resistant to high concentrations of As. These include a 28 % cumulative abundance of *Sideroxydans*,

Gallionella, *Sulfuricella*, and *Thiobacillus* genera (Fig. 8). In contrast, tailings material with a high average As valence at site B at D = 10 and 15 cm, contains: 1) 4 – 8 % *Sphingomonas*; 2) slightly elevated Eh values (Fig. 2); and 3) a community of microbes common in metal-contaminated environments, such as the methanotrophs *Methylobacter* and *Methylocystis* (Park et al., 2018; Shi et al., 2019), and *Nitrospira* (Daims, 2014).

The microbial structure at site C correlates well with various geochemical factors (see Table 4 in Appendix J). Here, a decrease in the average valence of As with depth (Fig. 4) results in a more complex microbial community structure than observed at site B. This complexity can be understood with a closer inspection at the abundance of the genera *Gaiella*, *Nitrospira*, *Nitrosospora*, *Sulfurifustis*, *Thiobacillus*, *Methylocystis* and *Nocardioides* as well as the order Thermodesulfovibrionia. The first three (here now referred to as group 1), include species involved in nitrate-reduction (Albuquerque et al., 2011), nitrite-oxidation (Daims, 2014), and ammonia-oxidation (Prosser et al., 2013), respectively, whereas the latter five (referred to as group 2) include those capable of S-reduction (Thermodesulfovibrionia; Gao et al., 2015), S-oxidation (*Sulfurifustis* and *Thiobacillus*; Liu et al., 2019a) or As⁵⁺-reduction (*Methylocystis* and *Nocardioides*; Shi et al., 2019 and Bagade et al., 2016). The cumulative abundance of groups 1 and 2 show an inverse correlation; with the abundance of groups 1 and 2 decreasing and increasing with depth, respectively (Table 2). Therefore, the occurrence and activity of microorganisms within groups 1 and 2 correlate with the valence of As and thus with the proportion of arsenides over arsenates.

Table 2. The variation in groups of microbes as related to the average As valence and depth of site C's tailings profile.

	Genera / Class abundance	C-05 (%)	C-10 (%)	C-15 (%)	C-20 (%)	C-25 (%)	C-30 (%)
Group 1	<i>Gaiella</i>	12.4	7.5	7.6	3.1	17.6	4.6
	<i>Nitrospira</i>	3.9	8.4	7.9	3	0	0
	<i>Nitrosospira</i>	0	0	0	7.3	2.7	0
	Sum	16.3	15.9	15.5	13.4	20.3	4.6
Group 2	<i>Sulfurifustis</i>	0	5.5	7	7	27.6	5.6
	<i>Thiobacillus</i>	0	0	0	0	0	7.5
	<i>Nocardioides</i>	0	0	0	0	0	2.7
	<i>Methylocystis</i>	0	0	0	0	0	2.4
	Thermodesulfovibrionia	0	0	0	0	5	41
	Sum	0	5.5	7	7	32.6	45.6

7.2.5.1 The role of nitrogen-cycling “group 1” bacteria with respect to the valence of arsenic

At site B and C there occurs a large abundance of N-cycling bacteria (e.g. *Gaiella* and *Nitrosospira*) and others that couple nitrate-reduction to Fe and/or S-oxidation (e.g. *Thiobacillus*). The high abundance of these microbes could be due to the implemented cyanide or cyanide-Hg amalgamation technique for ore processing and the disposal of the corresponding waste at site B and C, respectively (Anderson, 1993; Dumaresq, 1993). Ammonium and As have been seen to co-occur in mining environments that used cyanide during ore-processing (EPA, 2003; Dave et al., 2008), with the release of ammonium being partially attributed to primarily biotic oxidation of arseno-sulfide minerals, such as arsenopyrite (Bissen & Frimmel, 2003; Tapley & Yan, 2003). However, cyanide species are easily biodegradable in the environment, due to being an important N-source for microorganisms (Ebbs, 2004), and thus cyanide species (likely) do not exist anymore in the tailings. Nevertheless, N-cycling microbial communities most likely colonized the tailings due to the early presence of cyanide.

Nitrifying bacteria are those that can oxidize ammonium, ammonia and nitrite to nitrate (such as the nitrite-oxidizing, *Nitrospira spp.* (Papirio et al., 2014). Papirio et al. (2014) also identified the co-occurrence of ammonium- and As^{3+} -oxidation under oxic conditions at neutral pH in the absence of As-oxidizers. In this regard, Papirio et al. (2014) showed that the activity of nitrifying and As-tolerant bacteria such as *Nitrospira* and *Lysobacter spp.* can be negatively affected by the presence of As^{3+} . The observed lower abundance of N-cycling genera of group 1 at greater depth is thus most likely the result of a lower average As valence.

A higher or similar abundance of *Gaiella* relative to *Nitrospira* occur at site C (Table 2). Li et al. (2008) observed the coexistence of denitrifiers (e.g. *Gaiella*) and nitrifiers, with their occurrence being due to anoxic or low-oxygen zones in the inner-part of flocs and biofilms. In addition, members of the *Gaiella* genus commonly occur in metal-contaminated sites (Liu et al. 2019b) and influence the concentration of As within non-ferrous, neutral-pH metal(loid) tailings (Liu et al., 2019a). Yet *Gaiella* species capable of reducing As^{5+} in the presence of nitrate species have not been identified. However, Dowdle et al. (1996) stated that within nitrate-respiring sediments, the reduction of As^{5+} could occur once all of the nitrate was removed.

7.2.5.2 The role of bacteria capable of S, Fe and As cycling with respect to As valence

Hollibaugh et al. (2006) showed that S-oxidation was coupled to As-reduction within a microbial community in Mono Lake, California, USA. The authors also identified:

- 1) different “guilds” of arsenate-reducing bacteria, such as S-oxidizers (oxidation of sulfide and other reduced S-compounds), heterotrophs, and organisms that could oxidize H_2 and Fe^{2+} ; and
- 2) arsenate-reducing, S-oxidizers which use nitrate as an electron acceptor.

Two of the identified SOB (*Sulfuricella*, and *Sulfurifustis*) are able to couple S-oxidation and As-reduction. Furthermore, Guan et al. (2017) identified *Thiobacillus* as well as other SOB (*Sulfuricurvum* and *Sulfurimonas*) capable of reducing As^{5+} to As^{3+} by using nitrate as the preferred electron donor. These observations suggest that a large increase in *Gaiella* between D = 20 cm and D = 30 cm at site C is a result of a nutrient-cycling between the previously mentioned nitrifying *Nitrospira* genus and the SOB capable of nitrate-reduction (Table 2).

In the past few decades, it has been recognized that the activity of SRB plays an essential role in the geochemical cycling of As (e.g. Oremland et al., 2009; Saalfield and Bostick, 2009; Handley et al., 2013), the mobilization of As (Buschmann and Berg, 2009; Li, et al., 2014) or in the reduction of arsenate (Saalfield and Bostick, 2009; Kocar et al., 2010). More recently, Zacarías-Estrada et al. (2020) show that SRB are capable of simultaneously reducing sulfate and arsenate species which results in the precipitation of biogenic Fe-As-S minerals. Kelly et al. (2007) proposed a similar process for the sequestration of metal(loid)s in wetland sediments of the CMC without providing any mineralogical evidence. Similarly, this study did not find any textural evidence for the biotic-controlled formation of (sulf-)arsenides.

Iron oxidation by FeOB is commonly associated with bacterial oxidation of As, rather than reduction (e.g. Seith & Jekel, 1997; Katsoyiannis & Zouboulis, 2004, 2006; Hohmann, 2010). However, *Gallionella*, a neutrophilic and Fe-oxidizing genera, is capable of reducing As^{5+} (Katsoyiannis & Zouboulis, 2004), and is present at D = 25 and 30 cm of site B. Another As-reducing bacteria (AsRB) genus, *Nocardioides* (Bagade et al., 2016), occurs at D = 30 cm of site C, which also include bacteria that are capable of degrading complex and unusual substrates (Tóth & Borsodi, 2014). Also, As-oxidizing bacteria within the family Sphingomonadaceae,

such as *Sphingomonas* (Macur et al., 2001; Kinegam et al., 2008) occur in the upper parts of site B where As has a higher average valence.

7.2.5.3 Relation of methanotrophic bacteria to As-reduction

In the lower 15 cm of the CMC tailings, especially at site A, there are higher relative abundances of methane-oxidizing bacteria (MOB) (e.g. *Methylocystis*, *Methylocapsa*, and *Methylovirgula*) and their occurrence correlates with higher ratios of primary arsenides to secondary arsenates.

Due to the occurrence of a methanotroph-specific broad-spectrum enzyme termed methane monooxygenase (MMO), there is significant evidence for methanotrophs to play an integral role in degrading and/or co-oxidizing a variety of metals, therefore demonstrating their potential use in environmental bioremediation (Pandey et al., 2014). Methanotrophic bacteria, such as those within the genera *Methylocystis*, *Methylocapsa*, and *Methylobacter* have been identified in metal and/or As-contaminated environments (e.g. those impacted by AMD, Gorra et al., 2012; Park et al., 2018). The speciation and bioavailability of metals in these environments suggest that their mobilization and sequestration was controlled by methanotrophs (Jenkins et al., 1994; Choi et al., 2006). Shi et al. (2019) showed that 10 of the studied methano- or methylotrophic genera (MOB), including, for example, *Methylocystis*, *Methylocapsa* and *Methylovirgula*, have As^{5+} and Hg^{2+} -reduction capabilities. Hence, the occurrence of this CH_4 -cycling bacteria at greater depths potentially played a role in the speciation of As.

Methanotrophic bacteria are commonly present in waterlogged soils (Dedysh, 2001) and their larger abundance at site A could be due to the tailings site being situated next to (and within) a large lake. Furthermore, site C is directly adjacent to a small low-lying wetland, which

could account for the presence of *Methylocystis* at the lower 10 cm. At this depth, the larger abundance of the Fe- and S-cycling bacteria *Sulfurifustis*, *Thiobacillus*, and SRB of the Thermodesulfovibrionia class most likely played a greater role in the speciation of As. The occurrence of the MOB at site B corresponds to a higher valence of As at D = 15 cm, which could be simply due to the fact that the tailings were once (perhaps) water-logged.

To summarize, changes in the bacterial communities with respect to the average valence of As suggest that:

- (1) A decrease in the abundance of nitrifying bacteria with depth is a result of a decreasing average As valence, potentially due to a higher proportion of As^{3+} -species;
- (2) As-oxidation may occur with ammonia oxidation due to ammonia-oxidizing bacteria (AOB) action;
- (3) S-oxidation may be coupled to As-reduction;
- (4) Methane-oxidizing bacteria have the potential to be linked to As^{5+} -reduction and environmental bioremediation; and
- (5) In the bottom layer of site B the genera *Gallionella*, *Methylocystis*, and *Nocardioides* may have played an active role in the reduction of As^{5+} , whereas the SRB class Thermodesulfovibrionia could have had such a role in the bottom layer of site C.

Future transmission electron microscopy (TEM) and/or SEM studies on selected tailings material should reveal whether these species are in close association with arsenides or arsenates.

Although there is no mineralogical or geochemical evidence for reduction of As^{5+} , it is intuitive that potential AsRB use some of the As^{5+} to reduce As-species to a lower valence as a matter of gaining energy.

7.2.6 Silver relation to microbial communities

Within the bulk microbial community structure and that of site A, Ag plays a governing role in shaping the overall community composition. Material from sites A and C have a similar range of Ag concentrations (10 – 50 ppm), while those of site B are higher (75 to 110 ppm) (Table 1 in Appendix G). This correlates with the similarity of microbial communities at sites A and C (Fig. 11). Additionally, all three sites have a slight increasing amount of Ag with depth (Appendix L). Silver is widely recognized in the literature as having a highly toxic effect on bacteria, with as little as 0.5 to 5 ppm for Ag⁺ ions and 12.50 to 50 ppm of silver nanoparticles (AgNPs) affecting bacterial cell growth (Greulich et al., 2012).

At D = 25 cm of site B, the presence of secondary Ag-minerals (Ca-Fe-Ag arsenates or as unidentified Fe-As-Sb-S-Ag-O phases, as identified with SEM; Appendix H) may have formed as a result of oxidative dissolution of Ag-arsenosulfides such as argentopyrite, proustite, or stephanite. This could have been potentially controlled or induced by FeOB and SOB (*Gallionella*, *Sideroxydans*, *Sulfuricella* and *Thiobacillus*) at greater depths of site B, similar to the widely recognized biotic oxidation of pyrite in mine waste environments (Chen et al., 2013). These sulfides have been identified within the ore at Cobalt, ON (Appendix B; Joyce et al., 2012).

The oxidation of such minerals could have influenced the microbial communities within the CMC tailings. For example, Masrahi et al. (2014) suggest that the activity of nitrifying bacteria is significantly affected by the presence of Ag⁺ with concentrations as low as 0.08 mg/L. Hence, the Ag concentrations at site B could be one possible explanation for the observed decrease in nitrifying bacteria with depth in the tailings.

7.3 Iron mobilization in alkaline tailings

Iron-(hydr)oxides are the most thermodynamically stable Fe-phases under near-neutral to alkaline conditions, with their formation being inhibited by, for example, the presence of FeRB (Revesz et al., 2015). As described by Courchesne et al. (2020), Co-Ni-Zn arsenates rather than Fe-(hydr)oxides replace scorodite under circumneutral conditions in layers enriched in Co, As and Fe relative to the layers above or below. In Appendix A, Courchesne et al. (2020) argued that the replacement of scorodite was promoted by the formation of Fe-carbonate complexes and the sequestration of Fe through the intercalation of the element in the interlayer of 2:1 clay minerals.

The analyses of the microbial community compositions at site A, B and C indicate that the dissolution of scorodite and the mobilization of Fe as Fe²⁺-species may have also been promoted by FeRB such as *Bacillus* and *Paenibacillus* (Li et al., 2020). The latter species are phenotypically and genotypically very diverse as well as widespread in the environment (Porwal et al., 2009; Grady et al., 2016), nevertheless, species of these genera are capable of Fe-reduction through the production of siderophores in Fe-limited conditions (Raza and Shen, 2010). Siderophores can be synthesized by *Bacillus subtilis* and members of the *Bacillus cereus* sensu lato group (Hertlein et al., 2014). These species were not detected in any tailings samples from this study, but the production of siderophores by many aerobic bacteria is common in order to allow the efficient transport of Fe through the cell wall (Neilands, 1981; Albrecht-Gary and Crumbliss, 1998).

In S-rich mine tailings environments, the diversity and activity of FeRB is not well-known as they are potentially competing with SRB for common electron donors (Praharaj &

Fortin, 2008). A bacterium detected at the CMC tailings capable of reducing Fe^{3+} under anaerobic conditions is *Rhodoferax ferrireducens* (Finneran et al., 2003). This bacterium occurs (most likely) under anaerobic conditions at D = 30 cm of site C as the corresponding tailings material has a low average valence of As and a high concentration of $\text{S}_{(\text{T})}$ (Fig. 3, Fig. 4). Hence, there is direct evidence for the FeRB-mediated mobilization of Fe within some tailings material of the CMC. The lack of FeRB abundance in the CMC tailings could be potentially due to the high abundance of FeOB, which rarely coexist with FeRB (Weiss et al., 2003; Roden et al., 2004; Haaijer et al., 2012).

Bacteria involved in N-cycling may also play a role in Fe reduction through a process termed *Feammox* (Sawayama, 2006). *Feammox* is the coupling of Fe reduction and anaerobic oxidation of ammonium (NH_4^+) which results in the production of N_2 (Luther et al. 1997), NO_3^- (Luther et al., 1997) or NO_2^- (Clément et al., 2005; Sawayama, 2006; Shrestha et al., 2009). This process is mediated either abiotically or through microbial activity (Yang et al., 2012). Soils that are highly weathered and contain nanocrystalline Fe-minerals have the potential to support *Feammox* (Yang et al., 2012). The production of N_2 , NO_3^- , or NO_2^- is dependent on the pH, with N_2 being produced over a wide pH range whereas the production of NO_3^- and NO_2^- occurs below a pH of 6.5 (Yang et al., 2012). Ammonium-oxidizing bacteria (e.g. *Nitrosospira* spp.) may play an important part in the *Feammox* process, as several species are involved in the uptake and transport of Fe (Prosser et al., 2013) and the synthesis of siderophores (Norton et al., 2008). However, many microorganisms responsible for this process are largely unknown as *Feammox* is a recently discovered metabolic pathway (Melton et al., 2014). Comparatively to the *Feammox* process, there are microbial communities involved in denitrification that are capable of N-reduction coupled to the oxidation of Fe and/or S (see above).

The microbially-mediated reduction of Fe^{3+} (by, for example, species from the *Bacillus*, *Nitrospira*, *Rhodoferrax*, and *Paenibacillus* genera) are limited to larger micrometer-size pore spaces within the tailings material whereas the observed mineral replacement reactions of scorodite by Co, Ni, Zn-arsenates and the potential complexation of Fe^{3+} by carbonate species could occur in micro- and nanopores (Courchesne et al., 2020). The contribution of the former biotic and the latter abiotic processes to the mobilization of Fe in the tailings material of the CMC is unclear and would require an Fe-isotope study on the Fe-phases in the upper tailings material (source of Fe) and the limonite precipitates at greater depth (location of the sequestration of Fe) (Courchesne et al., 2020).

7.4 Summary of microbes potentially involved in As-cycling for use in bioleaching of As-rich neutral-pH tailings

Overall, the microbial structure of the CMC tailings consists of predominantly Fe and S-cycling bacteria, which are tied together with N and C-cycling bacteria, along with the occurrence of many genera involved in the cycling of these elements (and nutrients) being either indirectly involved in the biogeochemical cycling of As (i.e. the use of $(\text{AsO}_4)^{2-}$ as a terminal electron acceptor) or those found in As (or other metal) contaminated sites. Most importantly, these microbial communities include, 1) those that are capable of Fe, S, and/or N-cycling (e.g. the genera *Gallionella*, *Thiobacillus* and *Nitrospira*, and the class Thermodesulfobionia); and 2) methanotrophic communities (e.g. *Methylocystis*, *Methylocapsa*, *Methylovirgula*). Furthermore, the occurrence of novel As-cycling bacteria within the characterized CMC tailings is likely present, due to the ~ 25 – 55 % uncharacterized Genera and > 85 % uncharacterized Species (Fig. 10 and Figure 4 in Appendix I). Many of the microbial communities in the CMC

tailings have As resistant genes, encoded by the *ars* gene, such as *Bacillus*, *Sphingomonas* and *Sulfuricella*, as well as additional previously unmentioned genera such as *Escherichia* and *Xylophilus* (Jackson et al., 2005). Additionally, the findings by Jackson et al. (2005) support the widespread occurrence of bacteria resistant to As in the environment, even within nearly pristine soils. Guan et al. (2017) also concluded that microbes are capable of building up a tolerance to As over time. It is therefore possible that 1) identified bacteria had an existing tolerance to As and 2) due to the tailings being nearly a century-old, the bacterial populations could have developed an As-tolerance, possibly due to horizontal gene-transfer (Guan et al., 2017).

Mineralogical effects on the microbial community: a summary

The most apparent and distinct change in mineralogy and microbial communities occur at site C where the transition from the reduced to oxidized zone between D = 30 and 25 is indicated by 1) a decrease in Co# and S#, and an increase in Fe#, Eh and As valence (Fig. 3, 4 and 5); and 2) increasing and decreasing proportion of arsenates and (sulf-)arsenides, arsenides and sulfides. This transition is also evident in the change in the microbial composition which depicts a decreasing abundance of S and As-reducing bacteria from D = 30 to D = 20cm.

At site B, the presence of more abundant arsenates to arsenides higher in the depth profile (i.e. above a depth of 20 cm) correlates well with a higher abundance of methanotrophic bacteria, whereas a relative higher proportion of arsenides lower in the profile (D < 20 cm) correlates with a higher abundance of FeOB and SOB (i.e. *Gaiella* and *Thiobacillus*). This large difference in the microbial community composition between the bottoms of sites B and C may explain the presence of a relatively sharp transition between the oxidized and reduced zone.

The material from site A was characterized by a very high Fe# and very low Co#, corresponding to the abundance of (sulf-)arsenides over arsenates. However, as we do not have quantitative average As valence data for site A, it is difficult to speculate the exact proportions of As-mineral phases (i.e. the abundance of arsenides versus arsenates). What we however do observe is the increasing methanotrophic bacteria with depth (i.e. *Methylocapsa* and *Methylovirgula*) as well as increasing FeOB and SOB bacteria with depth (i.e. *Sulfurifustis*). The methanotrophic bacteria were previously mentioned as having As⁵⁺ reducing capabilities, similar to species of *Sulfurifustis* which have been observed as coupling S-oxidation to As-reduction. Hence, the low proportion of FeRB and SRB at the bottom of site A may explain the absence of a well-developed reduced zone.

8 Conclusions

This multi-variate and multi-disciplinary study on the geochemical, mineralogical, and microbiological characteristics of the tailings at the CMC have provided an in-depth understanding of the tailings material in order to perform an effective and efficient bioleaching study (Chapter 2). This study added valuable biogeochemical knowledge to tailings systems characterized by neutral-to-alkaline mine drainage. The main findings from this chapter include:

- 1) Sites A and B in this study share a similar geochemistry and mineralogy to that observed by Courchesne et al. (2020);
- 2) Site C is geochemically and mineralogically dissimilar to sites A and B, as site C has distinct reduced and oxidized zones, as observed in more acidic mine tailings environments;

- 3) The mineral replacement reaction, as observed in Courchesne et al. (2020), of scorodite by Co-Ni-Zn arsenates does not appear to be dominantly microbially-mediated, therefore this reaction could be due to the potential complexation of Fe^{3+} -carbonate species in the micro- and nanopores;
- 4) The groupings observed of the Co# vs Fe# and S# between each site, correlates well with site-specific microbial groupings;
- 5) The abundance of microbial communities involved in cycling Fe, S, N and C correlate with depth, i.e. the occurrence of SRB at greater depths coincides with a low average valence of As;
- 6) The presence of FeOB and SOB at greater depths within the CMC tailings could be due to the presence of (sulf-)arsenides;
- 7) Samples at site B with low Co#'s and high Fe and/or S# tend to have a proportionally higher abundance FeOB or SOB, due to the abundance of (sulf-)arsenides, whereas at site C, a low Fe# and high Co and S#'s show a large abundance of (sulf-)arsenides, sulfides, and SRB;
- 8) At individual sites, high Co# do not correlate with a higher presence of potential As-cycling bacteria; and
- 9) The low abundance or absence of FeRB and SRB at the bottom of site A and B may explain the non-existence of a reduced zone.

Chapter Four: The bioleaching potential of Co from selected alkaline legacy mine tailings sites from the Cobalt Mining Camp, Ontario

9 Introduction

Over the past 60 years, bioleaching technology has been developed to harness biocatalysts within mine wastes using bacteria such as *Acidithiobacillus ferrooxidans* (Singh, 2016). Bioleaching is defined as the dissolution of metal-bearing phases from their mineral resources through controlled biological oxidation, reduction, and/or complexation processes (Bosecker, 1997; Rohwerder et al., 2003; Rawlings & Johnson, 2007; Konhauser, 2007; Mammadov et al., 2016). This technique is commonly employed as: a pre-treatment for refractory gold recovery, a recovery method for copper sulfide ores, and as a useful option in legacy mine site remediation (Singh, 2016). The microorganisms commonly used in bioleaching are acidophilic and/or thermophilic microbes because of their high tolerance to acidic conditions, metal(loid) concentrations, and extreme temperatures (Singh, 2016). Compared to traditional mining techniques, bioleaching can be considered a green method, since the utilized microorganisms occur naturally in the environment, and after further processing, the resulting waste product can be non-toxic and stable in the environment for disposal. Such methods for neutral-to-alkaline waste materials is however lacking in the current literature as the roles of neutrophilic metal-cycling microbes with respect to bioleaching systems is not well understood.

This chapter serves as a continuation of the information gained from Chapter 3's geochemical, mineralogical, and microbial characterization of the neutral-pH, As and Co-rich legacy mine tailings of the Cobalt mining camp (CMC). More specifically, this chapter will focus on the bioleaching potential of the tailings from the CMC, with the following objectives:

- (1) Design and conduct an oxidative (aerobic) and reductive (anaerobic) bioleaching experiment in two bacterial enrichments, a chemolithotroph- and heterotroph-enrichment, as well as a third control experiment;

- (2) Characterize the bulk microbial community present in each experiment method;
- (3) Compare and contrast the existing microbial communities with that seen in Chapter 3 as well as the differences and similarities existing between the different experiments; and
- (4) Determine whether the bioleaching experiments were successful and outline a potential bioleaching method for the tailings material at the CMC.

9.1 Background Information

9.1.1 Past Microbial Studies on the Farr and Mill Creek Wetlands in Cobalt, ON

The past microbial studies on sediments around the CMC is described in detail in Chapter

3. The main findings from these studies include:

- (1) Acid-producing oxidizing bacteria occurred in similar abundance as reducing bacteria, therefore implying oxic and anoxic conditions exist through the Farr Creek wetland (Kelly et al., 2007);
- (2) The abundance of sulfate and iron-reducing bacteria, and acid-producing bacteria varied with depth in cores from the Farr Creek wetland sediments (Kelly et al., 2007); and
- (3) In the Farr and Mill Creek wetlands, Kwong et al. (2007) observed that microbial sulfate reduction occurred locally, with potential As co-precipitation occurring as sulfides, such as framboidal pyrite.

In addition, studies were implemented to identify the change in As stability (Beauchemin and Kwong, 2007) and speciation (Kwong et al., 2007) with changing redox conditions. Kwong et al. (2007) concluded that the mobilization of As in the Farr and Mill Creek wetlands is due to:

1) the dissolution of As-bearing minerals, rather than from As-desorption from amorphous Fe-

phases; and 2) a change in redox conditions from reducing to oxidizing conditions. Beauchemin and Kwong (2007) conducted a redox experiment using tailings from various locations along Mill and Farr Creek. The redox experiment included the suspension of tailings in 10 mM KCl at a ratio of 1:10 at 23 °C for 30 days under anaerobic conditions (while monitoring dissolved metal concentrations); the tailings were then air-dried as a means of re-oxidation. The authors showed that the amount of dissolved As and P varied with and without different amendments. In the glucose-amended treatment there was a low dissolved P level, whereas the opposite was seen in the treatment without glucose, thereby suggesting that increased microbial activity consumed P, as a product of glucose input. In the tailings samples characterized by reducing conditions and without the addition of soluble C, there was an As speciation transformation to more soluble As^{3+} and an increase in dissolved As and P. When soluble C was added, dissolved P was consumed, due again to potential increased microbial activity, and solid As^{-1} phases formed. Additionally, when P was added at different concentrations, at a constant contact pH of 8, the authors identified a positive correlation with the amount of P added to the amount of dissolved As concentrations. Beauchemin and Kwong (2007) concluded that C rather than P was the limiting factor for both microbial reduction and As stabilization in the Farr and Mill Creek wetlands.

9.1.2 Microbial Communities Involved in As-cycling

Both chemolithotroph and chemoheterotroph bacteria play an essential role in the biogeochemical cycling of nutrients (and metals) in the environment. The main difference between these two groups are that they utilize different carbon sources. Chemolithotrophs use CO_2 as their carbon source (Konhauser, 2007) and gain energy from the oxidation of inorganic

electron donors (Schäfer, 2013), whereas chemoheterotrophs utilize reduced organic compounds as a source of energy and carbon (Amils, 2001).

In the environment, As reduction can occur through one of two methods, the first being through detoxification, which involves the cytoplasmic reduction of arsenate to arsenite (e.g. *Pseudomonas* (Macur et al., 2001) and *Herbaspirillum* (Govarthanan et al., 2015)), and the second known as dissimilatory reduction, where bacteria use arsenate as a terminal electron acceptor during respiration (Drewniak et al., 2015). Several dissimilatory arsenate-reducing bacteria (DARB) may: 1) reduce arsenate; 2) release As from adsorbed minerals (e.g. goethite); and 3) be involved in the formation of insoluble As-minerals and thereby contribute to As immobilization (Drewniak et al., 2015). Bacteria involved in As-reduction include, for example, *Shewanella* sp. O23S and *Aeromonas* sp. O23A, which are able to mobilize As from minerals such as arsenopyrite, löllingite, and scorodite (Drewniak et al., 2015).

Conversely, both heterotrophic and chemolithotrophic bacteria can oxidize As, as either a mode of detoxification (heterotrophs) or as a method of gaining energy (chemolithotrophs; Oremland and Stolz, 2005). Chemolithotrophs also have the ability to couple the oxidation of arsenite to the reduction of oxygen or nitrate (the latter under anaerobic conditions; Lièvremonet et al., 2009), and, for example, can include species of the genera *Nitrospira*, *Hydrogenophaga*, and *Nitrosospira* (Cavalca et al., 2019). Also, in neutral-pH conditions, neutrophilic FeOB (such as *Gallionella ferruginea*) and anaerobic nitrate-reducing/Fe-oxidizing bacteria contribute to As immobilization through the formation of solid As-bound Fe-minerals (Cavalca et al., 2019). Sulfur-cycling bacteria such as *Thiobacillus*, have also been suggested as playing a role in the oxidative dissolution of minerals such as Fe-As-S minerals (e.g. arsenopyrite; Cavalca et al., 2019). Furthermore, there are microorganisms that have both As-reduction and -oxidation

capabilities, for example *Dechloromonas*, with As-oxidation linked to chlorate-reduction (Suhadolnik et al., 2017), the chemolithotroph *Delftia* (Biswas et al., 2019), and *Ralstonia* (Battaglia-Brunet et al., 2006; Mondal et al., 2008).

9.1.3 Bioleaching of Arsenide or Arsenate-ores

Very recently, the first report of the microbial leaching of arsenidic ore, composed mainly of safflorite (CoAs_2), was presented by Giebner et al. (2019a, b). This study was conducted on a single piece of arsenidic ore from Bou Azzer district in Irthem, Morocco, under acidic conditions, using the acido- and thermophilic microorganisms *Acidithiobacillus ferrooxidans* and *Leptospirillum ferriphilum*. Prior to bioleaching, the ore was acidified by mixing with 3 M HCl and subsequently rinsed with water. This resulted in the enrichment of both As and Co, as well as Ni to be washed out. The conclusions presented by Giebner et al. (2019b) show that 1) Co yield was higher when in the presence of citric acid (maxima of 92 % recovery); and 2) the bioleaching of Co-arsenidic ore is possible under acidic conditions.

Comparatively, Drewniak et al. (2010) utilized several bacterial species involved in arsenite-oxidation, As-resistance and/or dissimilatory arsenate-reduction (i.e. *Sinorhizobium* sp. M14, *Aeromonas* sp. O23A, *Shewanella* sp. O23S, and *Pseudomonas* sp. OS8 and OS20) to study As mobilization from the Zloty Stok gold mine in south-west Poland. The experiments by Drewniak et al. (2010) were conducted under both anaerobic and aerobic conditions, with resulting high As yields. The authors identified that under aerobic conditions, the two *Pseudomonas* strains had the highest amount of released As after the 7-day incubation, whereas high amount of As was released from *Shewanella* sp. in the anaerobic experiments after the 21-

day incubation. Furthermore, they suggested that As-mobilization from arsenopyrite was accomplished through the action of the arsenite-oxidizer *Sinorhizobium* sp. M14.

10 Materials and Methods

10.1 Study Area, Sampling Methods and Storage

The study area, sampling and storage methods are the same as Chapter 3, and can be found in Section 5.1. The tailings sites, again, are referred to as sites A, B and C.

10.2 Bioleaching Experiment Setup

10.2.1 Initial Preparation

The minimal salts media (MSM) was prepared following the method from Santini et al. (2000), with minor revisions including: 1) the lack of use of the electron donor arsenite (NaAsO_2) and the trace element solution SL8; and 2) rather than the vitamin solution these authors used (as described by Macy et al., 1996), vitamin supplements from ATCC® were instead used (ATCC® MD-VS™). The ATCC® vitamin supplement has been used in a variety of growth media, such as in Mehanna et al. (2009) and Yazdi et al. (2019). A total of 12 L of MSM was prepared, for experiment start up and topping up as the experiment progressed. Deionized (DI) water was used for the control experiments.

Each of the 54 100 mL mason jars, MSM, and DI water were autoclaved at 121 °C for 15 minutes. The 54 serum bottles used for the anaerobic experiments were not autoclaved but were left in the anaerobic chamber for over 24 hours. Following sterilization, 0.01 M of Ca-nitrate ($\text{Ca}(\text{NO}_3)_2 \cdot 4\text{H}_2\text{O}$) and 0.01 M of Ca-lactate pentahydrate ($[\text{CH}_3\text{CH}(\text{OH})\text{COO}]_2\text{Ca} \cdot 5\text{H}_2\text{O}$) were dissolved in 100 mL of sterile DI water, filter sterilized then added to the chemolithotrophic and

heterotrophic growth media, respectively. The vitamin solution (at a 1 % final concentration) was subsequently added to each 1 L MSM solution. The final 1 L MSM solution was brought to a final contact pH of 8, by adding NaOH.

10.2.2 Aerobic and Anaerobic Experiment Setup and Incubation

Aerobic experiments were performed on the bench-top, maintaining sterile conditions, whereas anaerobic experiments were conducted in an anaerobic glove box (AGB). If plastic was brought into the AGB, there was a 12 – 24-hour wait time before any further experimentation. Two samples per site were used for the aerobic and anaerobic experiments (which were initially characterized by XRD and SEM analyses in Chapter 3), as well as one bulk sample (per tailings site) for a total of 9 samples. The bulk samples were prepared by homogenizing a subset of each sample, per site, and sub-setting a second time. Each of the 9 samples were duplicated for each of the three treatments (control, chemolithotroph- and heterotroph-enrichments) in both anaerobic and aerobic methods, for a total of 108 samples (54 aerobic, 54 anaerobic). Within each bottle were 7.5 g of tailings and 75 mL of MSM or DI water for a total bulk density of 10 %. The experimental schematic is shown in Figure 17. There were three rotations of thirty-six samples incubated and shaken in an Innova 4400 Incubator Shaker at any given time, each for two days, at an RPM of 150 and a constant temperature of 28 °C.

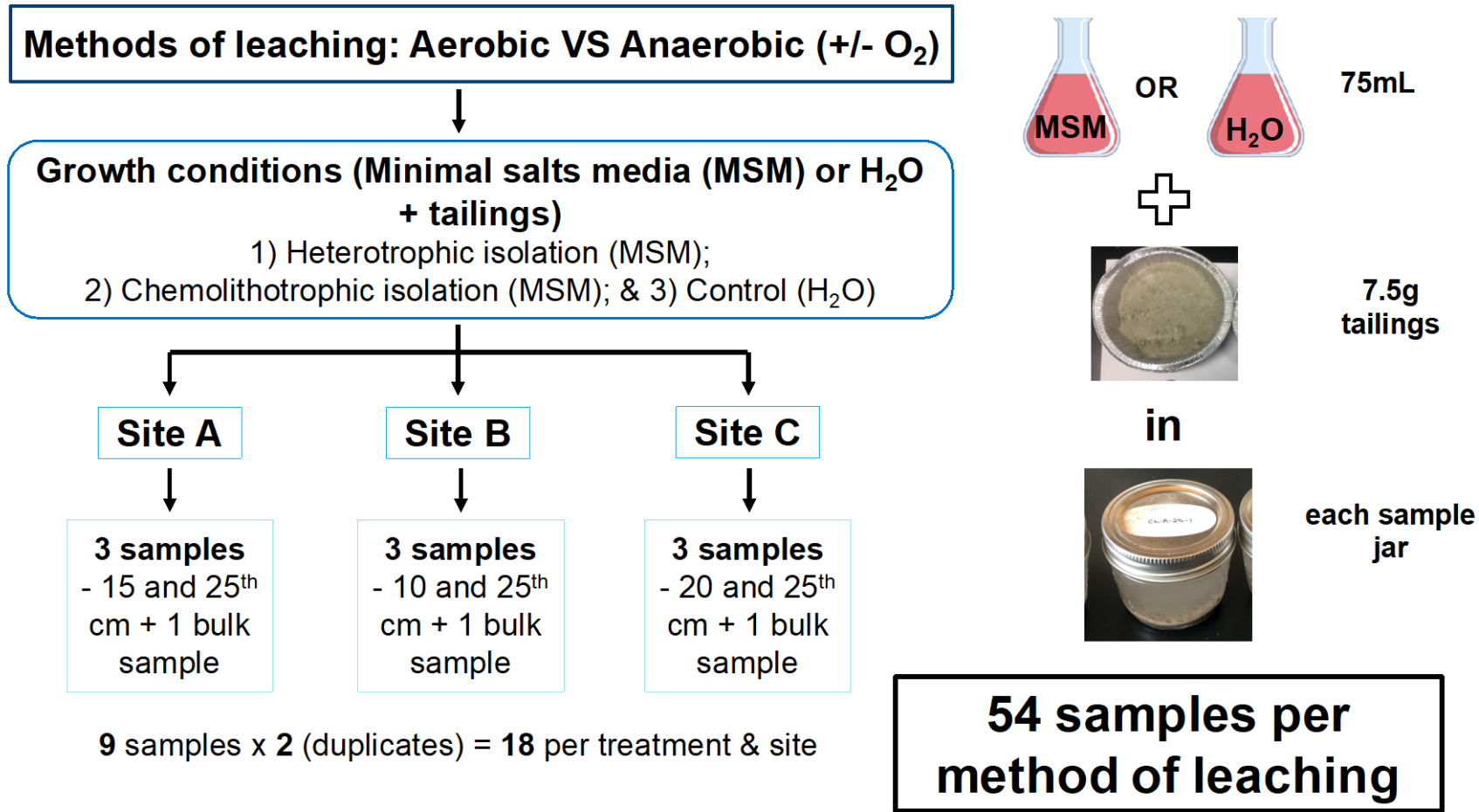


Figure 17. The bioleaching experiment schematic, showing two methods of leaching (aerobic or anaerobic) each of which in three growth conditions (control, heterotroph-enrichment, and chemolithotroph-enrichment).

10.3 Bi-weekly Analyses

10.3.1 Contact pH and ORP Measurements

Contact pH and ORP measurements were taken with an accumet® Tris Compatible Combination electrode using an accumet® AB150 pH/mV meter. The electrode was calibrated to a contact pH of 2, 4, 7 and 10 on each day of use, as well as an ORP value of 228 mV using Zobell's calibration solution. ORP was then converted to Eh by adding 200 mV (YSI Environmental, 2005). The accumet® electrode was only able to attain measurements of ORP relative to the pH value of each sample due to mechanical failure, therefore only the general trend of Eh (ORP converted) will be discussed. The Eh measurements taken over the 18-week experiment is shown in Appendix M.

10.3.2 Chemical Analysis

Every two weeks, 2.4 mL of liquid was extracted from each sample bottle, with 2.4 mL of sterile MSM or DI water added back in. Each extracted aliquot was divided in two for total and dissolved metal analyses. For dissolved metals, each sample was filtered through glass fiber filter papers with a 0.5 µm pore size. Samples were then diluted with DI water at a 1:2 ratio and brought down to a contact pH of 2, using 70 % nitric acid (HNO₃), and were then stored in a fridge to maintain a temperature of 4 °C. Chemical analysis of liquid samples were carried out at the Perdue Central Analytical Facility, Sudbury, Ontario. The internal standards Ru-101 and Re-185 were used for the corrections of drifts for the low to medium and heavy mass isotopes, respectively. Samples were diluted 100 times with 1 % HNO₃ (200 µL of liquid sample to 9.8 mL 1 % HNO₃). For quality assurances, a method blank, duplicate and a water trace elements certified reference material (NW-TMDA-64.3) was analyzed after every 15th sample. Please note

that the chemical composition of each site-specific bulk sample was not determined, therefore an average of each sample (per site) was used to calculate the percentage of Co and As recovered.

10.4 Experiment Shutdown and Sample Preservation

Two 1.5 mL microcentrifuge tubes were filled with liquid and tailings material for 16S rRNA analysis. All liquid was then taken out of each sample jar, disposed of, and the leftover tailings were dried at 80 °C for 2 days.

10.5 DNA Extraction and Computational Biology

The same 16S rRNA DNA extractions, PCR, and computational biology procedures employed for the original tailings samples (in Chapter 3, Section 5.8), was carried out on the 108 samples in the bioleaching experiments.

A table showing the raw sequence data information of all samples, including the total number of sequences, the percent of sequences that were filtered out, and the percent of sequences recovered, per sample, is provided in Table 1 and 2 of Appendix N. Post taxonomy assignment, six rarefaction curve graphs were generated (three for each treatment in the aerobic and anaerobic experiments), using the vegan package (Oksanen et al., 2019; see Fig. 1 of Appendix N).

10.6 Statistical Analysis

Statistical analyses were conducted using R with the identical statistical packages as explained in Chapter 3 (Section 5.10). However, only NMDS was implemented in this Chapter, the explanation of which can be found in Section 5.10 of Chapter 3.

11 Results

In the following results sections, the results from the 18-week aerobic and anaerobic bioleaching experiments will be discussed, in terms of the percent of Co and As recovered over the course of the experiments. Only the change in pH over time, the concentrations of total and dissolved Co and As released over time (Appendix O), and the cumulative percent of Co and As recovered will be explained, with the cumulative total and dissolved recovery percentages of Co and As, per biweekly analysis, in Tables 1 – 6 of Appendix P.

11.1 Trends of Contact pH

In the aerobic control (*C*) experiments, samples from site A have an increase in pH between weeks 0 to 4, while samples from site B and C have a slight decrease from week 0 to 2 (Fig. 18a). The pH remains relatively constant until week 16 and 18, where a decrease followed by an increase in pH occurs (Fig. 18a). The aerobic chemolithotroph-enrichment (*Ch*) experiments exhibit a large pH decrease at week 2, followed by either an increase for samples from site A from weeks 4 to 7, or stable pH values for samples from site B and C for the remainder of the 16 weeks (Fig. 18b). The pH values collected in the aerobic heterotroph-enrichment (*H*) experiments have a comparatively tight, constant range of pH values, with a slight fluctuation observed in site B's samples from week 2 to 6 (Fig. 18c).

Larger ranges of pH values are observed in the anaerobic experiments, with the anaerobic control (*AC*) experiments showing the largest variation (Fig. 18d). Within the *AC*-experiment site B and C's samples have a notable decrease in week 2 then remains relatively stable, whereas the samples from sites A have large fluctuates throughout the experiment, specifically those at weeks

2, 9, 11, 14 and 16 (Fig. 18d). The anaerobic chemolithotroph-enrichment (*ACh*) experiments have relatively consistent, stable pH values after an initial decrease at week 2, with slight decreases observed at weeks 11 and 16 (Fig. 18e). Both the *Ch* and *ACh*-experiments show that samples from sites A and C have the highest and lowest pH values throughout the 18-weeks, respectively (Fig. 18b, 18e). Finally, in the anaerobic heterotroph-enrichment (*AH*) experiments, there is an overall general decreasing trend from week 0 to 18, with site C's samples having relatively constant, high pH values, while site A and B samples fluctuate throughout the 18 weeks (Fig. 18f). Samples from site A show a large decreasing trend from week 0 to 4, followed by a gradual increase at weeks 7, 9 and 16, and decreases at weeks 11 and 14 and 18 (Fig. 18f). Comparatively, site B's samples exhibit a decrease in pH at week 4 to week 14, followed by an increase at week 16, and decrease at week 18 (Fig. 18f).

In general, the aerobic experiments are characterized as having a higher relative Eh value than the anaerobic experiments (Appendix M). The trend in relative Eh is inversely proportional to the trend of pH, i.e. a dip in pH is accounted for by a high relative Eh value; this is best visualized in the *Ch* and *ACh*-experiments (Fig. 1b, e in Appendix M).

11.2 Total and Dissolved Cobalt and Arsenic Concentration

The geochemical results from the 18-week bioleaching experiments are presented in Appendix O, with only the total and dissolved metal concentrations of Co and As being shown. All samples were analyzed for weeks 0, 9 and 18, with some having more samples analyzed; for example, those from site C, due to the tailings materials having the highest Co and As concentrations. The figures referred to in this section can be found in Appendix O.

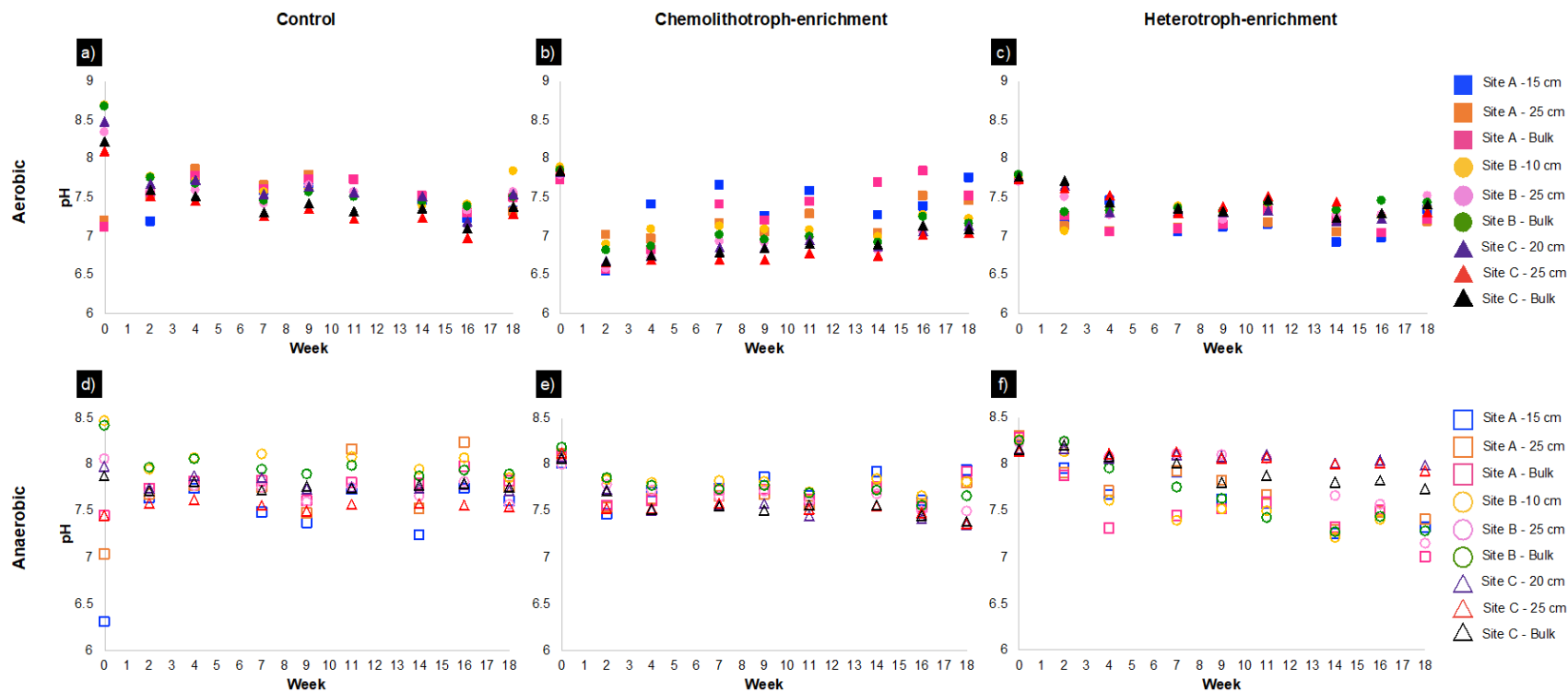


Figure 18. XY-plots showing the variation of pH within the 18-week experiments. The aerobic experiments are observed in a) – c) and the anaerobic experiments in d) – f).

In the control experiments, the amount of Co leached into solution was lower in the *C*-experiments (Fig. 1: 1), as compared to the *AC*-experiments (Fig. 1: 2; with the number after the colon denoting the column number). The opposite is observed for the amount of As released, with the exception of anaerobic samples from material from site A (Fig. 1: 2 and 1: 4). In both *C*- and *AC*-experiments, there are large fluctuations in the concentrations of As and Co. For example, Figure 1: 1 and 1: 2 exhibit large decreasing concentrations from week 0 to week 9, while Figure 1: 3b exhibits large increasing concentrations from week 0 to 9. In the *AC*-experiments specifically, the concentrations of Co and As are observed to increase (or remain fairly constant) between weeks 9 and 18 (Fig. 1: 2 and 1: 4). Also, there are notable sample-specific large dips in the concentrations of As in both *C*- and *AC*-experiments (Fig. 1: 3a, 3b and 1: 4c).

Higher concentrations of both Co and As are observed in the *Ch*-experiments, compared to the *ACh*-experiments (Fig. 2). Anomalously high As concentrations are observed in site A's 15th cm sample (Fig. 2: 3a). There is a (slight) increasing trend in the concentrations of Co and As leached over time in both *Ch*- and *ACh*-experiments, with this feature being more prominent in the aerobic, rather than anaerobic, method. Site C's samples during the *Ch*-experiment have the highest concentrations of Co and As released (Fig. 2: 1c and 2: 3c), while several of site C's samples during the *ACh*-experiments experience a large decrease from week 14 to week 18 (Fig. 2: 2c and 2: 4c).

Similar to the chemolithotroph-enrichments, the *H*-enrichments, rather than the *AH*-enrichments have higher concentrations of Co and As released during the experiments (Fig. 3). In the *H*- and *AH*-experiments, site A's 15th cm sample have anomalously high concentrations of Co and As (Fig. 1: 1a and 1: 3a). The material from site C have high concentrations of Co and As

in the *H*-experiments, with increases observed within the first 4 or 9 weeks (for Co and As, respectively), followed by slight decreasing concentrations at week 16 (Fig. 3: 1c and 3: 3c). The *AH*-experiments have comparatively low concentrations of Co and As released, with slight increasing trends in the release of Co or As observed (Fig. 3: 2 and 3: 4).

11.3 Percent Metal Recovery from Bioleaching Enrichment Experiments

11.3.1 Cobalt and Arsenic Recovery

The full table of total cumulative percent of Co and As released from each sample, can be found in Tables 1 – 6 in Appendix P (Co in Tables 1, 3, and 5 and As in Tables 2, 4 and 6), with the original concentrations of Co and As from each sample within Table 1 of Appendix G. In the control experiments, the highest % of Co and As released was observed in the anaerobic samples B – 10 (0.84 % total Co) and A – Bulk (2.39 % total As), respectively (Fig. 19), with 0.6 % Co and 1.78 % As from the aerobic samples A – Bulk and C - Bulk. The sample A – 15 from the chemolithotroph-enrichments had an anomalously high release of total Co and As (0.26 % Co and 9.66 % As) in the aerobic experiments (Fig. 20a). This same sample (A-15), in the *ACh*-enrichments, also had the highest % of total Co and As released, 0.119 % Co & 0.5 % As (Fig. 20d). Sample A – 15 however had a higher % of total Co and As released under aerobic conditions. Finally, in the heterotroph-enrichments, the aerobic C – 20 and A – 15 samples had the highest % of total Co and As released, 0.94 % Co and 30 % As (Fig. 21a, 21 c). While in the *AH*-enrichments, sample A - Bulk and B – Bulk had the highest % of total Co and As released, respectively (0.17 % Co and 1.57% total As).

The following conclusions can now be made, 1) sample A – 15 had high leaching efficiencies in the *Ch*-, *ACh*, and *H*-enrichments; 2) in the control experiments, samples under

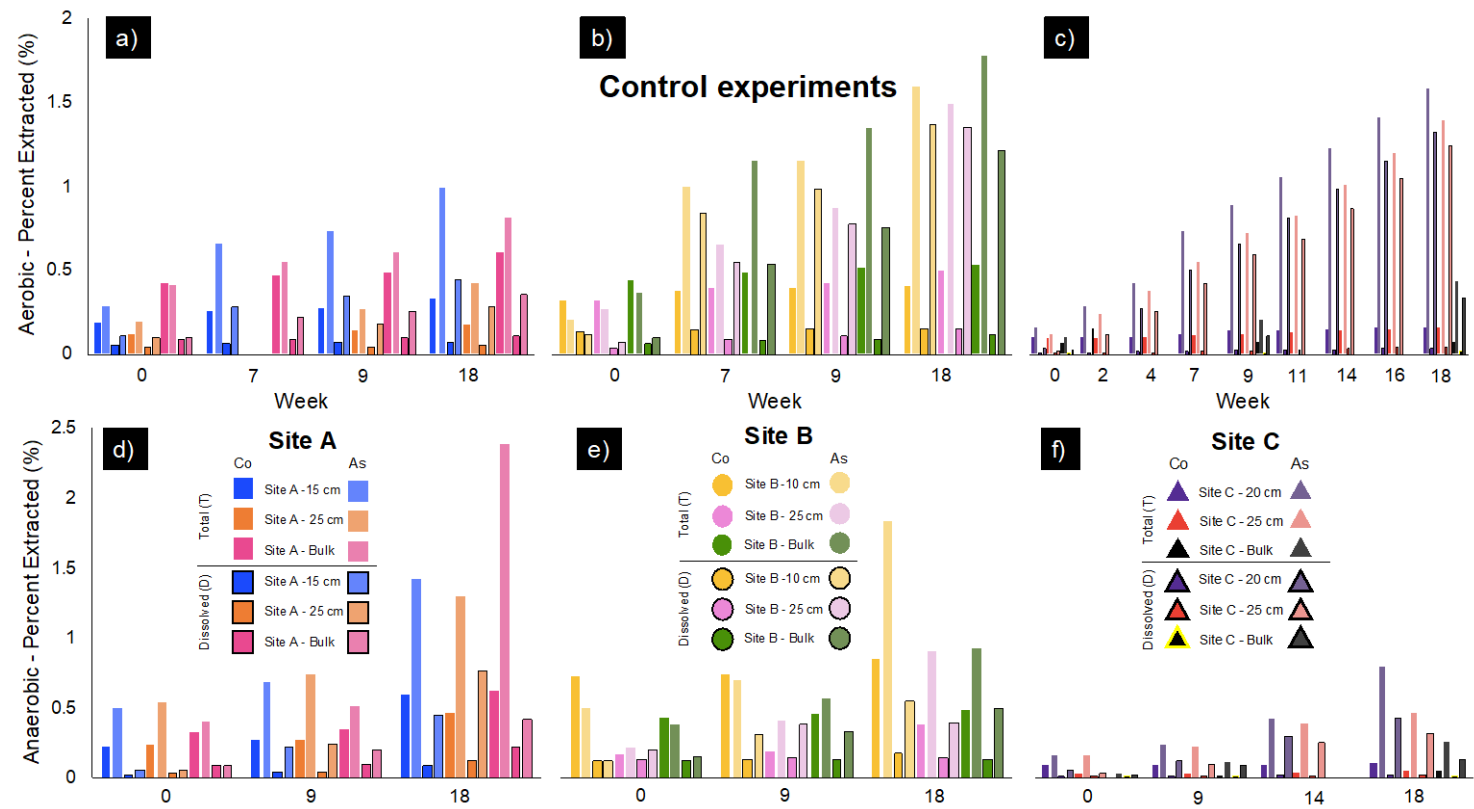


Figure 19. Six double-bar graphs illustrating the cumulative percent of total and dissolved Co and As released during the 18-week control bioleaching experiments. The aerobic experiments are shown in a) to c) and the anaerobic in d) to f).

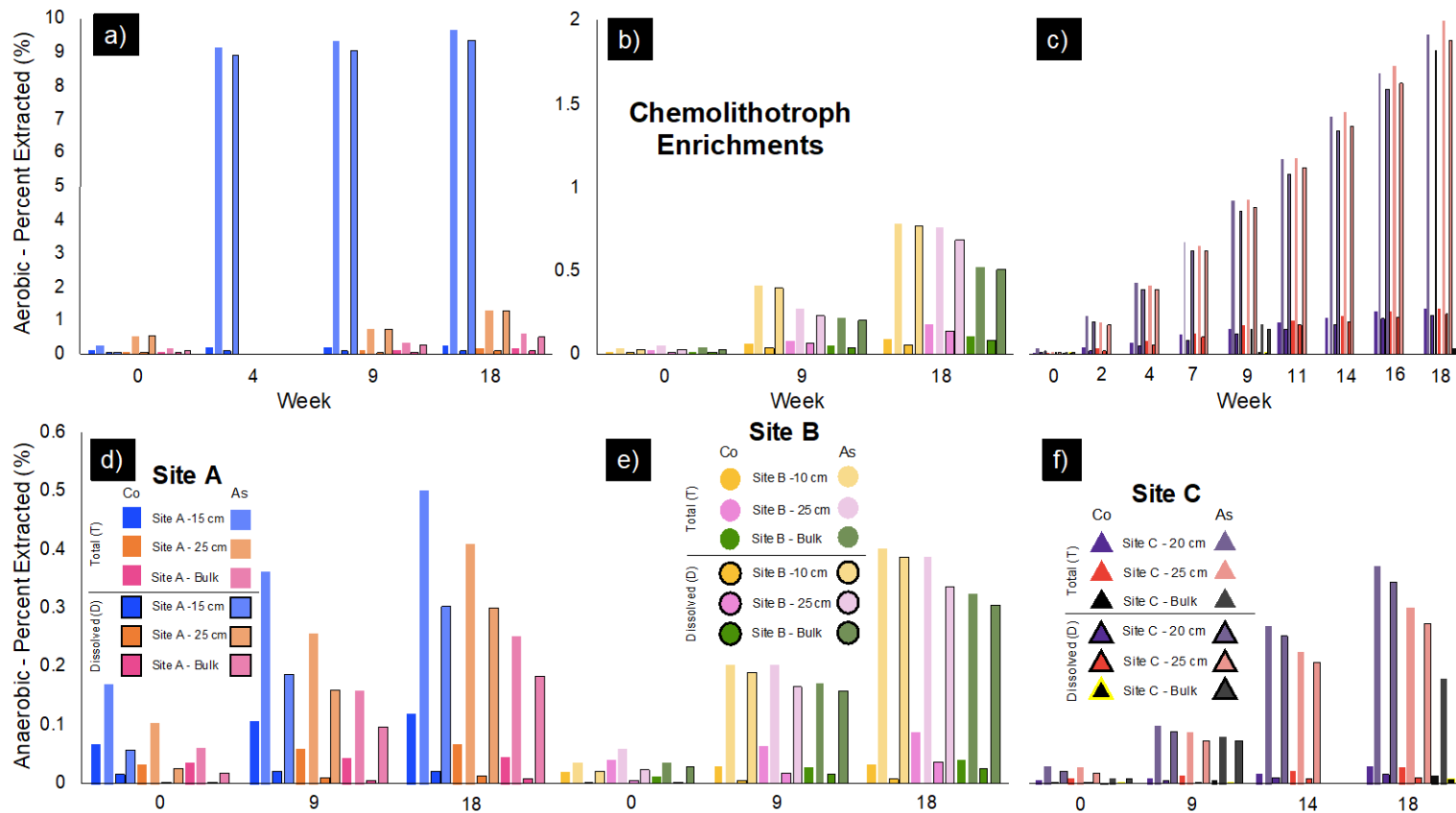


Figure 20. Six double-bar graphs showing the cumulative percent of total and dissolved Co and As released during the 18-week chemolithotroph-enrichment experiments. The aerobic experiments are shown in a) to c) and the anaerobic in d) to f).

anaerobic conditions were more efficient at leaching Co and As; 3) in both chemolithotroph- and heterotroph-enrichments, samples under aerobic conditions had the highest efficiencies; and 4) the heterotroph-enrichments had the total highest efficiency of releasing both Co and As.

11.4 Relation of As and Co concentrations to pH

In the bioleaching experiments, there was no pH increase or decrease larger than ~ 2 pH units. Nevertheless, the following may be observed with respect to the correlation of pH to the amount of As and Co in solution:

- 1) Positive correlation from weeks 9 to 18 in the *Ch*-experiments (Fig. 17),
- 2) Easily observable correlations between pH and the concentrations of As and Co in the *H*-experiments (e.g. week 4; Fig. 18 and Fig. 21),
- 3) In the highest leached sample from the *H*-experiments (A-15), there are easily observable correlations between pH and the amounts of As and Co (e.g. week 4; Fig. 18 and Fig. 21).
- 4) The *AH*-experiments have more subtle trends detected, i.e. a stable pH or decreasing pH causing slight increases in the concentration of As and Co (Fig. 18 and Fig. 21), and
- 5) No observable trends were seen in the control experiments.

11.5 Microbial Community Composition

In order to better characterize trends in the microbial data, the taxa that had a relative abundance of less than 2 % (or 0.5 % for Species-level description) were grouped together into a single category. Therefore, in the following sections, only those above a relative abundance > 2 % (or 0.5 % for Species) will be discussed. Additional taxonomic abundance graphs (Kingdom, Class, Family and Species) can be found in Appendix Q.

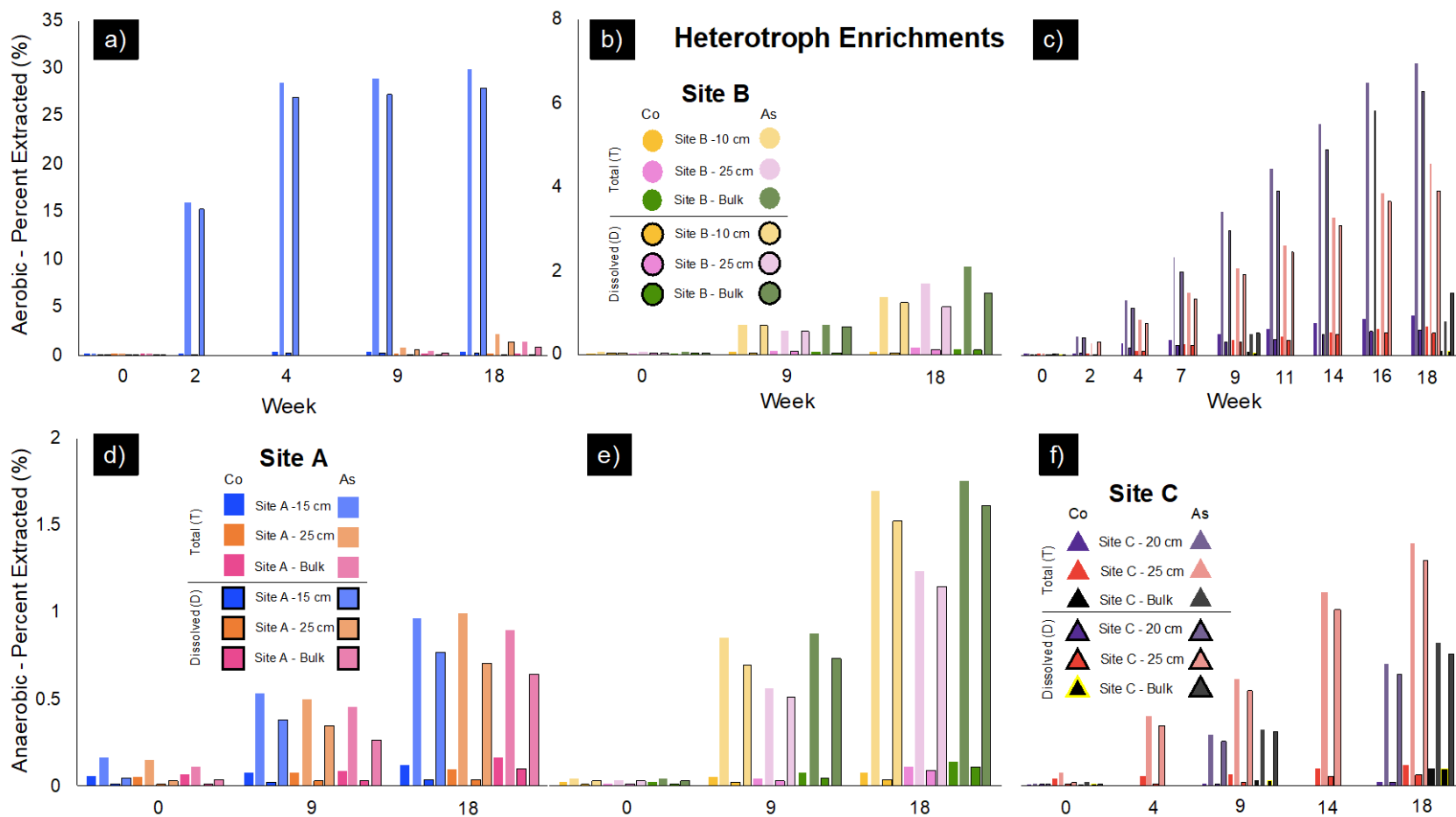


Figure 21. Six double-bar graphs showing the cumulative percent of total and dissolved Co and As released during the 18-week heterotroph-enrichment experiments. The aerobic experiments are shown in a) to c) and the anaerobic in d) to f).

11.5.1 Phylum-level Bulk Microbial Composition

Tailings material after bioleaching experiments consist mainly of the Proteobacteria (20 - 99 %), Acidobacteria (2 – 45 %), Bacteroidetes (2 - 48 %), Firmicutes (2 – 53 %), and Gemmatimonadetes (2 - 29 %), with lesser Chloroflexi (2 - 7 %) and Verrucomicrobia (2 - 7 %) (Fig. 22). In the *Ch*-experiments, there is a higher abundance of Bacteroidetes (5 - 48 %) *versus* more Acidobacteria (2 - 34 %) and Proteobacteria (20 – 87 %) in the *ACh*-experiments. The heterotrophic-enrichment experiments are not as diverse as the chemolithotrophic or control experiments. The *H*-experiments have less Firmicutes (2 - 18 %), and the occurrence of Bacteroidetes (2 - 13 %) and Acidobacteria (5 - 18 %), whereas the *AH*-experiments include Proteobacteria (47 - 99 %) and Firmicutes (2 - 53 %). Comparatively, the control experiments have the only occurrences of Actinobacteria (2 - 5 %), Armatimonadetes (9 %), Nanoarchaeota (2 %) and Rokubacteria (4 %), as well as less Acidobacteria (2 - 19 %) than the *Ch* and *ACh*-experiments and more than the *H* and *AH*-experiments. The aerobic, control (*C*) experiments have a higher abundance of Bacteroidetes (3 - 36 %) than that of the *AC*-experiments (2 - 11 %), the latter of which also has 2 – 5.5 % Gemmatimonadetes.

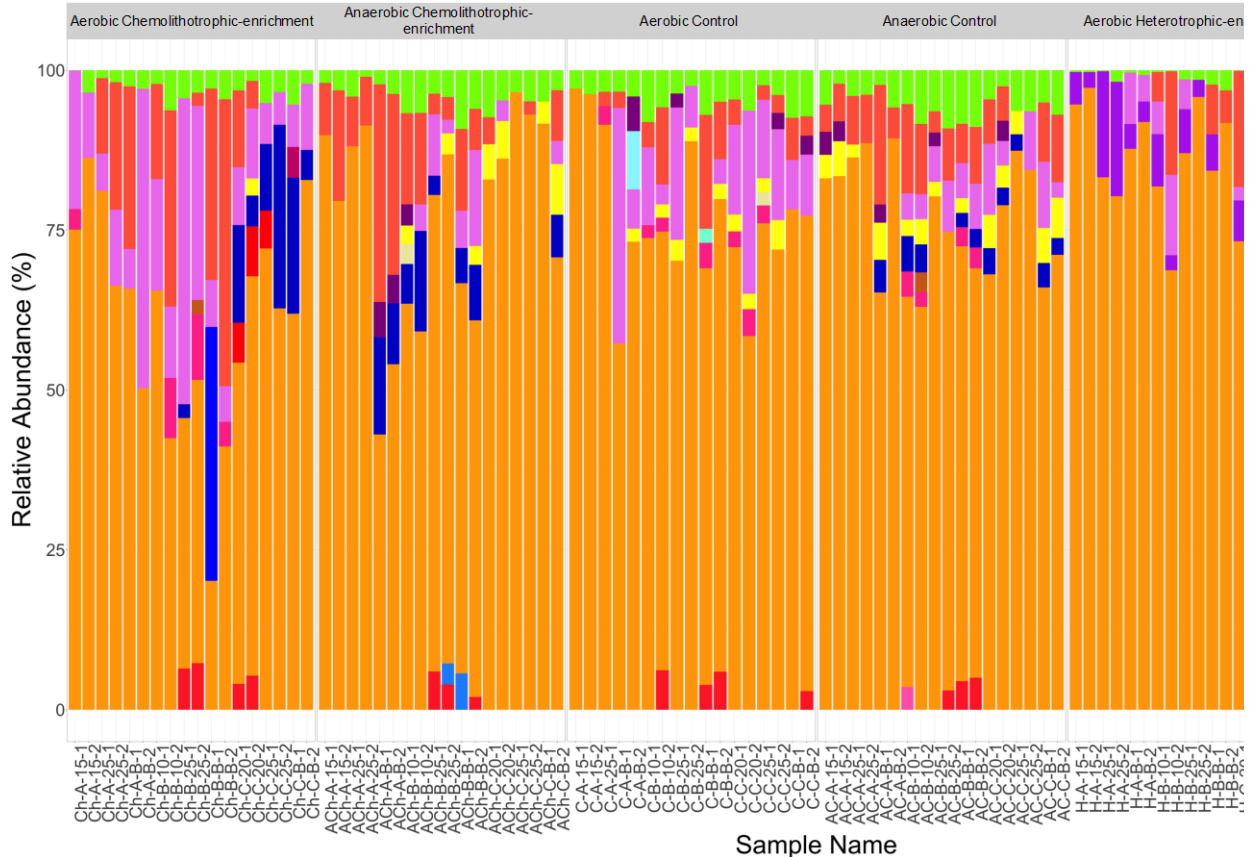


Figure 22. Normalized relative abundance taxonomic bar plot of the microbial communities after bioleaching experiments on the Phylum level.

11.5.2 Order-level Bulk Microbial Composition

Collectively, across all samples, Betaproteobacteriales, Pseudomonadales and Sphingomonadales are the three most dominant taxonomic orders identified. Within the *Ch*-experiments, Betaproteobacteriales (6 - 72 %), Chitinophagales (2 - 44 %), Acidobacteriales (11 - 43 %), Caulobacterales (2 - 37 %) and Pseudomonadales (2 - 46 %) have the highest relative abundance (Fig. 23). In the *ACh*-experiments, the dominant orders are site-specific; Sphingomonadales (13 - 72 %) in site A, Pseudomonadales (9 - 34 %) in site B, and Betaproteobacteriales (6 - 23 %) and Pseudomonadales (23 - 47 %) in site C. A large shift in dominant orders is observed in the *H*- and *AH*-experiments, with the majority of the *H*-samples characterized by a large abundance of Betaproteobacteriales (18 - 72 %), Pseudomonadales (6 -

57 %) and Xanthomonadales (2 - 32 %), and the *AH*-samples dominated by Pseudomonadales (22 - 97 %), Betaproteobacteriales (2 - 39 %) and Clostridiales (2 - 53 %) (Fig. 23). In both the *C* and *AC*-experiments, site A has a high abundance of Sphingomonadales (3 - 61 %; 2 - 57 %, respectively), with samples from sites B and C being more taxonomically diverse. The samples from sites B and C in the *C*-experiments have Betaproteobacteriales (12 - 40 %), Pseudomonadales (3.5 %), Chitinophagales (2 - 26 %), and much less Sphingomonadales (3 - 21 %) (Fig. 23). Compared to the *C*-experiments, the *AC*-experiments have a higher abundance of Betaproteobacteriales (10 - 65 %) and Acidiferrobacteriales (2 - 25 %), with minor Acidobacteriales, Immundisolibacteriales, Opitutales, and Gemmatimonadetes (Fig. 23).

11.5.3 Control Experiment Microbial Community Composition

Above a relative abundance of 4 %, the genera *Brevundimonas*, *Caenimonas*, *Ellin6055*, *Ellin6067*, *Limnobacter*, *Sphingomonas*, *Sphingorhabdus*, *Sulfurifustis*, *Thiobacillus* and *Xylophilus* (Fig. 24) are common to both *C* and *AC*-experiments, within the orders: Caulobacterales, Betaproteobacteriales, Sphingomonadales, and Acidiferrobacteriales (Fig. 23). The most abundant genera from the *C*-experiments include: *Bradyrhizobium* (8 – 11 %), *Brevundimonas* (23 %), *Caenimonas* (9-11 %), *Caulobacter* (11 – 23 %), *Ellin6055* (15 – 31 %), *Ellin6067* (13 %), *Lacibacter* (10 – 35 %), *Limnobacter* (10 %), *Sphingomonas* (24 %), *Sphingorhabdus* (10 – 40 %), and *Sulfurifustis* (9 %) (Fig. 24) within the orders Rhizobiales, Caulobacterales, Betaproteobacteriales, Sphingomonadales, Chitinophagales, and Acidiferrobacteriales (Fig. 23). Whereas within the *AC*-experiments, the most abundant genera

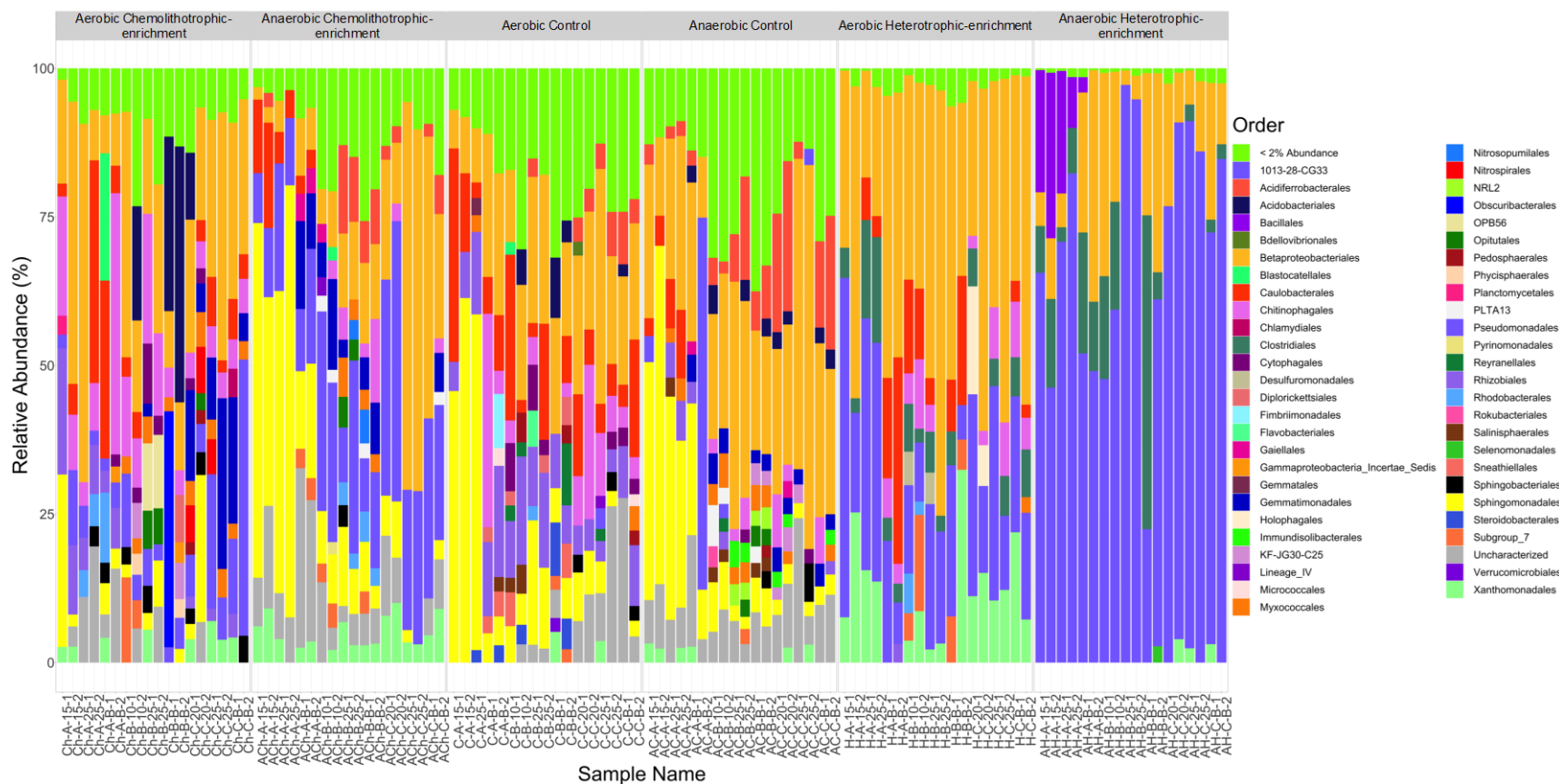


Figure 23. Normalized relative abundance taxonomic bar plot of the microbial communities after bioleaching experiments on the Order level.

consist of *Alterythrobacter* (12 – 14 %), *Brevundimonas* (8 – 11 %), *Caenimonas* (10 – 12 %), *Ellin6055* (16 – 17 %), *MNDI* (18%), *Pseudomonas* (one sample at 62 %), *Sphingomonas* (8 – 28 %), *Sphingorhabdus* (11 %), *Sulfurifustis* (9 – 25 %), *Terrimonas* (8 %) and *Thiobacillus* (9 – 45 %) (Fig. 24), of the Sphingomonadales, Caulobacterales, Betaproteobacterales, Pseudomonadales, Acidiferrobacterales, and Chitinophagales orders (Fig. 23). While

11.5.4 Chemolithotroph-enrichment Experiment Microbial Community Composition

The common genera above a relative abundance of 4 % in the *Ch* and *ACh*-experiments include *Brevundimonas*, *Lacunisphaera*, *Pseudomonas*, *Sphingomonas* and *Terrimonas*, of the orders Caulobacterales, Opitutales, Pseudomonadales, Sphingomonadales, and Chitinophagales. The genera *Bradyrhizobium* (8.5 %), *Brevundimonas* (28 – 35 %), *Caenimonas* (15 %), *Delftia* (14 %), *Herbaspirillum* (9 – 11 %), *Lacibacter* (9.5 %), *Limnohabitans* (9 – 29 %), *Pseudomonas* (12 – 46 %), *Ralstonia* (16 – 54 %), *Sphingomonas* (21 %), *Sphingopyxis* (29 %), and *Terrimonas* (8 – 17 %) are the most abundant in the *Ch*-experiments (Fig. 24), within the orders Rhizobiales, Caulobacterales, Betaproteobacterales, Chitinophagales, Pseudomonadales, and Sphingomonadales (Fig. 23). With the most abundant genera in the *ACh*-experiments including: *Brevundimonas* (12 – 18 %), *Dechloromonas* (15 %), *Ellin6055* (21 – 70 %), *Limnobacter* (10 – 51 %), *Luteimonas* (8 %), *Pseudomonas* (8 – 36 %), *Sphingomonas* (8 – 13 %), *Sulfurifustis* (9 – 15 %), *Terrimonas* (14 %), and *Thiobacillus* (8 – 10 %) (Fig. 24), of the Caulobacterales, Betaproteobacterales, Sphingomonadales, Xanthomonadales, Pseudomonadales, Acidiferrobacterales and Chitinophagales orders (Fig. 23).

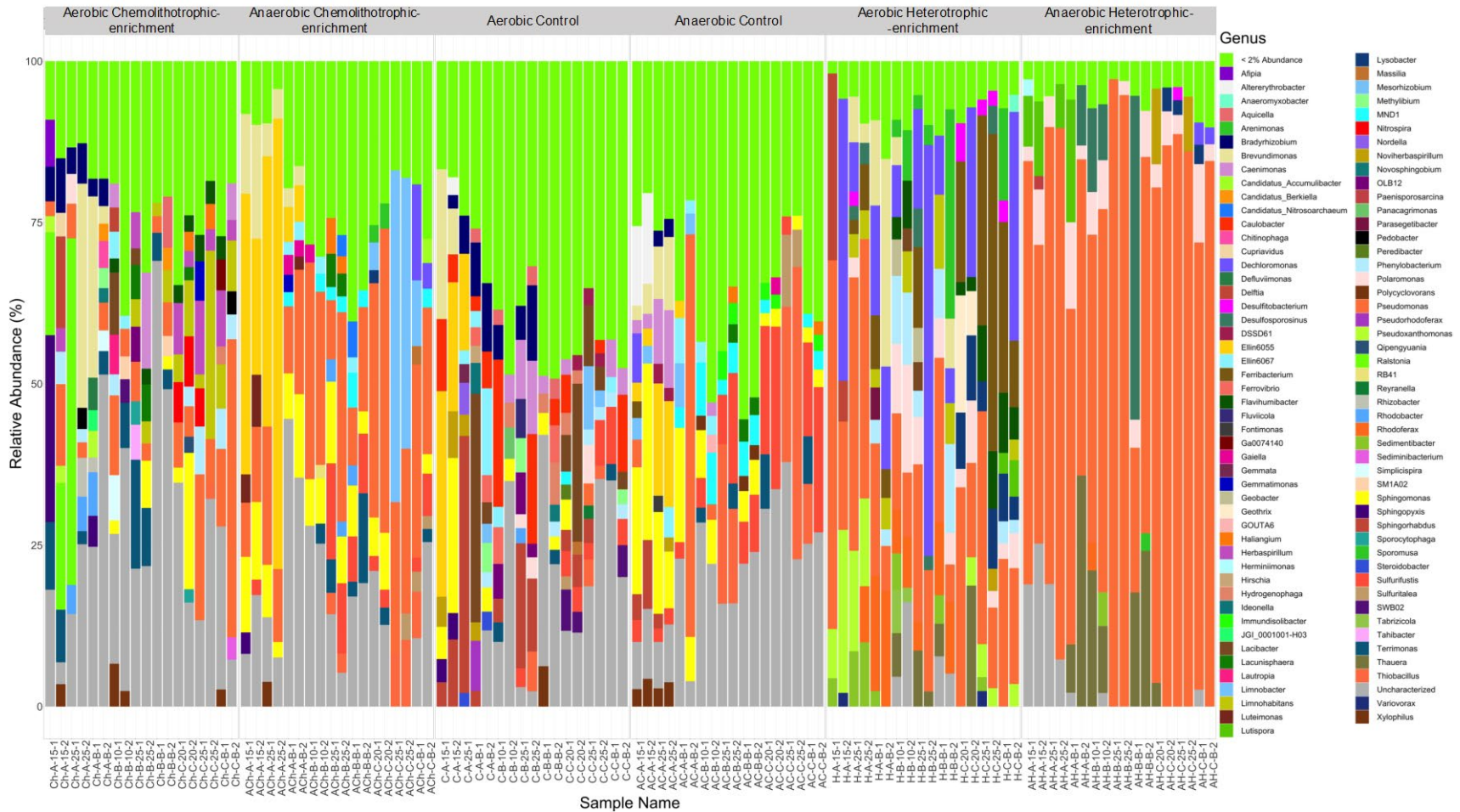


Figure 24. Normalized relative abundance taxonomic bar plot of the microbial communities after bioleaching experiments on the Genus level.

11.5.5 Heterotroph-enrichment Experiment Microbial Community Composition

The *H*-experiments include the genera: *Arenimonas* (14 – 32 %), *Brevundimonas* (13 – 32 %), *Dechloromonas* (8 – 64 %), *Delftia* (29 %), *Ferribacterium* (8 – 49 %), *Flavihumibacter* (~ 9 %), *Geothrix* (18 %), *Limnohabitans* (11.5 %), *Lysobacter* (9 – 10 %), *Phenylobacterium* (10.5 – 14 %), *Polaromonas* (10 – 17 %), *Pseudomonas* (10 – 57 %), *Pseudoxanthomonas* (14 – 25 %), *Rhodoferax* (9 – 18 %), *Sedimentibacter* (8.5 – 10 %), and *Thauera* (9 – 19 %) genera (Fig. 24), from the Xanthomonadales, Caulobacterales, Betaproteobacteriales, Chitinophagales, Holophagales, Pseudomonadales, and Clostridiales orders (Fig. 23). The microbial diversity of the *AH*-experiments are much less diverse than the *H*-experiments, with only 6 genera with a relative abundance over 8 %, including: *Desulfosporosinus* (9 – 50 %), *Lutispora* (7 – 19 %), *Noviherbaspirillum* (8 – 12 %), *Polaromonas* (5 – 13 %), *Pseudomonas* (22 – 97 %), and *Thauera* (7.5 – 36 %) (Fig. 24), from the Clostridiales, Betaproteobacteriales, and Pseudomonadales orders (Fig. 23). These genera are all common to the *H*-experiments, with the exclusion of *Noviherbaspirillum* (Fig. 24).

11.5.6 Diversity of As, S, Fe and N-cycling Microbial Communities Between Enrichments

Due to the fact that we are primarily interested in microbial communities that have been identified as playing a role in the biogeochemical cycling of As, only these communities (i.e. As, Fe, S and N-cycling communities) will be discussed, at a relative abundance of > 8%.

11.5.6.1 Control Experiments

Within the control experiments, the As (\pm S)-cycling genera dominate over those that have a role in Fe and/or N-cycling. The C-experiments only contain two genera, *Brevundimonas* and *Sphingomonas* (in two samples, 23 – 24 %), that have As-cycling capabilities. The AC-experiments are comparatively dominated by the As-cycling *Alterythrobacter*, *Brevundimonas*, *MND1*, *Pseudomonas*, and *Sphingomonas* genera (8 – 62 % total relative abundance) (Fig. 24). The genus *Pseudomonas* contains species identified as As-reducing bacteria (AsRB), Fe-reducing bacteria (FeRB) and nitrate-reducing bacteria (NRB), and, occurs in the highest abundance of 62 % in the AC-experiment sample AC-A-Bulk-2 (Fig. 24). Contrarily, the C-experiments have a higher abundance of strictly S-oxidizing bacteria (SOB; *Brevundimonas*, *Caenimonas*, and *Limnobacter*, 9 – 23 %), when compared to the AC-experiments (*Brevundimonas* and *Thiobacillus*, 8 – 11 %) (Fig. 24). The C-experiments have a lower abundance of bacteria able to cycle Fe, S and N, *Lacibacter* and *Sulfurifustis* (9 – 35 %; Fe- and/or S-cyclers), and *Bradyrhizobium*, *Caenimonas*, and *Ellin6067* (8 – 13 %; S- and N-cyclers), when compared to the AC-experiments, *Caenimonas* and *Sulfurifustis* (9 – 25 %; Fe and S-cycling), and *Caenimonas*, *Pseudomonas*, and *Terrimonas* (8 – 62 %, N-cycling) (Fig. 24).

11.5.6.2 Chemolithotroph-enrichments

The chemolithotroph-experiments microbial communities are dominated by As- and S-cycling bacteria, similar to the control experiments. However, contrary to the control experiments, there are multiple occurrences of genera that are known to be strictly As-oxidizing and/or -reducing bacteria (namely *Delftia* and *Dechloromonas*, occurring in the Ch and ACh-experiments, respectively). The Ch-experiments have the occurrence of 9 – 54 % of the genera

Delftia, *Herbaspirillum*, *Pseudomonas*, *Ralstonia*, *Sphingomonas*, and *Sphingopyxis*, whereas the *ACh*-experiments have *Brevundimonas*, *Dechloromonas*, *Luteimonas*, *Pseudomonas*, *Sphingomonas*, *Sulfurifustis* and *Thiobacillus* (8 – 36 %), in terms of their As-cycling bacteria (Fig. 24). The chemolithotroph-experiments have a higher relative abundance of SOB genera than the control experiments (9 – 51 %), namely *Brevundimonas*, *Caenimonas* and *Limnohabitans* (in the *Ch*-experiments) and *Brevundimonas* and *Limnobacter* (in *ACh*-experiments; Fig. 24). Additionally, there are abundant microbes that are involved in N-cycling, 8 – 46 % in the *Ch*-experiments and 8 – 36 % in the *ACh*-experiments. The N-cycling bacteria genera within the *Ch*-experiments include: *Brevundimonas*, *Caenimonas* and *Limnohabitans* (in the *Ch*-experiments), and *Dechloromonas*, *Luteimonas*, *Pseudomonas*, and *Terrimonas* within the *ACh*-experiments (Fig. 24). Finally, both *Ch*- and *ACh*-experiments have isolated Fe- and S-oxidizing genera, the Fe- and S-reducing genus *Lacibacter* in the *Ch*-experiments, and *Sulfurifustis* and *Thiobacillus* in *ACh*-experiments (Fig. 24).

11.5.6.3 Heterotroph-enrichments

Lastly are the heterotroph-enrichment experiments, which also have strictly As-cycling microbes under both anaerobic and aerobic conditions, specifically *Dechloromonas* and *Delftia* (8 – 64 %) in *H*-experiments, and *Desulfosporosinus* (9 – 50 %) in *AH*-experiments (Fig. 24). Similar to *Pseudomonas*, *Desulfosporosinus* sp. can also be involved in As, Fe, S, and N-cycling, more specifically in their reduction. Other identified microbial genera involved in the biogeochemical cycling of As include: *Brevundimonas*, *Ferribacterium*, *Polaromonas*, *Pseudomonas*, *Pseudoxanthomonas*, and *Thauera* (8 – 57%) and *Noviherbaspirillum*, *Polaromonas*, *Pseudomonas*, and *Thauera* (8 – 97 %), in the *H*- and *AH*-experiments,

respectively (Fig. 24). Sulfur-cycling microbes in the *H*-experiments include *Brevundimonas* and *Limnohabitans* (Fig. 24), with no strict SOB or SRB identified in the *AH*-experiments. The *H*-experiments contain a lower abundance of N-cycling bacteria than the *AH*-experiments, with *Thauera*, a bacteria genus involved in denitrification, being common to both (Fig. 24). In the *H*-experiments, *Limnohabitans*, *Lysobacter*, *Polaromonas*, *Pseudomonas*, *Pseudoxanthomonas* and *Thauera* (9 – 57%) are involved in N-cycling, with *Desulfosporosinus*, *Noviherbaspirillum*, *Polaromonas*, *Pseudomonas* and *Thauera* (8 – 97 %) in the *AH*-experiments (Fig. 24).

11.5.6.4 Arsenic-cycling Populations

There are lesser abundant As-oxidizing bacteria (AsOB), e.g. *Herminiimonas* (2.5 %), *Hydrogenophaga* (2 – 7 %), *Noviherbaspirillum* (2 – 12 %), *Simplicispira* (3 – 7 %), and *Variovorax* (~ 2 %). The AsOB population tends to be treatment-specific, with the exception however of *Noviherbaspirillum* occurring in *H*-, *AH*-, *C*-, and *AC*-experiments, which is more predominant in the *AH*-experiments, where the highest relative abundance of AsOB occurs (i.e. *Noviherbaspirillum*).

The AsRB population is much more diverse and widespread, with some genera isolated to one treatment method (e.g. *Desulfitobacterium*, which only occurs in the heterotrophic experiments), and others spanning multiple experiments, for example, *Pseudomonas*, which occurs in all treatments/enrichments. The AsRB-population consists of: *Afipia*, *Altererythrobacter*, *Anaeromyxobacter*, *Brevundimonas*, *Cupriavidus*, *Desulfitobacterium*, *Ferribacterium*, *Geobacter*, *Herbaspirillum*, *Lacibacter*, *Massilia*, *Mesorhizobium*, *Methylibium*, *Pedobacter*, *Polaromonas*, *Pseudomonas*, *Pseudoxanthomonas*, *Rhodobacter*, *Sphingomonas*, *Sphingopyxis*, *Sporomusa*, and *Sulfuritalea*. In decreasing AsRB-population abundance are the

heterotroph-enrichments (average = 21 % ± 24 %), followed by the chemolithotroph-enrichments (average = 11 ± 11 %), and the control experiments (average = 8.4 % ± 10 %).

Additionally, there are genera that are capable of both As-reduction and As-oxidation, including *Delftia*, *Dechloromonas*, and *Ralstonia*. The heterotrophic experiments have the highest relative abundance of microorganisms that can perform both (*Dechloromonas* and *Delftia*, 5 – 63 %), followed by the chemolithotroph-enrichments (*Delftia* and *Ralstonia*, 4 – 53 %), and the control experiments (*Dechloromonas*, 7.5 %).

11.5.7 Identified Species in the Bioleaching Experiments

On average, the aerobic experiments have a lower relative abundance of uncharacterized species, and are more diverse as only 9 of the characterized species are not found within the aerobic experiments (*Lacunisphaera anatis*, *Herminiimonas aquatilis*, *Hydrogenophaga atypica*, *Immundisolibacter cernigliae*, *Arenimonas daechungensis*, *Sphingomonas flava*, *Paenisporosarcina quisquillarium*, *Peredibacter starrii*, *Methylobacter tundripaludum*) and therefore only in the anaerobic experiments (Fig. 4 in Appendix Q). Within the aerobic experiments, there were several species specific to each treatment method. The C-experiments were the only samples to have: *Caulobacter daechungensis*, *Steroidobacter flavus*, *Caulobacter fusiformis*, *Ramlibacter ginsenosidimutans*, *Hydrogenophaga palleronii*, and *Sphingosaurantiacus polygranulatus* identified (Fig. 4 in Appendix Q). The Ch-experiments were the only samples to have: *Hydrogenophaga atypica*, *Lacunisphaera limnophila*, *Terrimonas lutea*, *Pedobacter luteus*, *Cupriavidus pauculus*, *Caulobacter profundus* and *Sediminibacterium salmoneum* identified, and the H-experiments were the only samples to have: *Tabrizicola aquatica*, *Flavobacterium buctense*, *Rhodoferax ferrireducens*, *Desulfosporosinus hippei*,

Ferribacterium limneticum, *Parasegetibacter luojensis*, *Arenimonas metalli*, *Phenylobacterium muchangponense*, and *Sphingomonas soli* characterized.

The species that were confidently identified in the anaerobic tailings experiments were less diverse than the aerobic experiments. These identified species, above an abundance of 0.5 %, include the following, with the treatment or enrichment name code in brackets meaning that this species was only identified in that specific treatment or enrichment: *Lacunisphaera anatis* (ACh), *Arenimonas aquatica*, *Herminiimonas aquatilis* (AC), *Immundisolibacter cernigliae* (AC), *Sphingomonas daechungensis* (ACh), *Rhodoferax ferrireducens* (AH), *Sphingomonas flava* (AC), *Ramlibacter ginsenosidimutans* (AC), *Desulfosporosinus hippie* (AH), *Ferribacterium limneticum*, *Lacunisphaera limnophila*, *Noviherbaspirillum massiliense*, *Methylibium petroleophilum*, *Paenisporsarcina quisquiliarum* (AH), *Flaviumibacter sediminis* (AC), *Peredibacter starrii* (AC), *Limnobacter thiooxidans*, and *Methylobacter tundripaludum* (AC).

The species *Rhodoferax ferrireducens*, *Ramlibacter ginsenosidimutans*, *Desulfosporosinus hippei*, *Ferribacterium limneticum*, *Noviherbaspirillum massiliense*, *Methylibium petroleophilum*, *Flaviumibacter sediminis* and *Limnobacter thiooxidans* were common to both anaerobic and aerobic experiments (Fig. 4 in Appendix Q).

The above genera can be grouped into the following categories: 1) water and soil-dwellers; 2) bacteria capable of degrading carbon compounds; 3) Fe, As and S-cycling microbes (mainly reducers); and 4) lesser methano- and methylotrophs. The species potentially involved in As-cycling consist of: *R. ferrireducens*, *S. flava*, *V. paradoxus*, *M. petroleophilum*, and *S. soli*.

11.5.8 Comparison of the Background Microbial Community to the Enriched Microbial Communities

Within the next section, the background microbial community as identified in Chapter 3 will be compared and contrasted to that seen in the bioleaching experiments conducted to enhance the growth of different bacterial communities.

At the Phylum level, similar to that of the background microbial community (Fig. 8), all communities from the bioleaching experiments are dominated by Proteobacteria (Fig. 22). On the Order level, however, dissimilarities are better visualized. In the background community, the dominant orders are Betaproteobacteriales and Rhizobiales ± Sphingomonadales and Acidiferrobacterales (Fig. 9). Within the community enrichments there is still a high abundance of Betaproteobacteriales and Sphingomonadales (in the *C*-, *ACh*-, *AC*-experiments), however the sometimes high occurrence of the order Pseudomonadales appears with lesser Rhizobiales mainly occurring within the unenriched, *C*-experiments (Fig. 23). Moreover, the communities observed after the experiments, are recognized as being more taxonomically diverse than the background communities.

On the Genus level, there are many observations that can be made (Fig. 24):

- 1) The abundance of lake- and soil-dwelling organisms not observed in the background communities (e.g. *A. aquatica*, *T. aquaticus*, and *H. aquatilis*);
- 2) The high abundance of the new (to the background community) genus *Pseudomonas*, the occurrence of which is most abundant in the *AH*-experiments;
- 3) The previous high abundance of methano- and methylotrophic communities observed are comparatively lacking in the experiment communities;
- 4) In the microbial community identified after the leaching experiments, out of the 97 genera, only 12 occur within the original tailings material, which all either occurred in the control experiments or chemolithotroph-enrichments;

- 5) There was an increase in the relative abundances of: 1) the thiosulfate-oxidizing genera, *Limnobacter*; and 2) *Sphingomonas* genera;
- 6) Proportionally, there are much higher abundances of Fe, S, As, and N-cycling bacteria, due primarily to the occurrence of *Pseudomonas*, however, there are also high occurrences of the thiosulfate-oxidizing *Limnobacter* (10 – 51 % in the ACh-experiments);
- 7) Many FeRB were found in greater diversity and abundance (i.e. *Ferribacterium*, *Geothrix*, *Desulfitobacterium*, *Desulfosporosinus*, *Lactibacter*, and *Pedobacter*), along with the previously identified *Rhodoferax ferrireducens*;
- 8) The presence of new As-cycling bacteria emerge in the microbial communities after the experiments (e.g. the new occurrences of *Brevundimonas*, *Dechloromonas*, *Delftia*, and *Desulfosporosinus*); and
- 9) There are also a lesser amount of Uncharacterized genera and species observed here.

11.6 Multivariate Statistical Analysis

11.6.1 Non-metric Multidimensional Scaling Analysis

Non-metric multidimensional scaling (NMDS) plot of the microbial community structure of all six different experimental methods shown in Fig. 25. As previously noted, the closer two points are together, the similar is there microbial composition; the inverse is also true. A stress value produced for an NMDS plot which is less than 0.2 is considered to be good, as it means that the ordination distances (and therefore the axes from which they are derived) explains 80 % of the variability in the data. Hence, the lower the stress value, the higher our confidence is in

capturing the major patterns in the data. The circles on the NMDS plot correspond to 95 % confidence intervals.

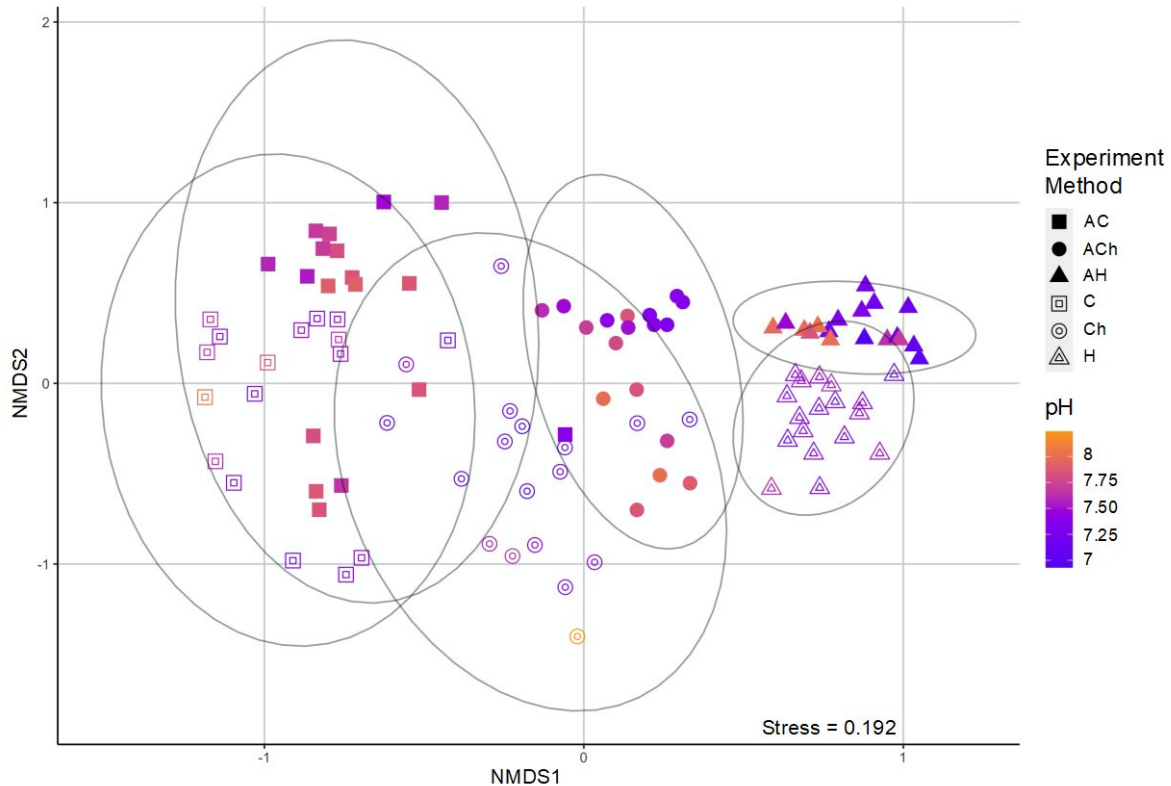


Figure 25. NMDS plot showing the similarities and differences in the microbial communities per six bioleaching experiments.

The microbial community composition within the *C*- and *AC*-experiments are very similar to each other, with their diversity distribution across both the NMDS1 and NMDS2 axes. Both the *C*- and *AC*-experiments have a moderately similar microbial composition to the *Ch*-experiments (shown by overlapping 95 % confidence intervals), whereas the microbial community composition of the *Ch*-experiments is fairly similar to only the *ACh*-experiments. Furthermore, the microbial diversity of the *Ch*- and *ACh*-experiments are seen to change dominantly across the NMDS2 axes. In contrast, the *H*- and *AH*-experiments are similar to each other and more similar to the *Ch*- and *ACh*-experiments, than the *C*- and *AC*-experiments.

Moreover, the microbial diversity of the *H*- and *AH*-experiments are distributed across different NMDS axes, the *H*-experiments strongly distributed across both axes, and the *AH*-experiments across the NMDS1 axes. The confidence intervals for the *H*- and *AH*-experiments are also much smaller than the *Ch*-, *C*-, *ACh*-, and *AC*-experiments.

12 Discussion

12.1 Contact pH as Related to the Concentration Fluctuations of As and Co

As observed from the negative correlation of pH and As and Co in sample A-15 in the *H*-enrichments, the slightly acidic pH potentially favours the mobilization of Co, Fe-(sulf-)arsenides mineral species, as identified in Chapter 3. This slightly decreasing pH could have also favoured the increased activity of metal-cycling bacteria. The authors Xingyu et al. (2010) found that even with a pH unit difference of 0.3 (1.2 – 1.5), the abundances of their bioleaching organisms *Leptospirillum* and *Acidithiobacillus* spp. were significantly affected, which in turn influenced their bioleaching efficiency. Further statistical analysis will show whether the pH fluctuations in this study enhanced or depressed the leaching. Future work will also be to determine whether pH affected the microbial communities present within each of the three treatments, using multi-variate statistical analyses.

12.2 Potential Precipitation as a Solid Phase

As mentioned, within the three experiment treatment methods, there are large fluctuations in the concentrations of As and Co in solution, occurring at specific weeks (Appendix O). These decreasing concentration trends could be attributed to the precipitation of As and/or Co as a solid

phase. This suggestion, however, would require SEM and/or TEM analyses of the remaining tailings residue from the leaching experiments.

It is not uncommon for a secondary processing step to occur in an industrial bioleaching process in order to maximize metal recoveries, after a metal-precipitation step. A process such as this is conducted in the bioheapleaching operation at the Talvivaara mine in Finland, where they are mainly interested in the extraction of Ni ± Cu, Co and Zn from sulfides, using the native consortia to the ore. The Talvivaara process has been extensively described by Saari & Riekkola-Vanhanen (2012). In this bioleaching operation, a 10% circulating liquid, known as the pregnant leach solution (or PLS), is sent to a metal recovery phase, where Cu, Zn and Ni-Co sulfides are precipitated and subsequently sent to refineries. It is possible that a secondary process such as this could be an option for the tailings within the CMC.

Phosphate-bearing salt solutions are commonly used to enhance microbial activities in waste rocks materials and may precipitate cobalt phosphates such as pakhomovskiyite ($\text{Co}_3(\text{PO}_4)_2 \cdot 8\text{H}_2\text{O}$). This mineral may have played an important role during the bioleaching of the CMC tailings. Cobalt phosphates are sparingly soluble salts with $\text{Co}_3(\text{PO}_4)_2(\text{s})$ being the compound with the lowest solubility ($\text{Co} = 2.56^{-13}$ mg/kg, at equilibrium) as determined via the geochemical speciation program Visual Minteq (Gustafsson, 2019). Moreover, erythrite, a common secondary As-mineral seen in the CMC tailings, and pakhomovskiyite are both members of the vivianite-mineral group ($A_3(\text{XO}_4)_2 \cdot 8\text{H}_2\text{O}$, where A = divalent, Mg, Fe, Co, Ni, Zn, and X = As, P). Hence, it is not uncommon for P to substitute for As inside the crystal lattice of erythrite during bioleaching experiments (Frost et al., 2003). Future SEM and/or TEM analyses will determine whether there was a factor that inhibited the leaching of As and Co within these

experiments, and potentially whether this was a biologically-controlled or -induced form of mineralization.

12.3 Microbial Communities in Treatments versus the Tailings Background Microbial Community

In comparison to the tailings background community, the microbial community identified after the bioleaching experiments exhibit, most importantly: 1) a significantly larger diversity in terms of bulk composition, as only 12 of 97 genera (above a relative abundance of 2 %) are native to the original materials; and 2) a greater abundance and diversity of Fe, S, As, and N-cycling microorganisms. Of the identified As-cycling communities in the experiments, only the potential AsRB *Polaromonas* and *Sphingomonas* were observed in the background community.

Arsenic reduction by the identified AsRB activity could be achieved through either a dissimilatory reduction pathway by, for example, *Desulfitobacterium*, *Mesorhizobium*, and *Sulfuritalea* (Niggemyer et al., 2001, Sá-Pereira et al., 2007, Watanabe et al., 2017), through cytoplasmic reduction (e.g. *Afipia* and *Cupriavidu*; Guo et al., 2020), or As-reduction through methylation pathways (e.g. *Sphingomonas* and *Rhodobacter*; Macur et al., 2001, Lv et al., 2012). In the identified AsOB, As-oxidation can be achieved via: As³⁺-oxidation coupled to nitrate-reduction (e.g. *Hydrogenophaga* and *Simplicispira*; Cui, J et al., 2018a), detoxification (*Variovorax*; Satola et al., 2013), or by using As³⁺ as the sole electron acceptor, growing lithotrophically (*Herminiimonas*; Cai et al., 2009).

As previously mentioned, there is a significantly larger group of AsRB than AsOB and the population that can perform both reduction and oxidation, with the heterotroph-enrichments having the largest relative abundance of all three treatments/enrichments, followed by the

chemolithotroph-enrichments and control experiments. Therefore, we can suggest that the enrichments did in fact successfully favour neutrophilic As-cycling communities, and that the higher abundance of AsRB could be due to high As valence in the tailings samples selected for the experiments (Fig. 4 and Table 2 of Appendix G). The heterotrophic-communities may also have a higher proportion of AsRB than the latter two due to their affinity to primarily reduce oxidized compounds by coupling this reduction to the oxidation of organic carbon (Konhauser, 2007). Also, the presence of heterotrophic bacteria in the chemolithotroph-enrichments can be due to the synthesized organic substances by the chemolithotrophs (Battaglia-Brunet et al., 2002). This existence was also observed by Drewniak et al. (2010). The authors isolated three bacteria from the Zloty Stok Au-mine, of which two could perform dissimilatory As-reduction heterotrophically (*Shewanella* sp. O23S and *Aeromonas* sp. O23A) and the third as a lithotrophic, arsenite-oxidizer (*Sinorhizobium* sp. M14).

12.4 Microbial Community Structure as Related to High Concentrations of Co and As in Solution

Select sample(s) with the highest leaching efficiency will now be discussed in terms of the possible microbial communities that enhanced the leaching process. Tables 1 – 6 in Appendix P show the cumulative percent of Co and As released for all samples, in each treatment. Sample B-10 will be discussed for the anaerobic control experiments, A-15 for the aerobic chemolithotroph-enrichments, and C-20 and A-15 for the aerobic heterotroph-enrichments. Here the focus is on bacteria known to be able to reduce and/or oxidize As. Also, similar to the suggestion made in Chapter 3, there is no direct evidence for the biologically-controlled dissolution of As-minerals, however biologically-induced dissolution of As-minerals

most likely occurred during the bioleaching experiments, due to the high abundance of As-cycling bacteria.

12.4.1 Leaching Patterns in the Control Experiments

The anaerobic control experiment sample B-10 consists of the identification of only *Pseudomonas* as potentially being able to perform As-reduction. There are higher occurrences of S and N-cycling genera (compared to As-cycling) within this sample, such as the occurrence of the S-oxidizing bacterial genus, *Sulfurifustis*, species of which have been suggested to perform As-reduction through S-oxidation, using nitrate as a terminal electron acceptor (Guan et al., 2017). It should be noted that this was not observed in this specific SOB genera, but in the commonly-associated SOB genera *Thiobacillus* (Guan et al., 2017). As mentioned, there are higher abundances of As-resistant bacteria in the control samples. This is possibly due to suggestions by Cai et al. (2009) and Guan et al. (2017), stating that the long-term As contamination in soils may result in the horizontal gene transfer of As-resistant genes, leading to a diverse set of bacteria capable of As-resistance. Therefore, as there are no definitive bacteria within the anaerobic control experiment (in this sample) capable of As-reduction, the leaching mechanics of this sample cannot be fully understood at this time.

12.4.2 Leaching Patterns in Chemolithotroph-enrichments

Sample A-15 from the aerobic chemolithotroph-enrichment experiments have a slightly higher proportion of AsOB to AsRB (~ 40 % and 30 %, respectively), with some of these bacterial genera capable of both oxidation and reduction (i.e. *Ralstonia* and *Delftia*). This original tailings sample had a higher proportion of primary arsenides to secondary arsenates, as

observed on the SEM (Fig. 7), therefore the oxidation of arsenides would have potentially been the main form of Co and As released into solution.

12.4.3 Leaching Patterns in Heterotroph-enrichments

Comparatively, within the aerobic heterotroph-enrichment experiments, the highest extraction efficiency of total and dissolved Co was from tailings of site C (C-20), which as discussed in Chapter 3, primarily contains more Co-Ni-Zn arsenates, with a corresponding high As valence (Table 2 of Appendix G). The existing microbial communities within this sample include many FeRB, such as *Ferribacterium*, *Desulfitobacterium*, *Geothrix* and *Ferribacterium* (Niggemyer et al., 2001, Mehta, 2013, Jiang et al., 2019). As previously mentioned, both *Ferribacterium* and *Desulfitobacterium* have been suggested to possess As⁵⁺-reduction capabilities (Jiang et al., 2019), thereby potentially aiding the release of Co into solution. The same tailings sample (as seen in the previous section, A-15) had a high As release in the aerobic heterotroph-enrichment experiments, comprising *Delftia* and *Dechloromonas* (Suhadolnik et al., 2017) as the most abundant AsRB and AsOB. Therefore, tailings material from the CMC with a higher proportion of primary Fe, Co-arsenides to secondary Co-Ni-Zn arsenates could be more efficiently bioleached through the use of aerobic, chemolithotroph (*Delftia*) or heterotroph (*Dechloromonas*) microorganisms.

12.5 Mechanisms of Microbial Leaching

Although the bioleaching experiments did not yield the best results, the microbial leaching mechanisms that may have occurred throughout the course of the experiment are here described. Similar to Chapter 3, there is no direct evidence for microbial-controlled or -induced

dissolution of minerals, however, future SEM and/or TEM analyses will hopefully shed light on this subject.

As observed by Drewniak et al. (2015), the isolated *Shewanella* strains from the Zloty Stok Au-mine site were capable of reductive dissolution of scorodite through direct contact, as bacterial colonies attached to the surface of scorodite secreted enzymes and metabolites promoting chemical reactions enhancing dissolution (Konhauser, 2007). Bacterial attachment can enhance the bioleaching process due to the bacterial synthesis of extracellular polysaccharides (EPS) (Konhauser, 2007; Drewniak et al., 2015). Extracellular polysaccharides can fuel processes such as mineral fracturing, chemical reactions, as well as by serving as substrates for heterotrophic bacteria, of which produce organic agents promoting chemical dissolution (Welch et al., 1999; Konhauser, 2007). The production of organic agents (such as acids) increase the dissolution of minerals by either: 1) protonation through destabilizing the metal-O bond; 2) promoting the formation of metal chelates; or 3) by indirectly lowering the state of saturation in solution as a result of metal complexation (Bennett et al., 1988). This dissolution process by organic acids has been observed in the microorganism *Burkholderia fungorum* by Mailloux et al. (2009) on As-bearing apatite. As the heterotrophic *Dechloromonas* was within the community identified in the sample with the highest leached As efficiency (A-15, within the *H*-experiments), it is therefore likely that EPS production and/or the formation of organic acids took place to enhance this process.

Alternatively, chemolithotrophic organisms, such as *Delftia* (also occurring in A-15, within the *H* and *Ch*-experiments), rely on metabolic pathways to oxidize reduced As-minerals, with their dissolution being achieved through direct or indirect mechanisms (Drewniak and Sklodowska, 2013). An indirect interaction occurs when microbial-oxidative reactions (e.g.

oxidation of Fe^{2+} to Fe^{3+}) drive further mineral breakdown through oxidative attack (Konhauser, 2007; Singh, 2016).

Thus, any or all of these mineral dissolution mechanisms could have enhanced the dissolution of As-minerals within the bioleaching experiments of the CMC tailings, however, at this point, it is only speculative. These microbial-processes are highly likely due to the variation in leaching efficiency and in the identified microbial communities between the control experiments and the chemolithotroph- and heterotroph-enrichments.

12.6 Suggestions for Future Bioleaching of the Cobalt Mining Camp Tailings

In the best leached tailings samples dominated by Fe, Co-arsenides, the As-cycling genera *Delftia* and *Dechloromonas* or *Delftia* and *Ralstonia* (for the *H* and *Ch*-enrichments, respectively) were identified, whereas FeRB with As-reduction capabilities (e.g. *Ferribacterium* and *Desulfitobacterium*) dominated in leaching Co from the heterotroph-enriched tailings samples primarily consisting of Co, Ni, Zn-arsenates. Therefore, if bacteria such as these are kept within their optimal growth conditions and are provided with their essential nutrients, they may be capable of efficiently and effectively bioleaching the mine tailings of the CMC.

13 Conclusions

Despite the very low percent extraction of Co and As from all tailings material within the three treatments, this was an important step in determining the neutrophilic As-cycling bacteria that could be enriched in the neutral-to-alkaline pH legacy mine tailings of the CMC via chemolithotroph and heterotroph-enrichments. The provided growth conditions within the chemolithotroph and heterotroph-amended experiments were, however, suitable for the growth

of the As-oxidizing and -reducing bacteria not previously identified in the microbial communities characterized in Chapter 3. Additional important findings include:

- 1) The highest percent of Co and As was released in the aerobic, heterotroph-enrichments, which may be due to the higher relative abundances of AsRB over AsOB;
- 2) The low microbial diversity in the anaerobic heterotroph-enrichments could have inhibited Co and As release;
- 3) AsRB, AsOB and FeRB were identified as the prime bacterial communities for the most effective leaching; and
- 4) Anaerobic experiments were not as efficient as aerobic experiments, possibly due to the As-cycling bacteria preferentially preferring aerobic conditions.

Chapter Five: General Conclusions and Project Implications

14 Conclusions

14.1 General Conclusions

This study demonstrates the importance of integrating geochemical, mineralogical and microbial analytical methods, in order to achieve a sufficient comprehension of the biogeochemical relationships occurring within tailings material. Moreover, this study has added to the current lack of scientific knowledge and understanding of neutrophilic bioleaching organisms.

The overarching objectives of this project were to characterize the geochemical, mineralogical and microbial relationships in materials from selected tailings sites in the Cobalt Mining Camp (Chapter 3) and second to integrate these results in order to perform bench-scale,

neutrophilic bioleaching enrichment experiments under aerobic and anaerobic conditions (Chapter 4). The most important conclusions from Chapter 3 include: 1) the site-specific groupings observed on the Co# vs Fe# and S# plots correlate to those observed in the microbial data; 2) S, Fe, N and C-cycling bacteria are the most abundant groups in the selected CMC tailings, of which are highly dependent on depth; 3) the average arsenic valence was observed to statistically influence the microbial communities present within site C; 4) samples at site B with low Co#'s and high Fe and/or S#'s tend to have a proportionally higher abundance of SOB or FeOB, due to the higher relative abundance of (sulf-)arsenides, whereas at site C, a low Fe# and high Co and S#'s show a large abundance of (sulf-)arsenides, sulfides and SRB; and 5) materials from site C have a distinct reduced and oxidized zone, which correlates to the abundance of Fe-reducing and sulfate-reducing bacteria, and a very low average As valence. Chapter 4's most important findings are that: 1) the chemolithotroph- and heterotroph-growth conditions were suitable for the new development of As-cycling bacteria; 2) aerobic conditions were more suitable for both chemolithotroph- and heterotroph-enrichments; 3) the aerobic heterotroph-enrichments had the best leaching efficiency of Co and As, potentially due to the higher relative abundance of AsRB over AsOB; and 4) five genera consisting of AsRB, AsOB and/or FeRB were identified in the samples that had the highest percent of Co and As released.

15 Future Work

Additional analyses following the thesis defence will take place in order to more fully grasp the underlying bioleaching mechanics that were at play during the enrichment experiments. These analyses will include: 1) running a t-test in order to statistically determine the leaching efficiency difference between treatments and enrichments; 2) conduct additional statistical

analyses such as performing a redundancy analysis (RDA), creating more NMDS plots and/or principal component analysis (PCA) graphs; and 3) and micro- to nanometre-scale studies on an SEM and transmission electron microscope (TEM), respectively, on the leached tailings residue.

16 Project Implications and Potential Applications

Despite the low leaching efficiency observed in the bioleaching enrichment experiments, these results served as an important first step in determining the neutrophilic As-cycling bacterial communities that could be enriched in tailings material for future bioleaching operations in the CMC or in other tailings sites, or low-grade ores, characterized by a neutral-to-alkaline pH and high Co and As concentrations. This study identified five genera in the samples with the highest percent Co and As released, that have been acknowledged as having As-oxidizing and/or -reducing capabilities (*Dechloromonas*, *Delftia*, *Ralstonia*, *Desulfitobacterium*, and *Ferribacterium*). Therefore, future experiments could be focused on the growth and enrichment of these identified As-cycling bacteria through classic culturing methods, by determining the nutrients and optimal growth conditions these bacteria require, so that they are able to: 1) catalyze necessary redox reactions; and 2) outcompete other accessory organisms. This study therefore additionally has potential applications to tailings sites or waste rock piles that are characterized by a neutral-to-alkaline drainage with high Co and As concentrations.

17 References

- AANDC (Aboriginal Affairs and Northern Development Canada). (2012). Internal Audit Report: Value for Money Audit of the Giant Mine Remediation Project. Audit and Assurances Survey Branch Project 12-32, <http://www.aadnc-aandc.gc.ca/eng/1366814305245/1366814424097>
- Abercrombie, S.M. (1991). Geology of the Ketz River Gold Mine. *Mineral Deposits of the Northern Canadian Cordillera, Yukon-Northeastern British Columbia (Field Trip 14)*. (Abbott, J.G. and Turner, R.J.W, Ed.) p. 259-267.
- Aceró, P., Ayora, C., Torrentó, C., & Nieto, J. M. (2006). The behavior of trace elements during schwertmannite precipitation and subsequent transformation into goethite and jarosite. *Geochimica et Cosmochimica Acta*, 70(16), 4130–4139.
<https://doi.org/10.1016/j.gca.2006.06.1367>
- Acevedo, F., Gentina, J. C., & Garcia, N. (1998). CO₂ supply in the biooxidation of an enargite–pyrite gold concentrate. *Biotechnology Letters*, 20(3), 257–259.
- Adams, N. W., & Kramer, J. R. (1998). Reactivity of Ag⁺ ion with thiol ligands in the presence of iron sulfide. *Environmental Toxicology and Chemistry: An International Journal*, 17(4), 625-629.
- Ahmann, D., Krumholz, L. R., Hemond, H. F., Lovley, D. R., & Morel, F. M. M. (1997). Microbial mobilization of arsenic from sediments of the Aberjona watershed. *Environmental Science and Technology*, 31(10), 2923–2930.
<https://doi.org/10.1021/es970124k>

- Albrecht-Gary, A. M., & Crumbliss, A. L. (1998). Coordination chemistry of siderophores: thermodynamics and kinetics of iron chelation and release. *Metal ions in biological systems*, 35, 239.
- Albuquerque, L., França, L., Rainey, F. A., Schumann, P., Nobre, M. F., & Da Costa, M. S. (2011). *Gaiella occulta* gen. nov., sp. nov., a novel representative of a deep branching phylogenetic lineage within the class Actinobacteria and proposal of Gaiellaceae fam. nov. and Gaiellales ord. nov. *Systematic and Applied Microbiology*, 34(8), 595–599. <https://doi.org/10.1016/j.syapm.2011.07.001>.
- Amils, R. (2011). Chemotroph. In: Gargaud M. et al. (eds) Encyclopedia of Astrobiology. Springer, Berlin, Heidelberg. https://doi.org/10.1007/978-3-642-11274-4_278
- Ams, D. A., Maurice, P. A., Hersman, L. E., & Forsythe, J. H. (2002). Siderophore production by an aerobic *Pseudomonas mendocina* bacterium in the presence of kaolinite. *Chemical Geology*, 188(3-4), 161-170.
- Anderson, P. (1993). Cobalt mining camp tailings inventory, Cobalt, Ontario. *Unpublished report, Ontario Ministry of Northern Development and Mines, 196pp*.
- Andrews, AJ, Owsiacki, L., Kerrich, R., & Strong, DF (1986). The silver deposits at Cobalt and Gowganda, Ontario. I: Geology, petrography, and whole-rock geochemistry. *Canadian Journal of Earth Sciences* , 23 (10), 1480-1506.
- Andrade, C. F., Jamieson, H. E., Kyser, T. K., Praharaaj, T., & Fortin, D. (2010). Biogeochemical redox cycling of arsenic in mine-impacted lake sediments and co-existing pore waters near Giant Mine, Yellowknife Bay, Canada. *Applied Geochemistry*, 25(2), 199–211. <https://doi.org/10.1016/j.apgeochem.2009.11.005>

- Apprill, A., McNally, S., Parsons, R., & Weber, L. (2015). Minor revision to V4 region SSU rRNA 806R gene primer greatly increases detection of SAR11 bacterioplankton. *Aquatic Microbial Ecology*, 75(2), 129-137.
- Babechuk, M. G., Weisener, C. G., Fryer, B. J., Paktunc, D., & Maunders, C. (2009). Microbial reduction of ferrous arsenate: Biogeochemical implications for arsenic mobilization. *Applied Geochemistry*, 24(12), 2332–2341.
- Bagade, A. V., Bachate, S. P., Dholakia, B. B., Giri, A. P., & Kodam, K. M. (2016). Characterization of Roseomonas and Nocardioides spp. for arsenic transformation. *Journal of Hazardous Materials*, 318, 1–31.
<https://doi.org/10.1016/j.jhazmat.2016.07.062>
- Barkay, T., & Schaefer, J. (2001). Metal and radionuclide bioremediation: issues, considerations and potentials. *Current opinion in microbiology*, 4(3), 318-323.
- Barker, W. W., Welch, S. A., Chu, S., & Banfield, J. F. (1998). Experimental observations of the effects of bacteria on aluminosilicate weathering. *American Mineralogist*, 83(11-12_Part_2), 1551-1563.
- Battaglia-Brunet, F., Itard, Y., Garrido, F., Delorme, F., Crouzet, C., Greffié, C., & Joulian, C. (2006). A simple biogeochemical process removing arsenic from a mine drainage water. *Geomicrobiology Journal*, 23(3-4), 201-211.
- Battaglia-Brunet, F., Dictor, M. C., Garrido, F., Crouzet, C., Morin, D., Dekeyser, K., ... & Baranger, P. (2002). An arsenic (III)-oxidizing bacterial population: selection, characterization, and performance in reactors. *Journal of applied microbiology*, 93(4), 656-667.

- BBDuk Guide. (n.d.). Retrieved from <https://jgi.doe.gov/data-and-tools/bbtools/bb-tools-user-guide/bbduk-guide/>
- Beauchemin, S., & Kwong, Y. T. J. (2007). Fluctuating Redox Conditions and Phosphorus Competition: Contributors To Arsenic Release From Wetland Tailings in Cobalt, Ontario 1, 2(07). Mining and the Environment IV Conference, Sudbury, Ontario, Canada, October 19-27, 2007
- Beinert, H., Holm, R. H., & Münck, E. (1997). Iron-sulfur clusters: nature's modular, multipurpose structures. *Science*, 277(5326), 653-659.
- Bell, R. A., & Kramer, J. R. (1999). Structural chemistry and geochemistry of silver-sulfur compounds: Critical review. *Environmental Toxicology and Chemistry*, 18(1), 9–22.
[https://doi.org/10.1897/1551-5028\(1999\)018<0009:SCAGOS>2.3.CO;2](https://doi.org/10.1897/1551-5028(1999)018<0009:SCAGOS>2.3.CO;2)
- Bennett, P. C., Melcer, M. E., Siegel, D. I., & Hassett, J. P. (1988). The dissolution of quartz in dilute aqueous solutions of organic acids at 25 C. *Geochimica et Cosmochimica Acta*, 52(6), 1521-1530.
- Bigham, J. M., Schwertmann, U., Carlson, L., & Murad, E. (1990). A poorly crystallized oxyhydroxysulfate of iron formed by bacterial oxidation of Fe (II) in acid mine waters. *Geochimica et Cosmochimica Acta*, 54(10), 2743-2758.
- Bigham, J. M., Schwertmann, U., Traina, S. J., Winland, R. L., & Wolf, M. (1996). Schwertmannite and the chemical modeling of iron in acid sulfate waters. *Geochimica et Cosmochimica Acta*, 60(12), 2111-2121.
- Bissen, M., & Frimmel, F. H. (2003). Arsenic—a review. Part I: occurrence, toxicity, speciation, mobility. *Acta hydrochimica et hydrobiologica*, 31(1), 9-18.

- Biswas, R., Vivekanand, V., Saha, A., Ghosh, A., & Sarkar, A. (2019). Arsenite oxidation by a facultative chemolithotrophic *Delftia* spp. BAS29 for its potential application in groundwater arsenic bioremediation. *International Biodeterioration & Biodegradation*, *136*, 55-62.
- Bosecker, K. (1997). Bioleaching: metal solubilization by microorganisms. *FEMS Microbiology Reviews*, *20*(1–2), 591–604. Retrieved from:
<http://www.sciencedirect.com/science/article/pii/S0168644597000363>
- Bowell, R. J., Alpers, C. N., Jamieson, H. E., Nordstrom, D. K., & Majzlan, J. (2014). The environmental geochemistry of arsenic - An overview. *Reviews in Mineralogy and Geochemistry*, *79*(1), 1–16. <https://doi.org/10.2138/rmg.2014.79.1>
- Bowell, R. J., & Craw, D. (2014). The management of arsenic in the mining industry. *Reviews in Mineralogy and Geochemistry*, *79*(1), 507–532.
<https://doi.org/10.2138/rmg.2014.79.11>
- Bowen, H. J. M. (1979). *Environmental Chemistry of the Elements*. Academic Press, London.
- Boyle, R. W., & Jonasson, I. R. (1973). The geochemistry of arsenic and its use as an indicator element in geochemical prospecting. *Journal of Geochemical Exploration*, *2*(3), 251-296.
- Brandl, H. (2001). Microbial leaching of metals. *Biotechnology*, *10*, 191-224.
- Bruneel, O., Duran, R., Koffi, K., Casiot, C., Fourçans, A., Elbaz-Poulichet, F., & Personné, J. C. (2007). Microbial diversity in a pyrite-rich tailings impoundment (Carnoulès, France). *Geomicrobiology Journal*, *22*(5), 249–257. <https://doi.org/10.1080/01490450590947805>
- Bryce, C., Blackwell, N., Schmidt, C., Otte, J., Huang, Y. M., Kleindienst, S., ... Kappler, A. (2018). Microbial anaerobic Fe(II) oxidation – Ecology, mechanisms and environmental

- implications. *Environmental Microbiology*, 20(10), 3462–3483.
- <https://doi.org/10.1111/1462-2920.14328>
- Burford, E. P., Fomina, M. & Gadd, G. M. (2003). Fungal involvement in bioweathering and biotransformation of rocks and minerals. *Mineral Mag* 67, 1127–1155.
- Burke, M., Rakovan, J., & Krekeler, M. P. (2017). A study by electron microscopy of gold and associated minerals from Round Mountain, Nevada. *Ore Geology Reviews*, 91, 708-717.
- Burton, E. D., Johnston, S. G., & Bush, R. T. (2011). Microbial sulfidogenesis in ferrihydrite-rich environments: Effects on iron mineralogy and arsenic mobility. *Geochimica et Cosmochimica Acta*, 75(11), 3072–3087.
- Buschmann, J., & Berg, M. (2009). Impact of sulfate reduction on the scale of arsenic contamination in groundwater of the Mekong, Bengal and Red River deltas. *Applied Geochemistry*, 24(7), 1278-1286.
- Caccavo, F., Schamberger, P. C., Keiding, K., & Nielsen, P. H. (1997). Role of hydrophobicity in adhesion of the dissimilatory Fe (III)-reducing bacterium *Shewanella alga* to amorphous Fe (III) oxide. *Applied and Environmental Microbiology*, 63(10), 3837-3843.
- Cai, L., Liu, G., Rensing, C., & Wang, G. (2009). Genes involved in arsenic transformation and resistance associated with different levels of arsenic-contaminated soils. *BMC Microbiology*, 9, 1–11. <https://doi.org/10.1186/1471-2180-9-4>.
- Callahan, B. J., McMurdie, P. J., Rosen, M. J., Han, A. W., Johnson, A. J. A., & Holmes, S. P. (2016). DADA2: high-resolution sample inference from Illumina amplicon data. *Nature methods*, 13(7), 581-583.

- Canuel, E. A. (2007). Molecular Geomicrobiology. *Reviews in Mineralogy and Geochemistry*, Banfield, Jillian F., Cervini-Silva, Javiera, Nealson, Kenneth M.(Eds.), 2005, vol. 59, Mineralogical Society of America and Geochemical Society, Chantilly, VA, 294 pp.
- Cavalca, L., Zecchin, S., Zaccheo, P., Abbas, B. A., Rotiroti, M., Bonomi, T., & Muyzer, G. (2019). Exploring biodiversity and arsenic metabolism of microbiota inhabiting arsenic-rich groundwaters in Northern Italy. *Frontiers in microbiology*, 10, 1480.
- CCME. (2001). Canadian environmental quality guidelines. Hull, QC: Canadian Council of Ministers of the Environment.
- Chan, C. S., Fakra, S. C., Emerson, D., Fleming, E. J., & Edwards, K. J. (2011). Lithotrophic iron-oxidizing bacteria produce organic stalks to control mineral growth: implications for biosignature formation. *The ISME journal*, 5(4), 717-727.
- Chandrababha, M. N., & Natarajan, K. A. (2011). Mechanism of arsenic tolerance and bioremoval of arsenic by *Acidithiobacillus ferrooxidans*. *Journal of Biochemical Technology*, 3,257–265.
- Chen, L. X., Li, J. T., Chen, Y. T., Huang, L. N., Hua, Z. S., Hu, M., & Shu, W. S. (2013). Shifts in microbial community composition and function in the acidification of a lead/zinc mine tailings. *Environmental microbiology*, 15(9), 2431-2444.
- Chen, Y. W., Yu, X., & Belzile, N. (2019). Arsenic speciation in surface waters and lake sediments in an abandoned mine site and field observations of arsenic eco-toxicity. *Journal of Geochemical Exploration*, 205(July), 106349.
<https://doi.org/10.1016/j.gexplo.2019.106349>.
- Choi, D. W., Antholine, W. E., Do, Y. S., Semrau, J. D., Kisting, C. J., Kunz, R. C., ... & DiSpirito, A. A. (2005). Effect of methanobactin on the activity and electron

- paramagnetic resonance spectra of the membrane-associated methane monooxygenase in *Methylococcus capsulatus* Bath. *Microbiology*, 151(10), 3417-3426.
- Choi, D. W., Do, Y. S., Zea, C. J., McEllistrem, M. T., Lee, S. W., Semrau, J. D., ... & Boyd, E. S. (2006). Spectral and thermodynamic properties of Ag (I), Au (III), Cd (II), Co (II), Fe (III), Hg (II), Mn (II), Ni (II), Pb (II), U (IV), and Zn (II) binding by methanobactin from *Methylosinus trichosporium* OB3b. *Journal of inorganic biochemistry*, 100(12), 2150-2161.
- Clarke, K. R. (1993). Non-parametric multivariate analysis of changes in community structure. *Australian Journal of Ecology* 18, 117--143.
- Clément, J. C., Shrestha, J., Ehrenfeld, J. G., & Jaffé, P. R. (2005). Ammonium oxidation coupled to dissimilatory reduction of iron under anaerobic conditions in wetland soils. *Soil Biology and Biochemistry*, 37(12), 2323-2328.
- Cloke, P. L. (1963). The geologic role of polysulfides—Part I The distribution of ionic species in aqueous sodium polysulfide solutions. *Geochimica et Cosmochimica Acta*, 27(12), 1265-1298.
- Corkhill, C. L., Wincott, P. L., Lloyd, J. R., & Vaughan, D. J. (2008). The oxidative dissolution of arsenopyrite (FeAsS) and enargite (Cu₃AsS₄) by *Leptospirillum ferrooxidans*. *Geochimica et Cosmochimica Acta*, 72(23), 5616–5633.
- Corriveau, M. C., Jamieson, H. E., Parsons, M. B., & Hall, G. E. M. (2011a). Mineralogical characterization of arsenic in gold mine tailings from three sites in Nova Scotia. *Geochemistry: Exploration, Environment, Analysis*, 11(3), 179–192.
- <https://doi.org/10.1144/1467-7873/09-246>

- Corriveau, M. C., Jamieson, H. E., Parsons, M. B., Campbell, J. L., & Lanzirrotti, A. (2011b). Direct characterization of airborne particles associated with arsenic-rich mine tailings: Particle size, mineralogy and texture. *Applied Geochemistry*, 26(9–10), 1639–1648.
<https://doi.org/10.1016/j.apgeochem.2011.04.021>
- Corsini, A., Cavalca, L., Crippa, L., Zaccheo, P., & Andreoni, V. (2010). Impact of glucose on microbial community of a soil containing pyrite cinders: Role of bacteria in arsenic mobilization under submerged condition. *Soil Biology and Biochemistry*, 42(5), 699–707.
- Creclius, E. A. (1993, August). The concentration of silver in mussels and oysters from NOAA National Status and Trends mussel watch sites. In *Proceedings* (pp. 8-10).
- Crowe, S.A., O'Neill, A.H., Weisener, C.G., Kulczycki, E., Fowle, D.A., & Roberts, J.A., 2007. Reductive dissolution of trace metals from sediments. *Geomicrobiol. J.* 24, 157–165.
- Cui, J., Du, J., Tian, H., Chan, T., & Jing, C. (2018a). Rethinking anaerobic As (III) oxidation in filters: Effect of indigenous nitrate respirers. *Chemosphere*, 196, 223-230.
- Cui, X., Gu, Q., Liu, X., Wen, J., Lu, A., Ding, H., ... Wang, X. (2018b). Contact-bioleaching mechanism of Ni and Co from sulfide concentrate at neutral pH by heterotrophic bacteria. *Minerals and Metallurgical Processing*, 35(4), 221–229.
<https://doi.org/10.19150/mmp.8599>
- Cui, X., Wang, X., Li, Y., Lu, A., Hao, R., Wang, C., & Ding, H. (2015). *Bioleaching of a Complex Co-Ni-Cu Sulfide Flotation Concentrate by Bacillus megaterium QM B1551 at Neutral pH. Geomicrobiology Journal* (Vol. 33).
<https://doi.org/10.1080/01490451.2015.1085470>

- Cui, Y., Fang, L., Guo, X., Wang, X., Wang, Y., Li, P., ... & Zhang, X. (2018). Responses of soil microbial communities to nutrient limitation in the desert-grassland ecological transition zone. *Science of the total environment*, 642, 45-55.
- Cummings, D. E., Caccavo, F., Fendorf, S., & Rosenzweig, R. F. (1999). Arsenic mobilization by the dissimilatory Fe(III)- reducing bacterium *Shewanella alga* BrY. *Environmental Science and Technology*, 33(5), 723–729.
- Cymes, B. A., Krekeler, M. P., Nicholson, K. N., & Grigsby, J. D. (2017). A transmission electron microscopy (TEM) study of silver nanoparticles associated with mine waste from New Caledonian nickel deposits: potential origins of silver toxicity in a World Heritage Site. *Environmental Earth Sciences*, 76(18), 640.
- Dahl, C., Friedrich, C. G. (2008). *Microbial Sulfur Metabolism*. Springer-Verlag, Heidelberg, Germany, 303 pp.
- Daims, H. (2014). The Family Nitrospiraceae. In E. Rosenberg et al. (Ed.), *The Prokaryotes: Other Major Lineages of Bacteria and The Archaea* (pp. 733–749). Springer-Verlag Berlin Heidelberg. <https://doi.org/10.1007/978-3-642-38954-2>.
- Das, S., Hendry, M. J., & Essilfie-Dughan, J. (2011). Effects of adsorbed arsenate on the rate of transformation of 2-line ferrihydrite at pH 10. *Environmental science and technology*, 45(13), 5557-5563.
- Dave, S. R., Gupta, K. H., & Tipre, D. R. (2008). Characterization of arsenic resistant and arsenopyrite oxidizing *Acidithiobacillus ferrooxidans* from Hutti gold leachate and effluents. *Bioresource technology*, 99(16), 7514-7520.

- Davis, N. M., Proctor, D. M., Holmes, S. P., Relman, D. A., & Callahan, B. J. (2018). Simple statistical identification and removal of contaminant sequences in marker-gene and metagenomics data. *Microbiome*, 6(1), 226.
- Dedysh, S. N. (2002). Methanotrophic bacteria of acidic Sphagnum peat bogs. *Microbiology*, 71(6), 638-650.
- Dedysh, S. N., Horz, H. P., Dunfield, P. F., & Liesack, W. (2001). A novel pmoA lineage represented by the acidophilic methanotrophic bacterium *Methylocapsa acidophila* B2. *Archives of microbiology*, 177(1), 117-121.
- DeSisto, S. L., Jamieson, H. E., & Parsons, M. B. (2016). Subsurface variations in arsenic mineralogy and geochemistry following long-term weathering of gold mine tailings. *Applied Geochemistry*, 73, 81–97. <https://doi.org/10.1016/j.apgeochem.2016.07.013>
- Diaby, N., Dold, B., Pfeifer, H. R., Holliger, C., Johnson, D. B., & Hallberg, K. B. (2007). Microbial communities in a porphyry copper tailings impoundment and their impact on the geochemical dynamics of the mine waste. *Environmental Microbiology*, 9(2), 298-307. <https://doi.org/10.1111/j.1462-2920.2006.01138.x>.
- Dockrey, J., Lindsay, M., Mayer, K., Beckie, R., Norlund, K., Warren, L., & Southam, G. (2014). Acidic Microenvironments in Waste Rock Characterized by Neutral Drainage: Bacteria–Mineral Interactions at Sulfide Surfaces. *Minerals*, 4(1), 170–190. <https://doi.org/10.3390/min4010170>
- Donahue, R., Hendry, M. J., & Landine, P. (2000). Distribution of arsenic and nickel in uranium mill tailings, Rabbit Lake, Saskatchewan, Canada. *Applied Geochemistry*, 15(8), 1097–1119. [https://doi.org/10.1016/S0883-2927\(99\)00114-6](https://doi.org/10.1016/S0883-2927(99)00114-6)

- Dong, H., Jaisi, D. P., Kim, J., & Zhang, G. (2009). Microbe-clay mineral interactions. *American Mineralogist*, 94(11-12), 1505-1519.
- Dong, H. (2010). Mineral-microbe interactions: A review. *Frontiers of Earth Science in China*, 4(2), 127–147. <https://doi.org/10.1007/s11707-010-0022-8>.
- Dong, H., & Lu, A. (2012). Mineral-Microbe Interactions and Implications for Remediation. *Elements*, 8(2), 95–99.
- Dopp, E., Hartmann, L. M., Florea, A. M., Von Recklinghausen, U., Pieper, R., Shokouhi, B., ... & Obe, G. (2004). Uptake of inorganic and organic derivatives of arsenic associated with induced cytotoxic and genotoxic effects in Chinese hamster ovary (CHO) cells. *Toxicology and applied pharmacology*, 201(2), 156-165.
- Dopson, M., Baker-Austin, C., Koppineedi, P. R., & Bond, P. L. (2003). Growth in sulfidic mineral environments: metal resistance mechanisms in acidophilic micro-organisms. *Microbiology*, 149(8), 1959-1970.
- Dove, P. M. (2010). The rise of skeletal biominerals. *Elements*, 6(1), 37-42.
- Dowdle, P. R., Laverman, A. M., & Oremland, R. S. (1996). Bacterial dissimilatory reduction of arsenic (V) to arsenic (III) in anoxic sediments. *Applied and Environmental Microbiology*, 62(5), 1664-1669.
- Drahota, P., & Filippi, M. (2009). Secondary arsenic minerals in the environment: A review. *Environment International*, 35(8), 1243–1255. <https://doi.org/10.1016/j.envint.2009.07.004>
- Drewniak, L., & Sklodowska, A. (2013). Arsenic-transforming microbes and their role in biomining processes. *Environmental Science and Pollution Research*, 20(11), 7728–7739. <https://doi.org/10.1007/s11356-012-1449-0>

- Drewniak, L., Styczek, A., Majder-Lopatka, M., & Sklodowska, A. (2008a). Bacteria, hypertolerant to arsenic in the rocks of an ancient gold mine, and their potential role in dissemination of arsenic pollution. *Environmental Pollution*, *156*(3), 1069–1074.
<https://doi.org/10.1016/j.envpol.2008.04.019>
- Drewniak, L., Matlakowska, R., & Sklodowska, A. (2008b). Arsenite and arsenate metabolism of *Sinorhizobium* sp. M14 living in the extreme environment of the Zloty Stok gold mine. *Geomicrobiology Journal*, *25*(7–8), 363–370.
<https://doi.org/10.1080/01490450802402836>
- Drewniak, L., Matlakowska, R., Rewerski, B., & Sklodowska, A. (2010). Arsenic release from gold mine rocks mediated by the activity of indigenous bacteria. *Hydrometallurgy*, *104*(3–4), 437–442. <https://doi.org/10.1016/j.hydromet.2010.02.025>
- Drewniak, L., Stasiuk, R., Uhrynowski, W., & Sklodowska, A. (2015). *Shewanella* sp. O23S as a driving agent of a system utilizing dissimilatory arsenate-reducing bacteria responsible for self-cleaning of water contaminated with arsenic. *International Journal of Molecular Sciences*, *16*(7), 14409–14427. <https://doi.org/10.3390/ijms160714409>
- Duker, A., Carranza, E., & Hale, M. (2005). Arsenic geochemistry and health. *Environment International*, *31*(5), 631–641. doi:10.1016/j.envint.2004.10.020
- Dumaresq, C. (2009). Tailings of the Cobalt Area. Retrieved from:
<http://www.cobaltmininglegacy.ca/tailings.php>
- Dumaresq, C. G. (1993). *The occurrence of arsenic and heavy metal contamination from natural and anthropogenic sources in the Cobalt area of Ontario* (Doctoral dissertation, Carleton University).

- Duquesne, K., Lebrun, S., Casiot, C., Bruneel, O., Personné, J. C., Leblanc, M., ... & Bonnefoy, V. (2003). Immobilization of arsenite and ferric iron by *Acidithiobacillus ferrooxidans* and its relevance to acid mine drainage. *Applied and Environmental Microbiology*, 69(10), 6165-6173.
- Dyck, W. (1968). Adsorption and coprecipitation of silver on hydrous ferric oxide. *Can. J. Chem.* 46, 1441–1444.
- Ebbs, S. (2004). Biological degradation of cyanide compounds. *Current opinion in Biotechnology*, 15(3), 231-236.
- Eckelman, M. J., & Graedel, T. E. (2007). Silver emissions and their environmental impacts: A multilevel assessment. *Environ. Sci. Technol.* 41, 6283–6289.
- Ehrlich, H. L. (1996). How microbes influence mineral growth and dissolution. *Chem Geol* 132, 5–9.
- Ehrlich, H. L. & Newman, D. K. (2009). *Geomicrobiology*, 5th edn. Boca Raton, FL: CRC Press/Taylor and Francis.
- Eilers, K. G., Debenport, S., Anderson, S., & Fierer, N. (2012). Digging deeper to find unique microbial communities: The strong effect of depth on the structure of bacterial and archaeal communities in soil. *Soil Biology and Biochemistry*, 50, 58–65.
<https://doi.org/10.1016/j.soilbio.2012.03.011>
- Elberling, B., Schippers, A., & Sand, W. (2000). Bacterial and chemical oxidation of pyritic mine tailings at low temperatures. *Journal of Contaminant Hydrology*, 41(3-4), 225-238.
- Elkhatib, E. A., Bennett, O. L., & Wright, R. J. (1984). Kinetics of Arsenite Sorption in Soils. *Soil Science Society of America Journal*, 48(4), 758–762.
<https://doi.org/10.2136/sssaj1984.03615995004800040012x>

- Ellis, R. J., Morgan, P., Weightman, A. J., & Fry, J. C. (2003). Cultivation-dependent and-independent approaches for determining bacterial diversity in heavy-metal-contaminated soil. *Applied and environmental microbiology*, 69(6), 3223-3230.
- Emsley, J. (2001). *Nature's Building Blocks*. Oxford University Press, Inc., New York.
- EPA. (2003). *EPA and Hardrock Mining: A Source Book for Industry in the Northwest and Alaska* (p. 64) (U.S. Environmental Protection Agency, Seattle). Seattle: EPA.
- EPA. (1996). Method 3052: Microwave Assisted Acid Digestion of Siliceous and Organically Based Matrices. EPA.
- EPA (2011). Secondary Drinking Water Regulations: Guidance for Nuisance Chemicals. U.S. EPA, Washington. 816-F-10-079. Accessed: 02 July 2020, <https://www.epa.gov/sdwa/secondary-drinking-water-standards-guidance-nuisance-chemicals>.
- Espiell, F., Roca, A., Cruells, M., & Nuñez, C. (1986). Gold and silver recovery by cyanidation of arsenopyrite ore. *Hydrometallurgy*, 16(2), 141-151.
- Essilfie-Dughan, J., Hendry, M. J., Warner, J., & Kotzer, T. (2013). Arsenic and iron speciation in uranium mine tailings using X-ray absorption spectroscopy. *Applied Geochemistry*, 28, 11–18. <https://doi.org/10.1016/j.apgeochem.2012.10.022>
- Fawcett, S. E., Jamieson, H. E., Nordstrom, D. K., & McCleskey, R. B. (2015). Arsenic and antimony geochemistry of mine wastes, associated waters and sediments at the Giant Mine, Yellowknife, Northwest Territories, Canada. *Applied Geochemistry*, 62, 3–17. <https://doi.org/10.1016/j.apgeochem.2014.12.012>
- Filippou, D., & Dernopoulos, G.P. (1997). Arsenic Immobilization by Controlled Scorodite Precipitation. *JOM*, 49(12): 52-55.

- Finneran, K. T., Johnsen, C. V., & Lovley, D. R. (2003). *Rhodoferax ferrireducens* sp. nov., a psychrotolerant, facultatively anaerobic bacterium that oxidizes acetate with the reduction of Fe (III). *International Journal of Systematic and Evolutionary Microbiology*, 53(3), 669-673.
- Fisher, N. S., & Wang, W. X. (1998). Trophic transfer of silver to marine herbivores: A review of recent studies. *Environmental Toxicology and Chemistry: An International Journal*, 17(4), 562-571.
- Fordham, A. W., & Norrish, K. (1979). Arsenate-73 uptake by components of several acidic soils and its implications for phosphate retention. *Soil Research*, 17(2), 307-316.
- Frankel, R. B., & Bazylinski, D. A. (2003). Biologically induced mineralization by bacteria. *Reviews in mineralogy and geochemistry*, 54(1), 95-114.
- Frost, R. L., Martens, W., Williams, P. A., & Klopogge, J. T. (2003). Raman spectroscopic study of the vivianite arsenate minerals. *Journal of Raman Spectroscopy*, 34(10), 751–759. <https://doi.org/10.1002/jrs.1049>.
- Frueh, A. J. (1958). The crystallography of silver sulfide, Ag₂S. *Z. Kristallogr*, 110(2), 136-144.
- Gadd, G. M. (1993). Interactions of fungi with toxic metals. *New Phytol* 124, 25–60.
- Gadd, G. M. (2004). Microbial influence on metal mobility and application for bioremediation. *Geoderma*, 122(2-4 SPEC. IIS.), 109–119. <https://doi.org/10.1016/j.geoderma.2004.01.002>
- Gadd, G. M. (2010). Metals, minerals and microbes: Geomicrobiology and bioremediation. *Microbiology*, 156(3), 609–643. <https://doi.org/10.1099/mic.0.037143-0>
- Gao, S., Zhang, R. G., Cao, W. D., Fan, Y. Y., Gao, J. S., Huang, J., ... & Thorup-Kristensen, K. (2015). Long-term rice-rice-green manure rotation changing the microbial communities

- in typical red paddy soil in south china. *Journal of integrative agriculture*, 14(12), 2512-2520.
- Garris, H. W., Baldwin, S. A., Taylor, J., Gurr, D. B., Denesiuk, D. R., Van Hamme, J. D., & Fraser, L. H. (2018). Short-term microbial effects of a large-scale mine-tailing storage facility collapse on the local natural environment. *PLoS ONE*, 13(4), 1–25.
<https://doi.org/10.1371/journal.pone.0196032>
- Gharieb, M. M., Kierans, M., & Gadd, G. M. (1999). Transformation and tolerance of tellurite by filamentous fungi: accumulation, reduction and volatilization. *Mycol Res* 103, 299–305.
- Giebner, F., Kaden, L., Wiche, O., Tischler, J., Schopf, S., & Schlömann, M. (2019a). Biorecovery of cobalt from an arsenidic ore. *Minerals Engineering*, 131(October 2018), 73–78. <https://doi.org/10.1016/j.mineng.2018.10.020>
- Giebner, F., Helmich, J., Wiche, O., Kaden, L., Schlömann, M., & Schopf, S. (2019b, January). Biorecovery of a natural arsenide ore. In *Geophysical Research Abstracts* (Vol. 21).
- Gihring, T. M., Druschel, G. K., McCleskey, R. B., Hamers, R. J., & Banfield, J. F. (2001). Rapid arsenite oxidation by *Thermus aquaticus* and *Thermus thermophilus*: Field and laboratory investigations. *Environmental Science and Technology*, 35(19), 3857–3862.
- Giri, A. K., Patel, R. K., Mahapatra, S. S., & Mishra, P. C. (2013). Biosorption of arsenic (III) from aqueous solution by living cells of *Bacillus cereus*. *Environmental Science and Pollution Research*, 20(3), 1281–1291.
- Glasauer, S., Beveridge, T. J., Burford, E. P., Harper, F. A. & Gadd, G. M. (2004). Metals and metalloids, transformations by microorganisms. In *Encyclopedia of Soils in the*

- Environment, pp. 438–447. Edited by D. Hillel, C. Rosenzweig, D. S. Powlson, K. M. Scow, M. J. Singer, D. L. Sparks and J. Hatfield. Amsterdam: Elsevier.
- Gorby, Y. A., Yanina, S., McLean, J. S., Rosso, K. M., Moyles, D., Dohnalkova, A., ... & Culley, D. E. (2006). Electrically conductive bacterial nanowires produced by *Shewanella oneidensis* strain MR-1 and other microorganisms. *Proceedings of the National Academy of Sciences*, *103*(30), 11358-11363.
- Gorra, R., Webster, G., Martin, M., Celi, L., Mapelli, F., & Weightman, A. J. (2012). Dynamic Microbial Community Associated with Iron-Arsenic Co-Precipitation Products from a Groundwater Storage System in Bangladesh. *Microbial Ecology*, *64*(1), 171–186.
<https://doi.org/10.1007/s00248-012-0014-1>
- Govarthanan, M., Lee, S. M., Kamala-Kannan, S., & Oh, B. T. (2015). Characterization, real-time quantification and in silico modeling of arsenate reductase (*arsC*) genes in arsenic-resistant *Herbaspirillum* sp. GW103. *Research in microbiology*, *166*(3), 196-204.
- Grady, E. N., MacDonald, J., Liu, L., Richman, A., & Yuan, Z. C. (2016). Current knowledge and perspectives of *Paenibacillus*: a review. *Microbial cell factories*, *15*(1), 203.
- Greulich, C., Braun, D., Peetsch, A., Diendorf, J., Siebers, B., Epple, M., & Köller, M. (2012). The toxic effect of silver ions and silver nanoparticles towards bacteria and human cells occurs in the same concentration range. *RSC advances*, *2*(17), 6981-6987.
- Groves, D. I., Goldfarb, R. J., Gebre-Mariam, M., Hagemann, S. G., & Robert, F. (1998). Orogenic gold deposits: a proposed classification in the context of their crustal distribution and relationship to other gold deposit types. *Ore geology reviews*, *13*(1-5), 7-27.

- Guan, X., Yan, X., Li, Y., Jiang, B., Luo, X., & Chi, X. (2017). Diversity and arsenic-tolerance potential of bacterial communities from soil and sediments along a gold tailing contamination gradient. *Canadian Journal of Microbiology*, 63(9), 788–805. <https://doi.org/10.1139/cjm-2017-0214>
- Guo, T., Zhou, Y., Chen, S., Lu, H., He, Y., Tang, X., & Xu, J. (2020). The influence of periphyton on the migration and transformation of arsenic in the paddy soil: Rules and mechanisms. *Environmental Pollution*, 114624.
- Gustaffson, J.P. (2019). Visual Minteq 3.1. Kth, Seed, Stockholm, Sweden.
- Haaijer, S. C. M., Crienen, G., Jetten, M. S. M., & Op den Camp, H. J. M. (2012). Anoxic iron cycling bacteria from an iron sulfide-and nitrate-rich freshwater environment. *Frontiers in Microbiology*, 3(FEB), 1–8. <https://doi.org/10.3389/fmicb.2012.00026>
- Hamilton, E. I. (1994). The geobiochemistry of cobalt. *Science of the Total Environment, The*, 150(1–3), 7–39. [https://doi.org/10.1016/0048-9697\(94\)90126-0](https://doi.org/10.1016/0048-9697(94)90126-0)
- Handley, K. M., McBeth, J. M., Charnock, J. M., Vaughan, D. J., Wincott, P. L., Polya, D. A., & Lloyd, J. R. (2013). Effect of iron redox transformations on arsenic solid-phase associations in an arsenic-rich, ferruginous hydrothermal sediment. *Geochimica et Cosmochimica Acta*, 102, 124-142.
- Harrison, J. J., Turner, R. J., Marques, L. L., & Ceri, H. (2005). Biofilms: a new understanding of these microbial communities is driving a revolution that may transform the science of microbiology. *American Scientist*, 93(6), 508-515.
- Hegler, F., Schmidt, C., Schwarz, H., & Kappler, A. (2010). Does a low-pH microenvironment around phototrophic FeII-oxidizing bacteria prevent cell encrustation by FeIII minerals?. *FEMS Microbiology Ecology*, 74(3), 592-600.

- Heikkinen, P. M., Räisänen, M. L., & Johnson, R. H. (2009). Geochemical characterisation of seepage and drainage water quality from two sulphide mine tailings impoundments: acid mine drainage versus neutral mine drainage. *Mine Water and the Environment*, 28(1), 30-49.
- Hem, J.D., (1985). Study and Interpretation of the Chemical Characteristics of Natural Water, 3rd Edition. U.S. Geological Survey Water Supply Paper 2254.
- Henke, K. R. (2009). *Arsenic: Environmental Chemistry, Health Threats and Waste Treatment*.
Arsenic: Environmental Chemistry, Health Threats and Waste Treatment.
<https://doi.org/10.1002/9780470741122>
- Hersman, L. E., Forsythe, J. H., Ticknor, L. O., & Maurice, P. A. (2001). Growth of *Pseudomonas mendocina* on Fe (III)(hydr) oxides. *Applied and Environmental Microbiology*, 67(10), 4448-4453.
- Hertlein, G., Müller, S., Garcia-Gonzalez, E., Poppinga, L., Süssmuth, R. D., & Genersch, E. (2014). Production of the catechol type siderophore bacillibactin by the honey bee pathogen *Paenibacillus* larvae. *PLoS One*, 9(9), e108272.
- Hohmann, C., Winkler, E., Morin, G., & Kappler, A. (2010). Anaerobic Fe (II)-oxidizing bacteria show As resistance and immobilize As during Fe (III) mineral precipitation. *Environmental Science & Technology*, 44(1), 94-101.
- Holden, J. F. & Adams, M. W. W. (2003). Microbe–metal interactions in marine hydrothermal vents. *Curr Opin Chem Biol* 7, 160–165.
- Hollibaugh, J. T., Budinoff, C., Hollibaugh, R. A., Ransom, B., & Bano, N. (2006). Sulfide oxidation coupled to arsenate reduction by a diverse microbial community in a soda lake. *Applied and environmental microbiology*, 72(3), 2043-2049.

- Hu, W., Long-feng, L., and Ke-qiang, W. (1983). Flotation [M].
- Hu, Z., & Gao, S. (2008). Upper crustal abundances of trace elements: a revision and update. *Chemical Geology*, 253(3-4), 205-221.
- Huang, J. H. (2014). Impact of microorganisms on arsenic biogeochemistry: A review. *Water, Air, and Soil Pollution*, 225(2). <https://doi.org/10.1007/s11270-013-1848-y>.
- Huang, J.-H., Voegelin, A., Pombo, S. A., Lazzaro, A., Zeyer, J., & Kretzschmar, R. (2011c). Influence of arsenate adsorption to ferrihydrite, goethite, and boehmite on the kinetics of arsenate reduction by *Shewanella putrefaciens* strain CN-32. *Environmental Science and Technology*, 45(18), 7701–7709.
- Huerta-Rosas, B., Cano-Rodríguez, I., Gamiño-Arroyo, Z., Gómez-Castro, F. I., Carrillo-Pedroza, F. R., Romo-Rodríguez, P., & Gutiérrez-Corona, J. F. (2020). Aerobic processes for bioleaching manganese and silver using microorganisms indigenous to mine tailings. *World Journal of Microbiology and Biotechnology*, 36(8), 1-16.
- Jackson, C. R., Dugas, S. L., & Harrison, K. G. (2005). Enumeration and characterization of arsenate-resistant bacteria in arsenic free soils. *Soil Biology and Biochemistry*, 37(12), 2319–2322. <https://doi.org/10.1016/j.soilbio.2005.04.010>
- Jacobson, A. R., McBride, M. B., Baveye, P., & Steenhuis, T. S. (2005). Environmental factors determining the trace-level sorption of silver and thallium to soils. *Sci. Total Environ.* 345, 191–205.
- Jamieson, H. E. (2014). The Legacy of Arsenic Contamination from Mining and Processing Refractory Gold Ore at. *Reviews in Mineralogy and Geochemistry*, 79 (Mvrb 2013), 533–551.

- Jefferson, C. W., Thomas, D. J., Gandhi, S. S., Ramaekers, P., Delaney, G., Brisbin, D., Cutts, C., Portella, P., & Olson, R. A. (2007). Unconformity-associated uranium deposits of the Athabasca Basin, Saskatchewan and Alberta, in Goodfellow, W.D., ed., *Mineral Deposits of Canada: A Synthesis of Major Deposit-Types, District Metallogeny, the Evolution of Geological Provinces, and Exploration Methods: Geological Association of Canada, Mineral Deposits Division, Special Publication No. 5*, p. 273-305.
- Jenkins, M. B., Chen, J. H., Kadner, D. J., & Lion, L. W. (1994). Methanotrophic bacteria and facilitated transport of pollutants in aquifer material. *Applied and environmental microbiology*, 60(10), 3491-3498.
- Ji, H., Zhang, Y., Bararunyeretse, P., & Li, H. (2018). Characterization of microbial communities of soils from gold mine tailings and identification of mercury-resistant strain. *Ecotoxicology and Environmental Safety*, 165(30), 182–193.
<https://doi.org/10.1016/j.ecoenv.2018.09.011>
- Jiang, S., Lee, J.-H., Kim, D., Kanaly, R. A., Kim, M.-G., & Hur, H.-G. (2013). Differential arsenic-mobilization from As-bearing ferrihydrite by iron-respiring *Shewanella* strains with different arsenic-reducing activities. *Environmental Science and Technology*, 47(15), 8616–8623.
- Jiang, Z., Li, P., Wang, Y., Liu, H., Wei, D., Yuan, C., & Wang, H. (2019). Arsenic mobilization in a high arsenic groundwater revealed by metagenomic and Geochip analyses. *Scientific reports*, 9(1), 1-10.
- Jones, C. A., Langner, H. W., Anderson, K., McDermott, T. R., & Inskeep, W. P. (2000). Rates of microbially mediated arsenate reduction and solubilization. *Soil Science Society of America Journal*, 64(2), 600–608.

- Joyce, D. K., Tait, K., Vertoli, V., Back, M., & Nicklin, I. (2012). The Cobalt Mining District, Cobalt, Ontario, Canada. *Mineralogical Record*, 43(6), 685-713.
- Jurjovec, J., Ptacek, C. J., & Blowes, D. W. (2002). Acid neutralization mechanisms and metal release in mine tailings: a laboratory column experiment. *Geochimica et Cosmochimica Acta*, 66(9), 1511-1523.
- Karavaiko, G. I., Smolskaja, L. S., Golyshina, O. K., Jagovkina, M. A., & Egorova, E. Y. (1994). Bacterial pyrite oxidation: Influence of morphological, physical and chemical properties. *Fuel processing technology*, 40(2-3), 151-165.
- Katsoyiannis, I. A., & Zouboulis, A. I. (2004). Application of biological processes for the removal of arsenic from groundwaters. *Water research*, 38(1), 17-26.
- Katsoyiannis, I. A., & Zouboulis, A. I. (2006). Use of iron-and manganese-oxidizing bacteria for the combined removal of iron, manganese and arsenic from contaminated groundwater. *Water Quality Research Journal*, 41(2), 117-129.
- Kelley, B. C., & Tuovinen, O. H. (1988). Microbiological oxidations of minerals in mine tailings. In *Chemistry and biology of solid waste* (pp. 33-53). Springer, Berlin, Heidelberg.
- Kelly, J., Champagne, P., & Michel, F. (2007). Assessment of metal attenuation in a natural wetland system impacted by alkaline mine tailings, Cobalt, Ontario, Canada. *Mine Water and the Environment*, 26(3), 181–190. <https://doi.org/10.1007/s10230-007-0007-3>.
- Kemmitt, S. J., Wright, D., Goulding, K. W., & Jones, D. L. (2006). pH regulation of carbon and nitrogen dynamics in two agricultural soils. *Soil biology and biochemistry*, 38(5), 898-911.

- Kinegam, S., Yingprasertchai, T., Tanasupawat, S., Leepipatpiboon, N., Akaracharanya, A., & Kim, K. W. (2008). Isolation and characterization of arsenite-oxidizing bacteria from arsenic-contaminated soils in Thailand. *World Journal of Microbiology and Biotechnology*, 24(12), 3091-3096.
- King, H. M. (2020). Silver. Retrieved from <https://geology.com/minerals/silver.shtml>
- Kirby, C. S., & Cravotta III, C. A. (2005). Net alkalinity and net acidity 2: practical considerations. *Applied Geochemistry*, 20(10), 1941-1964.
- Kissin, S. A. (1992). Five-element (Ni-Co-As-Ag-Bi) veins. *Geoscience Canada*.
- Kocar, B. D., Borch, T., & Fendorf, S. (2010). Arsenic repartitioning during biogenic sulfidization and transformation of ferrihydrite. *Geochimica et Cosmochimica Acta*, 74(3), 980-994.
- Kock, D., & Schippers, A. (2008). Quantitative microbial community analysis of three different sulfidic mine tailing dumps generating acid mine drainage. *Applied and Environmental Microbiology*, 74(16), 5211–5219. <https://doi.org/10.1128/AEM.00649-08>.
- Koizumi, Y., Kojima, H., & Fukui, M. (2003a). Characterization of depth-related microbial community structure in lake sediment by denaturing gradient gel electrophoresis of amplified 16S rDNA and reversely transcribed 16S rRNA fragments. *FEMS Microbiology Ecology*, 46(2), 147–157. [https://doi.org/10.1016/S0168-6496\(03\)00212-5](https://doi.org/10.1016/S0168-6496(03)00212-5)
- Koizumi, Y., Takii, S., Nishino, M., & Nakajima, T. (2003b). Vertical distributions of sulfate-reducing bacteria and methane-producing archaea quantified by oligonucleotide probe hybridization in the profundal sediment of a mesotrophic lake. *FEMS Microbiology Ecology*, 44(1), 101-108.
- Konhauser, K. (2007). Introduction to Geomicrobiology. Oxford: Blackwell.

- Konhauser, K. O., Kappler, A., & Roden, E. E. (2011). Iron in microbial metabolisms. *Elements*, 7(2), 89-93.
- Kontak, D.K., & Smith, P.K. (1988). Meguma gold studies IV: chemistry of vein mineralogy. In: Report of Activities 1987 Part B: Nova Scotia Department of Mines and Energy, Mines and Minerals Branch, Report 88-1, 85-101.
- Korenevsky, A., & Beveridge, T. J. (2007). The surface physicochemistry and adhesiveness of *Shewanella* are affected by their surface polysaccharides. *Microbiology*, 153(6), 1872-1883.
- Korte, N. E., & Fernando, Q. (1991). A review of arsenic (III) in groundwater. *Critical Reviews in Environmental Science and Technology*, 21(1), 1-39.
- Kramer JR. (1996). Aqueous silver in the environment: Conceptual. *Argentum* 4:19–30.
- Krause, E., & Ettel, V. A. (1989). Solubilities and stabilities of ferric arsenate compounds. *Hydrometallurgy*, 22(3), 311-337.
- Kwong, Y. T. J., Beauchemin, S., Hossain, M. F., & Gould, W. D. (2007). Transformation and mobilization of arsenic in the historic Cobalt mining camp, Ontario, Canada. *Journal of Geochemical Exploration*, 92(2-3), 133-150.
- Laird, K. R., Das, B., & Cumming, B. F. (2014). Enrichment of uranium, arsenic, molybdenum, and selenium in sediment cores from boreal lakes adjacent to northern Saskatchewan uranium mines. *Lake and Reservoir Management*, 30(4), 344–357.
<https://doi.org/10.1080/10402381.2014.933987>
- Langmuir, D.A. (1999). Formation of scorodite in McClean Lake prototype tailings. Pers. Comm.

- Langner, H. W., & Inskeep, W. P. (2000). Microbial reduction of arsenate in the presence of ferrihydrite. *Environmental Science and Technology*, 34(15), 3131–3136.
- Li, L., Jia, R., Qu, Z., Li, T., Shen, W., & Qu, D. (2020). Coupling between nitrogen-fixing and iron (III)-reducing bacteria as revealed by the metabolically active bacterial community in flooded paddy soils amended with glucose. *Science of The Total Environment*, 716, 137056.
- Li, Y. Z., He, Y. L., Ohandja, D. G., Ji, J., Li, J. F., & Zhou, T. (2008). Simultaneous nitrification–denitrification achieved by an innovative internal-loop airlift MBR: Comparative study. *Bioresource Technology*, 99(13), 5867-5872.
- Liau, S. Y., Read, D. C., Pugh, W. J., Furr, J. R., & Russell, A. D. (1997). Interaction of silver nitrate with readily identifiable groups: Relationship to the antibacterial action of silver ions. *Lett. Appl. Microbiol.* 25, 279–283.
- Liermann, L. J., Kalinowski, B. E., Brantley, S. L., & Ferry, J. G. (2000). Role of bacterial siderophores in dissolution of hornblende. *Geochimica et Cosmochimica Acta*, 64(4), 587-602.
- Lievremont, D., Bertin, P. N., & Lett, M. C. (2009). Arsenic in contaminated waters: biogeochemical cycle, microbial metabolism and biotreatment processes. *Biochimie* 91, 1229–1237. doi: 10.1016/j.biochi.2009. 06.016
- Lindsay, M. B., Blowes, D. W., Condon, P. D., & Ptacek, C. J. (2009). Managing pore-water quality in mine tailings by inducing microbial sulfate reduction. *Environmental science & technology*, 43(18), 7086-7091.
- Little, A. J., Sivarajah, B., Frendo, C., Sprague, D. D., Smol, J. P., & Vermaire, J. C. (2020). The impacts of century-old, arsenic-rich mine tailings on multi-trophic level biological

- assemblages in lakes from Cobalt (Ontario, Canada). *Science of the Total Environment*, 709, 136212. <https://doi.org/10.1016/j.scitotenv.2019.136212>.
- Liu, J., Yao, J., Wang, F., Min, N., Gu, J., Li, Z., Sunahara, G., Duran, R., Solevic-Knudsen, T., Hudson-Edwards, & K., Alakangas, L. (2019a). Bacterial diversity in typical abandoned multi-contaminated nonferrous metal(loid) tailings during natural attenuation. *Environmental Pollution*, 247, 98–107. <https://doi.org/10.1016/j.envpol.2018.12.045>.
- Liu, J., Yao, J., Sunahara, G., Wang, F., Li, Z., & Duran, R. (2019b). Nonferrous metal(loid)s mediate bacterial diversity in an abandoned mine tailing impoundment. *Environmental Science and Pollution Research*, 26(24), 24806–24818. <https://doi.org/10.1007/s11356-019-05092-3>.
- Lloyd, J R. (2002). Bioremediation of metals; the application of microorganisms that make and break minerals. *Microbiology Today*, 29: 67–69
- Lloyd, J. R. (2003). Microbial reduction of metals and radionuclides. *FEMS Microbiol Rev* 27, 411–425.
- Lloyd, J. R., Lovley, D. R. & Macaskie, L. E. (2003). Biotechnological application of metal-reducing microorganisms. *Adv Appl Microbiol* 53, 85–128.
- Lombardi, A. T., & Garcia, O. (2002). Biological leaching of Mn, Al, Zn, Cu and Ti in an anaerobic sewage sludge effectuated by *Thiobacillus ferrooxidans* and its effect on metal partitioning. *Water Research*, 36(13), 3193–3202. [https://doi.org/10.1016/S0043-1354\(02\)00008-8](https://doi.org/10.1016/S0043-1354(02)00008-8).
- Lottermoser, B. G. (2007). Tailings. In: *Mine Wastes: Characterization, Treatment, Environmental Impacts*, 153-181. https://doi.org/10.1007/978-3-540-48630-5_4
- Lovely, D. R. (1993) Dissimilatory metal reduction. *Ann. Rev. Microbiol.* 47, 263-290.

- Lovley, D. R. (2013). Dissimilatory Fe(III)- and Mn (IV)- Reducing Prokaryotes. The Prokaryotes-Prokaryotic Physiology and Biochemistry, doi:10.1007/978-3-642-30141-4_69, Springer-Verlag Berlin Heidelberg.
- Lovley, D. R. (2000). *Environmental microbe-metal interactions*. ASM.
- Lu, A., Li, Y., & Jin, S. (2012). Interactions between semiconducting minerals and bacteria under light. *Elements*, 8(2), 125-130.
- Lu, X., & Wang, H. (2012). Microbial oxidation of sulfide tailings and the environmental consequences. *Elements*, 8(2), 119-124.
- Luoma, S. N. (1993). Bioavailability of silver to bivalves in estuaries. In *Proceedings* (pp. 8-10).
- Luoma, S. N., & Rainbow, P. S. (2008). Metal contamination in aquatic environments: science and lateral management. Cambridge university press.
- Luther III, G. W., Sundby, B., Lewis, B. L., Brendel, P. J., & Silverberg, N. (1997). Interactions of manganese with the nitrogen cycle: alternative pathways to dinitrogen. *Geochimica et Cosmochimica Acta*, 61(19), 4043-4052.
- Lv, C., Zhao, C., Yang, S., & Qu, Y. (2012). Arsenic metabolism in purple nonsulfur bacteria. *Wei sheng wu xue bao= Acta microbiologica Sinica*, 52(12), 1497.
- Lynch, J.J. (1990). Provisional elemental values for eight new geochemical lake sediment and stream sediment reference materials LKSD1, LKSD-2, LKSD-3, LKSD-4, STSD-1, STSD2, STSD-3 and STSD-4, *Geostandards Newsletter*, 14: 153-167.
- Ma, Y. Q., & Lin, C. X. (2012). Arsenate immobilization associated with microbial oxidation of ferrous ion in complex acid sulfate water. *Journal of Hazardous Materials*, 217, 238–245.

- Macur, R. E., Wheeler, J. T., McDermott, T. R., & Inskeep, W. P. (2001). Microbial populations associated with the reduction and enhanced mobilization of arsenic in mine tailings. *Environmental Science and Technology*, 35(18), 3676–3682.
<https://doi.org/10.1021/es0105461>
- Macy, J. M., Nunan, K., Hagen, K. D., Dixon, D. R., Harbour, P. J., Cahill, M., & Sly, L. I. (1996). *Chrysiogenes arsenatis* gen. nov., sp. nov., a new arsenate-respiring bacterium isolated from gold mine wastewater. *International Journal of Systematic and Evolutionary Microbiology*, 46(4), 1153-1157.
- Mailloux, B. J., Alexandrova, E., Keimowitz, A. R., Wovkulich, K., Freyer, G. A., Herron, M., ... & Dong, H. (2009). Microbial mineral weathering for nutrient acquisition releases arsenic. *Applied and Environmental Microbiology*, 75(8), 2558-2565.
- Majzlan, J., Lalinská, B., Chovan, M., Bläß, U., Brecht, B., Göttlicher, J., Steininger, R., Hug, K., Ziegler, & S., Gescher, J. (2011). A mineralogical, geochemical, and microbiological assessment of the antimony- and arsenic-rich neutral mine drainage tailings near Pezinok, Slovakia. *American Mineralogist*, 96(1), 1–13. <https://doi.org/10.2138/am.2011.3556>.
- Mammadov, K., Doutora, P., & Queiroz, A. M. (2016). Dephosphorization of Iron Ore through Bioleaching.
- Manceau, A., & Drits, V. A. (1993). Local structure of ferrihydrite and ferroxhyte by EXAFS spectroscopy. *Clay minerals*, 28(2), 165-184.
- Marquez, M. A., Ospina, J. D., & Morales, A. L. (2012). New insights about the bacterial oxidation of arsenopyrite: A mineralogical scope. *Minerals Engineering*, 39, 248–254.
- Marrero, J., Coto, O., Goldmann, S., Graupner, T., & Schippers, A. (2015). Recovery of nickel and cobalt from laterite tailings by reductive dissolution under aerobic conditions using

- Acidithiobacillus* species. *Environmental Science and Technology*, 49(11), 6674– 6682.
<https://doi.org/10.1021/acs.est.5b00944>
- Martinez-Villegas, N., Briones-Gallardo, R., Ramos-Leal, J. A., Avalos-Borja, M., Castanon-Sandoval, A. D., Razo-Flores, E., & Villalobos, M. (2013). Arsenic mobility controlled by solid calcium arsenates: A case study in Mexico showcasing a potentially widespread environmental problem. *Environmental Pollution*, 176,114–122.
- Masrahi, A., VandeVoort, A. R., & Arai, Y. (2014). Effects of silver nanoparticle on soil-nitrification processes. *Archives of environmental contamination and toxicology*, 66(4), 504-513.
- Mateos, L. M., Ordóñez, E., Letek, M., & Gil, J. A. (2006). *Corynebacterium glutamicum* as a model bacterium for the bioremediation of arsenic. *International Microbiology*, 9(3), 207–215.
- Matlakowska, R., Drewniak, L., & Sklodowska, A. (2008). Arsenic-hypertolerant *Pseudomonads* isolated from ancient gold and copper-bearing black shale deposits. *Geomicrobiology Journal*, 25(7–8), 357–362.
- Maurice, P. A., Haack, E. A., & Mishra, B. (2009). Siderophore sorption to clays. *Biometals*, 22(4), 649-658.
- Maurice, P. A., Lee, Y. J., & Hersman, L. E. (2000). Dissolution of Al-substituted goethites by an aerobic *Pseudomonas mendocina* var. bacteria. *Geochimica et Cosmochimica Acta*, 64(8), 1363-1374.
- Mayzlan, J., Drahota, P., & Filippi, M. (2014) Parageneses and Crystal Chemistry of Arsenic Minerals. *Reviews in Mineralogy and Geochemistry* 79, 17-184.

- McMurdie, P. J., & Holmes, S. (2013). phyloseq: an R package for reproducible interactive analysis and graphics of microbiome census data. *PloS one*, 8(4), e61217.
- Mehanna, M., Basseguy, R., Delia, M. L., Gubner, R., Sathirachinda, N., & Bergel, A. (2009). Geobacter species enhances pit depth on 304L stainless steel in a medium lacking with electron donor. *Electrochemistry communications*, 11(7), 1476-1481.
- Mehta, M. G. (2013). Metal reduction by Geothrix fermentans. Retrieved from the University of Minnesota Digital Conservancy, <http://hdl.handle.net/11299/158863>.
- Melton, E. D., Swanner, E. D., Behrens, S., Schmidt, C., & Kappler, A. (2014). The interplay of microbially mediated and abiotic reactions in the biogeochemical Fe cycle. *Nature Reviews Microbiology*, 12(12), 797-808.
- Mendez, M. O., Glenn, E. P., & Maier, R. M. (2007). Phytostabilization potential of quailbush for mine tailings: growth, metal accumulation, and microbial community changes. *Journal of Environmental Quality*, 36(1), 245-253.
- Meunier, L., Walker, S. R., Wragg, J., Parsons, M. B., Koch, I., Jamieson, H. E., & Reimer, K. J. (2010). Effects of soil composition and mineralogy on the bioaccessibility of arsenic from tailings and soil in gold mine districts of nova scotia. *Environmental Science and Technology*, 44(7), 2667–2674. <https://doi.org/10.1021/es9035682>
- Mielke, R. E., Pace, D. L., Porter, T., & Southam, G. (2003). A critical stage in the formation of acid mine drainage: Colonization of pyrite by Acidithiobacillus ferrooxidans under pH-neutral conditions. *Geobiology*, 1(1), 81-90.
- Mondal, P., Majumder, C. B., & Mohanty, B. (2008). Treatment of arsenic contaminated water in a batch reactor by using Ralstonia eutropha MTCC 2487 and granular activated carbon. *Journal of hazardous materials*, 153(1-2), 588-599.

- Morin, G., & Calas, G. (2006). Arsenic in soils, mine tailings, and former industrial sites. *Elements*, 2(2), 97–101. <https://doi.org/10.2113/gselements.2.2.97>.
- Mulligan, C. N., & Yong, R. N. (2004). Natural attenuation of contaminated soils. *Environment international*, 30(4), 587-601.
- Murray, J. W., & Dillard, J. G. (1979). The oxidation of cobalt (II) adsorbed on manganese dioxide. *Geochimica et Cosmochimica Acta*, 43(5), 781-787.
- MVRB (Mackenzie Valley Review Board). (2013). Report of Environmental Assessment and Reasons for Decision, Giant Mine Remediation Project. EA0809-001, 245 p, Retrieved from: http://reviewboard.ca/upload/project_document/EA0809-001_Giant_Report_of_Environmental_Assessment_June_20_2013.PDF
- Myagkaya, I. N., Lazareva, E. V., Gustaytis, M. A., & Zhmodik, S. M. (2016). Gold and silver in a system of sulfide tailings. Part 1: Migration in water flow. *Journal of Geochemical Exploration*, 160, 16-30.
- Neilands, J. B. (1981). Microbial iron compounds. *Annual review of biochemistry*, 50(1), 715-731.
- Natural Resources Canada. (1998). Canadian U Statistics Fact Sheet. Natural Resources Canada, U and Radioactive Waste Division, Energy Resources Branch.
- Neumann, T., Scholz, F., Kramar, U., Ostermaier, M., Rausch, N., & Berner, Z. (2013). Arsenic in framboidal pyrite from recent sediments of a shallow water lagoon of the Baltic Sea. *Sedimentology*, 60(6), 1389-1404.
- Newman, D. K. (2001). How bacteria respire minerals. *Science*, 292(5520), 1312-1313.

- Newman, D. K., Kennedy, E. K., Coates, J. D., Ahmann, D., Ellis, D. J., Lovley, D. R., & Morel, F. M. M. (1997b). Dissimilatory arsenate and sulfate reduction in *Desulfotomaculum auripigmentum* sp. nov. *Archives of Microbiology*, 168(5), 380–388.
- Newsome, L., Solano Arguedas, A., Coker, V. S., Boothman, C., & Lloyd, J. R. (2020). Manganese and cobalt redox cycling in laterites; Biogeochemical and bioprocessing implications. *Chemical Geology*, 531(October 2019), 119330.
<https://doi.org/10.1016/j.chemgeo.2019.119330>.
- Nielsen, L. P., Risgaard-Petersen, N., Fossing, H., Christensen, P. B., & Sayama, M. (2010). Electric currents couple spatially separated biogeochemical processes in marine sediment. *Nature*, 463(7284), 1071-1074.
- Nies, D. H. (1999). Microbial heavy-metal resistance. *Appl Microbiol Biotechnol* 51, 730–750.
- Niggemyer, A., Spring, S., Stackebrandt, E., & Rosenzweig, R. F. (2001). Isolation and characterization of a novel As (V)-reducing bacterium: implications for arsenic mobilization and the genus *Desulfitobacterium*. *Applied and Environmental Microbiology*, 67(12), 5568-5580.
- Nordstrom, D. K. (2000). An overview of arsenic mass poisoning in Bangladesh and West Bengal, India. *Minor elements*, 21-30.
- Nordstrom, D. K., Majzlan, J., & Königsberger, E. (2014). Thermodynamic properties for arsenic minerals and aqueous species. *Reviews in Mineralogy and Geochemistry*, 79(1), 217-255.
- Norton, J. M., Klotz, M. G., Stein, L. Y., Arp, D. J., Bottomley, P. J., Chain, P. S. G., ... Starkenburg, S. R. (2008). Complete genome sequence of *Nitrosospira multiformis*, an

- ammonia-oxidizing bacterium from the soil environment. *Applied and Environmental Microbiology*, 74(11), 3559–3572. <https://doi.org/10.1128/AEM.02722-07>
- Nyombolo, B. M., Neale, J. W., & van Staden, P. J. (2000). Neutralization of bioleach liquors. *Journal of the South African Institute of Mining and Metallurgy*, 100(7), 403–408.
- Oberdorster, G., Oberdorster, E., & Oberdorster, J. (2005). Nanotoxicology: An emerging discipline evolving from studies of ultrafine particles. *Environ. Health Perspect.* 113, 823–839.
- Oksanen, J., Blanchet, F., Friendly, M., Kindt, R., Legendre, P., McGlenn, D., Minchin, P., O'Hara, R.B., Simpson, G., Solymos, P., Stevens, M.H.H., Szoecs, E., & Wagner, H. (2019, September 1). *Package 'vegan'*. Retrieved July 23, 2020, from <https://cran.r-project.org/web/packages/vegan/vegan.pdf>.
- Ontario Ministry of the Environment. (2011). *Final Report: Cobalt-Coleman Mining Camp Soil Assessment*. Retrieved from: <https://collections.ola.org/mon/25010/313445.pdf>
- Ordóñez, E., Letek, M., Valbuena, N., Gil, J. A., & Mateos, L. M. (2005). Analysis of genes involved in arsenic resistance in *Corynebacterium glutamicum* ATCC 13032. *Applied and environmental microbiology*, 71(10), 6206-6215.
- Oremland, R. S., & Stolz, J. F. (2005). Arsenic, microbes and contaminated aquifers. *Trends in microbiology*, 13(2), 45-49.
- Oremland, R. S., Saltikov, C. W., Wolfe-Simon, F., & Stolz, J. F. (2009). Arsenic in the evolution of earth and extraterrestrial ecosystems. *Geomicrobiology Journal*, 26(7), 522-536.
- Páez-Espino, D., Tamames, J., de Lorenzo, V., & Cánovas, D. (2009). Microbial responses to environmental arsenic. *Biometals*, 22(1), 117-130.

- Paktunc, D., Foster, A., & Laflamme, G. (2003). Speciation and Characterization of Arsenic in Ketz River Mine Tailings Using X-ray Absorption Spectroscopy. *Geochimica et Cosmochimica Acta*, 68(5), 969–983. <https://doi.org/10.1016/j.gca.2003.07.013>.
- Paktunc, D., Foster, A., Heald, S., & Laflamme, G. (2004). Speciation and characterization of arsenic in gold ores and cyanidation tailings using X-ray absorption spectroscopy. *Geochimica et Cosmochimica Acta*, 68(5), 969–983. <https://doi.org/10.1016/j.gca.2003.07.013>
- Paktunc, D., Thibault, Y., & Weisener, C. (2015). Sulfide oxidation and mobilization of arsenic in the Ketz River Mine tailings. *Proceedings of the 10th International Congress for Applied Mineralogy (ICAM)*. (M. A. T. M. Broekmans, Ed.) (Vol. 3). Springer-Verlag Berlin Heidelberg. https://doi.org/10.1007/978-3-642-27682-8_60. p. 503-511.
- Pandey, V. C., Singh, J. S., Singh, D. P., & Singh, R. P. (2014). Methanotrophs: promising bacteria for environmental remediation. *International Journal of Environmental Science and Technology*, 11(1), 241-250.
- Papirio, S., Zou, G., Ylinen, A., Di Capua, F., Pirozzi, F., & Puhakka, J. A. (2014). Effect of arsenic on nitrification of simulated mining water. *Bioresource technology*, 164, 149-154.
- Parada, A. E., Needham, D. M., & Fuhrman, J. A. (2016). Every base matters: Assessing small subunit rRNA primers for marine microbiomes with mock communities, time series and global field samples. *Environmental Microbiology*, 18(5), 1403–1414. <https://doi.org/10.1111/1462-2920.13023>.
- Park, J. E., Lee, B. T., Kim, B. Y., & Son, A. (2018). Bacterial community analysis of stabilized soils in proximity to an exhausted mine. *Environmental Engineering Research*, 23(4), 420–429. <https://doi.org/10.4491/eer.2018.040>

- Parkes, R. J. (1998). JH Banfield and KH Nealson (Eds.) Geomicrobiology: Interactions between Microbes and Minerals. Washington. (Mineralogical Society of America: Reviews in Mineralogy Vol 35), 1997, 448 pp. ISBN 0-939950-43-X. *Mineralogical Magazine*, 62(5), 725-726.
- Patterson, J. P. E. (1938). Some observations on a disease of sheep on Dartmoor. *Empire Journal of Experimental Agriculture*, 6, 262-267.
- Percival, J.B., Kwong, Y.T.J., Dumaresq, C.G., & Michel, F.A. (2004) Transport and attenuation of arsenic, cobalt and nickel in an alkaline environment (Cobalt, Ontario) Geological Survey of Canada Open File 1680.
- Pettit, C. M., Scharer, J. M., Chambers, D. B., Halbert, B. E., Kirkaldy, J. L., & Bolduc, L. (1999). Neutral mine drainage. *Proceedings of Mining and the Environment, Sudbury, Canada*, 829-838.
- Piret, N.L. (1999). Arsenic Management in Copper Smelting. In: *Copper 99-Cobre 99*, Volume II: Mineral Processing/Environment, Health and Safety, 321-340.
- Porwal, S., Lal, S., Cheema, S., & Kalia, V. C. (2009). Phylogeny in aid of the present and novel microbial lineages: diversity in Bacillus. *PLoS One*, 4(2), e4438.
- Praharaj, T., & Fortin, D. (2008). Seasonal variations of microbial sulfate and iron reduction in alkaline Pb–Zn mine tailings (Ontario, Canada). *Applied Geochemistry*, 23(12), 3728-3740.
- Prosser, J. I., Head, I. M., & Stein, L. Y. (2013). The Family Nitrosomonadaceae. In E. Rosenberg (Ed.), *The Prokaryotes: Alphaproteobacteria and Betaproteobacteria* (pp. 901–918). Springer-Verlag Berlin Heidelberg.
<https://doi.org/10.1007/978-3-642-30197-1>.

- Purcell, T. W., & Peters, J. J. (1998). Sources of silver in the environment. *Environmental Toxicology and Chemistry*, 17(4), 539–546.
[https://doi.org/10.1897/15515028\(1998\)017<0539:SOSITE>2.3.CO;2](https://doi.org/10.1897/15515028(1998)017<0539:SOSITE>2.3.CO;2)
- Quast, C., Pruesse, E., Yilmaz, P., Gerken, J., Schweer, T., Yarza, P., Peplies, J., & Glöckner, F. O. (2012). The SILVA ribosomal RNA gene database project: improved data processing and web-based tools. *Nucleic acids research*, 41(D1), D590-D596.
- R Core Team. (2018). R: A Language and Environment for Statistical Computing (Version 3.5.2, R Foundation for Statistical Computing, Vienna, Austria, 2018).
- Rabus, R., Hansen, T. A., & Widdel, F. (2006). Dissimilatory sulfate- and sulfur-reducing prokaryotes. *The prokaryotes*, 2, 659-768.
- Rajoka, M. S. R., Mehwish, H. M., Zhang, H., Ashraf, M., Fang, H., Zeng, X., ... & He, Z. (2020). Antibacterial and antioxidant activity of exopolysaccharide mediated silver nanoparticle synthesized by *Lactobacillus brevis* isolated from Chinese koumiss. *Colloids and Surfaces B: Biointerfaces*, 186, 110734.
- Ravenschlag, K., Sahm, K., Knoblauch, C., Jørgensen, B. B., & Amann, R. (2000). Community structure, cellular rRNA content, and activity of sulfate-reducing bacteria in marine Arctic sediments. *Applied and Environmental Microbiology*, 66(8), 3592-3602.
- Rawlings, D. E. (2007). *Biomining* (p. 314). D. B. Johnson (Ed.). Berlin: Springer.
- Raza, W., & Shen, Q. (2010). Growth, Fe³⁺ reductase activity, and siderophore production by *Paenibacillus polymyxa* SQR-21 under differential iron conditions. *Current microbiology*, 61(5), 390-395.
- Reich, M., Kesler, S., Utsunomiya, S., Palenik, S., Chryssoulis, S. L. (2005). Solubility of gold in arsenian pyrite. *Geochim Cosmochim Acta*, 69, 2781–2796

- Revesz, E., Fortin, D., & Paktunc, D. (2015). Reductive dissolution of scorodite in the presence of *Shewanella* sp. CN32 and *Shewanella* sp. ANA-3. *Applied Geochemistry*, *63*, 347-356.
- Riveros, P. A., Dutrizac, J. E., & Spencer, P. (2001). Arsenic disposal practices in the metallurgical industry. *Canadian Metallurgical Quarterly*, *40*(4), 395–420.
<https://doi.org/10.1179/cmq.2001.40.4.395>
- Roberts, J. A., Fowle, D. A., Hughes, B. T., & Kulczycki, E. (2006). Attachment behavior of *Shewanella putrefaciens* onto magnetite under aerobic and anaerobic conditions. *Geomicrobiology Journal*, *23*(8), 631-640.
- Roden, E. E., Sobolev, D., Glazer, B., & Luther, G. W. (2004). Potential for microscale bacterial Fe redox cycling at the aerobic-anaerobic interface. *Geomicrobiology Journal*, *21*(6), 379-391.
- Rohwerder, T., Gehrke, T., Kinzler, K., & Sand, W. (2003). Bioleaching review part A: Progress in bioleaching: Fundamentals and mechanisms of bacterial metal sulfide oxidation. *Applied Microbiology and Biotechnology*, *63*(3), 239–248.
<https://doi.org/10.1007/s00253-003-1448-7>.
- Rousk, J., Bååth, E., Brookes, P. C., Lauber, C. L., Lozupone, C., Caporaso, J. G., ... & Fierer, N. (2010). Soil bacterial and fungal communities across a pH gradient in an arable soil. *The ISME journal*, *4*(10), 1340-1351.
- Russell, H., & Hugo, W. B. (1994). Antimicrobial activity and action of silver. *Prog. Med. Chem.* *31*, 351–370.
- Ryan, R. J., & Smith, P. K. (1998). A review of the mesothermal gold deposits of the Meguma Group, Nova Scotia, Canada. *Ore Geology Reviews*, *13*(1-5), 153-183.

- Sá-Pereira, P., Rodrigues, M., e Castro, I. V., & Simoes, F. (2007). Identification of an arsenic resistance mechanism in rhizobial strains. *World Journal of Microbiology and Biotechnology*, 23(10), 1351-1356.
- Saalfeld, S. L., & Bostick, B. C. (2009). Changes in iron, sulfur, and arsenic speciation associated with bacterial sulfate reduction in ferrihydrite-rich systems. *Environmental Science & Technology*, 43(23), 8787-8793.
- Saari, P., & Riekkola-Vanhanen, M. (2012). Talvivaara bioheapleaching process. *Journal of the Southern African Institute of Mining and Metallurgy*, 112(12), 1013-1020.
- Sahm, K., MacGregor, B. J., Jørgensen, B. B., & Stahl, D. A. (1999). Sulphate reduction and vertical distribution of sulphate-reducing bacteria quantified by rRNA slot-blot hybridization in a coastal marine sediment. *Environmental Microbiology*, 1(1), 65-74.
- Saini, G., & Chan, C. S. (2013). Near-neutral surface charge and hydrophilicity prevent mineral encrustation of Fe-oxidizing micro-organisms. *Geobiology*, 11(2), 191–200.
<https://doi.org/10.1111/gbi.12021>
- Santini, J. M., Sly, L. I., Schnagl, R. D., & Macy, J. M. (2000). A new chemolithoautotrophic arsenite-oxidizing bacterium isolated from a gold mine: phylogenetic, physiological, and preliminary biochemical studies. *Applied and Environmental Microbiology*, 66(1), 92–97.
- Satola, B., Wübbeler, J. H., & Steinbüchel, A. (2013). Metabolic characteristics of the species *Variovorax paradoxus*. *Applied microbiology and biotechnology*, 97(2), 541-560.
- Satyanarayan, T., Littlechild, J., and Kawarabayasi, Y. (2013) Thermophilic microbes in environmental and industrial biotechnology: Biotechnology of thermophiles. DOI 10.1007/978-94-007-5899-5, Springer Science+Business Media Dordrecht.

- Sawayama, S. (2006). Possibility of anoxic ferric ammonium oxidation. *Journal of bioscience and bioengineering*, 101(1), 70-72.
- Schäfer, G. (2013). Membrane-associated energy transduction in bacteria and archaea.
- Schindler, M., & Hochella Jr, M. F. (2016). Nanomineralogy as a new dimension in understanding elusive geochemical processes in soils: The case of low-solubility-index elements. *Geology*, 44(7), 515-518.
- Schindler, M., Durocher, J. L., Kotzer, T. G., & Hawthorne, F. C. (2013). Uranium-bearing phases in a U-mill disposal site in Northern Canada: Products of the interaction between leachate/raffinate and tailings material. *Applied Geochemistry*, 29, 151–161.
<https://doi.org/10.1016/j.apgeochem.2012.11.007>
- Schröder, I., Johnson, E. & de Vries, S. (2003). Microbial ferric iron reductases. *FEMS Microbiol Rev* 27, 427–447.
- Schwertmann, U., & Murad, E. (1983). Effect of pH on the formation of goethite and hematite from ferrihydrite. *Clays and Clay Minerals*, 31(4), 277-284.
- Scow, K., Goyer, M., Nelken, L., Cruse, P., & Moss, K. (1981). Exposure and risk assessment for silver.
- Seith, R., & Jekel, M. (1997). Biooxidation of arsenic (III) in fixed bed reactors; Biologische Oxidation von Arsenat (III) in Festbettreaktoren.
- Shannon, R. D. (1976). Revised effective ionic radii and systematic studies of interatomic distances in halides and chalcogenides. *Acta crystallographica section A: crystal physics, diffraction, theoretical and general crystallography*, 32(5), 751-767.
- Shaw, S. A., Hendry, M. J., Essilfie-Dughan, J., Kotzer, T., & Wallschläger, D. (2011). Distribution, characterization, and geochemical controls of elements of concern in

- uranium mine tailings, Key Lake, Saskatchewan, Canada. *Applied Geochemistry*, 26(12), 2044–2056. <https://doi.org/10.1016/j.apgeochem.2011.07.002>
- Sheik, C. S., Mitchell, T. W., Rizvi, F. Z., Rehman, Y., Faisal, M., Hasnain, S., McInerney, M., Krumholz, L. R. (2012). Exposure of soil microbial communities to chromium and arsenic alters their diversity and structure. *PLoS ONE*, 7(6). <https://doi.org/10.1371/journal.pone.0040059>.
- Shi, L. D., Chen, Y. S., Du, J. J., Hu, Y. Q., Shapleigh, J. P., & Zhao, H. P. (2019). Metagenomic evidence for a *Methylocystis* species capable of bioremediation of diverse heavy metals. *Frontiers in Microbiology*, 10(JAN), 1–10. <https://doi.org/10.3389/fmicb.2018.03297>.
- Shrestha, J., Rich, J. J., Ehrenfeld, J. G., & Jaffe, P. R. (2009). Oxidation of ammonium to nitrite under iron-reducing conditions in wetland soils: Laboratory, field demonstrations, and push-pull rate determination. *Soil science*, 174(3), 156-164.
- Simanova, A.A., & Peña, J., 2015. Time-resolved investigation of cobalt oxidation by Mn (III)-rich δ -MnO₂ using quick X-ray absorption spectroscopy. *Environ. Sci. Technol.* 49, 10867- 10876.
- Simon, G., Huang, H., Penner-Hahn, J. E., Kesler, S. E., & Kao, L. S. (1999). Oxidation state of gold and arsenic in gold-bearing arsenian pyrite. *American Mineralogist*, 84(7-8), 1071-1079.
- Singh, R. L. (2016). *Principles and Applications of Environmental Biotechnology for a Sustainable Future*. Springer Nature. <https://doi.org/10.1007/978-981-10-1866-4>.
- Slack, J., Kimball, B. E., & Shedd, K. B. (2017). Cobalt. In *Critical Mineral Resources of the United States - Economic and Environmental Geology and Prospects for Future Supply* (pp. F1–F40). <https://doi.org/https://doi.org/10.3133/pp1802F>.

- Smedley, P. L., & Kinniburgh, D. G. (2002). A review of the source, behaviour and distribution of arsenic in natural waters. *Applied Geochemistry*, 17(5), 517–568.
- Smith, I., & Carson, B. (1997). *Silver*. Ann Arbor Science Publishers, Ann Arbor, Michigan.
- Smith, R. M., & Martell, A. E. (1977). Critical stability constants, Vol. 3. Other organic ligands. *Plenum Press*, 365, 161.
- Soprovich, E. A. (2000). Arsenic release from oxide tailings containing scorodite, Fe-Ca arsenates and As containing goethites. *Tailings and Mine Waste 2000*, 277-287.
- Southam, G., & Beveridge, T. J. (1992). Enumeration of thiobacilli within pH-neutral and acidic mine tailings and their role in the development of secondary mineral soil. *Applied and Environmental Microbiology*, 58(6), 1904-1912.
- Stiefel, E. I. (1996). Transition metal sulfur chemistry: Biological and industrial significance and key trends.
- Stolz, J. F., Basu, P., & Oremland, R. S. (2002). Microbial transformation of elements: The case of arsenic and selenium. *International Microbiology*, 5,201–207.
- Stonehouse, H. B. (1954). An association of trace elements and mineralization at Sudbury*. *American Mineralogist*, 39(5–6), 452–474.
- Styblo, M., Del Razo, L. M., Vega, L., Germolec, D. R., LeCluyse, E. L., Hamilton, G. A., ... & Thomas, D. J. (2000). Comparative toxicity of trivalent and pentavalent inorganic and methylated arsenicals in rat and human cells. *Archives of toxicology*, 74(6), 289-299.
- Suhadolnik, M. L., Salgado, A. P., Scholte, L. L., Bleicher, L., Costa, P. S., Reis, M. P., ... & Nascimento, A. M. (2017). Novel arsenic-transforming bacteria and the diversity of their arsenic-related genes and enzymes arising from arsenic-polluted freshwater sediment. *Scientific reports*, 7(1), 1-17.

- Sun, W., Su, J. F., Zhang, G., & Hu, Y. H. (2012). Separation of sulfide lead-zinc-silver ore under low alkalinity condition. *Journal of Central South University*, 19(8), 2307-2315.
- Sun, W., Xiao, E., Dong, Y., Tang, S., Krumins, V., Ning, Z., ... & Xiao, T. (2016). Profiling microbial community in a watershed heavily contaminated by an active antimony (Sb) mine in Southwest China. *Science of the Total Environment*, 550, 297-308.
- Swash, P. M., & Monhemius, A. J. (1995, May). Synthesis, characterisation and solubility testing of solids in the Ca-Fe-AsO₄ system. In Sudbury'95, Conference on Mining and the Environment, Sudbury, Ontario (Vol. 28).
- Talavera Mendoza, O., Yta, M., Moreno Tovar, R., Dótor Almazán, A., Flores Mundo, N., & Duarte Gutiérrez, C. (2005). Mineralogy and geochemistry of sulfide-bearing tailings from silver mines in the Taxco, Mexico area to evaluate their potential environmental impact. *Geofísica internacional*, 44(1), 49-64.
- Tanaka, K., Yu, Q., Sasaki, K., & Ohnuki, T. (2013). Cobalt (II) oxidation by biogenic Mn oxide produced by *Pseudomonas* sp. strain NGY-1. *Geomicrobiology Journal*, 30(10), 874-885.
- Tapley, B., & Yan, D. (2003). The selective flotation of arsenopyrite from pyrite. *Minerals engineering*, 16(11), 1217-1220.
- The Cobalt Institute. (2019). The Cobalt Institute. Webpage. Available at: <https://www.cobaltinstitute.org/> (Accessed June 28, 2020).
- Tóth, E. M., & Borsodi, A. K. (2014). The Family Nocardioideae. In E. Rosenberg (Ed.), *The Prokaryotes: Actinobacteria* (pp. 651–694). <https://doi.org/10.1007/978-3-642-30138-4>
- Tourtelot, H. A. (1964). Minor-element composition and organic carbon content of marine and nonmarine shales of Late Cretaceous age in the western interior of the United States. *Geochimica et Cosmochimica Acta*, 28(10-11), 1579-1604.

- Valenzuela, A. (2000). *Arsenic management in the metallurgical industry* (Doctoral dissertation, Université Laval).
- van Grinsven, S., Sinnighe Damsté, J. S., Abdala Asbun, A., Engelmann, J. C., Harrison, J., & Villanueva, L. (2020). Methane oxidation in anoxic lake water stimulated by nitrate and sulfate addition. *Environmental Microbiology*, 22(2), 766–782.
<https://doi.org/10.1111/1462-2920.14886>
- VandeVoort, A. R., & Arai, Y. (2012). *Environmental chemistry of silver in soils. Current and historic perspective. Advances in Agronomy* (1st ed., Vol. 114). Elsevier Inc.
<https://doi.org/10.1016/B978-0-12-394275-3.00005-5>.
- Vhay, J.S. (1952). Cobalt resources, Chap. 6 of Materials Survey-Cobalt: U.S. Bureau of Mines.
- Vink, B.W., 1996. Stability relations of antimony and arsenic compounds in light of revised and extended Eh–pH diagrams. *Chemical Geology* 130, 21–30.
- von Pechmann, E. (1981). Mineralogy of the Key Lake U–Ni orebodies, Saskatchewan, Canada; evidence for their formation by hypogene hydrothermal processes. In *Geology of Uranium Deposits: Proceedings of the CIM-SEG Uranium Symposium* (p. 27). September.
- Wakelin, S. A., Anand, R. R., Reith, F., Gregg, A. L., Noble, R. R. P., Goldfarb, K. C., Andersen, G. L., DeSantis, T. Z., Piceno, Y. M., & Brodie, E. L. (2012). Bacterial communities associated with a mineral weathering profile at a sulphidic mine tailings dump in arid Western Australia. *FEMS Microbiology Ecology*, 79(2), 298–311.
<https://doi.org/10.1111/j.1574-6941.2011.01215.x>.
- Walker, S. R., Jamieson, H. E., Lanzirotti, A., Hall, G. E. M., & Peterson, R. C. (2015). The effect of ore roasting on arsenic oxidation state and solid phase speciation in gold mine

- tailings. *Geochemistry: Exploration, Environment, Analysis*, 15(4), 273–291.
<https://doi.org/10.1144/geochem2013-238>
- Walker, S. R., Parsons, M. B., Jamieson, H. E., & Lanzirotti, A. (2009). Arsenic mineralogy of near-surface tailings and soils: Influences on arsenic mobility and bioaccessibility in the nova scotia gold mining districts. *Canadian Mineralogist*, 47(3), 533–556.
<https://doi.org/10.3749/canmin.47.3.533>
- Walsh, A., & Watson, G. W. (2005). The origin of the stereochemically active Pb(II) lone pair: DFT calculations on PbO and PbS. *Journal of Solid State Chemistry*, 178(5), 1422–1428.
<https://doi.org/10.1016/j.jssc.2005.01.030>
- Walsh, A., Payne, D. J., Egdell, R. G., & Watson, G. W. (2011). Stereochemistry of post-transition metal oxides: Revision of the classical lone pair model. *Chemical Society Reviews*, 40(9), 4455–4463. <https://doi.org/10.1039/c1cs15098g>
- Wang, S., & Mulligan, C. N. (2006). Occurrence of arsenic contamination in Canada: Sources, behavior and distribution. *Science of the Total Environment*, 366(2–3), 701–721.
<https://doi.org/10.1016/j.scitotenv.2005.09.005>
- Watanabe, T., Miura, A., Iwata, T., Kojima, H., & Fukui, M. (2017). Dominance of Sulfuritalea species in nitrate-depleted water of a stratified freshwater lake and arsenate respiration ability within the genus. *Environmental microbiology reports*, 9(5), 522-527.
- Weeks, T., & Wan, R.Y. (2000). Behaviour of Arsenic in Refractory Gold Ore Processing - a Case Study of PT Newmont Minahasa Raya. *Minor Elements 2000*, C.A. Young (editor), 125-133.
- Weisener, C. G., Guthrie, J. W., Smeaton, C. M., Paktunc, D., & Fryer, B. J. (2011). The effect of ca-fe-as coatings on microbial leaching of metals in arsenic bearing mine waste.

- Journal of Geochemical Exploration*, 110(1), 23–30.
- <https://doi.org/10.1016/j.gexplo.2011.03.004>
- Weiss, J. V., Emerson, D., Backer, S. M., & Megonigal, J. P. (2003). Enumeration of Fe (II)-oxidizing and Fe (III)-reducing bacteria in the root zone of wetland plants: implications for a rhizosphere iron cycle. *Biogeochemistry*, 64(1), 77-96.
- Welch, S. A., Barker, W. W., & Banfield, J. F. (1999). Microbial extracellular polysaccharides and plagioclase dissolution. *Geochimica et Cosmochimica Acta*, 63(9), 1405-1419.
- Wickham, H. (2016). *ggplot2: elegant graphics for data analysis*. springer.
- Wickham, H., François, R., Henry, L., & Müller, K. (2018). *dplyr: A grammar of data manipulation*, R package version 0.7. 6 [Computer software manual].
- Wigginton, N. S., de Titta, A., Piccapietra, F., Dobias, J., Nesatyy, V. J., Suter, M. J. F., & Bernier-Latmani, R. (2010). Binding of silver nanoparticles to bacterial proteins depends on surface modifications and inhibits enzymatic activity. *Environ. Sci. Technol.* 44, 2163–2168.
- Wilson, M. A., Burt, R., & Lee, C. W. (2006). Improved elemental recoveries in soils with heating boric acid following microwave total digestion. *Communications in soil science and plant analysis*, 37(3-4), 513-524.
- Wilson, S. C., Lockwood, P. V., Ashley, P. M., & Tighe, M. (2010). The chemistry and behaviour of antimony in the soil environment with comparisons to arsenic: a critical review. *Environmental pollution*, 158(5), 1169-1181.
- Wong-Pinto, L. S., Menzies, A., & Ordóñez, J. I. (2020). Bionanominating: biotechnological synthesis of metal nanoparticles from mining waste—opportunity for sustainable

- management of mining environmental liabilities. *Applied Microbiology and Biotechnology*, 104(5), 1859-1869.
- Xiao, E., Krumins, V., Xiao, T., Dong, Y., Tang, S., Ning, Z., ... Sun, W. (2017). Depth-resolved microbial community analyses in two contrasting soil cores contaminated by antimony and arsenic. *Environmental Pollution*, 221, 244–255.
<https://doi.org/10.1016/j.envpol.2016.11.071>
- Xingyu, L., Biao, W., Bowei, C., Jiankang, W., Renman, R., Guocheng, Y., & Dianzuo, W. (2010). Bioleaching of chalcocite started at different pH: Response of the microbial community to environmental stress and leaching kinetics. *Hydrometallurgy*, 103(1-4), 1-6.
- Yan, L., Yin, H. H., Zhang, S., Leng, F. F., Nan, W. B., & Li, H. Y. (2010). Biosorption of inorganic and organic arsenic from aqueous solution by *Acidithiobacillus ferrooxidans* BY-3. *Journal of Hazardous Materials*, 178(1–3), 209–217.
- Yang, W. H., Weber, K. A., & Silver, W. L. (2012). Nitrogen loss from soil through anaerobic ammonium oxidation coupled to iron reduction. *Nature Geoscience*, 5(8), 538-541.
- Yang, Y., Ferrier, J., Csetenyi, L., & Gadd, G. M. (2019). Direct and indirect bioleaching of cobalt from low grade laterite and pyritic ores by *Aspergillus niger*. *Geomicrobiology Journal*, 36(10), 940-949.
- Yazdi, S. R., Agrawal, P., Morales, E., Stevens, C. A., Oropeza, L., Davies, P. L., Escobedo, C., & Oleschuk, R. D. (2019). Facile actuation of aqueous droplets on a superhydrophobic surface using magnetotactic bacteria for digital microfluidic applications. *Analytica Chimica Acta*, 1085, 107-116.

- Young, R. S. (1957). The geochemistry of cobalt. *Geochimica et Cosmochimica Acta*, 13(1), 28–41. [https://doi.org/10.1016/0016-7037\(57\)90056-X](https://doi.org/10.1016/0016-7037(57)90056-X)
- Young, R. S. (1979). *Cobalt in biology and biochemistry*. Academic Press.
- YSI Environmental. (2005). *Measuring ORP on YSI 6-Series Sondes: Tips, Cautions and Limitations*. Retrieved from the YSI Environmental website:
<https://www.yei.com/File%20Library/Documents/Technical%20Notes/T608-Measuring-ORP-on-YSI-6-Series-Sondes-Tips-Cautions-and-Limitations.pdf>
- Zacarias-Estrada, O. L., Ballinas-Casarrubias, L., Montero-Cabrera, M. E., Loreda-Portales, R., Orrantia-Borunda, E., & Luna-Velasco, A. (2020). Arsenic removal and activity of a sulfate reducing bacteria-enriched anaerobic sludge using zero valent iron as electron donor. *Journal of hazardous materials*, 384, 121392.
- Zampella, G., Neupane, K. P., De Gioia, L., & Pecoraro, V. L. (2012). The importance of stereochemically active lone pairs for influencing PbII and AsIII protein binding. *Chemistry - A European Journal*, 18(7), 2040–2050.
<https://doi.org/10.1002/chem.201102786>
- Zhang, J. H., Zhang, X., Ni, Y. Q., Yang, X. J., & Li, H. Y. (2007). Bioleaching of arsenic from medicinal realgar by pure and mixed cultures. *Process Biochemistry*, 42(9), 1265–1271.
- Zhang, R., Hedrich, S., Römer, F., Goldmann, D., & Schippers, A. (2020). Bioleaching of cobalt from Cu/Co-rich sulfidic mine tailings from the polymetallic Rammelsberg mine, Germany. *Hydrometallurgy*. <https://doi.org/10.1016/j.ijbiomac.2020.06.291>
- Zhao, H., Wang, J., Gan, X., Hu, M., Zhang, E., Qin, W., & Qiu, G. (2015). Cooperative bioleaching of chalcopyrite and silver-bearing tailing by mixed moderately thermophilic

culture: An emphasis on the chalcopyrite dissolution with XPS and electrochemical analysis. *Minerals Engineering*, 81, 29-39.

Zobrist, J., Dowdle, P. R., Davis, J. A., & Oremland, R. S. (2000). Mobilization of arsenite by dissimilatory reduction of adsorbed arsenate. *Environmental Science and Technology*, 34(22), 4747–4753. <https://doi.org/10.1021/es001068h>

Appendix A: The mineralogy and geochemistry of Cobalt-bearing mine tailings in North-Eastern Ontario, Canada (Courchesne et al., 2020).

The mineralogy and geochemistry of Cobalt-bearing mine tailings in North-Eastern Ontario, Canada

Brittaney Courchesne¹, Michael Schindler^{*2}, Aaron J. Lussier³ and Nadia Mykytczuk¹

1. School of the Environment, Laurentian University, Sudbury, ON, Canada, P3E, 2C6
2. Department of Geological Sciences, University of Manitoba, Winnipeg, MB, Canada
R3T2N2
3. Canadian Museum of Nature, Minerals Sciences Division. P.O. Box 3443, Station D,
Ottawa, ON, Canada, K1P 6P4

*corresponding author: Michael.schindler@umanitoba.ca

ABSTRACT

The growing demand of cobalt in electric car batteries requires an evaluation of biomining as a potential method for extracting it from existing mine tailings. The mine tailings at the Cobalt Mining Camp in Northeastern Ontario, Canada, contain elevated Co concentration with up to 3.5 wt% Co. The potential biomining of this element demands a thorough understanding of the geochemical, mineralogical and microbiological features within the heterogenous tailing material at the Cobalt Mining Camp. In this first contribution, previously unrecognized mineralogical-geochemical relationships at two tailing sites of the Cobalt Mining Camp are presented. Sixty-samples from two depth profiles (0-30 cm; i.e., one sample per centimeter) are collected at two tailings sites (sites A and B) and are characterized for their major and minor chemical elements. Mineralogical features at the centimeter-, micrometer- and nanometer-scale are characterized in selected samples using powder X-ray diffraction, scanning electron microscopy, transmission electron microscopy, and the focused ion beam technique. The tailing material at both sites is predominantly composed of minerals of the amphibole, chlorite and feldspar groups as well as carbonates (calcite and dolomite). Minor phases are Fe-Co-Ni-Zn-sulfarsenides and -arsenates. The tailings material at site B contains on average higher concentrations of As, Co, Sb and Zn and lower concentrations of Fe than the material at site A. The alteration of primary sulfarsenides to secondary arsenates is accompanied by an enrichment in As, Co, Sb and Zn (increase in Co#) and depletion in Fe (decrease in Fe#) in tailings material at both sites. Nano-mineralogical studies indicate that one mechanism for an increase in Co# and decrease in Fe# during the alteration of the tailings material is based on the replacement of earlier formed Fe-arsenates (scorodite) by Co-Zn-Ni-arsenates. During this process, Ni-, Co- and Zn-arsenates precipitate initially as nanoparticles on the surface of scorodite and detrital silicates, followed by a coarsening through Oswald ripening. The release of Fe³⁺ during the replacement of scorodite can results in the formation of Fe-rich hydroxy-interlayered minerals and (FeOHCO₃)_{aq} species under weak alkaline conditions. The mineralogical-geochemical features depicted in this study

provide a better understanding on the geochemical behavior of Co, Fe and As in alkaline tailings and may assist in the interpretation of mineral-microbial community associations and the development of effective bioleaching strategies for Co.

INTRODUCTION

The growing demand of cobalt (Co) in electric car batteries (Armand & Tarascon, 2008) resulted in revived exploration activities around the mining camp near Cobalt, Northeastern Ontario, Canada. Currently, these mining activities do not include either green mining or biomining of mine tailings with Co concentrations as high as 3.5 wt% (Percival et al., 2004). Biomining is a low-cost extraction of metal(loid)s from mine waste is facilitated through their leaching from minerals by pre-existing or introduced microbial communities (Rawlings, 2002; Brierley 2008). The nature of the interaction between microbes and metal(loid)-bearing minerals is controlled by (1) crystal chemical parameters (i.e., mineral species, element oxidation state, local atomic order), (2) the species and activity of the microbes present, and (3) geochemical conditions such as pH, Eh and temperature (Rawlings, 2002). Biomining has been successfully applied to sulfide-bearing mine waste as the production of sulfuric acid through the biotic-mediated oxidation of the sulfides allows an efficient leaching of most of the metals under acidic conditions (Waitling, 2006; Mahmoud et al., 2017).

Biomining of material at the mine tailings around Cobalt Ontario is challenging as an effective bioleaching of the neutral to alkaline tailings material requires either (1) the acidification of the tailings material, or (2) the enhancement of mineral-bacteria interactions under near-neutral pH conditions. Both approaches would require a thorough characterization of the geochemical, mineralogical and microbial conditions within the chemically heterogeneous tailings. Here, we describe formerly unknown geochemical-mineralogical relationships at two sites at the Cobalt mining camp (CMC). These sites are referred from now on as site A and B.

Background information on the Ag-Co-sulfarsenide ore deposit at Cobalt, ON

Cobalt is a small town in northeastern Ontario and is considered to be the “birthplace of hardrock mining” in Canada. During railway constructions in 1903, Ag-bearing pebbles were discovered on the shores of Cobalt Lake. Subsequent mining activities included over 100 different mines, yielding a total production of circa 12.6 billion grams (or 444 million ounces) silver (Marshall & Watkinson, 2000).

The Cobalt Embayment occurs in the Southern Province of the Canadian Shield and is widely known for the abundance of silver-sulfide-arsenide-bearing carbonate veins (Potter et al., 2010; Joyce et al., 2012). The Cobalt Embayment is an approximately 30,000 km² area of Paleoproterozoic siliciclastic sedimentary rocks of the Huronian Supergroup (~2.4-2.2 Ga) laying unconformably upon the Archean volcanic basement rocks, both of which were intruded by 2.2 Ga Nipissing diabase dykes and sills (Young et al., 2001; Potter et al., 2010). The ore veins are hosted in the Nipissing diabase dykes and sills, the Archean volcanic basement rocks, and the Coleman Member unit (primarily conglomerate with siltstone and sandstone) of the Huronian Supergroup (Debicki, 1990; Young et al., 2001; Potter et al., 2010).

The mineralogical compositions of the silver-arsenide veins are notably consistent throughout the Cobalt-Gowganda area and do not vary with the type of host rock. The ore veins primarily consist of the primary gangue minerals calcite and/or lesser dolomite associated with Co, Fe, and Ni-arsenides and -sulfarsenides, native silver and bismuth as well as silver antimonides (Joyce et al., 2012). The veins are typically zoned; the carbonates make up the central or main part of the vein while silicates occur as thin, less than 0.5 inches thick, layers immediately adjacent to vein walls. The silver-bearing assemblages, when present, occur at or near the interface between the silicates and carbonates.

Previous studies on the Cobalt mine tailings camp (CMC)

The environmental impacts of mine tailings in Cobalt, ON, are addressed in many geochemical-mineralogical studies such as Dumaresq (1993), Kwong et al. (2000, 2007), Percival et al. (1996, 2004, 2007) and Sprague et al. (2016). The tailings at the CMC are of particular concern as they contain high concentrations (up to 0.7 wt%) of As, resulting from the enrichment of sulfarsenides from milling process and their subsequent oxidation (Dumaresq, 1993; Percival et al., 2004; Kwong et al., 2006).

The environmental impact of released metal(loid)s from the mine tailings on the surrounding environment was, for example, addressed by Percival et al. (2004) and Sprague et al. (2016) who studied the transport, attenuation and concentration of As, Co and Ni in the natural waters around the Cobalt mine tailings. The authors found that (1) the total dissolved concentrations of As often exceeds the accepted value for drinking water; and (2) the source of metals in the surface waters is likely the weathering of primary Co- and Ni-sulfarsenides in the tailings. Kwong et al. (2007) and Percival et al. (2004) showed that the tailings are predominantly composed of albite, plagioclase, quartz, chlorite, calcite, dolomite, clinocllore, and micas (i.e., illite and muscovite). Dumaresq (1993) identified additionally large lenses of limonite, $\text{FeO}(\text{OH}) \cdot n\text{H}_2\text{O}$ at depths greater than 25 cm.

The tailings material also contains traces of primary ore minerals such as cobaltite, safflorite, skutterudite, arsenopyrite and gersdorffite (Kwong et al., 2007) and secondary As-bearing minerals such as annabergite, erythrite, scorodite and pharmacolite (Percival et al., 2004). Kwong et al. (2000) noted that erythrite with minor annabergite occurred only in the unsaturated parts of the tailings whereas scorodite was observed in both saturated and unsaturated tailings. Percival et al. (2004, 2007) and Dumaresq (1993) reported that the tailings at site B were characterized by white to yellow surface crusts during the summer months. The crusts formed by efflorescence of capillary water, were enriched in Ni, Co and As and composed predominantly of gypsum or thenardite (Dumaresq, 1993). Table 1 lists the chemical

composition of all As-bearing minerals identified in the Cobalt mine tailings by Percival et al. (2004), Kwong et al. (2006) and this study.

Secondary minerals of the (Co, Cu, Ni, Pb, Zn)-Fe(III)-As(V)-S(VI)-H₂O system occur often as thin rims or powdery aggregates and crusts on the primary sulfarsenides rather than large masses and cements within the waste (Petrunic et al., 2006, 2009, Majzlan et al., 2014). The relatively low abundance of these minerals in many mine tailings is a result of the relatively low dissolved concentrations of Co, Cu, Ni, Pb, and Zn in the waste and the relatively high solubility of the majority of arsenate minerals containing these metals as main components (Drahota and Filippi 2009; Nordstrom et al., 2014, Majzlan et al., 2014). Secondary Co-Ni-Zn-arsenates minerals in mine tailings may sequester economically significant quantities of certain elements (such as Co and As) in the tailings, in addition to controlling their release into the proximal environment (Majzlan et al., 2014). However, there have not been any studies on the formation mechanisms and stability of Co-Ni-Zn-arsenates minerals in mine tailings systems.

MATERIALS and METHODS

Sampling area

The area around Cobalt, Ontario, Canada contains 16 tailings sites. Two tailings sites (A, B) were chosen for sampling as they were (1) among the larger tailings sites in Cobalt, (2) fed from different mills, and (3) were among sites characterized by high As and Co concentrations (Ontario Ministry of the Environment (MOE), 2011). The tailings at site A, now occupying parts of a prominent lake in the area, are up 2 m in thickness and were deposited into the north end of the lake (Anderson, 1993). The tailings were mostly generated by five nearby mines, which operated intermittently from 1908 to the late 1940s (Dumaresq, 1993). However, the lake at site A has served as a collection site for migrated tailings from other Cobalt camp sites *via* feeder streams such as Mill Creek. The configuration of the deposited tailings has changed little since the construction of a dam in the 1950s by the MOE at the northern extremity

of the Farr Creek wetland (Dumaresq, 1993). Site B was used to deposit mine waste from mills between 1910 and 1920. The mills processed large tonnages of explicitly low-grade ore and used cyanides rather than Hg for extraction purposes (Dumaresq, 1993). Revegetation efforts were made with moderate success at site B in the late 1990's, however, there are still open patches of tailings which have a thin thenardite-gypsum crust (Percival et al., 2004; Dumaresq, 2009). Due to erosion and/or dam failure, a considerable amount of tailings material from site B has been drained into Mill Creek. Both sites A and B are part of the Farr Creek drainage basin.

Sampling methods

One tailings profile was sampled from each site (Fig. 1a and b). The sites for the two depth profiles had minimal organic cover, flat topography, and sufficient depth to the bedrock (as determined with a soil sampler probe). Along the two 30 cm profiles (Fig. 1a and b), samples were extracted every centimeter, resulting in a total of 60 samples. These were sealed in plastic bags and, within two hours, placed in the geochemical laboratories of Laurentian University in Sudbury (circa 2-hour drive).

Sample preparation

Upon arrival at the laboratories, the contact pH was measured after mixing 5 g of each tailings sample with 10 mL of deionized water. For quality assurance, the pH of a standard solution was measured after every 10th sample. The pH meter was calibrated with 4.00, 7.00 and 10.00 buffers from Fisher Scientific Canada; the measurement uncertainty was ± 0.1 . After the pH measurements, each sample was immediately dried in an oven at 80°C for 2 days and stored under dry conditions.

Chemical analysis

Chemical analysis of all 60 samples was carried out in the Elliot Lake Research Field Station, Sudbury, Ontario. A single digest per sample was obtained by heating a mixture of 0.5 g sample, 9 mL concentrated HF and 1 mL HCl in block heaters at 110°C followed by conversion with 15 mL concentrated HCl and HNO₃ (1:1 ratio) and 0.5 mL HF, 1 mL HCl and 10 mL HNO₃. A 1:10 dilution with 18.3 MΩ nanopure water was performed directly before ICP-MS analysis, with a total dilution factor of 1000. The samples were analyzed on a Varian 810 ICP-MS using the calibration standard from Inorganic Ventures. The internal standards used were Ru-101, for correcting drift in low medium mass isotopes, and Re-185, for correcting drift in heavier isotopes. For quality assurance, blank, duplicate and certified reference materials were analyzed after every 25th sample.

Powder X-ray Diffraction and Scanning Electron Microscopy

Samples taken two centimeters apart (starting at the surface layer (depth = 1 cm)) were powdered and prepared for X-ray powder diffraction (i.e., 15 samples from each depth profile). Powder X-ray diffraction patterns were recorded with a Philips 159 PW 1729 X-ray diffractometer using Cu-Kα radiation ($\lambda = 1.5418 \text{ \AA}$) at 40 kV and 30 mA. Diffraction patterns were collected over a range of 5-75° 2θ with a step size of 0.02° and a counting time of 2 s step⁻¹. All recorded X-ray diffraction patterns are listed in the Supplementary Materials, Appendix A.

Three selected samples from site A collected at depth (D) = 1, 11 and 20 cm and two samples from site B at D = 11 and 25 cm were prepared for Scanning Electron Microscopy (SEM) studies. The samples were embedded into epoxy pucks and polished using MicroPolish Alumina powder on 8-inch Nylon PSA Buehler discs. The carbon coated epoxy pucks were analyzed using a JEOL 6400 SEM operating at 20 kV, equipped with both backscattered (BSE) and secondary (SE) electron detectors and an Energy Dispersive X-ray Spectrometer (EDS).

Focused Ion Beam Technology (FIB) and Transmission Electron Microscopy (TEM)

A FIB section was extracted from a selected mineral surface coating with a FEI Dualbeam 235 SEM-FIB at 4D Labs, Simon Fraser University, BC, Canada. The extracted section was subsequently lifted using a platinum gas-glue and thinned to electron transparency by ion gas milling (Gaions). TEM studies were conducted with a field emission TEM FEI Talos F200x at the Manitoba Institute of Material Science. Imaging and selected area electron diffraction was performed with an accelerating voltage of 200 kV in bright and dark field mode with a 16 MB Ceta camera and a Fischione high angle annular dark field (HAADF) detector. Compositional analysis by EDS was performed in a Scanning Transmission Electron Microscope (STEM) mode with 4 SDD detectors.

RESULTS

The tailing samples acquired at both sites are grey with occasional red-coloured inclusions (Fig. 1a and b) and their average measured contact pH values were 8.5 (site A) and 8.1 (site B) (Supplementary Data B). The distribution of the metal(loid)s As, Co, Fe, Ni, Sb, and Zn vary with depth (Fig. 2-3, supplementary data C). At site B, elevated concentrations for Co, Fe Ni, Sb, and Zn occur at D = 10 - 24 cm and coincides at this range with elevated concentrations of As (Fig. 2). However, profile depths with maximum concentrations of Co, Fe Ni, Sb, and Zn do not necessarily coincide; for example, at D = 11 and 20 cm, high concentrations of Co are coincident with relatively low concentrations for Fe and Sb. Large variations in the chemical distributions of As, Co, Fe, Ni, Sb, and Zn with depth also occur at site B (Fig. 3). Similarly, at D = 9 and 11 cm, high concentrations of As, Co, Ni, Sb, and Zn are coincident with relatively low concentrations of Fe. Enrichment in Fe occurs at D = 0 cm (i.e., surface) and 25 to 29 cm, and coincides at D= 25 cm with an enrichment in As, Sb, and Zn (Fig. 3).

Bulk-mineralogical composition

The tailings material at site A is predominantly composed of quartz, albite, clinocllore, \pm calcite and dolomite with minor anorthite, muscovite, illite, epidote, stilbite, diopside, hedenbergite, magnesioriebeckite, magnesioarfvedsonite, and pargasite (Supplementary Data A). In the top 7 - 8 cm of the profile, calcite is the dominant carbonate mineral, whereas in the lower portion of the profile, dolomite predominantly occurs in association with Mg-rich silicates such as magnesioriebeckite and magnesioarfvedsonite. The mineralogical composition of the material at site B is similar to that of the site A. The tailings material is predominantly composed of quartz, clinocllore, albite, dolomite, and calcite and some minor sulfarsenides (gersdorffite, NiAsS). Conversely to the tailings material at site A, dolomite and calcite occur in similar proportions throughout the entire 30 cm profile at site B.

Observations at the micrometer scale

SEM characterization of tailings material from D = 1, 11 and 20 cm at site A included imaging and chemical characterization of 31, 27 and 20 As-bearing grains and mineral surface coatings, respectively. These examinations indicate that (a) sulfarsenides predominate at D = 1 cm, (b) sulfarsenides and arsenates occur in similar proportions at D = 11, and (c) arsenates predominate at D = 20 cm (Fig. 2). SEM examinations of tailings material from D = 11 and 20 cm at site B included the characterization of 26 and 16 As-bearing grains and mineral surface coatings, respectively and indicated that arsenates predominate over sulfarsenides at both depths (Fig. 3).

The characterized sulfarsenides in the tailings from both sites are predominantly arsenopyrite (FeAsS) and safflorite $(\text{Co,Fe,Ni})\text{As}_2$, (Fig. 4a and b) with minor chalcopyrite (CuFeS_2), löllingite (FeAs_2) and an unidentified Fe-Cu-Ag-As-S phase (possibly argentopyrite (AgFe_2S_3 ; Table 1). The observed arsenates are a mixture of Co-, Ni- and Zn-arsenates, which are commonly depleted in Fe and enriched in Ni relative to the observed sulfarsenides (Table 1,

Supplementary Data D1 and D2). The arsenates occur predominantly in mineral surface coatings on silicates (e.g. albite), carbonates and primary sulfarsenides (Fig. 4c and d). Iron-(hydr)oxides are rare and occur as mineral surface coatings on altered Fe-bearing sulfarsenides such as arsenopyrite (Fig. 4c and d).

Change in bulk chemical composition versus degrees of alteration

The higher abundance of arsenates relative to sulfarsenides in the tailings material at site B relative to that from site A correlates with higher average concentrations of As, Co, Sb, Zn and Ag and lower average concentration of Fe (Fig. 5). The depletion of Fe and enrichment in As, Co, Sb and Zn during the weathering of the sulfarsenides can be visualized by plotting the Co-number (Co#) versus Fe number (Fe#; Fig. 5). These numbers are defined as

$$\text{Co\#} = \frac{\text{Co} + \text{Zn} + \text{Sb} + \text{As}}{\text{Al} + \text{Co} + \text{Zn} + \text{Sb} + \text{As}} \times 100\% \quad (2)$$

$$\text{Fe\#} = \frac{\text{Fe}}{\text{Al} + \text{Fe}} \times 100\% \quad (3)$$

The calculations of these numbers assume that Al is an immobile element and can be thus used to calculate the depletion of Fe and enrichment Co, As, Sb, Zn and Ag in the tailings material. The following observations can be made when comparing the distribution of elements with the Co# and Fe # (Fig. 2 and 3, Supplementary Data C) and the occurrence and chemical composition of arsenides and arsenates (Fig. 2 and 3, supplementary data D1-D2) numbers (Fig 5):

- (1) Sulfarsenides are enriched in Fe relative to arsenates and predominate in tailings material with high Fe# and low Co#;
- (2) Arsenates are enriched in Ni and depleted in Fe relative to sulfarsenides and predominate in tailings material with high Co# and low Fe #.

Open questions prior to the examinations of the tailing material at the nano-scale

The chemical and mineralogical characterization of the tailings material using chemical analyses, XRD and SEM indicate the rare occurrence of Fe-(hydr)oxide minerals, the depletion in Fe during the weathering of the sulfarsenide-bearing mine waste, the sequestration of Co, Ni, Zn, Fe and As in certain layers of the tailings and the occurrence of arsenate-bearing mineral surface coatings depleted in Fe relative to sulfarsenide grains. However, the characterization of the tailings material on the micron-to-centimeter scale could not determine (1) the underlying mechanisms for the depletion of Fe in layers enriched in arsenates and (2) the paragenetic relationships and formation mechanisms of the Co-Ni-Zn-arsenates. Hence, a mineralogical study at the nanoscale was conducted on a FIB section extracted from an arsenate-bearing mineral surface coating with similar proportions of Fe, Co, Ni and Zn (Fig. 6a and b). The coating occurs on an albite grain from the sample at D = 25 cm of site B, which has the highest concentrations of Fe, Sb and Zn of all samples collected at this site (Fig. 3 and 6a, b).

Chemical and mineralogical trends across the FIB section

The FIB section from the mineral surface coating is subdivided into 12 distinct areas, which are numbered from 1 to 12 (Fig. 6c). We will refer to the corresponding area number when describing a chemical and mineralogical feature. The FIB section is predominantly composed of Co-Zn-Ni-bearing arsenates (yellow and red in Fig. 6d) and Fe-bearing minerals of the chlorite group (violet in Fig. 6d) with minor brookite, titanite and minerals of the feldspar group (black areas in Fig. 6d). Selected Area Diffraction pattern, Fast Fourier Transformation pattern of lattice fringes and semi-quantitative chemical analyses for all phases identified in the FIB section are listed in the Supplementary Data E.

One of the most prominent mineralogical features in the FIB section occurs in area 2 of the FIB section. Here, the Zn-arsenate arsenohopeite and Co-Ni-Zn-rich arsenate minerals with the vivianite-structure type (Table 1, Fig. 7a - f) occur in zones around a core composed of

scorodite (violet in Fig. 7b and blue in Fig. 7e, supplementary data E). Arsenates of the vivianite structure-type have the general composition $(M_3(AsO_4)_2 \cdot 8H_2O)$ with $M = Co, Ni$ and Zn and include the minerals erythrite, annabergite and köttigite (Table 1). The chemical distribution maps of Co (green), Ni (red) and Zn (blue) indicate that the immediate zone around the scorodite core is enriched in Ni (red in Fig. 7b, c and e), followed by a zone enriched in Co (yellow-green in Fig. 7b, c and e) and an outer zone enriched in Zn (mainly arsenohopeite; blue in Fig. 7c). A Scanning TEM image (Fig. 7d), chemical distribution maps for Fe, Co and Ni (Fig. 7e) and TEM images of the scorodite core and surroundings (encircled in Fig. 7d, e and f) indicate the occurrence of a concave-shaped scorodite surface towards the Ni-rich arsenate, a characteristic feature for a mineral replacement process between a parent (scorodite) and daughter (Ni-rich arsenate) (Ineson, 2014). High-resolution TEM images indicate that the interface between the Ni-rich arsenate (annabergite) and scorodite is characterized by nanoparticles of the former mineral and a relative homogeneous matrix of the latter mineral (Fig. 8A-C). Although this interface can be quite sharp at the nano-scale (Fig. 8b), nanoparticles of annabergite can occur within the scorodite matrix (indicated with arrows in Fig. 8c).

Different generations and types of arsenates and silicates occur throughout the FIB section. For example, in the upper part of area 1 occurs a mineral assemblage composed of an Fe-rich mineral of the chlorite group and Co-Ni-Zn-rich arsenates. The latter arsenates have M/As ratios ($M = Co, Ni$ and Zn) and d -spacings similar to those observed for arsenohopeite (Table1, Supplementary Data E).

The Fe-rich mineral of the chlorite group with $Fe \gg Mg$ (violet in Fig. 9b) cross-cuts the Co-Ni-rich arsenate (yellow in Fig. 9b), suggesting its formation after the latter mineral. This proposed sequence is supported by the occurrence of alteration halos within the arsenate along the arsenate-Fe-rich chlorite interface. These alteration halos are composed of a mineral of the tsumcorite group which has partially replaced the earlier formed Co-Ni-rich arsenate (indicated with an arrow in Fig. 9c and in blue in Fig. 9d). Minerals of the tsumcorite group have the

general formula $Me_1M_2(XO_4)_2(OH,H_2O)_2$ and chemical analyses of the alteration halo indicates that the *Me* site is occupied exclusively by Ca, the *M*-site mainly by Fe^{3+} and minor Al, Zn, Co, Ni, and the *X* site exclusively by As (Table 1). The Fe-rich chlorite itself has been altered along its interface towards a Zn-rich arsenate (arsenohopeite; indicated with an arrow in Fig. 9c and in green in Fig. 9d), suggesting that the latter formed after the former mineral.

Alteration halos on the surface of minerals of the chlorite group and other silicates occur throughout the FIB section. For example, a highly altered Mg-rich chlorite grain with $Mg \gg Fe$ occurs in the areas 4 and 5 within a Co-Ni-rich arsenate matrix composed of minerals with the vivianite structure-type (Fig. 9e and f). Nano-size fractures within the chlorite grain have been penetrated by Co-Ni-As-rich solutions and contain nanoparticles of a Co-Ni-rich arsenate with d-spacings similar to those of arsenohopeite (Table 1, supplementary data E). In the same area, an albite grain is embedded in a Co-Ni-rich arsenate matrix (vivianite structure-type; Fig. 9g, h). Here, the arsenate occurs as a coarse precipitate in the surroundings and in the form of nanoparticles within pore spaces of the alteration rim of the albite (Fig. 9g, h).

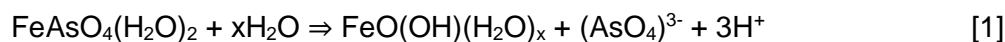
DISCUSSION

Examinations of a tailings sample at the nanoscale using a combination of FIB and TEM allows for a site-specific, in-depth chemical and mineralogical analysis of a highly localized area of interest. In a FIB section, the area thinned to electron transparency is typically about $5 \times 20 \mu m$. The high costs and levels of skill required for FIB/TEM analysis, limit the number of sections that can be thoroughly characterized. We do not claim that the results presented here represent the regional trends in the speciation of As, Fe, Co, Ni, Zn and Ag in the tailings at Cobalt, ON. However, the mineralogical and chemical features observed in the FIB section provide a better understanding of some of the chemical and mineralogical trends observed in the depth profiles at the two tailings sites. As such, we will first discuss alteration processes and mineral

replacement reactions observed at the nanoscale before addressing their relationship to the observed chemical trends within the depth profiles at site A and B.

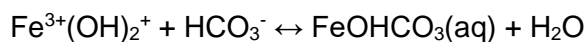
The replacement of scorodite by Co-Ni-Zn arsenates

The results above showed that scorodite is replaced under the alkaline conditions in the tailings by Co-Ni-Zn arsenates rather than by Fe-hydroxides. This is surprising as (a) scorodite has a lower solubility ($0.018 \mu\text{gL}^{-1}$; Dove & Rimstedt, 1985) than the Co-Ni-Zn arsenates with the vivianite structure-type ($\sim 0.38 \mu\text{gL}^{-1}$; Wei et al., 2013) and (b) scorodite is commonly replaced by As-rich Fe-hydroxides under weakly acidic to alkaline conditions, (Paktunc et al., 2008; Majzlan et al., 2014) via the reaction:



Although Fe-(hydr)oxides are the most stable Fe-phases in alkaline soils under oxidizing conditions, their formation can be limited by

(a) the complexation of Fe^{3+} -hydroxide species by carbonate species under near neutral pH and high $p\text{CO}_2$ conditions (Grive et al., 2014) via the reaction:



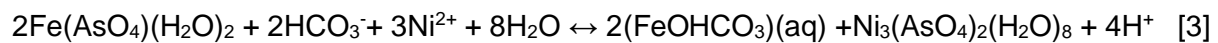
(b) clay minerals which can sequester Fe^{3+} through the intercalation of Fe-hydroxide oligomers into their interlayer (Georgiadis et al., 2020).

(c) the presence of Fe-reducing bacteria which can lead to the formation of Fe^{2+} -bearing aqueous species or Fe^{2+} -carbonates (Revesz et al., 2015)

Here, we will address the formation of the $\text{FeOHCO}_3(\text{aq})$ complex and those of the Fe^{3+} -hydroxy-interlayered minerals. The potential biotic dissolution of Fe^{3+} -minerals by Fe-reducing bacteria in the tailings material will be addressed elsewhere.

The potential occurrence of Fe^{3+} -carbonate species in pore waters at both tailings sites may be simulated using the geochemical speciation program Visual Minteq (Gustavson, 2019), selected pore water chemistry reported by Percival et al. (2004), the average contact pH of 8 in

the tailings material at site B (supplementary data B) and the thermodynamic data for calcite, scorodite, and the aqueous species $(\text{Fe}^{3+}\text{OHCO}_3)_{(\text{aq})}$ (Grive et al., 2014). The activity of CO_2 in the pore water will be simulated by considering an equilibrium between the pore water and either calcite or $\text{CO}_{2(\text{atm})}$. For both scenarios, the geochemical modelling shows that the observed pore waters were undersaturated with respect to scorodite, supersaturated with respect to ferrihydrite and goethite, and that the dominant Fe-bearing aqueous species was $\text{FeO}(\text{HCO}_3)_{(\text{aq})}$, respectively (supplementary data F). Although these simulations do not explain the formation of the observed scorodite and the absence of Fe-(hydr)oxides in the upper 30 cm of the tailings profile, they indicate that Fe^{3+} can be mobilized in the form of the $\text{FeO}(\text{HCO}_3)_{(\text{aq})}$ in the pore waters. Hence, the replacement of scorodite by annabergite in the presence of a carbonate-rich solution under abiotic conditions may be expressed by the equation:



A mineral replacement requires that dissolution of the phase to be replaced (in this case scorodite) and precipitation of the replacing phase (annabergite) are closely coupled in space and time (Putnis, 2009). Hence, the precipitation of annabergite required (1) a bicarbonate-bearing solution transporting Ni^{2+} to the growth/dissolution interface; and (2) the release of the common ion $(\text{AsO}_4)^{3-}$ during the dissolution of scorodite. The coupling of dissolution and precipitation may be recognized in Figures 7 and 8, which show the formation of annabergite nanoparticles at the scorodite interface and interior. According to Putnis (2009), the coupling between the dissolution of the parent (scorodite) and precipitation of the daughter (annabergite) can be achieved when the controlling mechanism is the dissolution rate of the parent, and the activation energy barrier for the nucleation of the daughter is low. Porosity also plays an important part in mineral replacement reactions, as an increase in porosity from the parent to the daughter phase allows a mass exchange between the pore water-solid interface and the bulk solution (Putnis, 2009). This increase in porosity was most likely provided by the occurrence of nanoparticles of annabergite along the annabergite-scorodite interface (Fig. 7f).

Textural evidence for the replacement of the earlier-formed annabergite by the Co-analogue erythrite or the replacement of erythrite by arsenohopeite is not apparent in the FIB section. However, the replacement of annabergite by erythrite would have been favoured by the lower solubility of the latter relative to the former mineral (Wei et al., 2013).

The formation of Fe-rich minerals of the chlorite group in the vicinity of the replacement reaction

There are two different generations of chlorite-group minerals in the FIB section. A younger more-or-less unaltered Fe-rich chlorite and a highly altered Mg-rich chlorite, most likely of detrital origin. As described above, the cross-cutting of the Ni-Co-arsenates by the Fe-rich chlorite indicates that the chlorite formed after the arsenates, most likely through the influx of Fe-rich pore fluids.

Minerals of the chlorite-group are hydroxy-interlayered minerals (HIM's). Iron-rich HIM's can form through ferrolysis (Brinkman, 1970, 1977), a process where Fe-hydroxide oligomers incorporate into the interlayers of micas or expandable 2 : 1 phyllosilicates or replace Mg-rich oligomers in the interlayer of primary Mg-rich chlorites (Schwertmann, 1976; Georgiadis et al., 2020).

In a recent review on the structure, composition and occurrence of HIM's, Georgiadis et al. (2020) showed that the intercalation of metal cations into expandable 2 : 1 phyllosilicates occurs preferentially under moderately acidic conditions (pH 4.6 to 5.8) and low soil organic matter (SOM) content. However, the authors also pointed out that (a) HIM's minerals have been also observed in soils of lower or higher pH and large SOM contents and (b) pH values at the micrometer scale on, for example, mineral surfaces or in confined pore spaces can significantly vary from those in the bulk soil. The difference between the formation of the HIM's in a neutral to alkaline *versus* weakly acidic solution is that the former pH conditions promote the fast precipitation of metal hydroxides either simultaneously or preferentially relative to the formation

of the HIM's (Carstea et al., (1970); Yamanaka & Brindley, 1978; Hsu, 1989; Violante et al., 1998; Dietel et al., 2019a, 2019b).

In the case of the neoformed Fe-rich chlorite in the FIB section, a combination of (a) the slow dissolution kinetic of the source of Fe^{3+} (most likely scorodite), (b) the formation of Fe^{3+} -carbonate aqueous complexes, (c) the generation of acidity through the replacement of scorodite by the Ni-Co-Zn arsenates (equation [3]) and (d) the presence of detrital chlorite-group minerals in the mineral surface coatings may have promoted and prevented the formation of the Fe-HIM's and Fe-(hydr)oxides, respectively.

The potential occurrence of weakly acidic to neutral pH conditions during the formation of the Fe-rich chlorite in the pore spaces of the mineral surface coatings is supported by the presence of the Ca-Fe-As-rich mineral of the tsumcorite group, which has most likely formed during the interaction of a Ca-Fe-rich solution with the Ni-Co-arsenate (Fig. 9C-D). Minerals of the tsumcorite group are important sinks for As in acidic alteration zones of base-metal ore deposits (acidity produced by the oxidation of the sulfides; Krause et al., 1998) and thus have been identified in mineral surface coatings formed under acidic pH conditions in Pb-Zn-As contaminated soils in Trail, British Columbia, Canada (Schindler & Hochella, 2017).

Formation mechanism of the Co-Ni-Zn arsenates of the vivianite structure-type

The formation of annabergite nanoparticles on the surfaces and interiors of scorodite and altered silicates (Fig. 8A-C, 9F-H) indicate that the formation of the particles has been mainly affected by the degree of supersaturation and the size of the pore spaces in the altered parts of the silicates.

A high degree of supersaturation increases the rate of formation for particles with radii larger than the critical radius of a particle (i.e., the radius at which a newly-formed particle does not completely re-dissolve in solution; Nguyen et al., 2014). The surface energy term (positive free energy) for the growth of a particle drastically reduces in the case of a heterogeneous

nucleation (i.e., growth on any kind of surface) resulting in higher nucleation rates of particles with radii smaller than the critical radius (Nguyen et al., 2014). The growth of a particle itself depends on the diffusion rate of monomers towards the surface of the growing nanoparticle, the rate of reaction of the monomer on the surface, the rate of Oswald ripening or aggregation of the particles themselves and in the case of a mineral replacement reaction, on the dissolution rate of the parent mineral.

Percival et al. (2004) reported that the concentrations of As (circa 100-150 mgL⁻¹) in the pore water at site B were two orders of magnitude higher than those for Co and Ni (1-4 mgL⁻¹) and argued that these concentrations are not controlled by the dissolution of annabergite and erythrite. However, these concentrations most likely control the influx of Ni and As into the pore spaces of mineral surface coatings. Hence, dissolution of scorodite by carbonate-bearing species and the influx of Ni and As-bearing species into the mineral surface coating likely result in a high degree of annabergite supersaturation and high rates of nanoparticle nucleation and aggregation. Surfaces of pre-existing minerals such as scorodite and detrital silicates favoured additionally the heterogeneous nucleation and stabilization of nanoparticles with radii smaller than the critical radius (Fig. 7, Fig. 8, Fig. 9).

The nucleation of a nanoparticle in a confined pore space on the surface and within altered scorodite (Fig. 8A-C) and silicate minerals (Fig. 9E-H) is controlled by (a) the sizes of the pore spaces which limit the size of the nuclei that precipitate inside them, (b) the physical and chemical properties of the constituents (solutes and solvents) within the pore spaces and (c) the chemical composition and reactivity of functional groups on the surface of the pore walls (Stack et al., 2015). It is not within the scope of this study to review in detail all these properties and so we want to address here only the effect of the pore size on the solubility of a nucleating nanoparticle. The physical limitations of a nano-size pore (i.e., nanopore) result in the formation of a nanoparticle which has, according to the classical nucleation theory, a higher surface energy and thus lower stability than a larger (micrometer-size) particle. Hence, a higher degree

of saturation with respect to the mineral is required to induce heterogeneous precipitation in the pore than would otherwise be required. This model is called the Pore-size Controlled solubility (Stack, 2015). In the case of the nucleation of the Co-Ni-Zn arsenate nanoparticles, the pore spaces within and on the surface of the altered scorodite and silicates (Fig. 8A-C, 9E-H) had to be large enough in order to allow the formation of a nanoparticle at a given state of supersaturation; i.e., the higher degree of supersaturation, the smaller the possible pore space in which nucleation can occur.

Observations on the nano- and micrometer scale versus chemical trends at the centimeter scale

The mineralogical studies at the nanoscale showed that

- (1) neutral to weak-alkaline conditions in the tailings material at site B favoured the replacement of the Fe-arsenates by Ni-Co-rich arsenates.
- (2) local variations in the pH value towards neutral to weak acidic conditions (at the nano to micrometer-scale) promoted most likely the neo-formation of Fe-rich HIM's;
- (3) Infiltration of Ni-, Co- and Zn-bearing solution into As-bearing mineral surface coatings resulted in pore solutions supersaturated with respect to minerals of the vivianite and arsenohopeite groups.

These observations and those obtained with SEM on the micrometer scale can be now used to explain some of the chemical trends observed in the two profiles at the centimetre scale.

1. Alteration of primary Fe-bearing sulfarsenides lead initially to the formation of scorodite;
2. Alteration of Co-Ni-Zn bearing sulfarsenides led to the interaction of Co-Ni-Zn rich fluids with earlier formed scorodite and the replacement of the latter by Co-Ni-Zn arsenates;
3. The occurrence of limonite lenses at greater depths ($D > 25$ cm; Dumaresq, 1993), the depletion in Fe with increasing degree of alteration of the sulfarsenides and the replacement of scorodite by Ni-Co-Zn arsenate (this study) indicate a high mobility of Fe

within the tailings profile, most likely due to the high stability of the (FeOHCO_3) aqueous species;

4. Fluctuations in the pH within the tailings column towards more acidic conditions resulted in the formation of Fe-rich hydroxy-interlayered minerals and explains the occurrence of Fe-rich layers without detectable amounts of Fe-(hydr)oxide minerals or scorodite.

Conclusions and Implications

This study revealed for the first time the underlying mechanisms for the mobility of Fe in the weak alkaline tailings at Cobalt, ON and its sequestration through the formation of Fe-HIM's in layers under weak acidic to neutral pH conditions. The observations in this study also indicated that

- (a) the sequestration of Co, Ni and Zn within the tailing column is controlled by the occurrence of previously formed Fe-arsenates;
- (b) the underlying crystallization mechanism of Co-, Ni- and Zn-arsenates is based on the formation of nanoparticles in confined pore spaces.

The occurrence of layers enriched in limonite, Fe^{2+} -bearing HIM's, Co-Ni-Zn-Fe-sulfarsenides and Co-Ni-Zn-Fe arsenate will have a strong impact on the microbial communities within the tailings profile as only specific species are able to adapt to high proportions of sulfarsenides or arsenates. An understanding of the composition of these microbial communities and their variations with the change in the mineralogical composition will be prerequisite for the efficient exploitation of these communities with respect to the bioleaching of Co from these tailings.

ACKNOWLEDGEMENTS

This work was supported by NSERC discovery grants to MS and NM and funding from the Canadian Museum of Nature to AL. We like to thank Xin Zhang and the 4D Lab at Simon Fraser University as well as Abdul Khan and the Manitoba Institute of Materials at the University of Manitoba for their technical assistance. We are very thankful to Dr. Graeme Spiers and Robert Meek for their assistance with the sampling of the tailings materials and their chemical analysis.

REFERENCES

- ANDERSON, P. (1993). Cobalt mining camp tailings inventory, Cobalt, Ontario. *Unpublished report, Ontario Ministry of Northern Development and Mines, 196pp.*
- BRINKMAN, R. (1970): Ferrollysis, a hydromorphic soil forming process. *Geoderma* **3**, 199-206.
- BRINKMAN, R. (1977): Surface-water gley soils in Bangladesh: genesis. *Geoderma* **17**, 111-144.
- BRIERLEY, C.L. (2008) How will biomining be applied in future? *Transactions of Nonferrous Metals Society of China* **18**, 6, 1302-1310
- CARSTEA, D. D., HARWARD, M. E. & KNOX, E. G. (1970): Comparison of iron and aluminum hydroxy interlayers in montmorillonite and vermiculite: I. Formation. *Soil Science Society of America Journal* **34**, 517-521.
- DIETEL, J., GROGER-TRAMPE, J., BERTMER, M., KAUFHOLD, S., UFER, K. & DOHRMANN, R. (2019a) Crystal structure model development for soil clay minerals - I. Hydroxy-interlayered smectite (HIS) synthesized from natural bentonite. A multi-analytical study. *Geoderma* **347**, 135-149.
- DIETEL, J., UFER, K., KAUFHOLD, S. & DOHRMANN, R. (2019b): Crystal structure model development for soil clay minerals - II. Quantification and characterization of hydroxy-interlayered smectite (HIS) using the Rietveld refinement technique. *Geoderma* **347**, 1-12.

- DEBICKI, R. L. (1990) *Stratigraphy, paleoenvironment and economic potential of the Huronian Supergroup in the southern Cobalt Embayment*. Vol. 148. Ontario, Ministry of Northern Development and Mines, 1990.
- DOVE, P.M., AND RIMSTEDT, J.D. (1985) The solubility and stability of scorodite, $\text{FeAsO}_4 \cdot 2\text{H}_2\text{O}$. *American Mineralogist* **70**, 838-844.
- DUMARESQ, C.G. (1993) The occurrence of arsenic and heavy metal contamination from natural and anthropogenic sources in the Cobalt area of Ontario. M.Sc. Thesis, Department of earth Sciences, Carleton University, Ottawa, 326 p.
- DUMARESQ, C. (2009). Tailings of the Cobalt Area. Retrieved from:
<http://www.cobaltmininglegacy.ca/tailings.php>
- DRAHOTA P. & FILIPPI M. (2009) Secondary arsenic minerals in the environment: A review. *Environmental International* **35**:1243-1255.
- GEORGIADIS A., DIETEL J., DOHRMANN, R., & D RENNERT, T. (2020) What are the nature and formation conditions of hydroxy-interlayered minerals (HIMs) in soil? *Journal of Plant Nutrition and Soil Science* **183**, 12-26.
- GRIVÉ, M., DURO, L. & BRUNO, J. (2014) Fe(III) mobilisation by carbonate in low temperature environments: Study of the solubility of ferrihydrite in carbonate media and the formation of Fe(III) carbonate complexes *Applied Geochemistry* **49**, 57–67.
- GUSTAVSON, J.P. (2019) Visual MINTEQ 3.1. KTH, SEED, Stockholm, Sweden.
- HSU, P. H. (1989): Aluminum Oxides and Oxyhydroxides, in Dixon, J. B., Weed, S. B. (eds.): Minerals in Soil Environments. SSSA, Madison, WI, USA, pp. 331-378
- INESON, P. R. (2014) Introduction to practical ore microscopy. Routledge Taylor & Francis Group London and New York.
- JOYCE, D. K., TAIT, K.T., VERTOLLI, V., BACK, M.E. & NICKLI, I. (2012) The Cobalt mining district, Cobalt, Ontario, Canada. *Mineralogical Record* **43**, 685-713.

- KRAUSE, W., BELENDORFF, K., BERNHARDT, H.J., MCCAMMON, C., EFFENBERGER, H. & MIKENDA, W. (1998) Crystal chemistry of the tsumcorite-group minerals. New data on ferrilotharmeyerite, tsumcorite, thometzekite, mounanaite, helmutwinklerite, and a redefinition of gartrellite. *European Journal of Mineralogy* **10**, 179-206.
- KWONG, Y.T.J., PERCIVAL, J.B. & SOPROVICH, E.A. (2000) Arsenic mobilization and attenuation in near-neutral drainage - implications for tailings and waste rock management for Saskatchewan uranium mines. *In Uranium 2000, International Symposium on the Process Metallurgy of Uranium*. E. Ozberk and A.J. Oliver (eds.). The Canadian Institute of Mining, Metallurgy and Petroleum (CIM), Montreal, p. 579-593.
- KWONG, Y.T.J., BEAUCHEMIN, S., HOSSAIN, M.F. & GOULD, W.D. (2007) Transformation and mobilization of arsenic in the historic Cobalt mining camp, Ontario, Canada. *Journal of Geochemical Exploration* **92**, 133-150.
- PERCIVAL, J.B., DUMARESQ, C.G., KWONG, Y.T.J., HENDRY, K.B. & MICHEL, F.A. (1996) Arsenic in surface waters, Cobalt, Ontario. *In Current Research 1996-C, Geological Survey of Canada* p. 137-146.
- MAHMOUD, A., CEZAC, P., HOADLEY, A.F.A., CONTAMINE, F. & D'HUGUES P. (2017) A review of sulfide minerals microbially assisted leaching in stirred tank reactors. *International Biodeterioration & Biodegradation* **19**, 118-146
- MAJZLAN, J., DRAHOTA, P. & FILIPPI, M. (2014) Parageneses and Crystal Chemistry of Arsenic Minerals. *Reviews in Mineralogy & Geochemistry* **79**, 17-184.
- MARSHALL, D. & WATKINSON, D. H. (2000) The Cobalt mining district: Silver sources, transport and deposition. *Exploration and Mining Geology* **9**, 81-90.
- NGUYEN T. K.T., MACLEAN, N. & MAHIDDINE, S. (2014) Mechanisms of Nucleation and Growth of Nanoparticles in Solution. *Chemistry Review* **114**, 7610–7630.

- NORDSTROM, D.K., MAJZLAN, J. & KONIGSBERGER E. (2014) Thermodynamic properties for arsenic minerals and aqueous species. *Reviews in Mineralogy and Geochemistry* **79**, 217-255.
- ONTARIO MINISTRY OF THE ENVIRONMENT (2011) *Final Report: Cobalt-Coleman Mining Camp Soil Assessment*. Retrieved from: <https://collections.ola.org/mon/25010/313445.pdf>
- PAKTUNC, D., DUTRIZAC, J. & GERTSMAN, V. (2008) Synthesis and phase transformations involving scorodite, ferric arsenate and arsenical ferrihydrite: Implications for arsenic mobility. *Geochimica et Cosmochimica Acta* **72**, 2649-2672.
- PERCIVAL, J.B., KWONG, Y.T.J., DUMARESQ, C.G. & MICHEL, F.A. (2004) Transport and attenuation of arsenic, cobalt and nickel in an alkaline environment (Cobalt, Ontario) Geological Survey of Canada Open File 1680.
- PERCIVAL, J.B., Y.T., KWONG, Y.T.J., DUMARESQ, C.G. & MICHEL, F.A. (2007) Distribution of As, Ni and Co in tailings and surface waters in the Cobalt area, Ontario. Sudbury 2007-Mining and the Environment International Conference.
- PETRUSIC, B.M., AL T.A. & WEAVER, L. (2006) A transmission electron microscopy analysis of secondary minerals formed in tungsten-mine tailings with an emphasis on arsenopyrite oxidation. *Applied Geochemistry* **21**, 1259-1273.
- PETRUSIC B.M., AL T.A., WEAVER L., & HALL D (2009) Identification and characterization of secondary minerals formed in tungsten mine tailings using transmission electron microscopy. *Applied Geochemistry* **24**, 2222-2233.
- POTTER, E. G., TAYLOR, R.P., JONES, P.C., REES, K. & CAMPBELL, I. (2010) The Geological Setting, Mineralogy, and Paragenesis of Gold- Bearing Polymetallic (Cu+Co+Ag+Au+Bi±Pb±Ni±U) Veins of the Merico-Ethel Property, Elk Lake, Northeastern Ontario, Canada. *Exploration and Mining Geology* **19**, 81-98.

- PUTNIS, A., (2009) Mineral replacement reactions. In: Thermodynamics and Kinetics of Water–Rock Interaction (eds. E. H. Oelkers and J. Schott). *Reviews in Mineralogy and Geochemistry* **30**, 87–124
- RAWLINGS, D.E. (2002) Heavy metal mining using microbes. *Annual Review in Microbiology* **56**, 65–91.
- REVESZ E., FORTIN D. & PAKTUNC, D. (2015) Reductive dissolution of scorodite in the presence of *Shewanella* sp. CN32 and *Shewanella* sp. ANA-3, *Applied Geochemistry* **63**, 347-356.
- SCHWERTMANN, U. (1976): Die Verwitterung mafischer Chlorite. *Zeitschrift fuer Pflanzenernaehrung und. Bodenkunde* **139**, 27-36.
- SCHINDLER, M. & HOCELLA, M.F. (Jr) (2017) Sequestration of Pb- Zn- Sb- and As-bearing incidental nanoparticles in mineral surface coatings and mineralized organic matter in soils. *Environmental Sciences: Processes and Impacts* **19**, 1016-1027.
- SPRAGUE D.D., MICHEL, F.A., & VERMAIRE, J.C. (2016) The effects of migration on ca. 100-year-old arsenic-rich mine tailings in Cobalt, Ontario, Canada. *Environmental Earth Sciences* **75**, 405-417.
- STACK, A.G. (2015) Precipitation in Pores: A Geochemical Frontier. *Reviews in Mineralogy & Geochemistry* **80**, 165-190.
- VIOLANTE, A., KRISHNAMURTI, G. S. R. & HUANG, P. M. (1998): Formation and stability of hydroxy aluminum-iron-montmorillonite complexes: influence of ferrous iron. *Soil Science Society of America. Journal* **62**, 1448-1454.
- WATLING, H.R. (2006) The bioleaching of sulphide minerals with emphasis on copper sulphides — A review. *Hydrometallurgy* **84**, 81-108
- WEI, C., YINIAN, Z., ZHANG, X., WANG, X. & LIU, J. (2013) Dissolution and Solubility of the Erythrite/Annabergite Solid Solution $[(\text{Co}_x\text{Ni}_{1-x})_3(\text{AsO}_4)_2 \cdot 8\text{H}_2\text{O}]$ at 25 °C *Asian Journal of Chemistry* **25**, 14, 7687-7696.

YAMANAKA, S. & BRINDLEY, G. W. (1978): Hydroxy-nickel interlayering in montmorillonite by titration method. *Clay. Clay Minerals* **26**, 21-24.

YOUNG, G. M., LONG, D.G.F., FEDO, C. & NESBITT, W. (2001) Paleoproterozoic Huronian basin: product of a Wilson cycle punctuated by glaciations and a meteorite impact. *Sedimentary Geology* **141**, 233-254.

Figure captions

Fig. 1 (a)-(b) Photos of the tailings profiles taken at (a) site A and (b) site B.

Fig. 2 (a)-(f) Concentration profiles of selected elements within the depth profile taken from tailings site A; the element for each profile is indicated; depths at 11, 15, 20 and 24 cm are highlighted with horizontal bars; the relative abundance of sulfarsenides versus arsenates is indicated for selected depths (see text for details)

Fig. 3 (a)-(f) Concentration profiles of selected elements within the depth profile taken from tailings site B; the element for each profile is indicated; depths at 9, 11 and 25 cm are highlighted with horizontal bars; the relative abundance of sulfarsenides versus arsenates is indicated for selected depths (see text for details)

Fig. 4 SEM images of selected sulfarsenide grains and arsenate- and Fe-(hydr)oxide bearing coatings; (a) EDS-SEM image in BSE mode and (b) chemical distribution map for Co and As of a safflorite, CoAs_2 grain; (c) EDS-SEM image in BSE mode and (d) chemical distribution map for Zn, Ni and Co of a Co-Ni-Zn arsenate coating on an albite grain and a Fe-(hydr)oxide coating on an arsenopyrite grain; grains and coatings are labelled accordingly.

Fig. 5 Scatter plot of the Co# versus Fe# calculated from chemical analyses of 30 samples collected at both tailings sites (see text for details); data plots for the sites A and B are highlighted in beige and light blue; the average concentrations of selected elements within the depth profiles are listed.

Fig. 6 (a) SEM-EDS image in BSE mode and (b) chemical distribution map for Fe, Ni and Co of a Co-Ni-Zn-Fe-arsenate coating on an albite grain; the coating was selected for a FIB extraction; the location of the extracted FIB section is indicated with a white rectangle; minerals and coatings are labelled accordingly in (a); (c) STEM-EDS image and (d) chemical distribution of Fe, Co and As for the extracted FIB sections; the section is divided into different areas which are indicated with a red-coloured boxes and numbered from 1 to 12

Fig. 7 (a) STEM-EDS image and chemical distribution maps for (b) Fe, Co and As and (c) Zn, Co and Ni for area 2 in the FIB section; the occurrence of a partially replaced scorodite fragment is encircled; (d)-(f) Higher magnification images of the scorodite fragment (encircled): (d) STEM-EDS image, (e) chemical distribution map of Fe, Co and Ni and (f) TEM image indicating the occurrence of a concave-shaped scorodite surface towards the Ni-rich arsenate which is highlighted with a red-dashed curved line; the location of areas depicted in Fig. 8a and 8c are indicated in (e) and (f) with white boxes.

Fig. 8 High-resolution TEM images of the interface between areas composed of a Ni-rich arsenate and scorodite; (a)-(b) the interface between nanoparticles of the Ni-rich arsenate and scorodite is visualized with white curved dashed lines; (a) the area depicted in (b) is indicated with a white box; (c) occurrence of nanoparticles of the Ni-rich arsenate within (indicated with arrows) and around a fragment of scorodite.

Fig. 9 (a) STEM-EDS image and (b) chemical distribution map of Fe, Co and As for a Fe-rich chlorite surrounded by various arsenates in area 1; the locations of the areas depicted in (c) and (d) are indicated with red boxes; (c) STEM-EDS image and (d) chemical distribution map for Fe, Zn and Ni for alteration halos in the Co-Ni-rich arsenate and Fe-rich chlorite (labelled with arrows); (e) STEM-EDS image of a highly-altered Mg-rich chlorite (labelled) and an albite fragment (shown in Fig. 9g and indicated with a white box) in the areas 4 and 5; the area shown in (f) is also indicated with a white box; (f) High-resolution TEM image of an area within the altered chlorite depicted in (e); areas composed of chlorite (chl) are characterized by lattice fringes parallel to (001) ($d \sim 14 \text{ \AA}$); nano-size pores with the chlorite contain nanoparticles of most likely a Ni-arsenate (Ni-As; identified on the basis of lattice fringes); (g) TEM (top) and STEM chemical distribution map for As (red) and Si (green) of a porous interface between an albite fragment and a Co-Ni-Zn-arsenate (vivianite structure-type); the area depicted in (h) is indicated with a white-framed square; (h) high-resolution TEM image of the interface between albite and a Co-Ni-Zn-arsenate, indicating the occurrence of nanoparticles of the arsenate in the pore spaces within the alteration rim of the albite.

Table 1 Arsenic-bearing minerals identified in the tailings of the Cobalt mining camp (excludes minerals identified in the ore veins and surrounding country rock)

Sulfarsenides			arsenates		
Mineral name	Formula	Ref.	Mineral name	Formula	Ref.
cobaltite	CoAsS	[1]-[3]	arsenohopeite	Zn ₃ (AsO ₄) ₂ ·4H ₂ O Zn can be partially replaced by Ni and Co	[3]
safflorite	(Co,Fe,Ni)As ₂	[1], [3]	tsumcorite-group ferrilotharmeyerite	Me ₁ M ₂ (XO ₄) ₂ (OH,H ₂ O) ₂ Me=Ca, M=Fe ³⁺ , X=As ⁵⁺	[3]
skutterudite	CoAs ₃	[1]	scorodite	FeAsO ₄ (H ₂ O) ₂	[2], [3]
arsenopyrite	FeAsS	[1], [3]	Arsenate minerals of the vivianite group erythrite annabergite köttigite	(M ₃ (AsO ₄) ₂ ·8H ₂ O with M = Co, Ni and Zn Co ₃ (AsO ₄) ₂ ·8H ₂ O Ni ₃ (AsO ₄) ₂ ·8H ₂ O Zn ₃ (AsO ₄) ₂ ·8H ₂ O	[2], [3]
gersdorffite	NiAsS	[1], [3]	pharmocolite	Ca(HAsO ₄)·2H ₂ O	[2]
löllingite	FeAs ₂	[3]	weilite brassite	Ca(HAsO ₄) Mg(HAsO ₄)·4H ₂ O	[2] [2]

[1] = Kwong et al., (2006), [2] = Percival et al., (2007); [3] = this study

a



b



Fig. 1

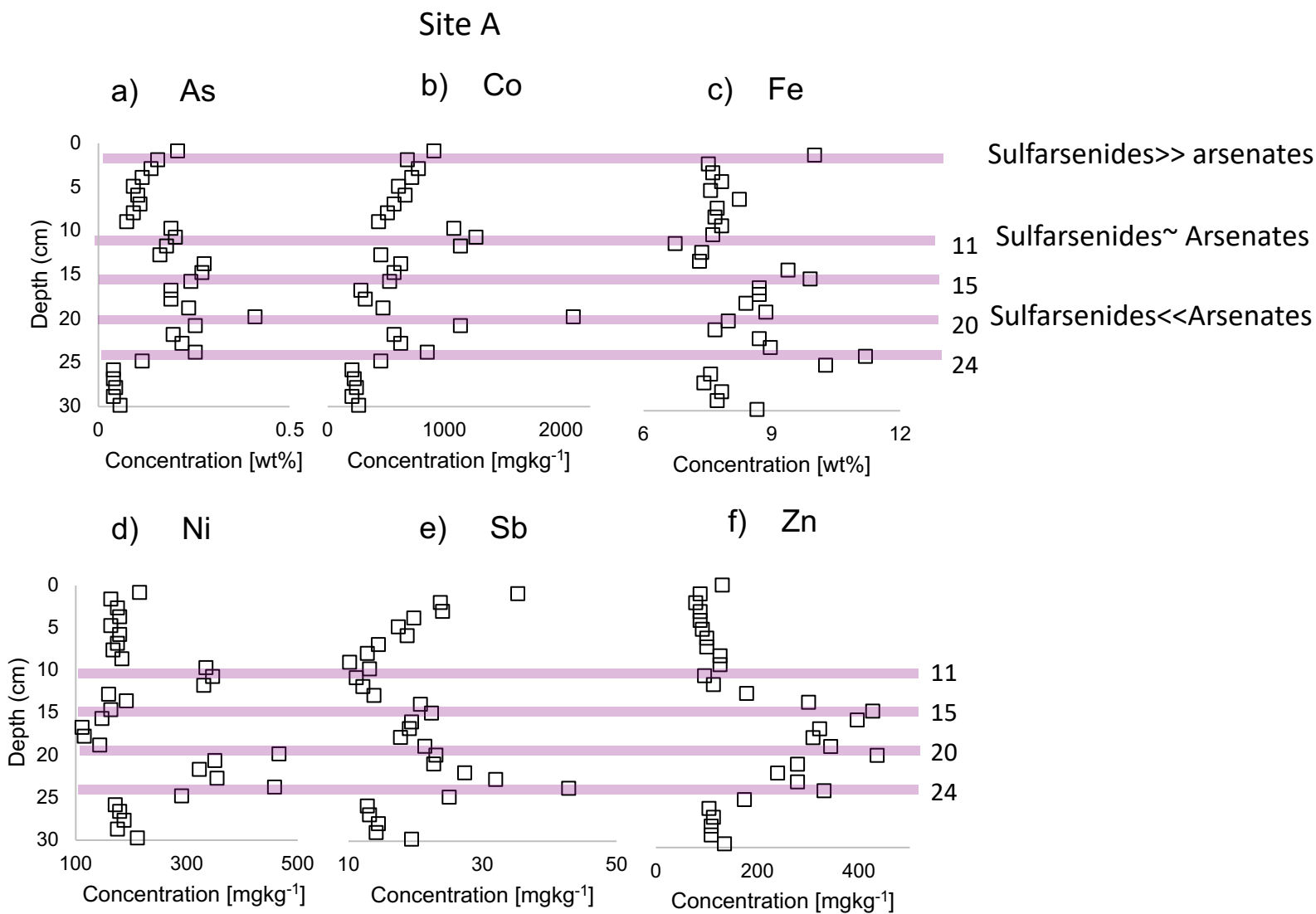


Fig. 2

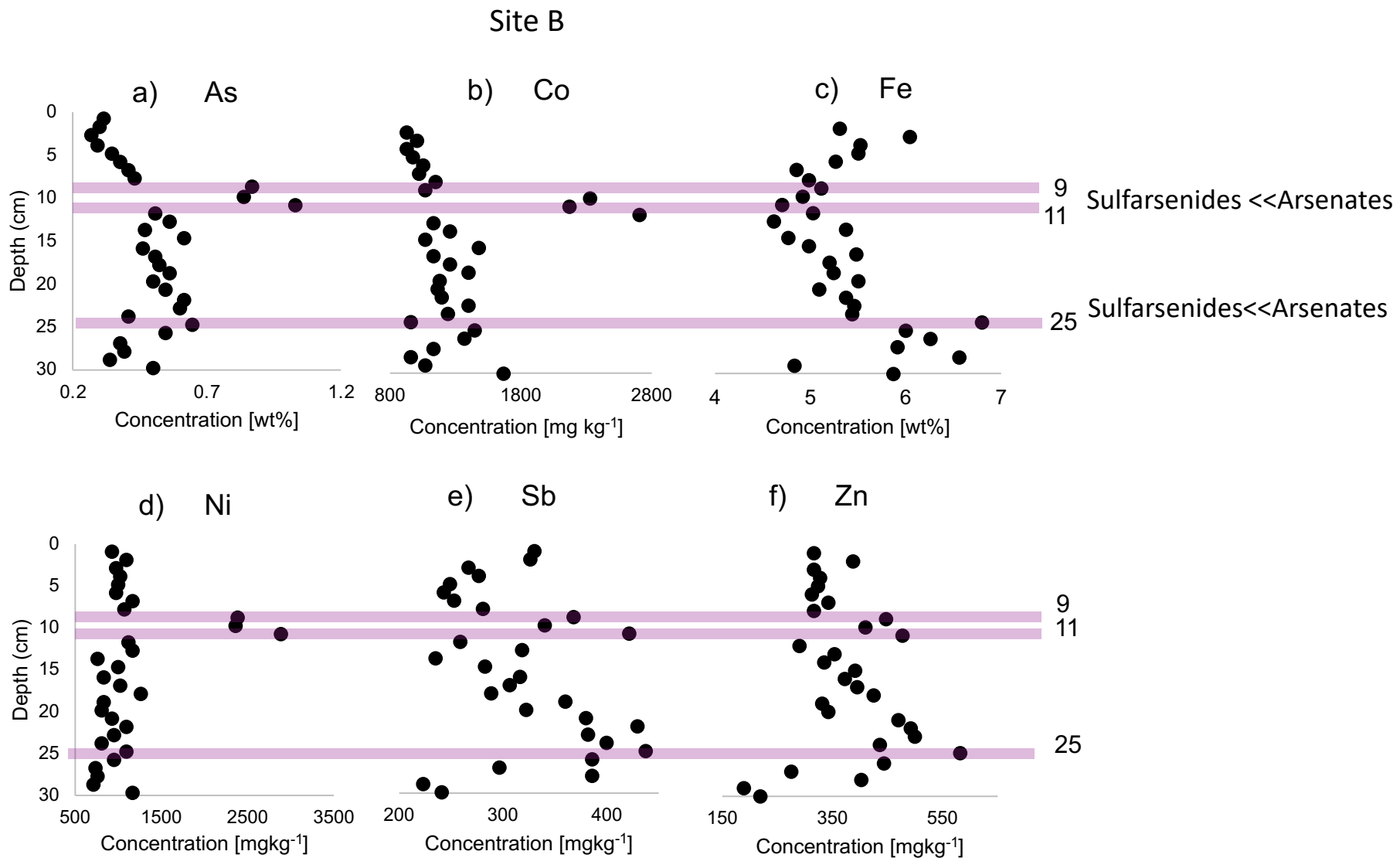


Fig. 3

a



b

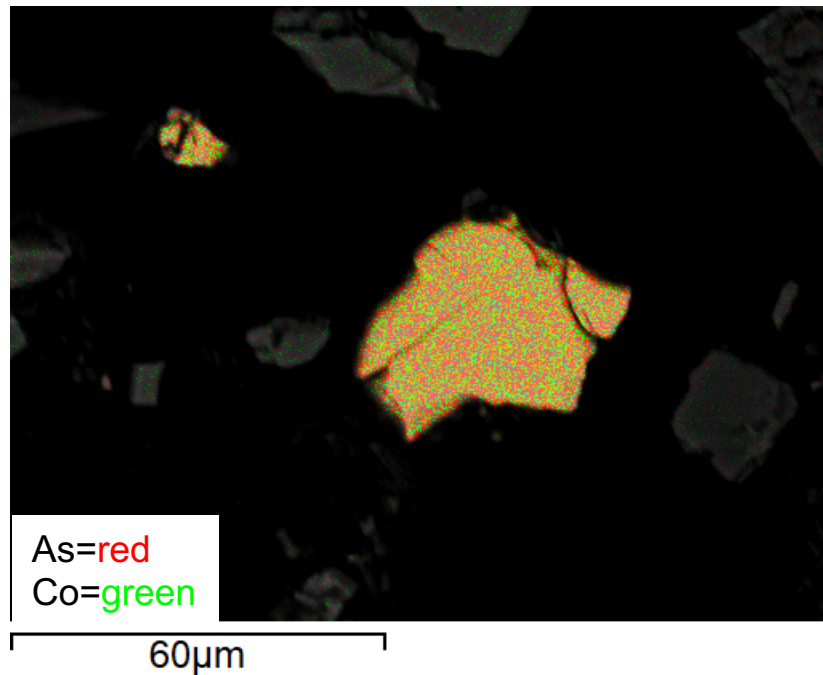
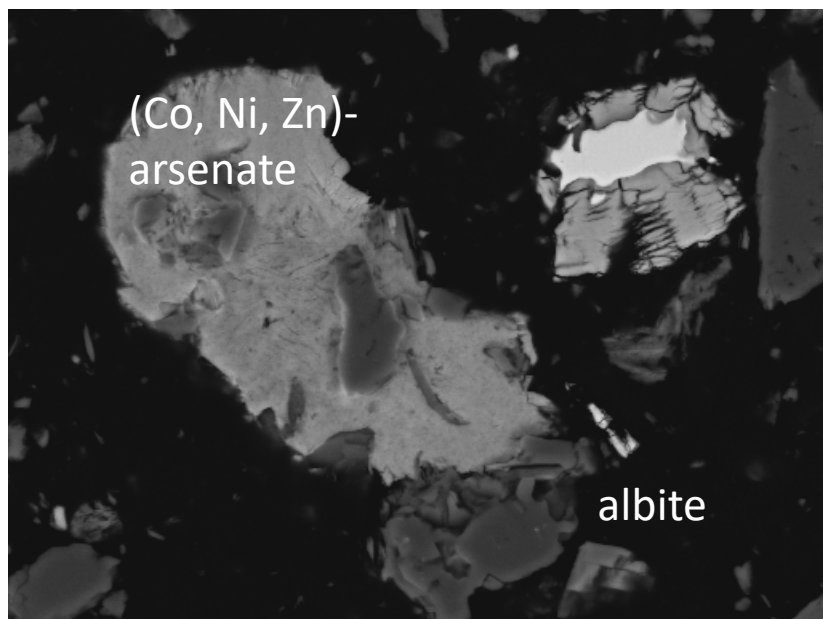
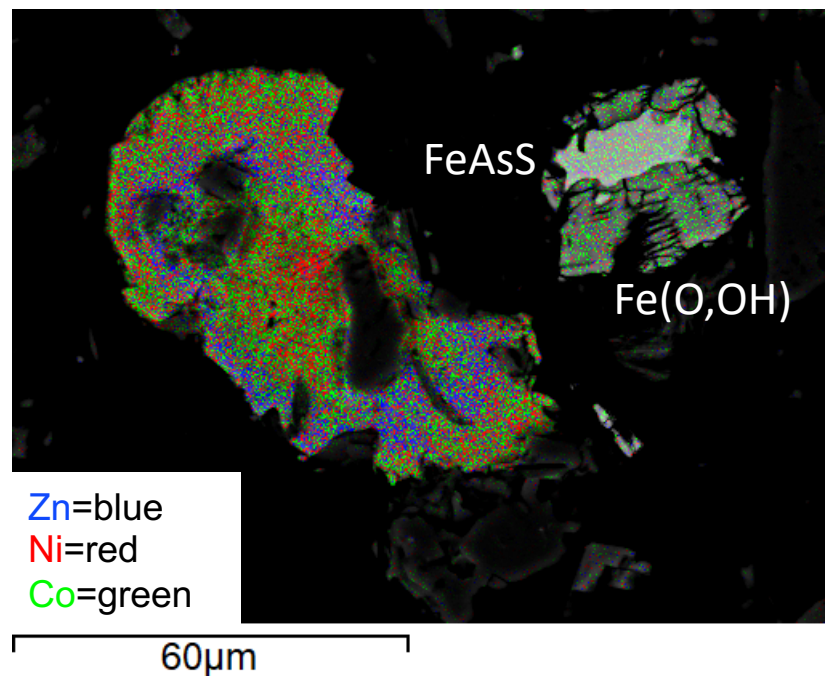


Fig. 4

c



d



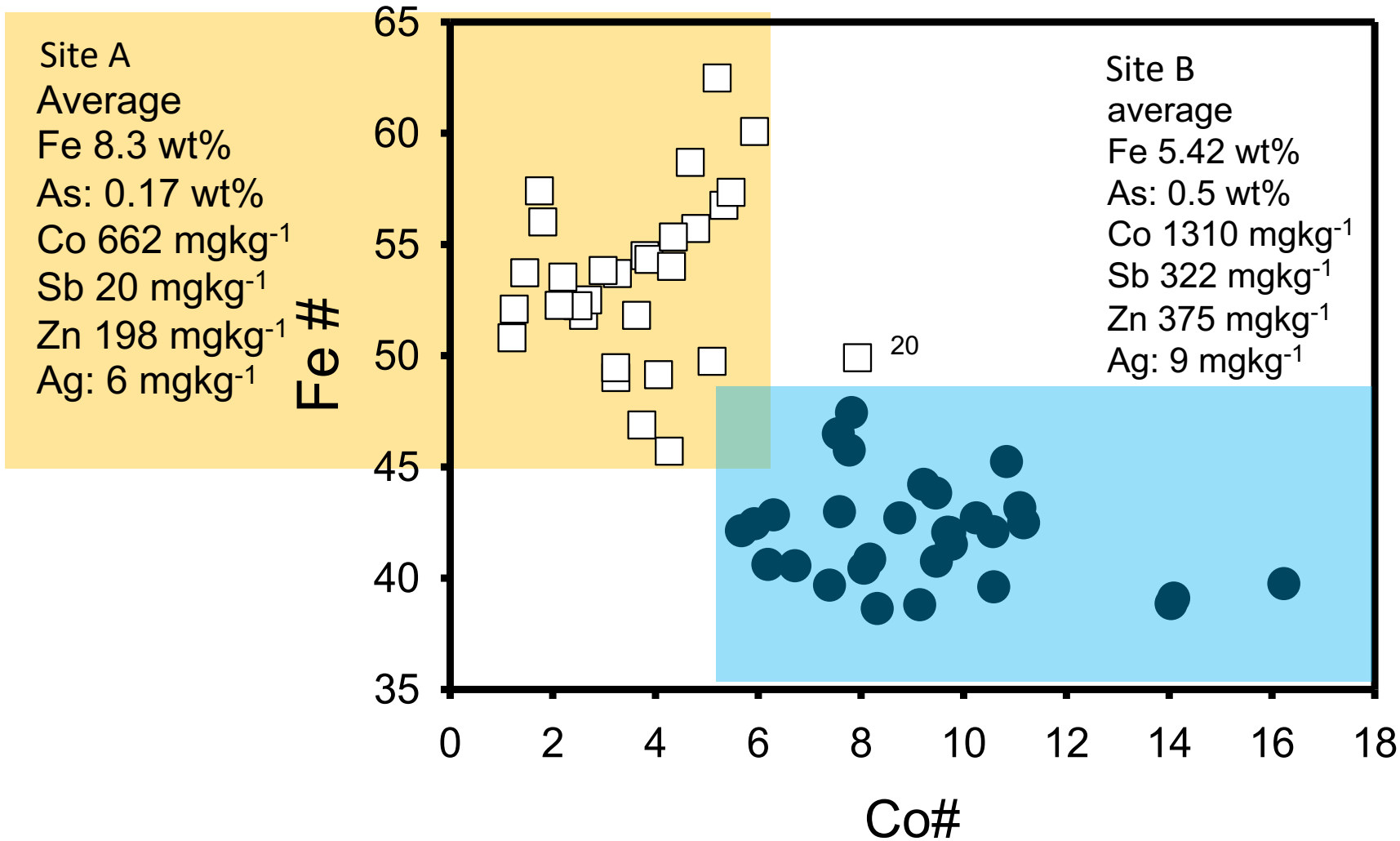


Fig. 5

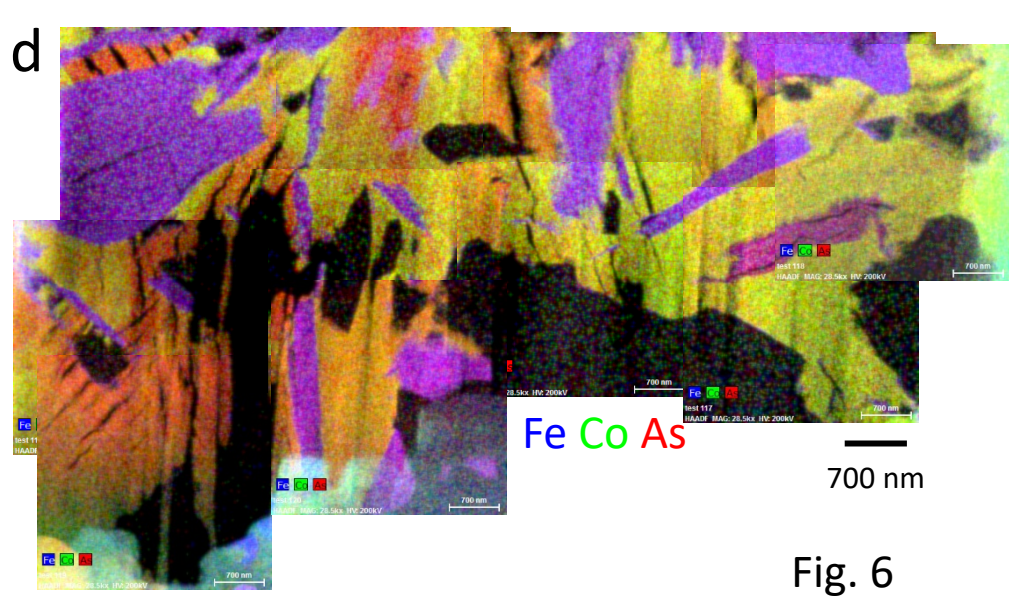
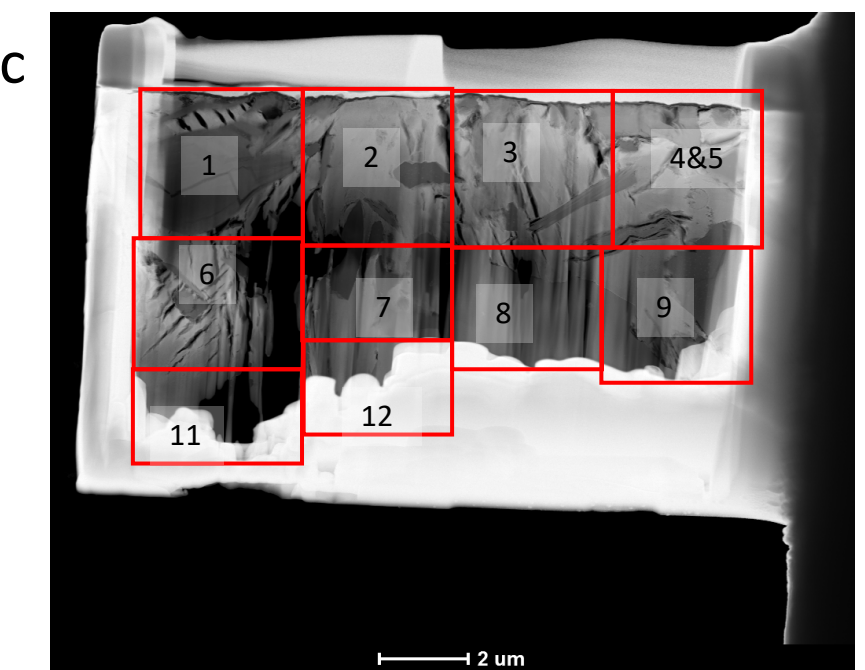
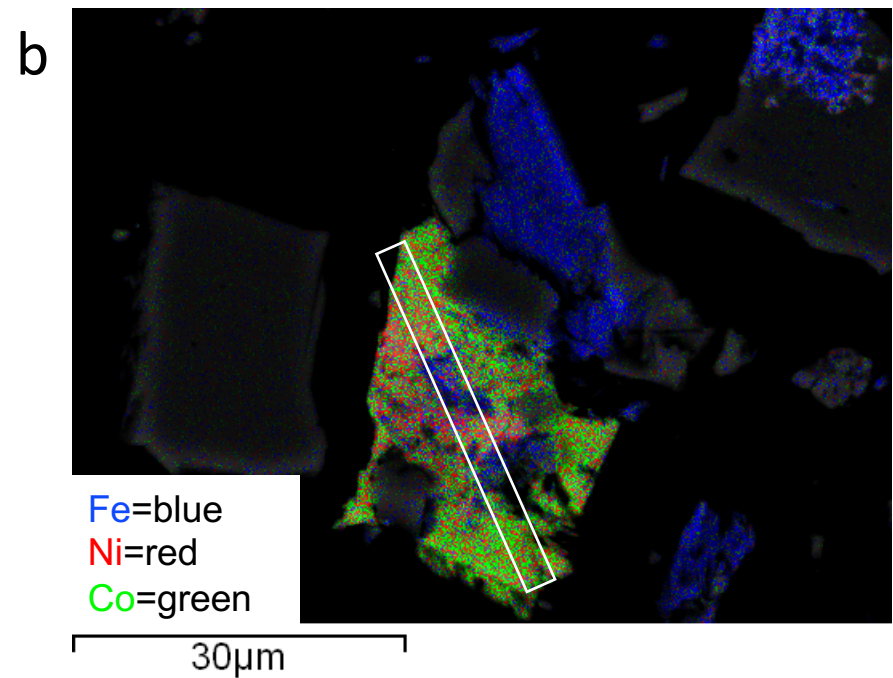
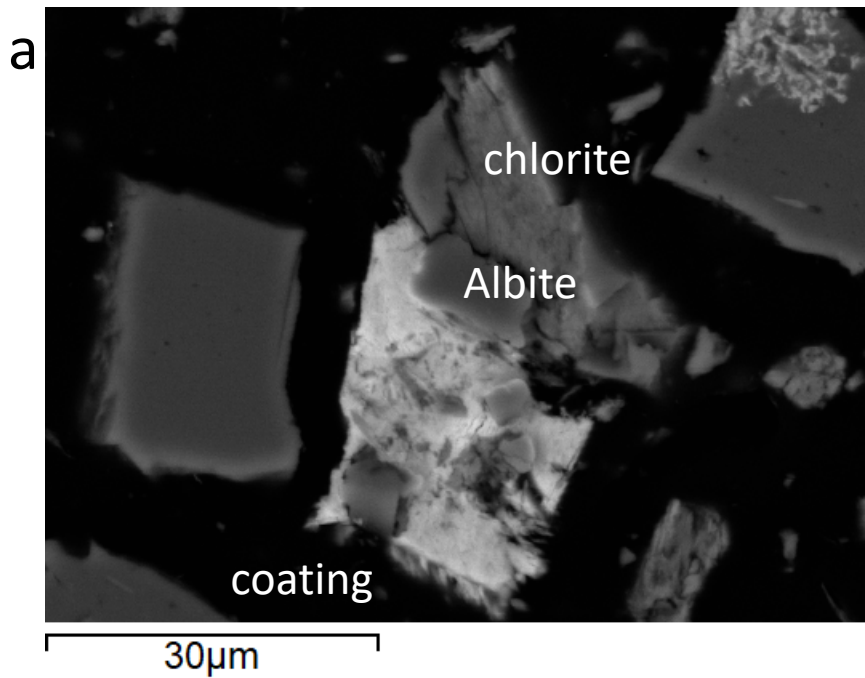


Fig. 6

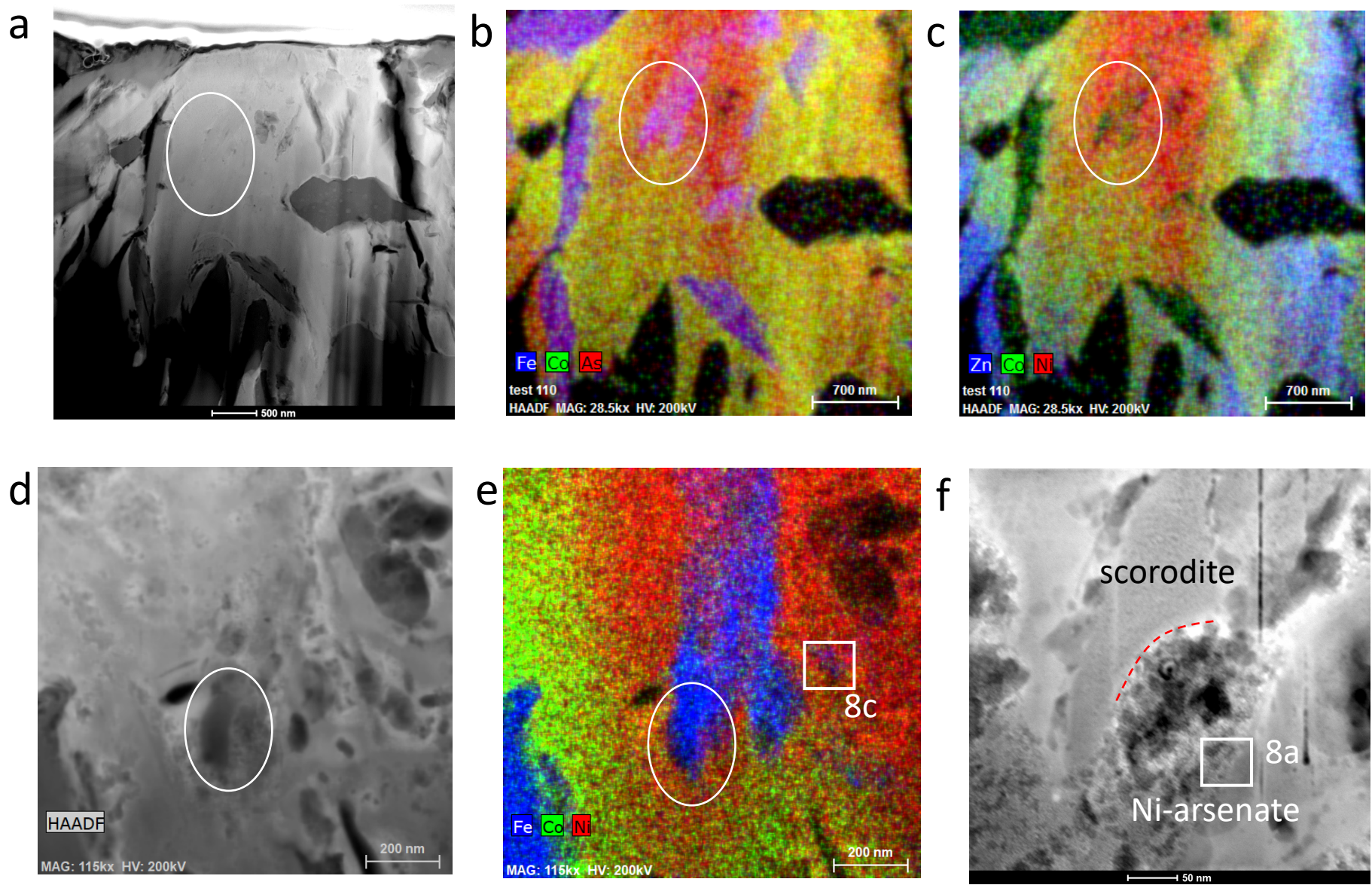


Fig. 7

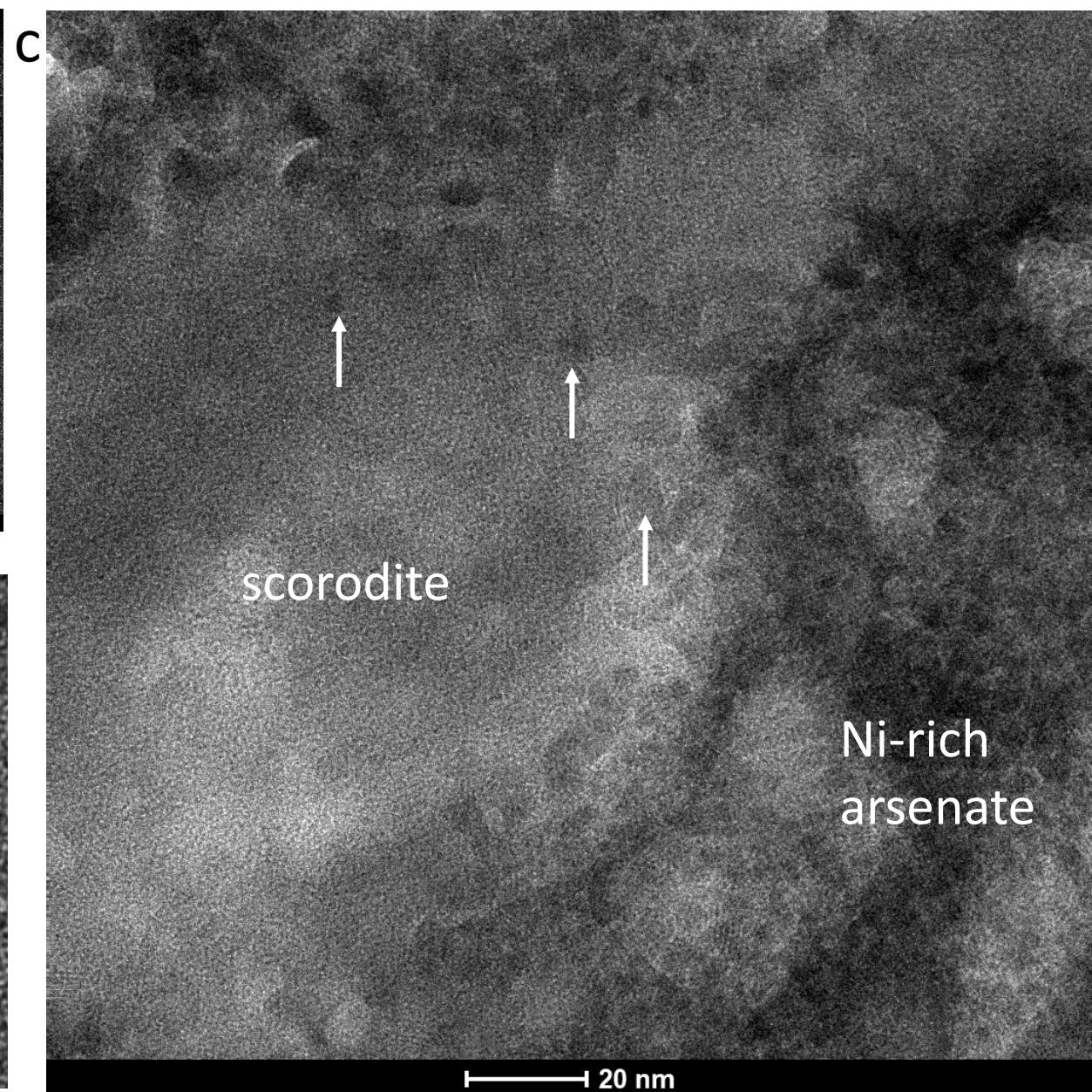
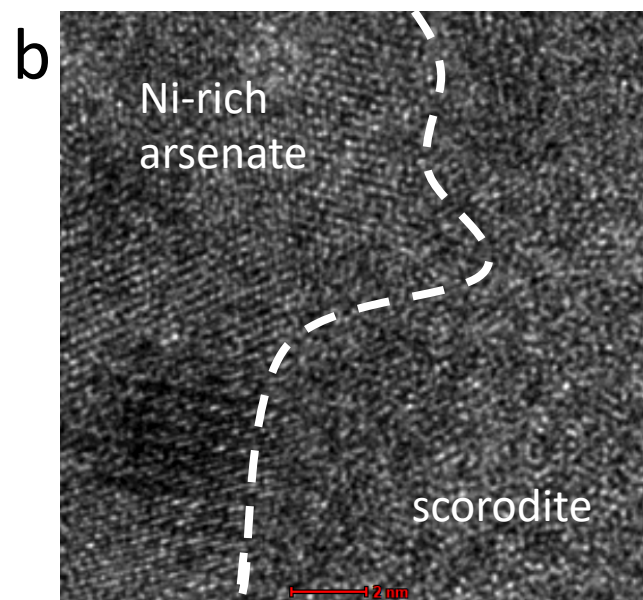
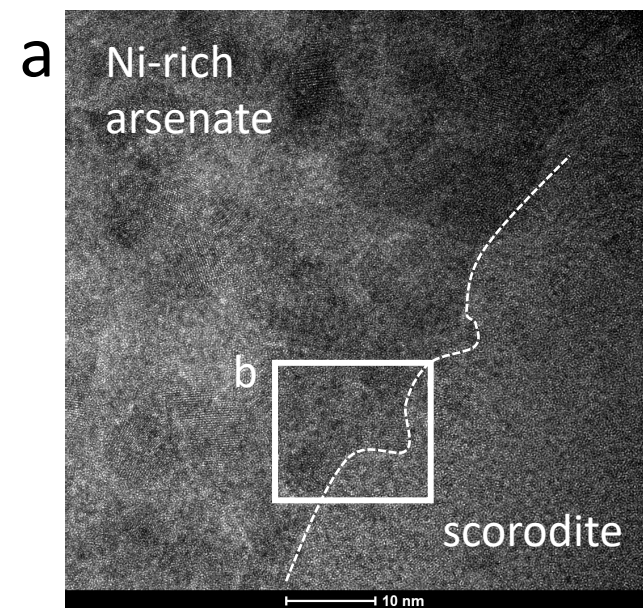


Fig. 8

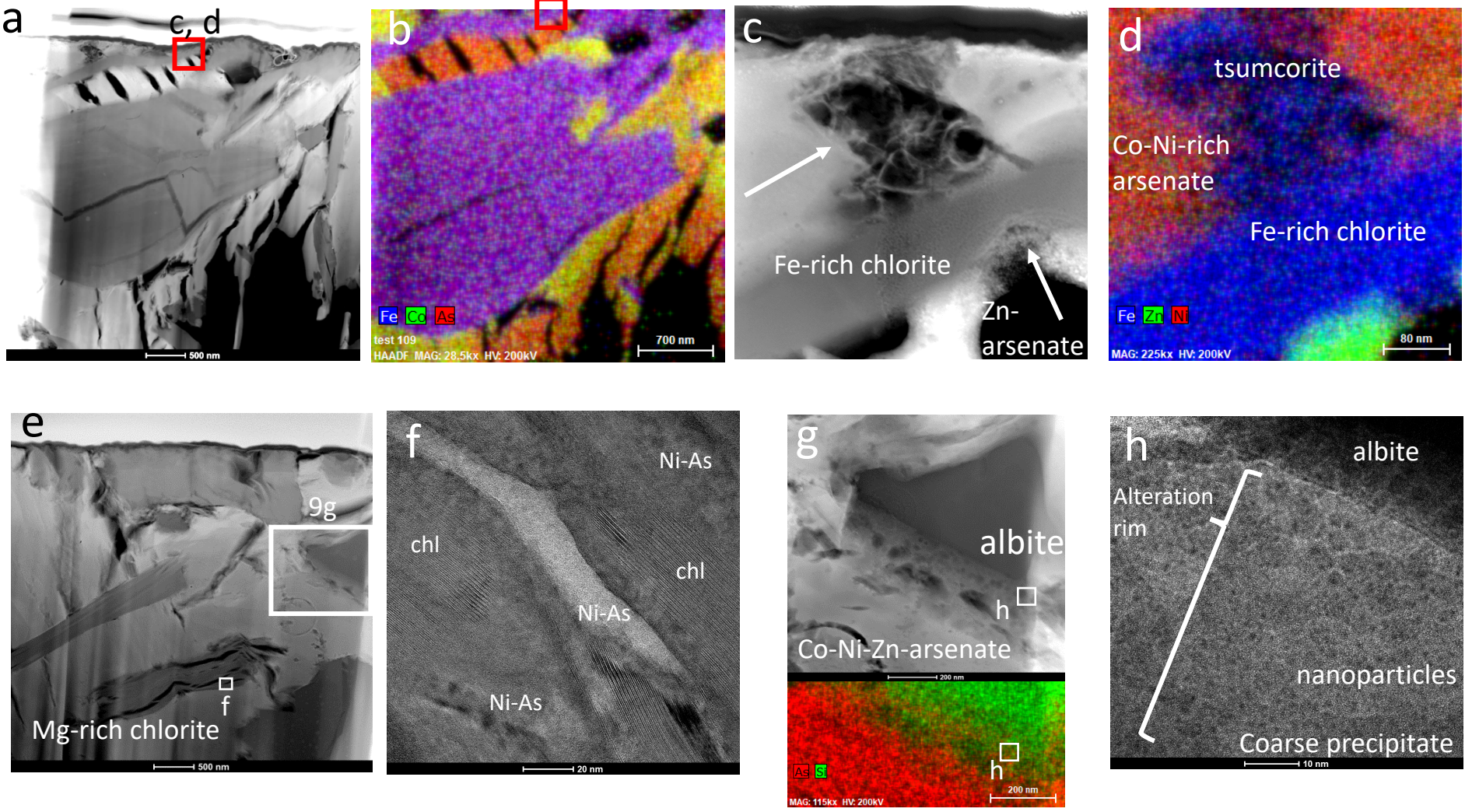
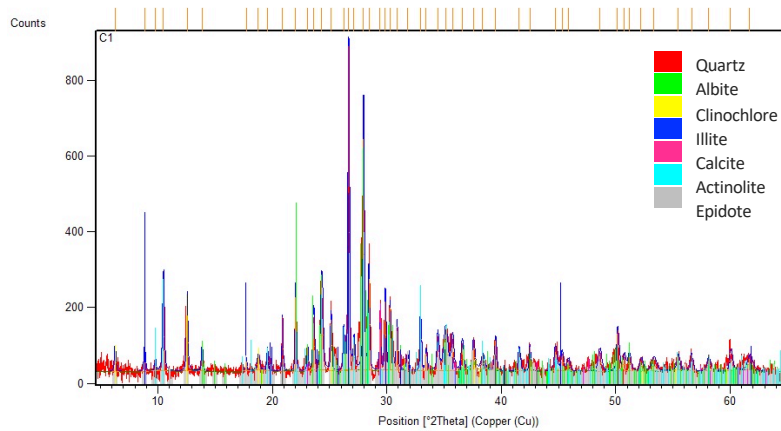


Fig. 9

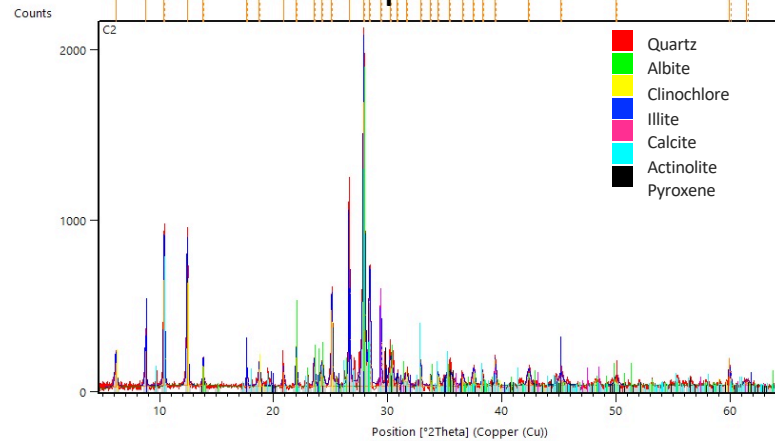
Supplementary Data A

X-ray diffraction pattern from samples collected at
site A and B tailings sites

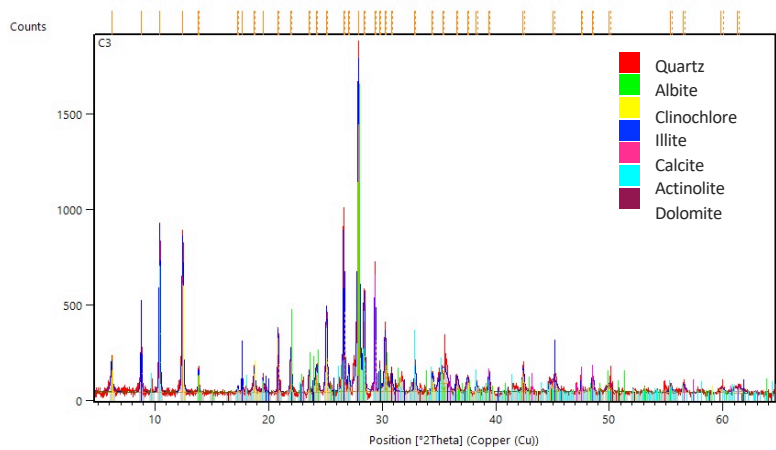
Sample No. A-1



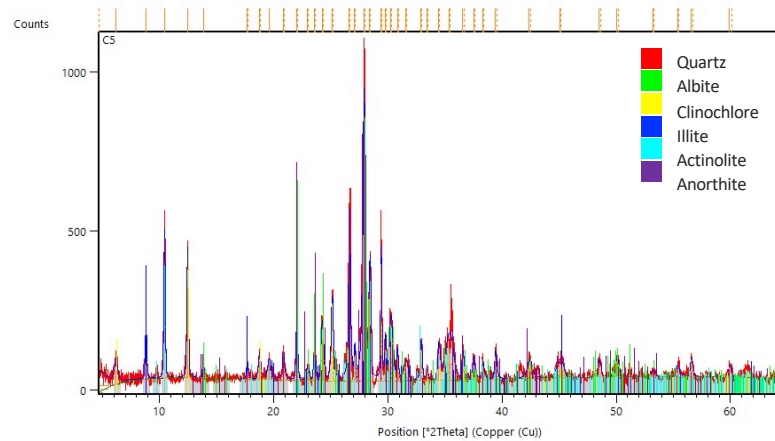
Sample No. A-2



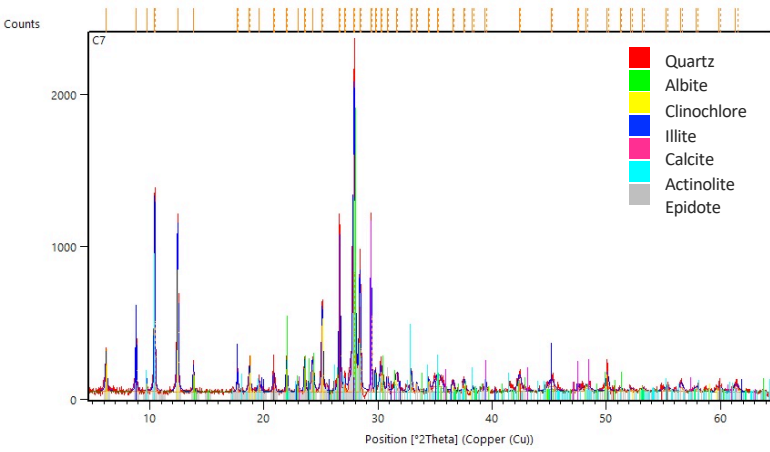
Sample No. A-3



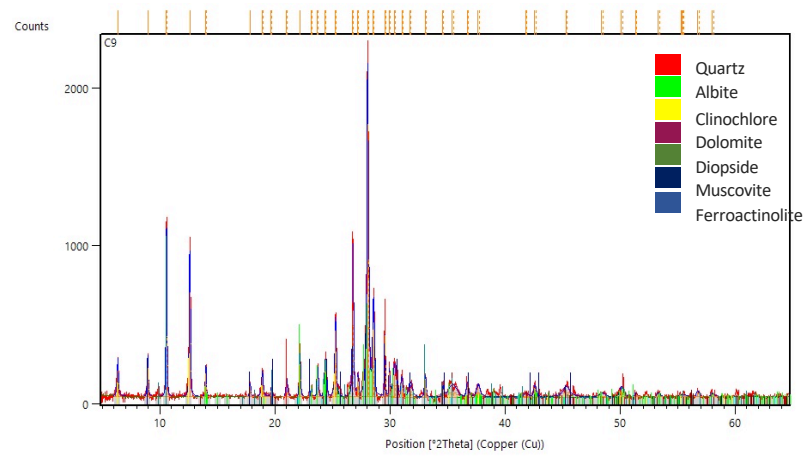
Sample No. A-5



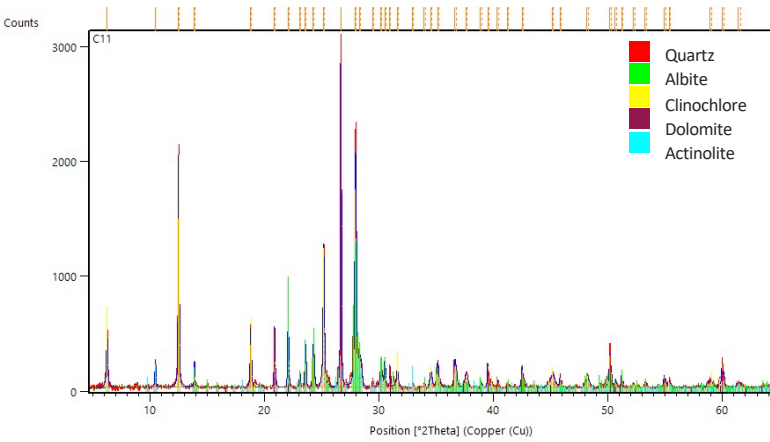
Sample No. A-7



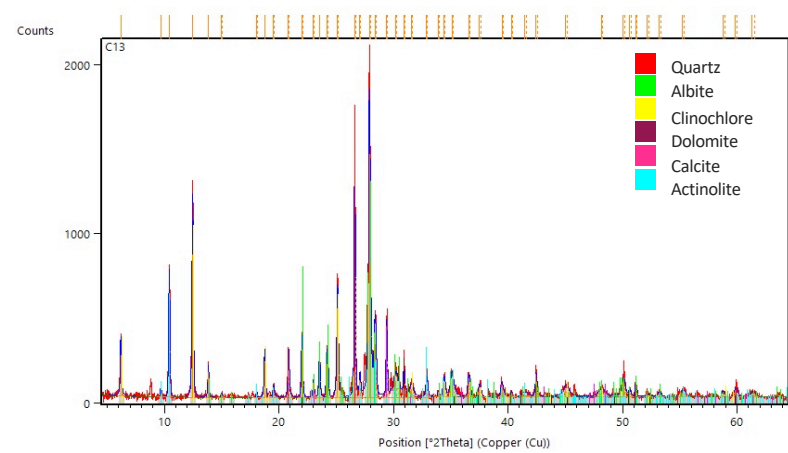
Sample No. A-9



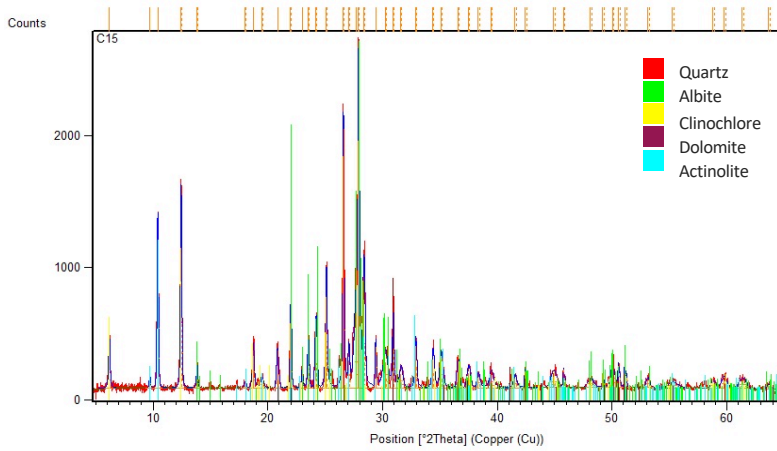
Sample No. A-11



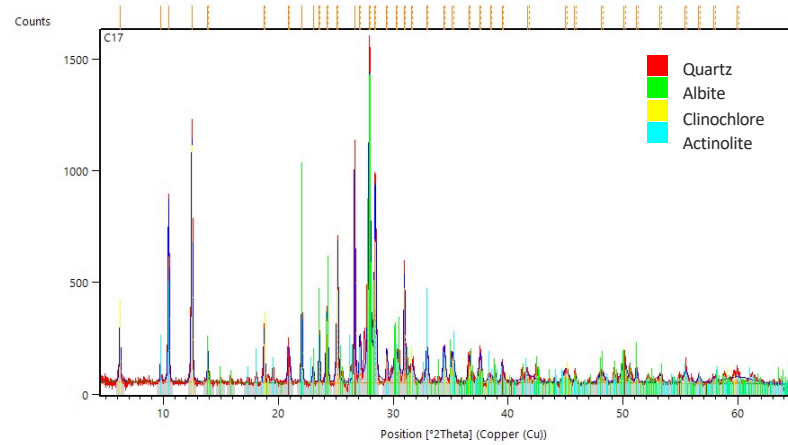
Sample No. A-13



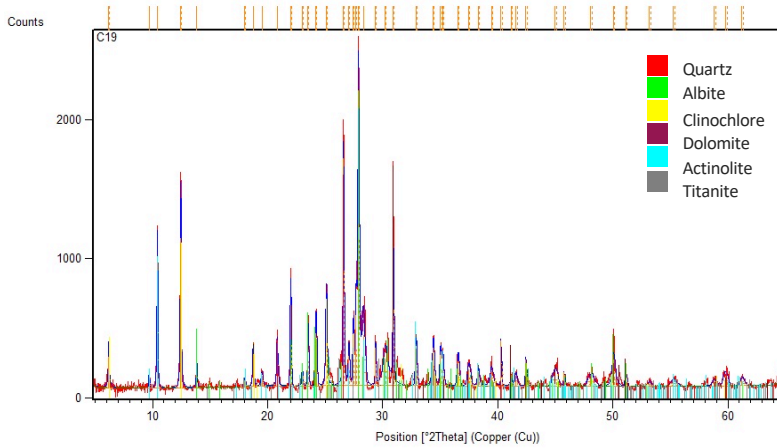
Sample No. A-15



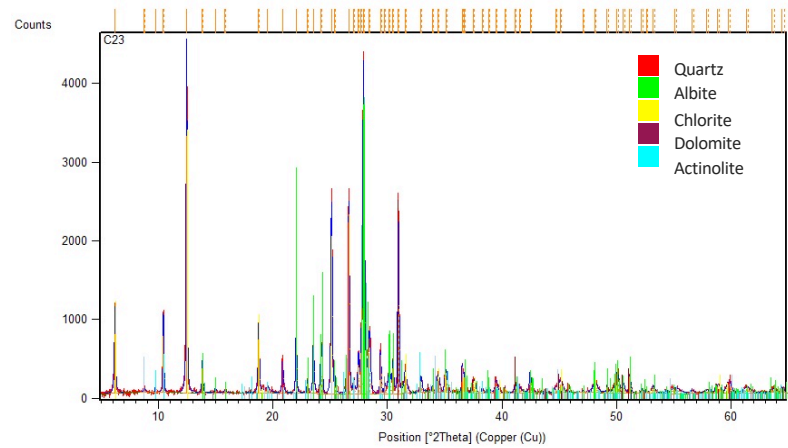
Sample No. A-17



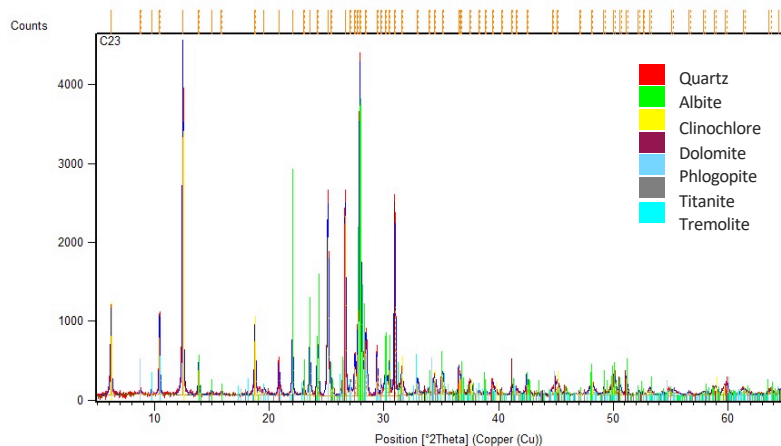
Sample No. A-19



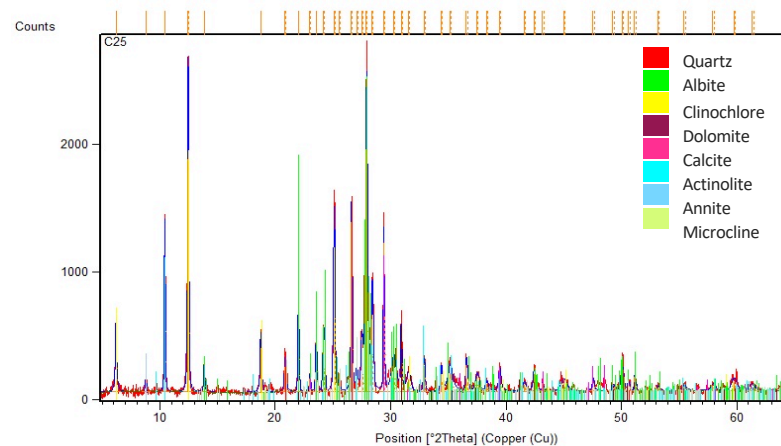
Sample No. A-21



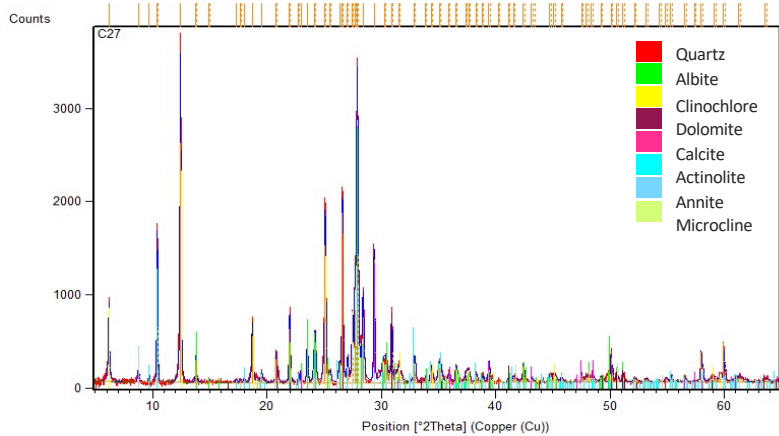
Sample No. A-23



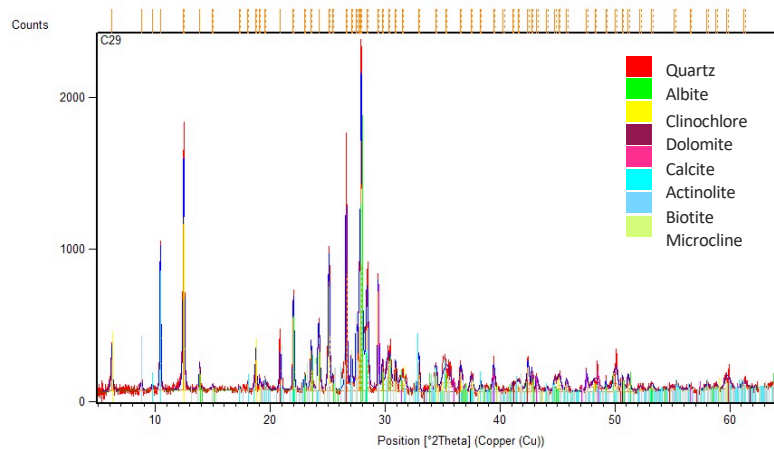
Sample No. A-25



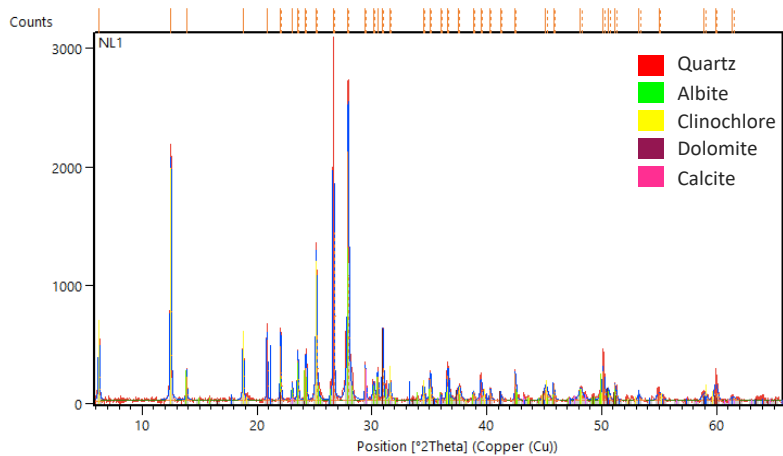
Sample No. A-27



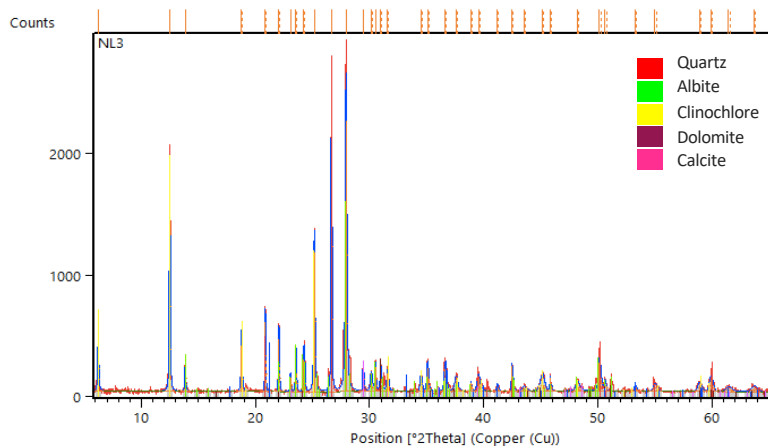
Sample No. A-29



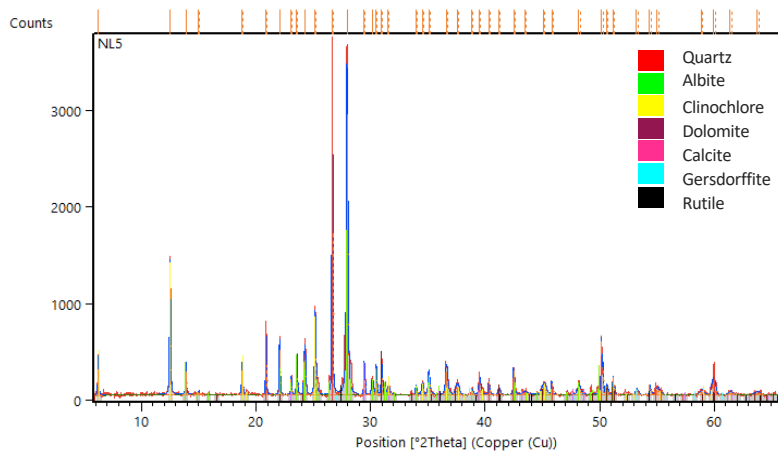
Sample No. B-1



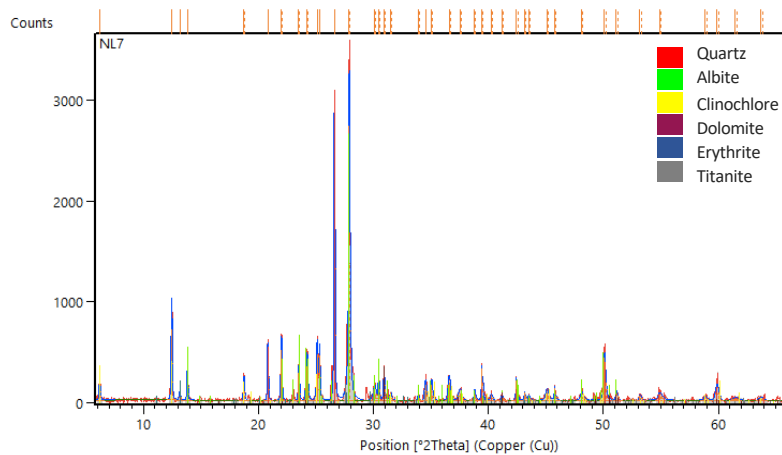
Sample No. B-3



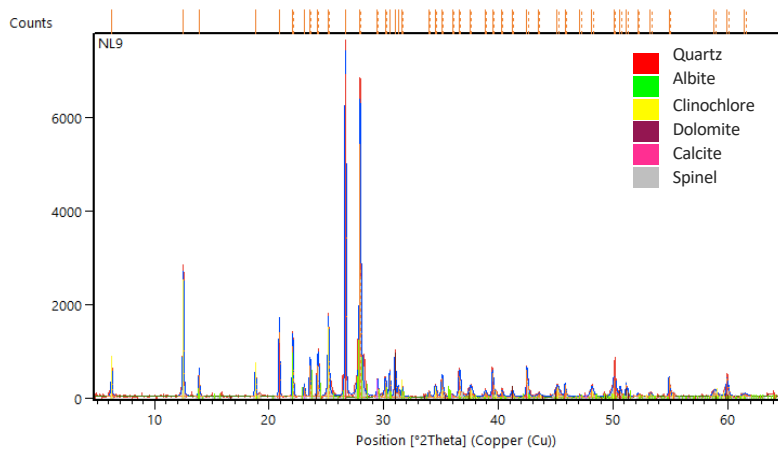
Sample No. B-5



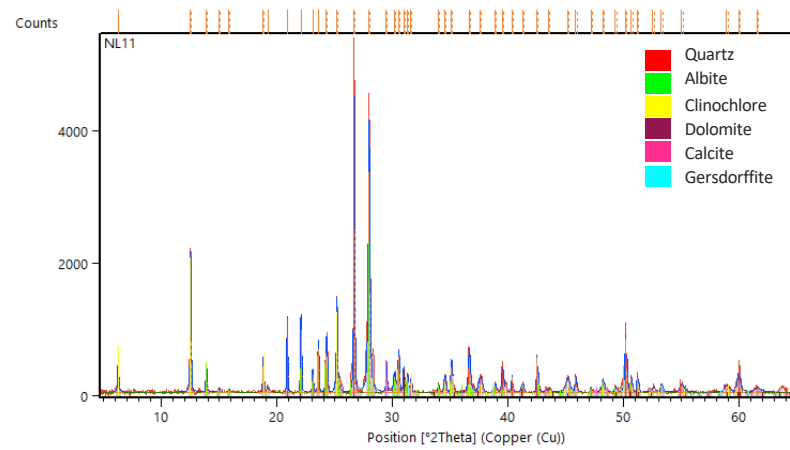
Sample No. B-7



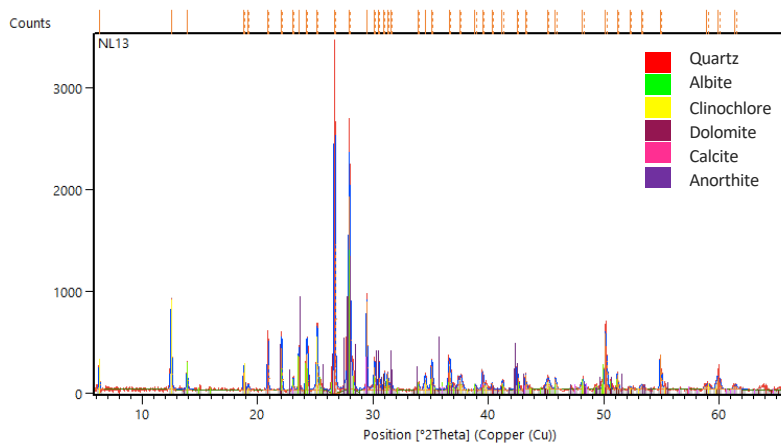
Sample No. B-9



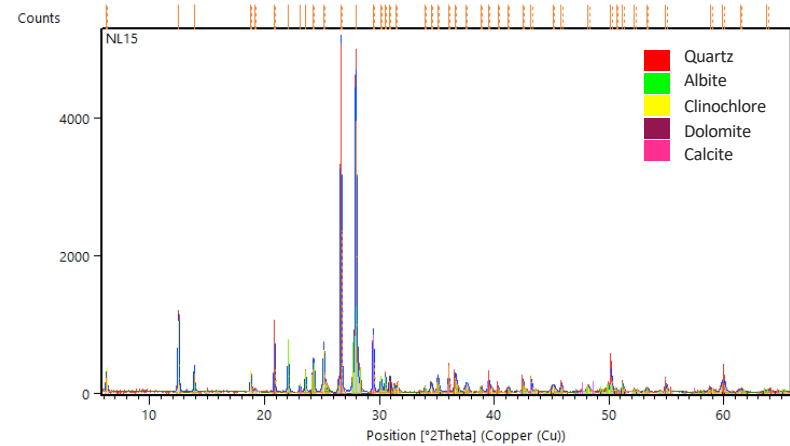
Sample No. B-11



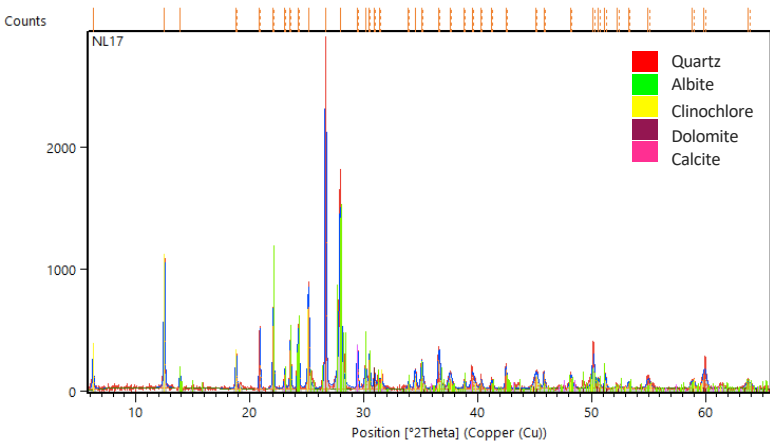
Sample No. B-13



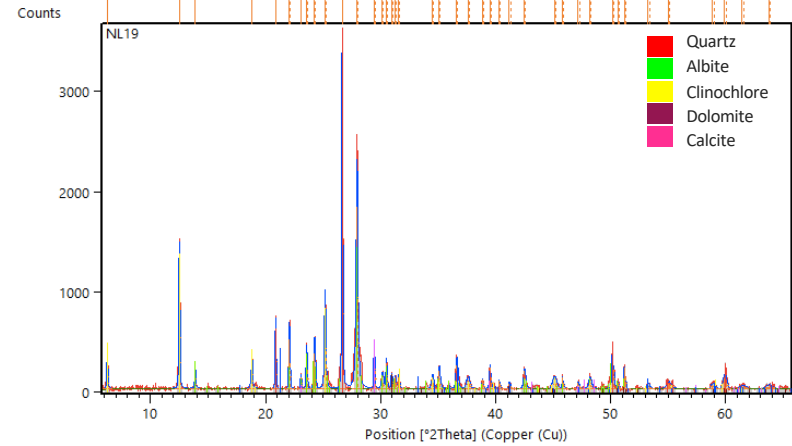
Sample No. B-15



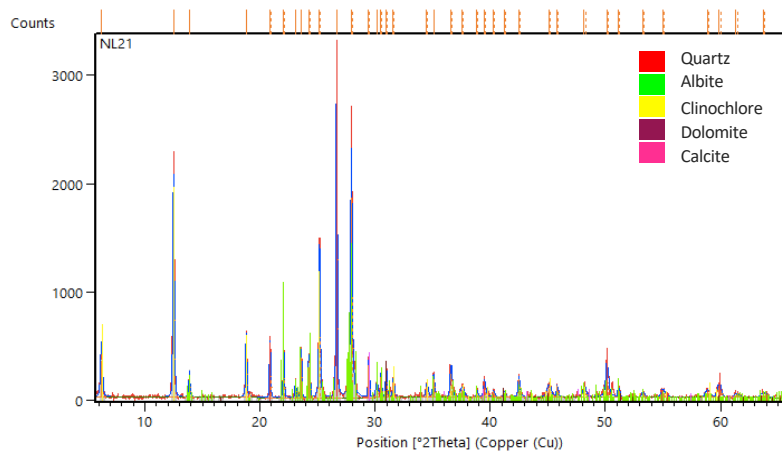
Sample No. B-17



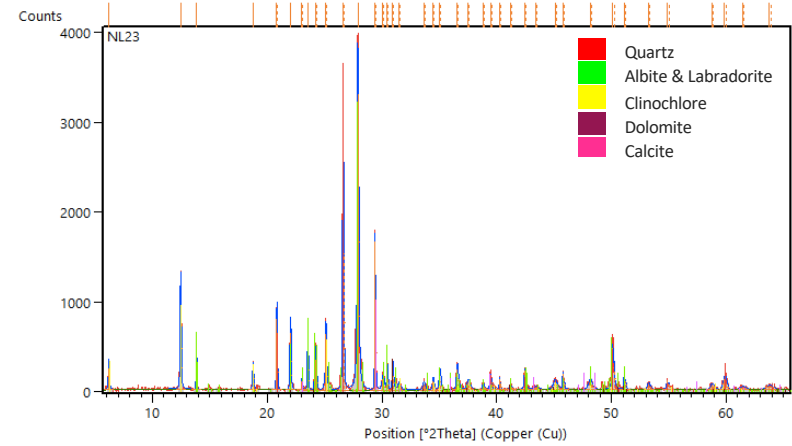
Sample No. B-19



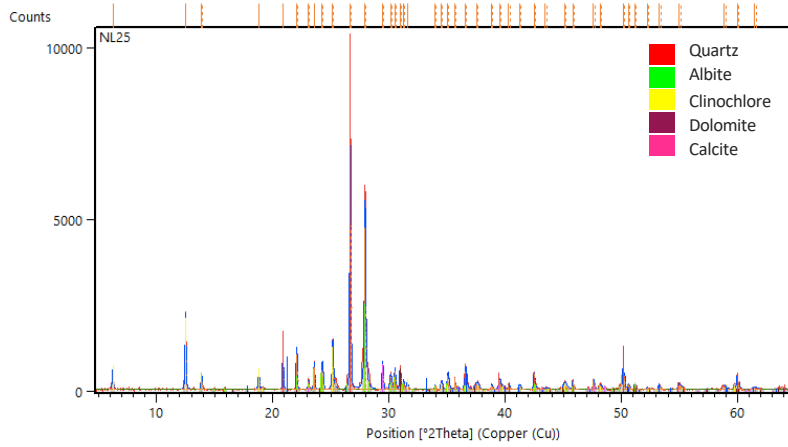
Sample No. B-21



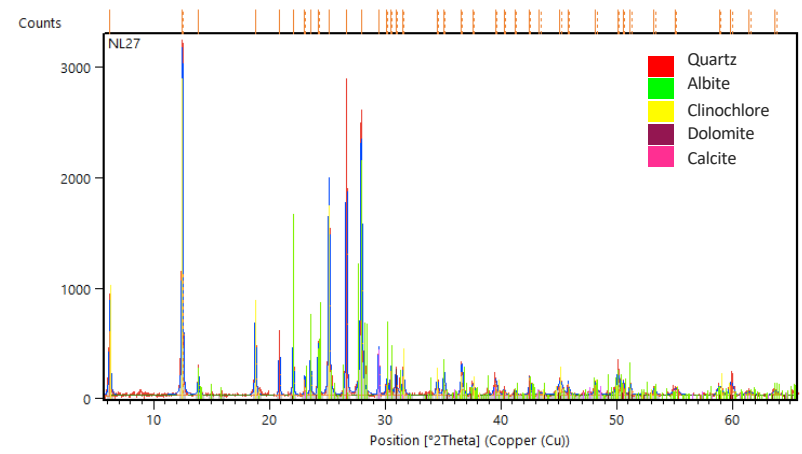
Sample No. B-23



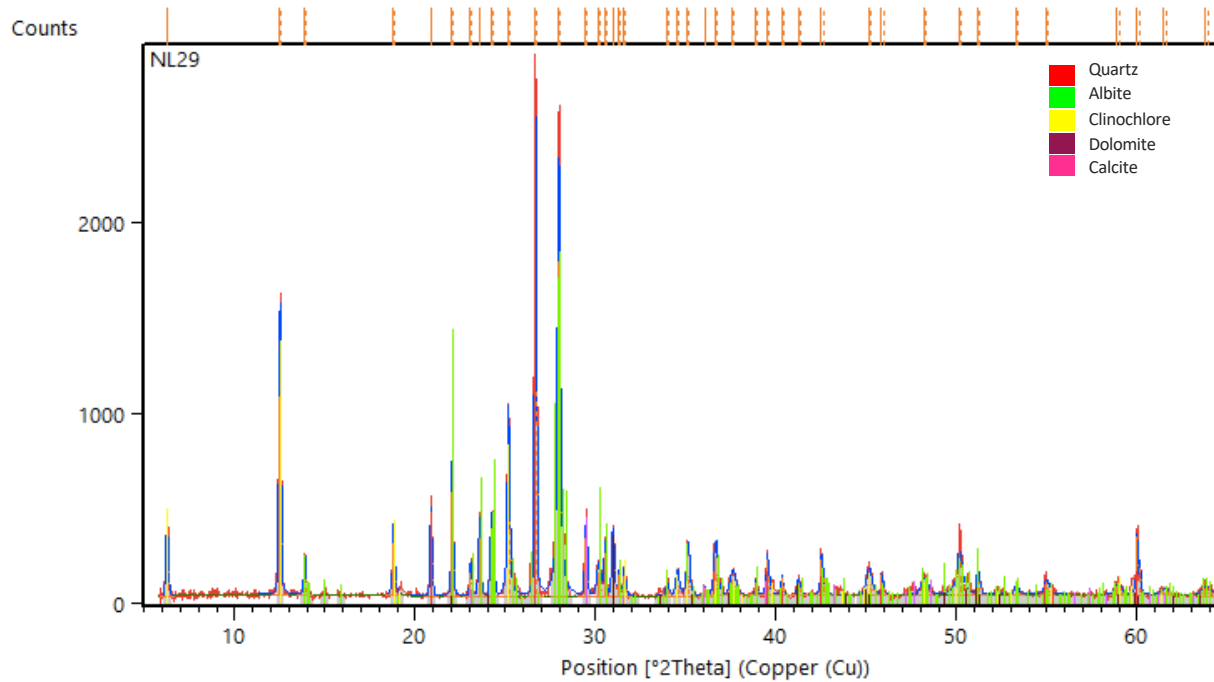
Sample No. B-25



Sample No. B-27

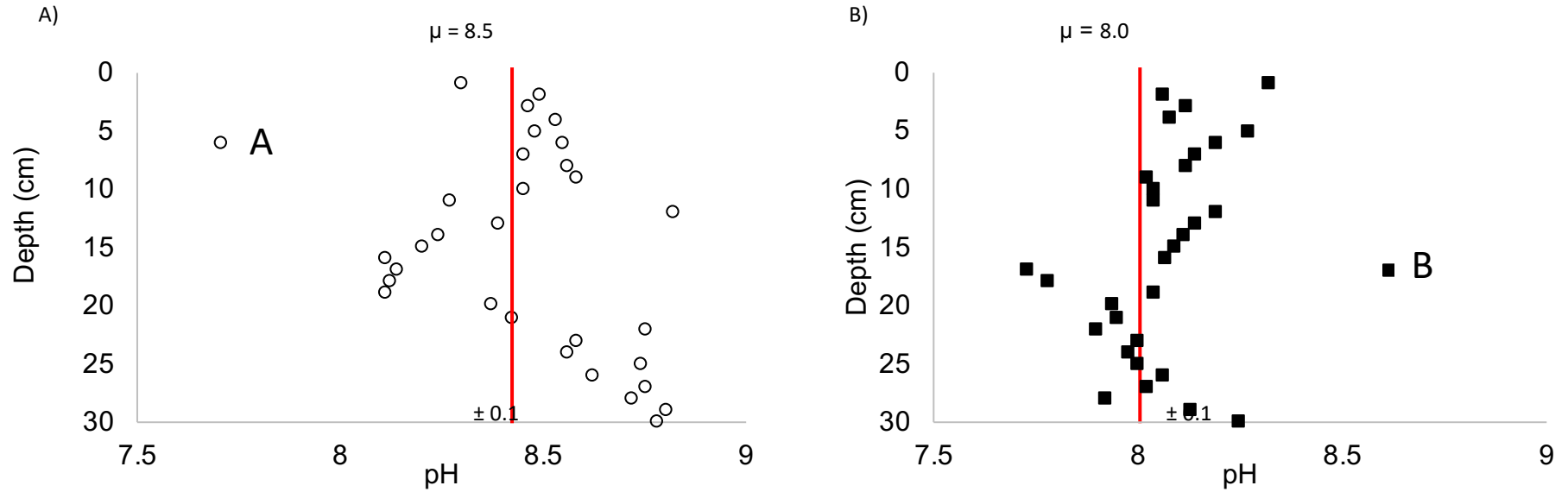


Sample No. B-29



Supplementary data B

Change of contact pH with depth



A and B: Plot of contact pH value versus depth for the two depth profiles

Supplementary data C

Chemical composition of the tailing samples, site B tailings

FINAL RESULTS wt% or (mg/Kg)																					
ELRFS LABEL	Ag	Al	As	Ca	Co	Cu	Fe	Hg	K	Mn	Mo	Na	P	Pb	Sb	Se	Ti	V	Zn	Zr	
Units	ppm	wt%	wt%	wt%	ppm	ppm	wt%	ppm	wt%	ppm	ppm	wt%	ppm	ppm	ppm	ppm	wt%	ppm	ppm	ppm	
NL = Nipissing- low tailings site																					
NL-1	4.19	7.78	0.313	2.37	937	414	5.32	1	0.587	906	1.5	3.62	577	396	333	2.81	0.424	155	318	101	
NL-2	6.91	8.22	0.303	2.45	1020	411	6.06	4.29	0.58	1020	1.5	3.63	651	467	328	3.06	0.46	172	388	106	
NL-3	6.95	7.61	0.268	2.25	936	375	5.54	3.52	0.562	928	1.5	3.43	595	416	268	2.4	0.437	158	317	102	
NL-4	6.41	7.38	0.296	2.19	997	396	5.53	4.7	0.514	926	1.5	3.38	578	455	278	2.49	0.429	156	329	99.1	
NL-5	8.67	7.74	0.344	2.31	1070	485	5.28	2.6	0.519	895	1.5	3.71	562	429	250	1.24	0.446	150	326	106	
NL-6	6.61	7.42	0.376	2.23	1040	560	4.88	4.51	0.463	841	1.5	3.62	496	442	245	2.13	0.407	137	314	94.1	
NL-7	5.82	7.24	0.411	2.2	1170	562	5	6.34	0.5	865	1.5	3.5	522	447	254	1.79	0.437	139	345	101	
NL-8	8.11	7.57	0.428	2.33	1090	661	5.14	2.57	0.462	909	1.5	3.67	510	526	283	2.82	0.423	143	319	97.7	
NL-9	14.5	7.76	0.868	2.08	2340	834	4.93	1	0.465	847	5.35	4	512	673	370	1.7	0.47	137	449	113	
NL-10	9.47	7.37	0.838	1.875	2190	761.5	4.73	1.93	0.4515	811	6.385	3.825	533	589	343	1.4675	0.4925	132.5	409.5	113	
NL-11	8.88	7.64	1.03	2.18	2720	882	5.04	1	0.469	861	8.25	3.93	587	777	423	1.64	0.503	137	478	125	
NL-12	10.1	7.32	0.506	2.27	1140	615	4.64	1	0.472	825	3.58	3.68	480	540	261	0.991	0.446	133	291	97.6	
NL-13	14.1	7.85	0.56	2.51	1270	663	5.4	1	0.505	946	3.75	3.73	536	642	321	1.95	0.468	153	356	105	
NL-14	12.3	7.61	0.471	2.19	1080	541	4.79	1	0.522	843	6.23	3.84	471	478	236	1.47	0.468	141	335	101	
NL-15	12.8	7.61	0.616	2.25	1490	681	4.99	1	0.513	871	6.93	3.76	524	588	285	1.29	0.488	143	391	110	
NL-16	9.24	7.38	0.463	2.39	1150	609	5.5	1	0.493	948	1.5	3.3	566	761	318	1.72	0.432	156	374	93.3	
NL-17	5.96	6.32	0.508	2.05	1280	614	5.22	8.96	0.481	904	3.19	2.88	559	730	309	1.18	0.437	146	396	94.7	
NL-18	11.5	7.41	0.524	2.25	1420	638	5.26	2.17	0.49	933	3.16	3.41	560	745	290	1.07	0.44	149	426	94.8	
NL-19	13	7.61	0.558	2.41	1190	735	5.52	1	0.51	948	3.31	3.53	548	902	363	0.3	0.445	154	332	97.9	
NL-20	7.88	7.04	0.503	2.23	1180	672	5.11	1	0.472	877	3.11	3.25	506	807.5	323.5	0.7675	0.3945	139.5	345.5	87.35	
NL-21	5.11	7.22	0.543	2.36	1210	746	5.38	2.43	0.482	942	3.27	3.22	559	896	382	1.73	0.398	148	472	89.3	
NL-22	11.2	7.42	0.613	2.35	1410	858	5.48	6.52	0.509	951	4.33	3.24	581	951	432	1.57	0.415	150	495	94.6	
NL-23	9.53	7.50	0.597	2.59	1260	750	5.45	1	0.485	956	3.42	3.45	595	1040	383	0.3	0.435	152	502	98.3	
NL-24	10	7.84	0.406	2.67	982	529	6.81	1	0.5	1100	1.5	3.18	658	856	401	1.6	0.435	191	438	97.7	
NL-25	13.9	7.93	0.65	2.69	1470	900	6.02	4.9	0.519	1050	4.34	3.53	646	1140	440	1.08	0.454	167	583	101	
NL-26	11.6	8.04	0.547	2.65	1390	701	6.27	1	0.544	1060	3.12	3.67	660	964	387	1.16	0.477	176	445	106	
NL-27	6.99	7.02	0.375	2.56	1150	443	5.92	9.92	0.504	1010	1.5	3.1	663	445	298	0.893	0.458	164	275	96.4	
NL-28	6.1	7.28	0.39	2.51	979	503	6.57	9.6	0.482	1060	1.5	2.92	634	832	388	1.42	0.416	181	403	93.5	
NL-29	6.16	6.42	0.341	2.33	1080	360	4.84	5.06	0.457	846	1.5	3.07	564	285	226	1.29	0.418	134	190	88.3	
NL-30	7.06	7.44	0.5	2.785	1680	412.5	5.895	2.325	0.668	1034	3.91	3.9	753.5	276.5	243	1.55	0.5635	161.5	220.5	122.5	

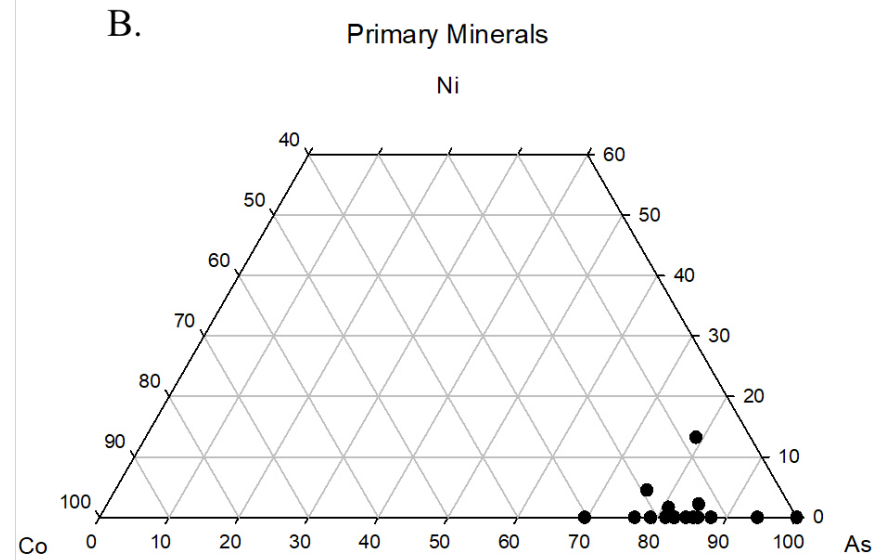
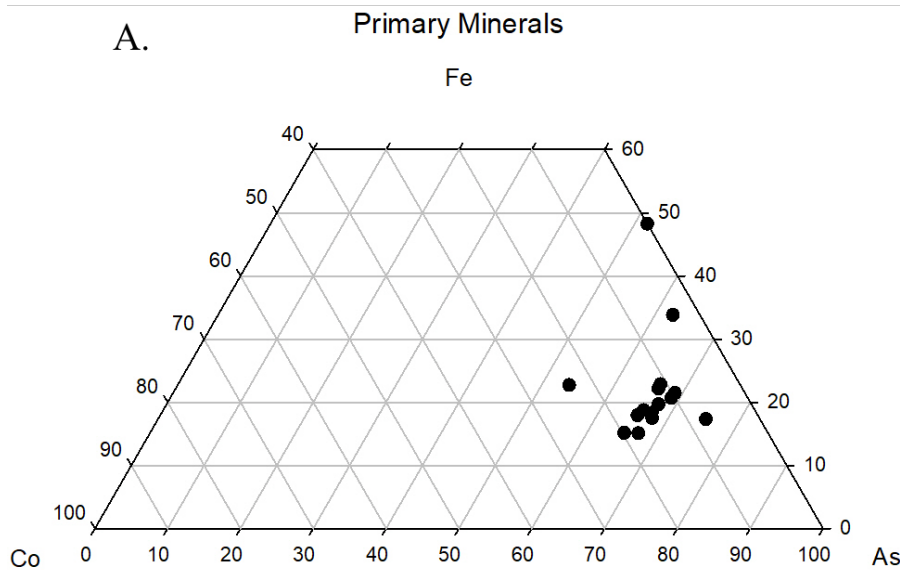
Supplementary data C

Chemical composition of the tailing samples, site A tailings

FINAL RESULTS (mg/Kg)																						
ELRFS LABEL	Ag	Al	As	Ca	Co	Cu	Fe	Hg	K	Mn	Mo	Na	P	Pb	Sb	Se	Ti	V	Zn	Zr		
C = Crosswise																						
Lake tailings site	ppm	wt%	wt%	wt%	ppm	ppm	wt%	ppm	wt%	ppm	ppm	wt%	ppm	ppm	ppm	ppm	wt%	ppm	ppm	ppm		
C-1		53	10.40	0.214	11.8	922	236	10	1	1.61	2550	1.5	2.11	542	84	35.5	1.34	0.554	314	135	97	
C-2		6.52	5.30	0.161	6.31	699	175	7.53	1	1.19	1900	1.5	1.28	327	67.2	23.8	1.96	0.491	207	92.2	63.5	
C-3		4.61	6.37	0.144	7.03	780	184	7.63	1	1.24	1920	1.5	1.51	321	51.1	24.1	0.824	0.451	227	84.2	59.7	
C-4		2.37	6.77	0.125	7.19	725	191	7.85	1	1.3	2040	1.5	1.66	329	50.9	19.8	2.24	0.492	247	94.5	60.3	
C-5		3.42	7.05	0.0975	7.07	616	181	7.58	1	1.25	1970	1.5	1.8	303	50.4	17.5	1.26	0.47	245	90.9	59.9	
C-6		4.44	7.48	0.108	7.68	674	189	8.27	1	1.39	2140	1.5	1.95	342	54.9	19.1	3.29	0.535	265	97.4	65.3	
C-7		4.16	6.63	0.115	6.68	579	187	7.73	1	1.28	1870	1.5	1.69	358	61.5	14.7	1.45	0.463	245	104	58.4	
C-8		4.01	7.01	0.0967	6.81	525	178	7.67	1	1.24	1860	1.5	1.95	376	67	13.1	1.56	0.493	263	106	62.3	
C-9		4.53	7.18	0.0796	5.38	452	169	7.86	1	1.08	1710	1.5	2.56	571	67	10.4	1.84	0.651	269	130	81.3	
C-10		5.4	7.90	0.196	2.44	1100	134.5	7.63	1	0.74	1093.5	1.5	2.885	748	67	13.35	2.79	0.524	202.5	130.5	110.5	
C-11		3.5	8.03	0.209	1.03	1280	93.4	6.76	1	0.57	695	1.5	3.14	805	67	11.3	1.76	0.404	155	103	113	
C-12		5.32	8.36	0.186	1.73	1140	113	7.38	1	0.676	930	1.5	3.2	792	67	12.4	2.13	0.464	186	117	111	
C-13		6.13	7.47	0.166	4.33	471	160	7.31	1	1.12	1720	1.5	3.05	801	67	14	1.15	0.65	249	184	103	
C-14		5.69	7.17	0.285	6.21	641	221	9.41	1	1.56	2750	1.5	2.45	882	67	20.8	1.31	0.732	329	304	87.6	
C-15		5.14	6.58	0.276	5.23	581	350	9.9	1	1.21	2870	1.5	2.61	1230	67	22.5	1.61	0.826	342	433	92.4	
C-16		4.81	6.51	0.251	4.84	547	288	8.75	1	0.999	2560	1.5	2.54	1120	67	19.6	1.24	0.733	319	402	81.8	
C-17		5.61	5.23	0.197	4.09	303	247	8.71	1	1.31	2400	1.5	2.7	1100	67	19.3	2.71	0.989	293	329	102	
C-18		5.17	7.07	0.196	4.75	325	228	8.41	1	1.18	2370	1.5	3.28	1050	67	17.8	0.663	0.909	319	316	93.6	
C-19		5.48	7.05	0.244	4.79	478	254	8.87	1	1.18	2430	1.5	3.2	1080	67	21.5	2.35	0.93	323	348	98.9	
C-20		5.68	8.04	0.417	1.585	2120	173	8.01	1	0.6295	1185	1.5	3.13	951.5	67	23.4	2.635	0.5015	205.5	439.5	122	
C-21		3.1	7.80	0.259	2.68	1150	148	7.72	1	0.913	1530	1.5	3.01	841	67	23	1.64	0.573	251	283	87.9	
C-22		4.4	8.10	0.201	4.95	586	181	8.71	1	1.26	2200	1.5	3.06	856	67	27.4	1.11	0.743	338	247	69.6	
C-23		4.86	7.67	0.229	4.85	636	213	9.01	1	1.23	2250	1.5	2.83	865	67	32.2	1.27	0.732	340	283	69.9	
C-24		5.83	9.04	0.262	6.19	865	247	11.2	1	1.45	2760	1.5	3.17	1060	67	43.1	2.14	0.81	406	335	84.4	
C-25		5.92	8.94	0.121	6.61	465	131	10.3	1	1.53	2540	1.5	3.26	1020	67	25.1	1.75	0.807	360	178	81.5	
C-26		2.87	7.37	0.0479	5.11	225	73.8	7.61	1	1.23	1860	1.5	2.7	727	67	13	1.29	0.625	262	109	63.2	
C-27		4.01	5.52	0.0484	4.56	233	128	7.44	1	1.23	1800	1.5	1.95	757	67	13.2	2.26	0.65	241	118	64.7	
C-28		4.38	6.77	0.0534	5.13	251	85.3	7.86	1	1.27	1920	1.5	2.46	783	67	14.7	1.71	0.674	262	115	68.9	
C-29		4.38	7.11	0.0449	5.15	221	101	7.73	1	1.25	1890	1.5	2.6	731	67	14.4	1.66	0.659	260	113	67.7	
C-30		4.71	6.82	0.0647	5.54	281	168.5	8.685	1	1.27	2180	1.5	2.38	873.5	67	19.7	1.197	0.8	282.5	138.5	73.7	

Supplementary data D1

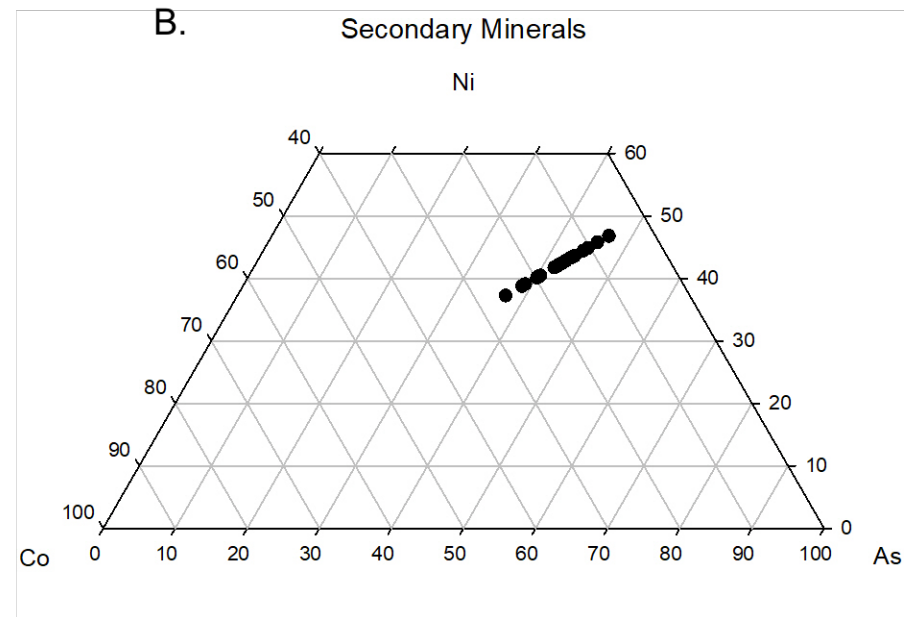
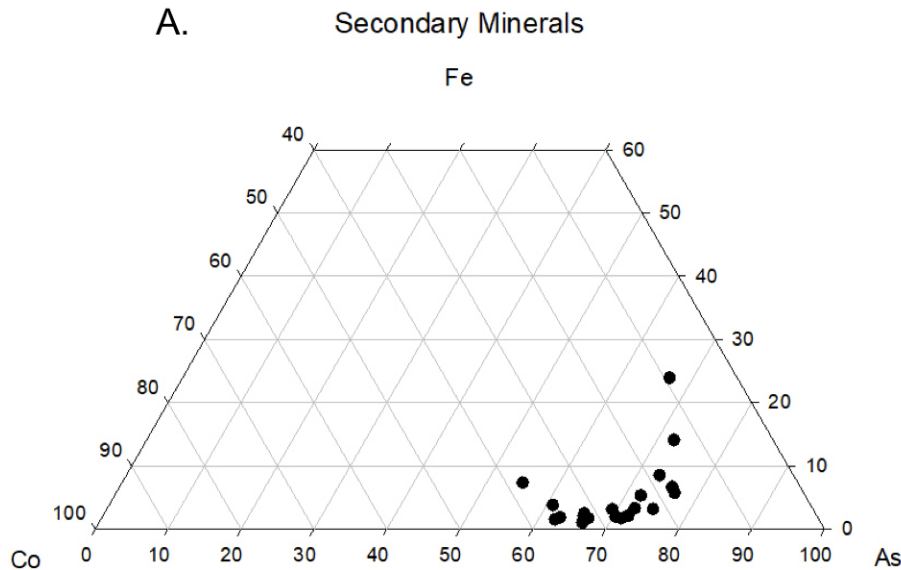
Composition of the arsenides (primary minerals) characterized with SEM



Triangle diagrams depicting the proportions of A. Co vs. Fe vs. As and B. Co vs. Ni vs. As

Supplementary data D2

Composition of the arsenates characterized with SEM



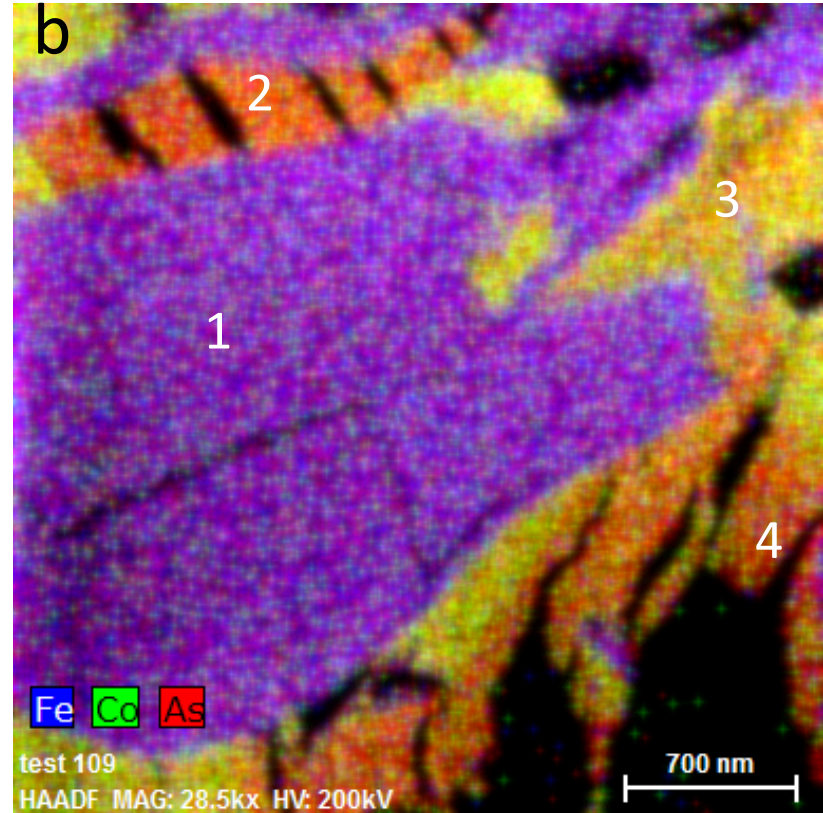
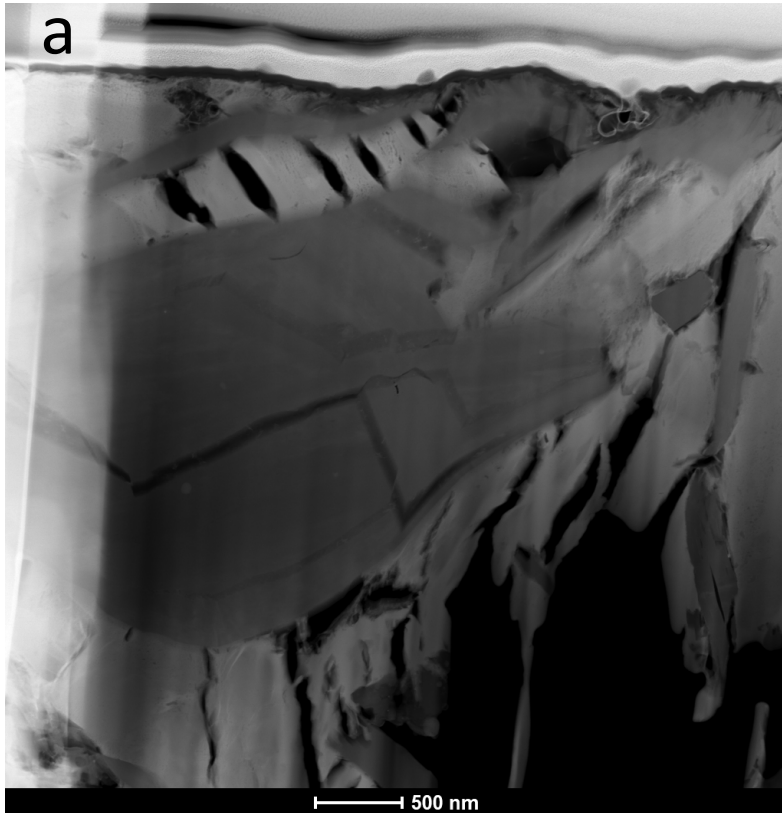
Triangle diagrams depicting the proportions of A. Co vs. Fe vs. As and B. Co vs. Ni vs. As

Supplementary data E
Selected Area diffraction pattern,
Fast Fourier Transformation pattern of lattice fringes
and semi-quantitative chemical analyses
for the major phases identified in the FIB section

Note that the concentrations for Oxygen are not listed in all chemical analyses

Area #1

Minerals of the arsenohopeite group and chlorite group



(a) STEM-EDS and (b) chemical distribution map for Fe (blue), Co (green) and As (red) for area 1; the chemical analyses listed in S17 are numbered from 1 to 4.

Semi-quantitative chemical analyses for the areas numbered 1 to 4 in S16b

1

Spectrum: 1

Element	Series	Net un.	C norm.	C Atom.	C Error (3 Sigma)	
		[wt.%]	[wt.%]	[at.%]	[wt.%]	
Magnesium	K-series	3621	9.02	9.02	7.97	1.00
Aluminium	K-series	3805	10.16	10.16	8.09	1.12
Iron	K-series	5019	17.98	17.98	6.92	1.89
Silicon	K-series	4833	12.68	12.68	9.70	0.63
Oxygen	K-series	17462	50.16	50.16	67.33	4.73
Total:		100.00	100.00	100.00		

2

Spectrum: 1

Element	Series	Net un.	C norm.	C Atom.	C Error (3 Sigma)	
		[wt.%]	[wt.%]	[at.%]	[wt.%]	
Oxygen	K-series	1514	32.35	32.35	67.36	3.91
Iron	K-series	6	0.18	0.18	0.11	0.30
Arsenic	L-series	1118	32.69	32.69	14.54	10.49
Zinc	L-series	1286	29.77	29.77	15.16	9.47
Nickel	K-series	90	2.67	2.67	1.51	1.01
Cobalt	K-series	81	2.34	2.34	1.32	0.93
Total:		100.00	100.00	100.00		

3

Spectrum: 1

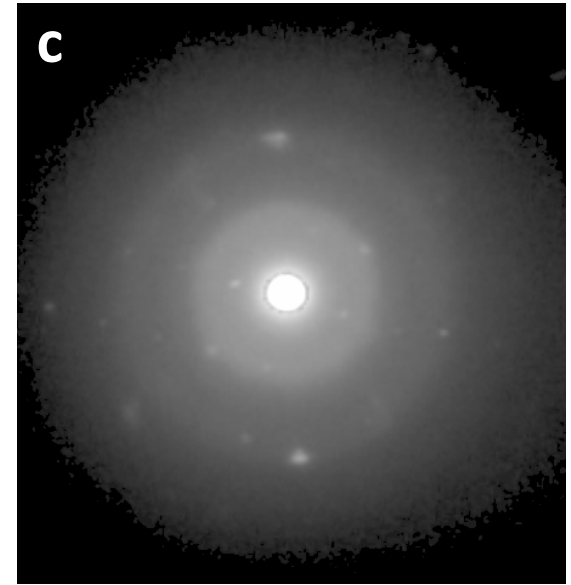
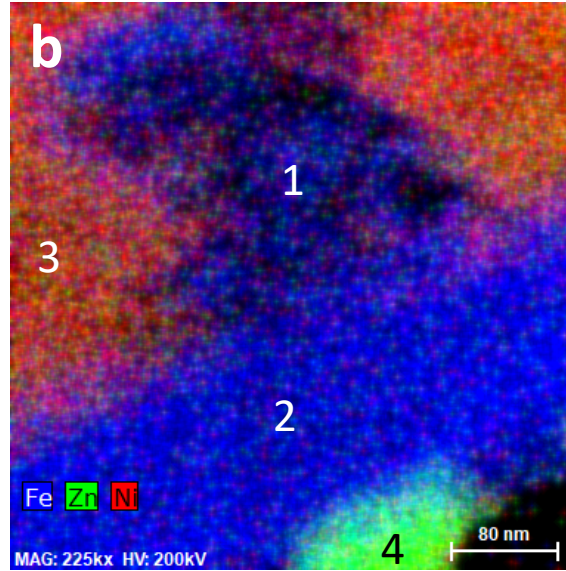
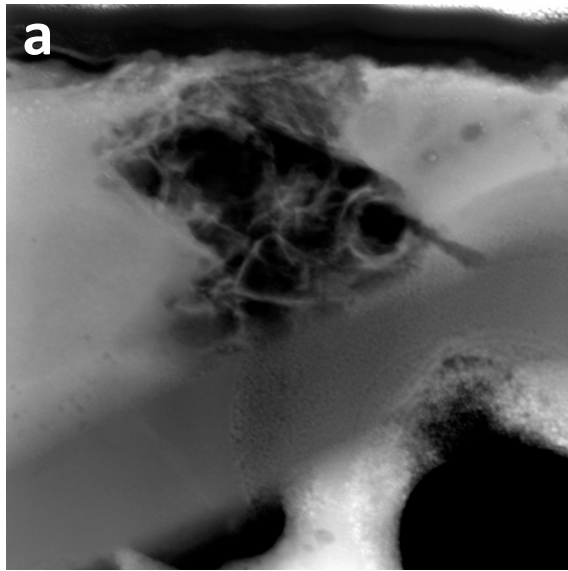
Element	Series	Net un.	C norm.	C Atom.	C Error (3 Sigma)	
		[wt.%]	[wt.%]	[at.%]	[wt.%]	
Oxygen	K-series	2536	33.50	33.50	67.77	3.69
Iron	K-series	7	0.11	0.11	0.07	0.21
Arsenic	L-series	1727	31.22	31.22	13.48	9.82
Zinc	K-series	558	12.14	12.14	6.01	2.06
Nickel	K-series	727	13.24	13.24	7.30	2.05
Cobalt	K-series	551	9.79	9.79	5.37	1.68
Total:		100.00	100.00	100.00		

4

Spectrum: 1

Element	Series	Net un.	C norm.	C Atom.	C Error (3 Sigma)	
		[wt.%]	[wt.%]	[at.%]	[wt.%]	
Oxygen	K-series	1061	30.49	30.49	65.28	4.00
Iron	K-series	0	0.00	0.00	0.00	0.00
Arsenic	L-series	784	30.83	30.83	14.09	10.13
Zinc	K-series	686	32.42	32.42	16.98	5.01
Nickel	K-series	80	3.13	3.13	1.83	1.24
Cobalt	K-series	82	3.14	3.14	1.83	1.23
Total:		100.00	100.00	100.00		

Occurrence of a mineral with the tsumcorite-group $A_1M_2(XO_4)_2(OH,H_2O)_2$ structure type



d tsumcorite-group
 $A_1M_2(XO_4)_2(OH,H_2O)_2$

D-spacing [Å]	(hkl)
4.6	(111)
2.85	(220)
1.59	(430)

S18 (a) STEM-EDS image, (b) chemical distribution map for Fe (blue), Zn (green) and Ni (red), c SAED pattern and d observed d spacings with (hkl) indices of a mineral of the tsumcorite group in an alteration halo (1) within an Co-Ni-arsenate mineral with the vivianite structure type (3) and in close association of a mineral of chlorite group (2) and Zn-arsenate (4); the chemical analyses for (1)-(4) are listed in S21

Semi-quantitative chemical analyses of the areas depicted in S20b

Spectrum: 1 **1**

Element	Series	Net un.	C norm.	C Atom.	C Error (3 Sigma)
		[wt.%]	[wt.%]	[at.%]	[wt.%]
Iron	K-series 1951	25.72	25.72	28.05	3.05
Cobalt	K-series 190	2.70	2.70	2.79	0.75
Nickel	K-series 191	2.79	2.79	2.89	0.77
Zinc	K-series 90	1.56	1.56	1.45	0.62
Silicon	K-series 357	3.44	3.44	7.45	0.63
Arsenic	L-series 2819	40.77	40.77	33.14	12.61
Aluminium	K-series 110	1.07	1.07	2.43	0.40
Calcium	K-series 1147	12.51	12.51	19.01	1.71
Lead	M-series 439	9.45	9.45	2.78	6.02

Total:		100.00	100.00	100.00	

Spectrum: 1 **2**

Element	Series	Net un.	C norm.	C Atom.	C Error (3 Sigma)
		[wt.%]	[wt.%]	[at.%]	[wt.%]
Magnesium	K-series 3210	20.25	20.25	27.07	2.19
Aluminium	K-series 2647	17.91	17.91	21.57	2.00
Silicon	K-series 4025	26.76	26.76	30.96	1.37
Iron	K-series 3862	35.07	35.07	20.40	3.71

Total:		100.00	100.00	100.00	

Spectrum: 1 **3**

Element	Series	Net un.	C norm.	C Atom.	C Error (3 Sigma)
		[wt.%]	[wt.%]	[at.%]	[wt.%]
Iron	K-series 254	2.29	2.29	2.64	0.58
Zinc	K-series 415	4.92	4.92	4.84	0.97
Nickel	K-series 1790	17.79	17.79	19.47	2.17
Cobalt	K-series 2614	25.36	25.36	27.65	2.86
Arsenic	L-series 4719	46.61	46.61	39.97	14.27
Silicon	K-series 125	0.86	0.86	1.96	0.31
Calcium	K-series 291	2.17	2.17	3.48	0.53

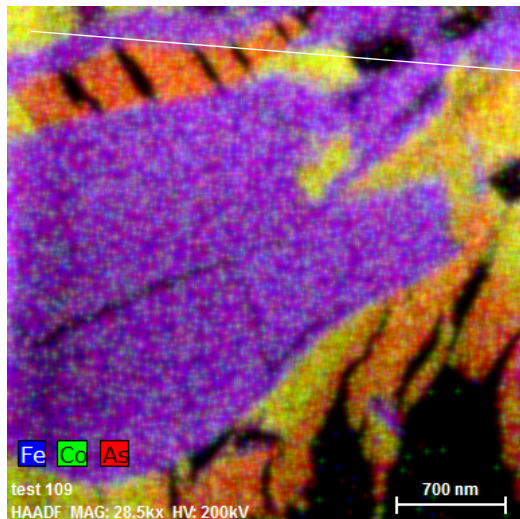
Total:		100.00	100.00	100.00	

Spectrum: 1 **4**

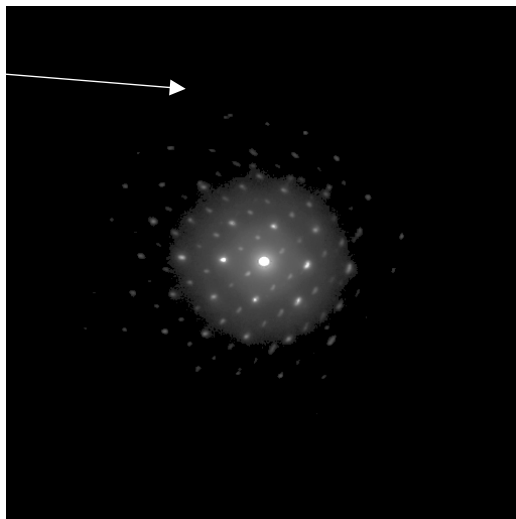
Element	Series	Net un.	C norm.	C Atom.	C Error (3 Sigma)
		[wt.%]	[wt.%]	[at.%]	[wt.%]
Cobalt	K-series 132	5.18	5.18	6.01	1.59
Nickel	K-series 106	4.21	4.21	4.91	1.45
Zinc	L-series 1385	43.45	43.45	45.47	13.74
Iron	K-series 49	1.74	1.74	2.13	0.89
Arsenic	L-series 1145	45.42	45.42	41.48	14.53

Total:		100.00	100.00	100.00	

a



b



c

D-spacing [Å]	(hkl)
5.21	(210)
3.45	(221)
3.63	(240)

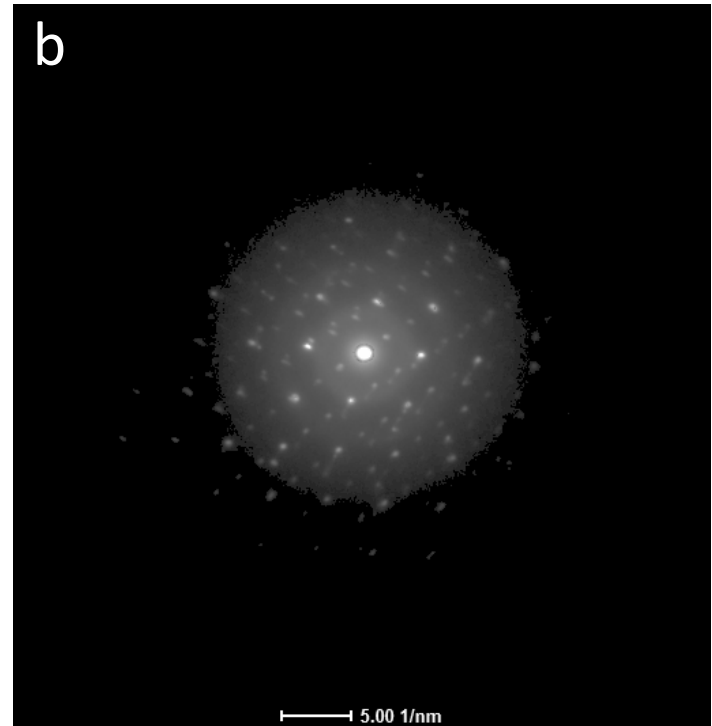
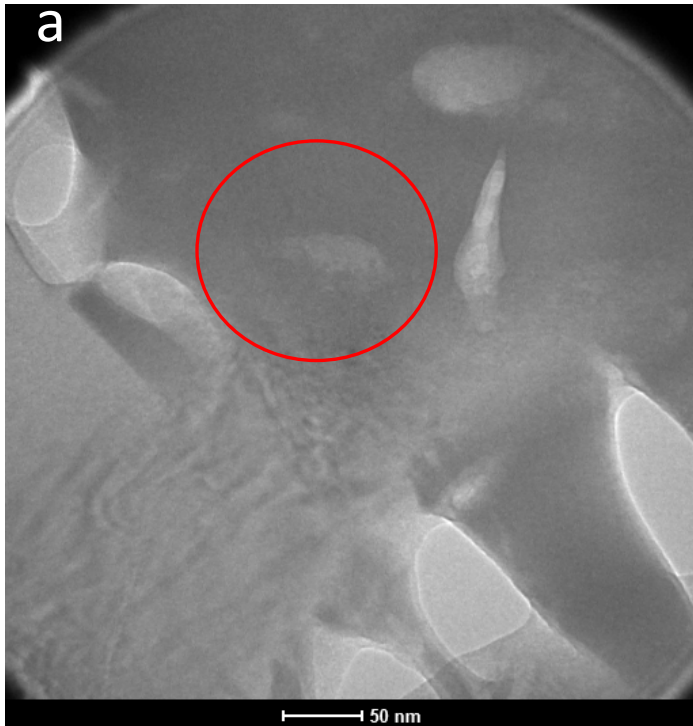
Co-Ni-As-rich mineral with the arsenohopeite structure type

d

Spectral Area 2		Colour = yellow (Zn Co Ni map)			
Element	Series	Net un. (wt%)	C norm. (wt%)	C atom. (at %)	C Error (3 sigma) (wt%)
Oxygen	K	36.93	36.93	70.86	4.79
Arsenic	L	32.13	32.13	13.17	10.67
Cobalt	K	17.61	17.61	9.17	3.36
Nickel	K	10.04	10.04	5.25	2.45
Zinc	L	3.29	3.29	1.54	1.64
Total		100	100	99.99	

S20 Chemical distribution maps for Fe (blue), Co (green) and As (red) of area 1, (b) SAED pattern (c) d-spacing and (hkl) indices and (d) semi-quantitative chemical analysis of a Co-Ni-rich mineral with arsenohopeite structure type

Mineral of the chlorite group $(\text{Mg,Fe})_5\text{Al}(\text{AlSi}_3\text{O}_{10})\text{OH}_8$

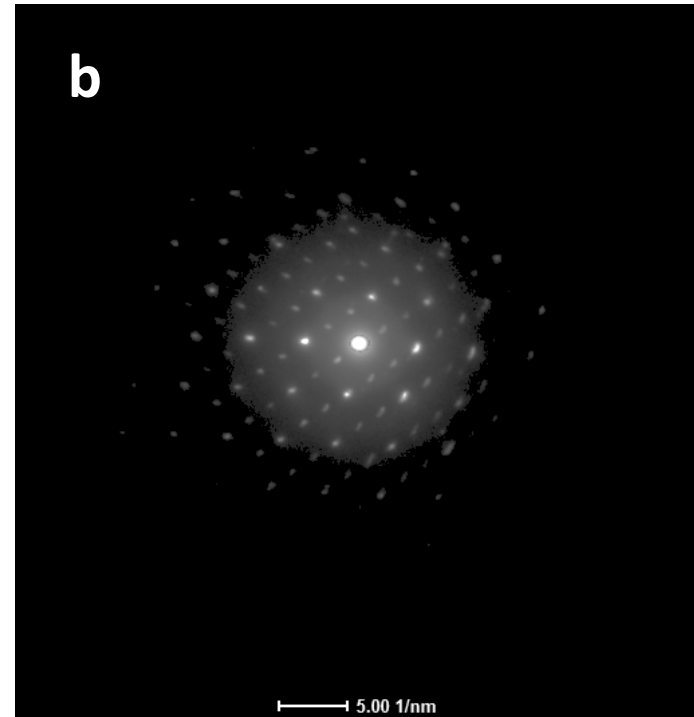


C

D-spacing [Å]	(hkl)
3.45	(-1 -1 3)
1.68	(-1 -3 7)
3.90	(-1 -1 3)
2.44	(-1 -3 3)

S21 (a) TEM image, (b) SAED pattern and (c) selected d-spacings and (hkl) for a mineral of the chlorite group in area 1; the area from which the SAED pattern was recorded is encircled in (a).

Co-Ni-rich arsenate with the Arsenohopeite structure type

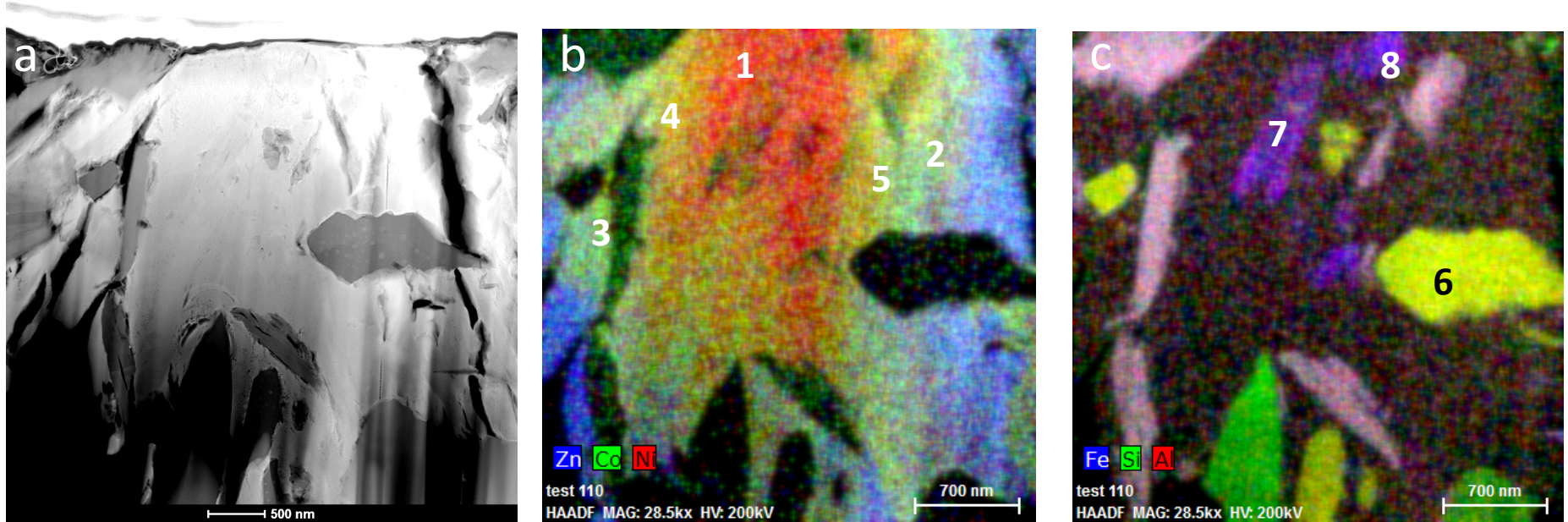


C

D-spacing [Å]	(hkl)
5.15	(2 1 0)
3.63	(2 4 0)
2.43	(2 7 0)
2.58	(4 2 0)

S22 (a) TEM image, (b) SAED pattern and (c) selected d-spacings and (hkl) mineral with the arsenohopeite structure type in area 1; the area from which the SAED pattern was recorded is encircled in (a).

Area #2



Minerals of the vivianite group
Scorodite
Albite
Minerals of the chlorite group

S23 (a) STEM-EDS image and (b)-(c) chemical distribution for (b) Zn (blue), Co (green) and Ni (red) and (c) Fe (blue), Si (green) and Al (red) of area 2; semi-quantitative chemical analyses for the phases numbered (1)-(8) are given in S24 and S25.

1

Q2	Element	Series	Net un.	C norm.	C Atom.	C Error (3 Sigma)
Ni~=As			[wt.%]	[wt.%]	[at.%]	[wt.%]
	Oxygen	K-series	1751	35.83	35.83	69.19 4.20
	Nickel	K-series	963	27.37	27.37	14.40 3.83
	Arsenic	L-series	1118	31.58	31.58	13.02 10.14
	Manganese	K-series	114	2.82	2.82	1.59 0.96
	Calcium	K-series	105	2.25	2.25	1.73 0.80
	Zinc	L-series	7	0.15	0.15	0.07 0.28
	Total: 100.00 100.00 100.00					

3

Q2	Element	Series	Net un.	C norm.	C Atom.	C Error (3 Sigma)
Co=Ni			[wt.%]	[wt.%]	[at.%]	[wt.%]
	Oxygen	K-series	1312	34.18	34.18	67.96 4.25
	Calcium	K-series	37	1.01	1.01	0.81 0.61
	Manganese	K-series	80	2.54	2.54	1.47 1.01
	Nickel	K-series	354	12.81	12.81	6.94 2.55
	Zinc	K-series	154	6.65	6.65	3.24 1.90
	Arsenic	L-series	851	30.57	30.57	12.98 9.99
	Cobalt	K-series	347	12.25	12.25	6.61 2.46
	Total: 100.00 100.00 100.00					

2

Q2	Element	Series	Net un.	C norm.	C Atom.	C Error (3 Sigma)
Zn+Co+Ni>As			[wt.%]	[wt.%]	[at.%]	[wt.%]
	Oxygen	K-series	1491	31.69	31.69	66.07 3.84
	Calcium	K-series	32	0.80	0.80	0.67 0.51
	Manganese	K-series	46	1.18	1.18	0.72 0.65
	Nickel	K-series	198	5.85	5.85	3.33 1.51
	Zinc	K-series	717	25.29	25.29	12.90 3.87
	Arsenic	L-series	1014	29.80	29.80	13.27 9.63
	Cobalt	K-series	186	5.38	5.38	3.05 1.43
	Total: 100.00 100.00 100.00					

4

Q2	Element	Series	Net un.	C norm.	C Atom.	C Error (3 Sigma)
Ni>>Co+Zn			[wt.%]	[wt.%]	[at.%]	[wt.%]
	Oxygen	K-series	1629	40.28	40.28	73.19 4.78
	Calcium	K-series	48	1.23	1.23	0.89 0.65
	Manganese	K-series	81	2.44	2.44	1.29 0.97
	Nickel	K-series	547	18.79	18.79	9.31 3.16
	Zinc	L-series	25	0.66	0.66	0.29 0.58
	Arsenic	L-series	841	28.76	28.76	11.16 9.41
	Cobalt	K-series	233	7.84	7.84	3.87 1.87
	Total: 100.00 100.00 100.00					

S24 semi-quantitative Chemical analysis for the areas numbered in S23b and c

5

5						
Q2	Element	Series	Net unn.	C norm.	C Atom.	C Error (3 Sigma)
CoNi-AsO			[wt.%]	[wt.%]	[at.%]	[wt.%]
	Oxygen	K-series	1633	35.76	35.76	69.61 4.25
	Calcium	K-series	31	0.80	0.80	0.62 0.51
	Manganese	K-series	42	1.13	1.13	0.64 0.64
	Nickel	K-series	463	14.09	14.09	7.47 2.53
	Zinc	L-series	383	9.17	9.17	4.37 3.28
	Arsenic	L-series	979	29.63	29.63	12.31 9.59
	Cobalt	K-series	317	9.42	9.42	4.98 1.97

	Total: 100.00 100.00 100.00					

6

Albite						
1 Element	Series	Net unn.	C norm.	C Atom.	C Error (3 Sigma)	
		[wt.%]	[wt.%]	[at.%]	[wt.%]	
	Silicon	K-series	4920	32.84	32.84	23.57 1.51
	Aluminium	K-series	1572	10.68	10.68	7.98 1.33
	Sodium	K-series	1220	7.11	7.11	6.23 0.96
	Oxygen	K-series	6810	49.37	49.37	62.21 4.87

	Total: 100.00 100.00 100.00					

8

8						
8 Element	Series	Net unn.	C norm.	C Atom.	C Error (3 Sigma)	
FeNi-AsO			[wt.%]	[wt.%]	[at.%]	[wt.%]
	Oxygen	K-series	1558	39.47	39.47	72.59 4.72
	Magnesium	K-series	0	0.00	0.00	0.00 0.00
	Iron	K-series	388	12.35	12.35	6.51 2.37
	Nickel	K-series	392	13.79	13.79	6.91 2.63
	Arsenic	L-series	931	32.56	32.56	12.79 10.57
	Zinc	K-series	10	0.48	0.48	0.22 0.54
	Calcium	K-series	50	1.35	1.35	0.99 0.69

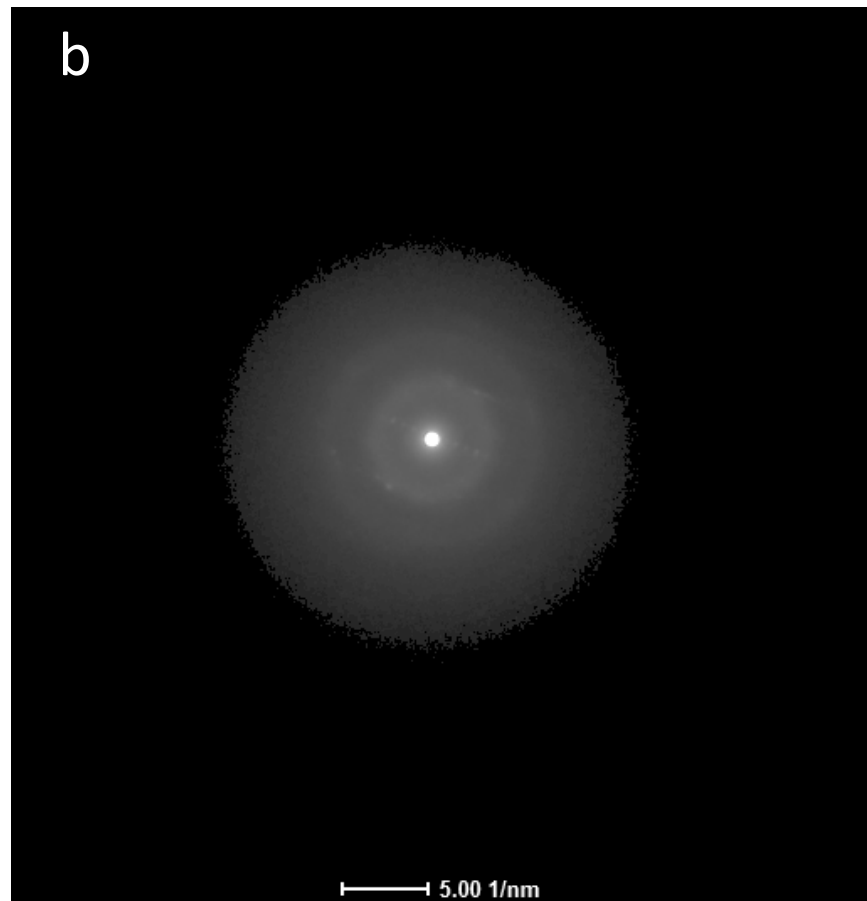
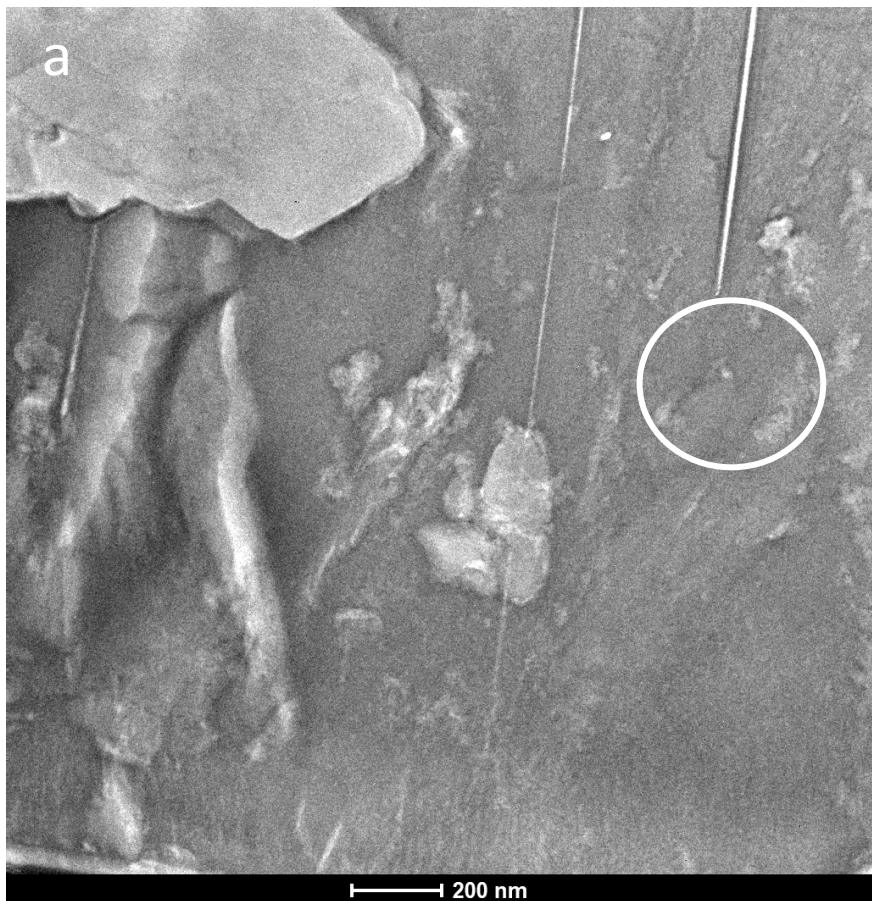
	Total: 100.00 100.00 100.00					

7

7						
14 Element	Series	Net unn.	C norm.	C Atom.	C Error (3 Sigma)	
Fe-AsO			[wt.%]	[wt.%]	[at.%]	[wt.%]
	Oxygen	K-series	898	33.99	33.99	66.48 4.65
	Iron	K-series	593	28.20	28.20	15.80 4.58
	Arsenic	L-series	631	32.89	32.89	13.73 11.01
	Aluminium	K-series	45	1.62	1.62	1.88 0.81
	Titanium	K-series	29	1.22	1.22	0.80 0.80
	Calcium	K-series	19	0.85	0.85	0.66 0.66
	Cobalt	K-series	24	1.23	1.23	0.66 0.89

	Total: 100.00 100.00 100.00					

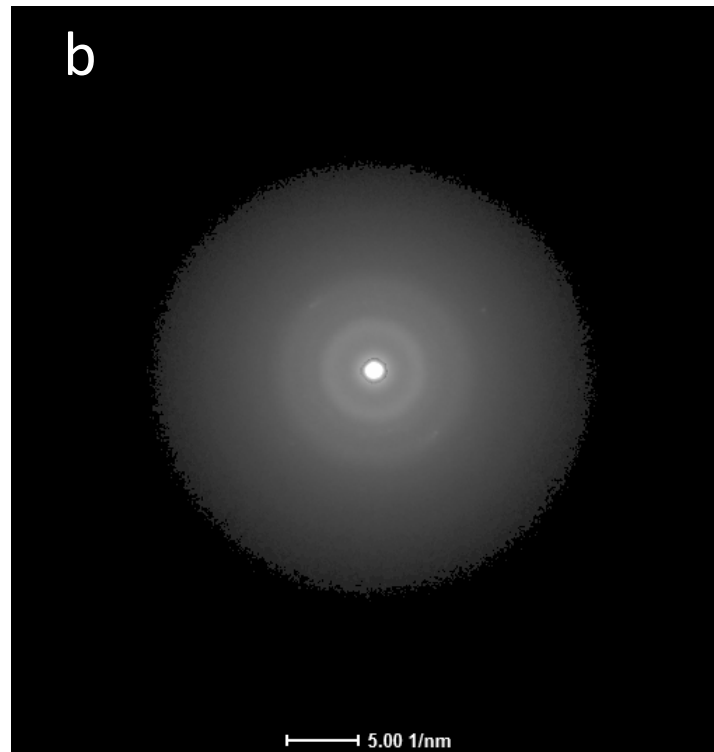
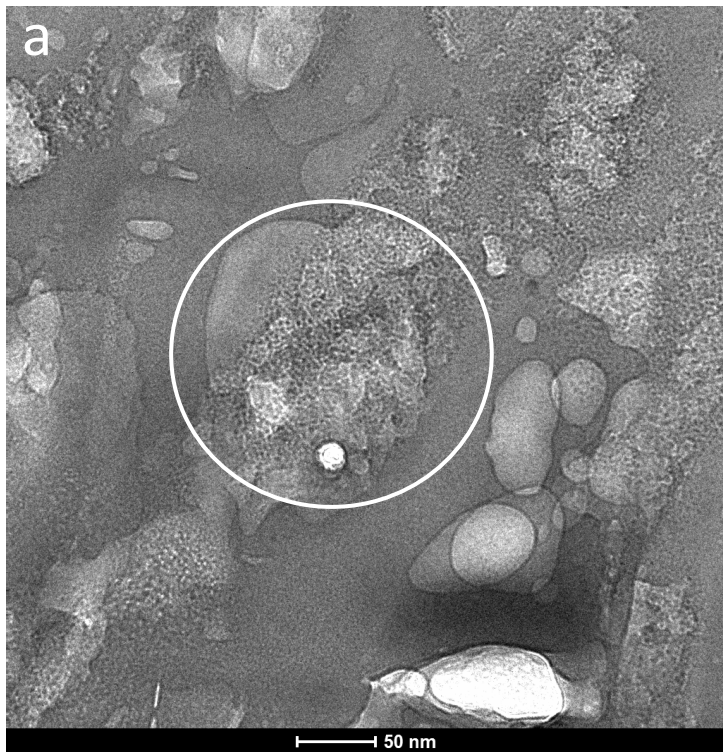
S25 Semi-quantitative chemical analysis for the areas numbered in S23b and c



C

Co-Ni-arsenate of the vivianite group	
D-spacing [Å]	(hkl)
2.66	(0 4 1)
3.86	(-2 0 1)

S26 (a) TEM image and (b) SAED pattern of a selected area in area 2 (encircled in (a)); (c) corresponding d-spacing and (hkl) of a Co-Ni-arsenate of the vivianite group

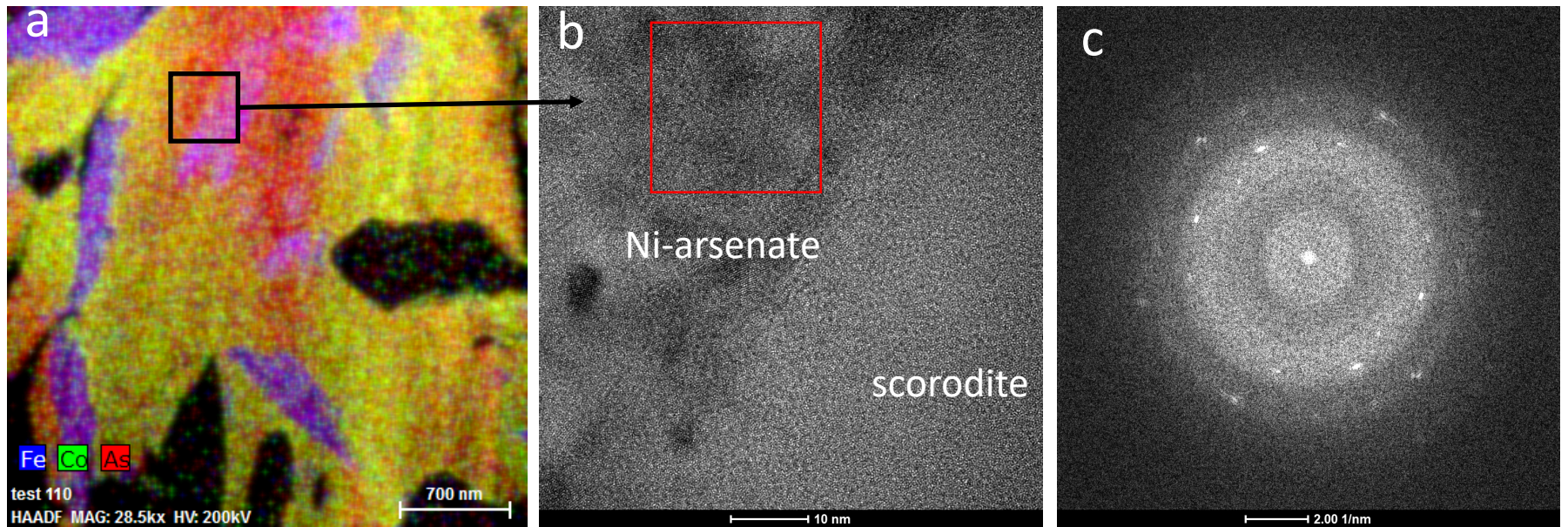


Co-Ni-rich arsenate with of the vivianite group

c

D-spacing [Å]	(hkl)
3.40	(-2 2 1)
1.62	(-5 5 1)
3.28	(-1 3 1)
2.45	(-4 0 1)

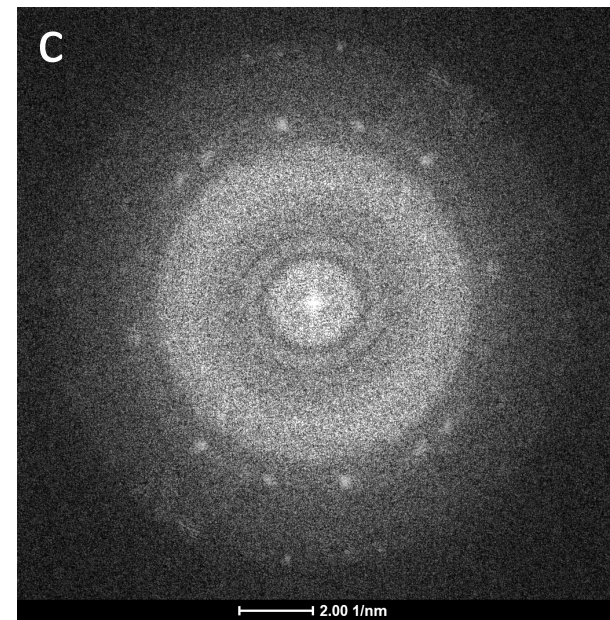
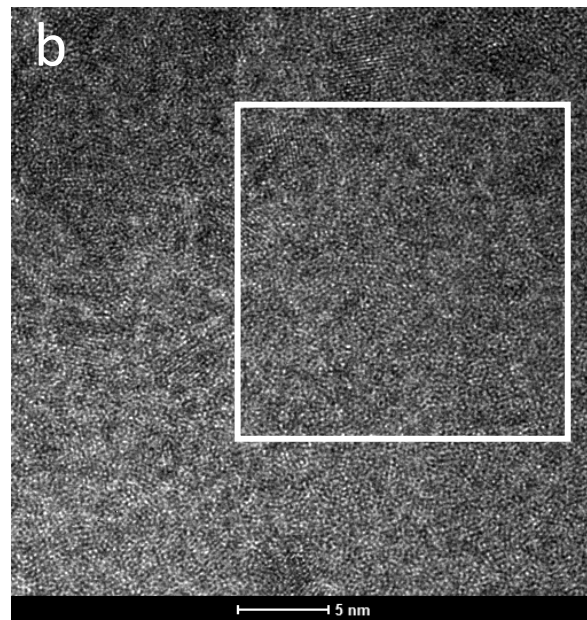
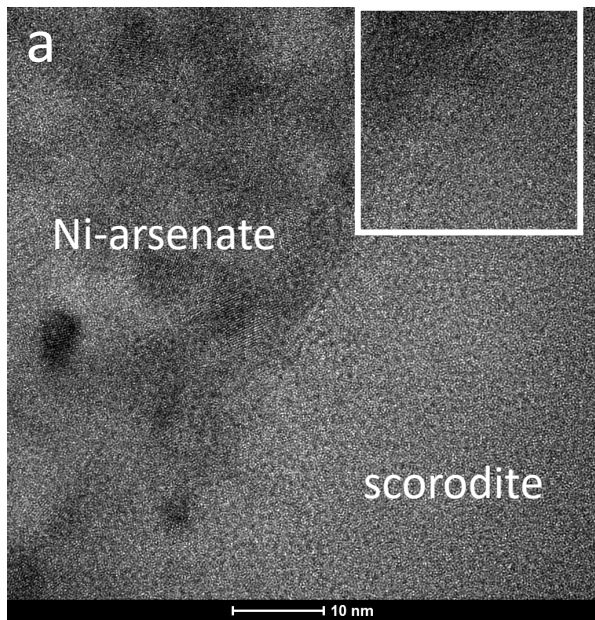
S27 (a) TEM image and (b) SAED pattern from a selected area (encircled in (a)) and (c) d-spacings and (hkl) indices of a Co-Ni-rich arsenate of the vivianite group



d

Ni-arsenate-bearing minerals of the vivianite group	
D-spacing [Å]	(hkl)
2.64	(330)
1.88	(202)
2.40	(-401)
1.90	(202)
1.97	(-441)

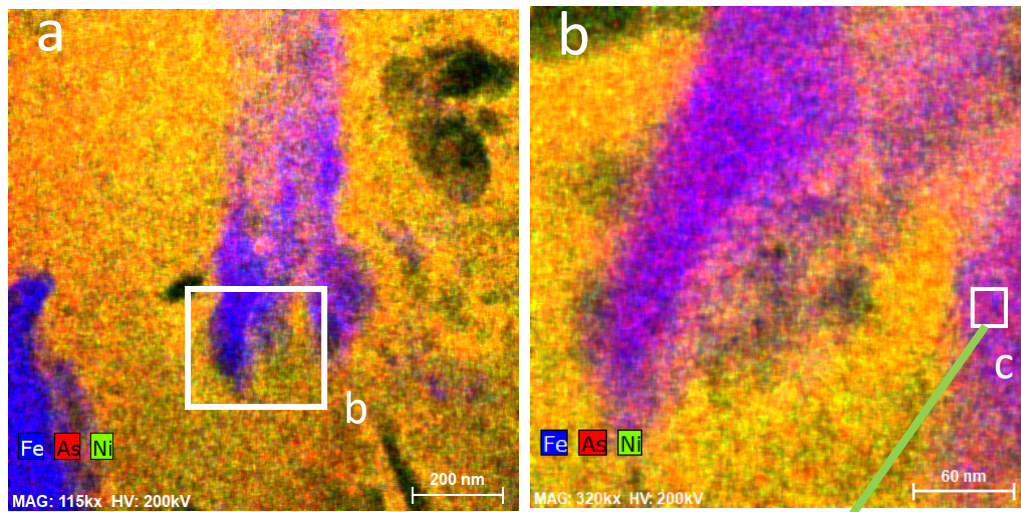
S28 (a) Chemical distribution map for Fe (blue), Co (green) and As (red) for area 2; (b) TEM of the interface between a Ni-arsenate of the vivianite group and scorodite (indicated with a black box in (a)); (c) FFT pattern of a selected area in (b) (indicated with a red box) and (d) D-spacings and (hkl) indices of a Ni-arsenate mineral of the vivianite group



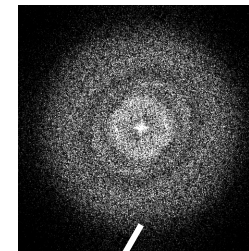
d

Scorodite $\text{FeAsO}_4 \cdot 2\text{H}_2\text{O}$	
D-spacing	hkl index
5.66	(1 1 1)
2.48	(2 3 1)
1.97	(5 1 1)

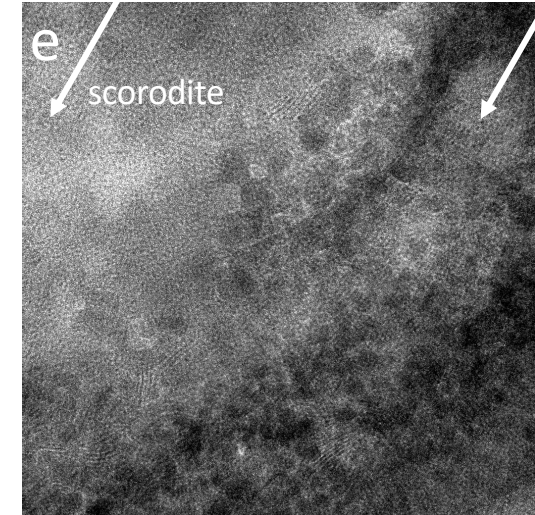
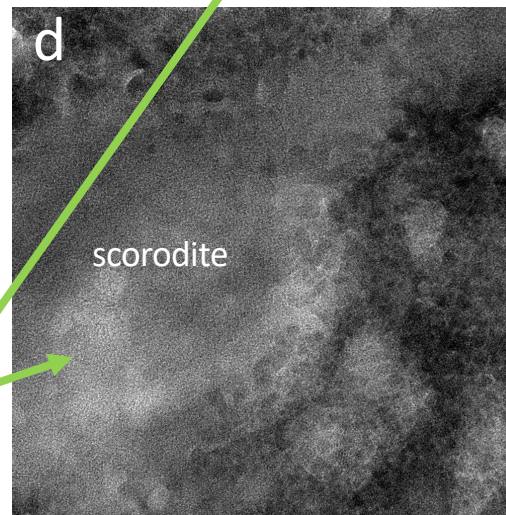
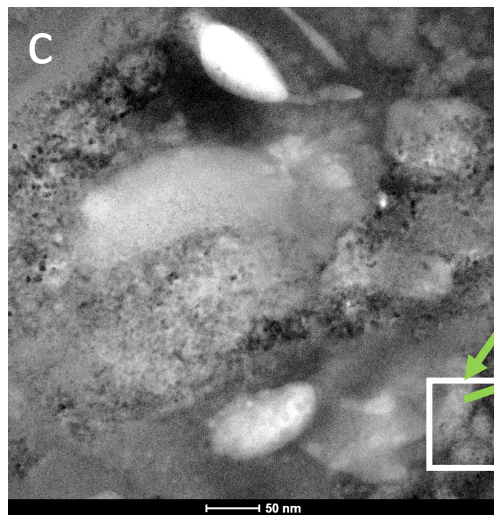
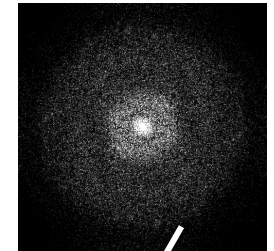
S29 (a) TEM of the interface between a Ni-arsenate of the vivianite group and scorodite (b) High-Resolution TEM of a selected area in (a) (indicated with a white box in (a)); (c) FFT pattern of a selected area in (b) (indicated with a white box) and (d) corresponding d-spacings and (hkl) indices of scorodite



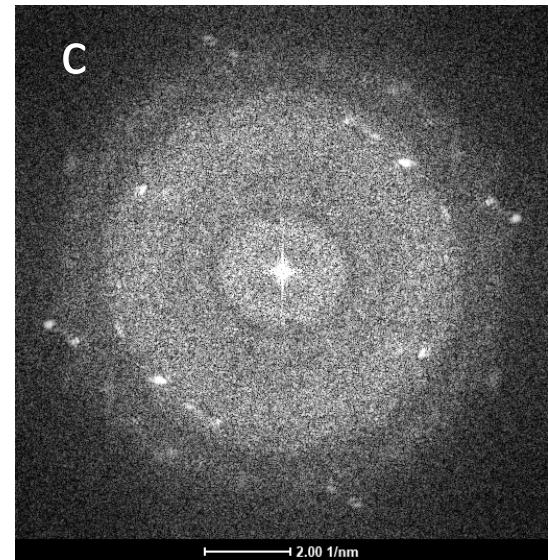
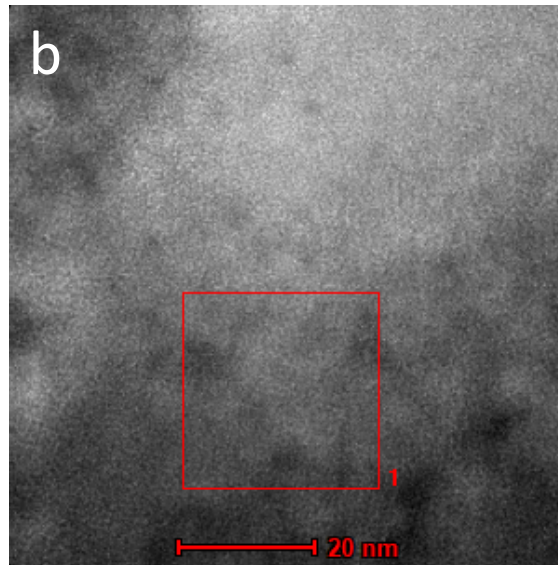
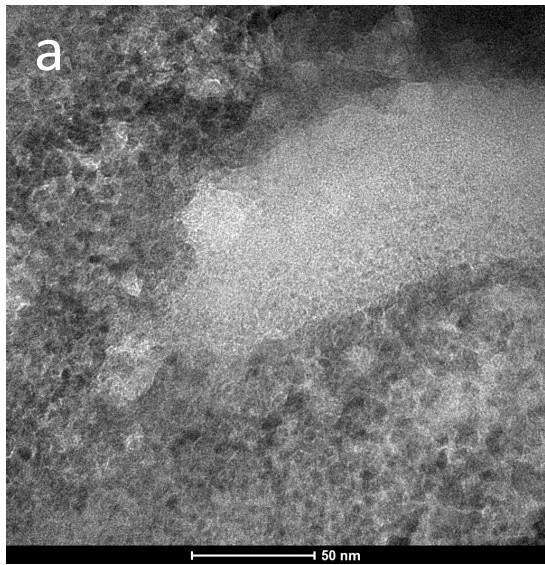
D=5.6 (111)
scorodite



D=7.9 (110)
vivianite



S30 (a)-(b) STEM-EDS chemical distribution maps for Fe (blue), As (red) and Ni (green) and (c)-(e) TEM images of the replacement of scorodite by (Co, Ni)-arsenates of the vivianite group; the areas shown in (b), (c) and (d) are indicated with squares in (a), (b) and (c), respectively; (e) FFT pattern from areas composed of scorodite and a mineral of the vivianite group.

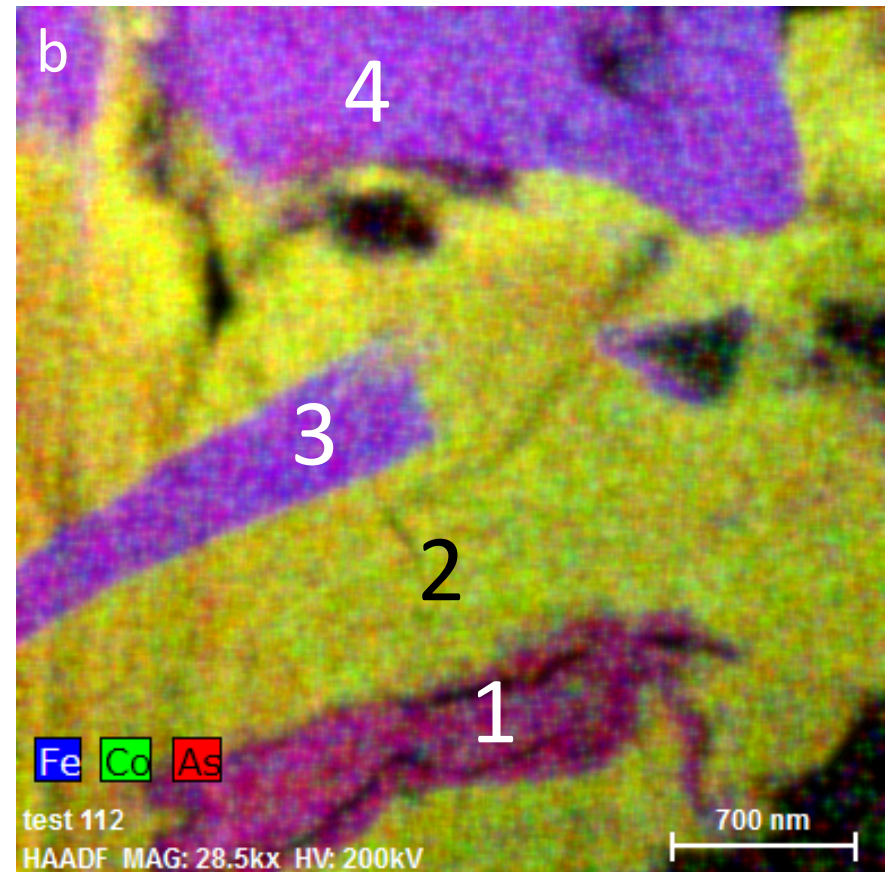
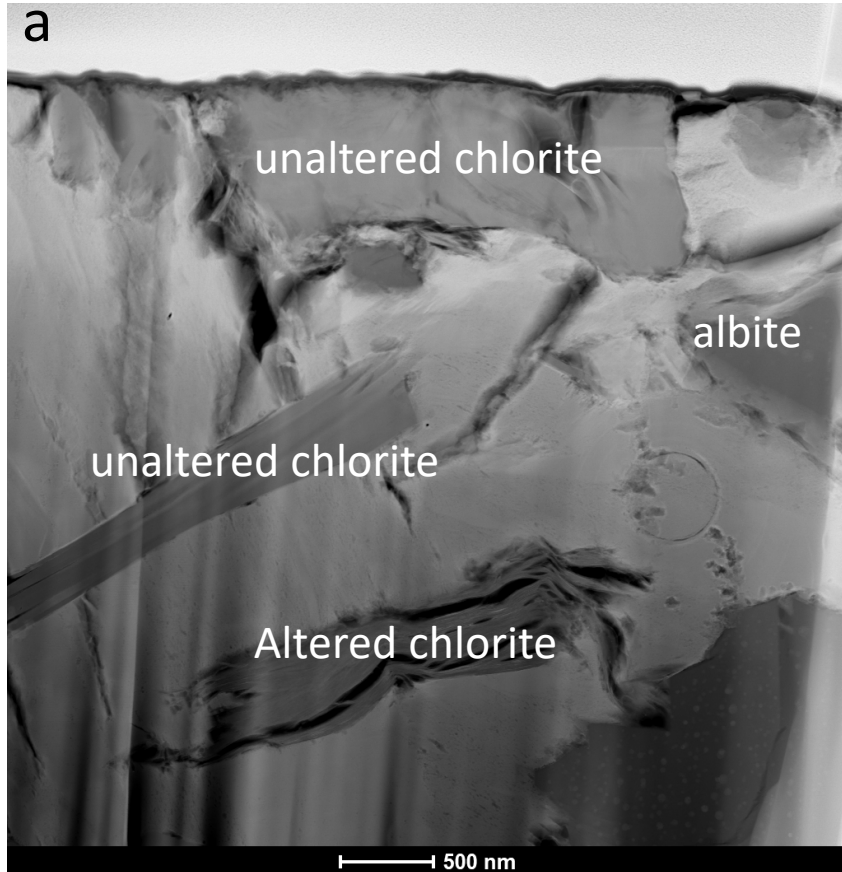


e

Arsenate-bearing minerals of the vivianite group	
D-spacing	hkl Index
2.65	(330)
3.03	(201)
1.96	(510)
1.79	(261)

S31 (a)-(b) TEM images and (c) FFT pattern for the area indicated with a red square in (b); (e) Table listing the observed d-spacing in the FFT pattern, which are characteristic for those observed for a mineral of the vivianite group.

Area #4



S32 (a) STEM-EDS image and (b) chemical distribution for (b) Fe (blue), Co (green) and As (red); semi-quantitative chemical analyses for the chlorite numbered (1)-(4) are given in S33.

Spectrum: 1 **1**

Element	Series	Net unn. [wt.%]	C norm. [wt.%]	C Atom. [at.%]	C Error (3 Sigma) [wt.%]
Nickel	K-series 433	21.17	21.17	13.39	3.86
Iron	K-series 423	18.71	18.71	12.44	3.45
Aluminium	K-series 189	6.23	6.23	8.57	1.56
Silicon	K-series 812	26.39	26.39	34.89	2.91
Magnesium	K-series 508	15.66	15.66	23.92	2.59
Calcium	K-series 59	2.12	2.12	1.97	0.99
Arsenic	L-series 200	9.72	9.72	4.82	3.90

Total:		100.00	100.00	100.00	

Spectrum: 1 **2**

Element	Series	Net unn. [wt.%]	C norm. [wt.%]	C Atom. [at.%]	C Error (3 Sigma) [wt.%]
Arsenic	L-series 3377	32.30	32.30	27.21	9.97
Zinc	K-series 698	8.03	8.03	7.75	1.29
Nickel	K-series 2693	25.91	25.91	27.86	2.90
Cobalt	K-series 3255	30.60	30.60	32.77	3.32
Iron	K-series 151	1.31	1.31	1.48	0.44
Calcium	K-series 258	1.86	1.86	2.93	0.48

Total:		100.00	100.00	100.00	

Spectrum: 1 **3**

Element	Series	Net unn. [wt.%]	C norm. [wt.%]	C Atom. [at.%]	C Error (3 Sigma) [wt.%]
Arsenic	L-series 41	1.46	1.46	0.72	1.00
Iron	K-series 1575	50.44	50.44	33.13	6.18
Magnesium	K-series 555	12.34	12.34	18.62	2.00
Aluminium	K-series 646	15.41	15.41	20.95	2.37
Silicon	K-series 867	20.35	20.35	26.58	2.19

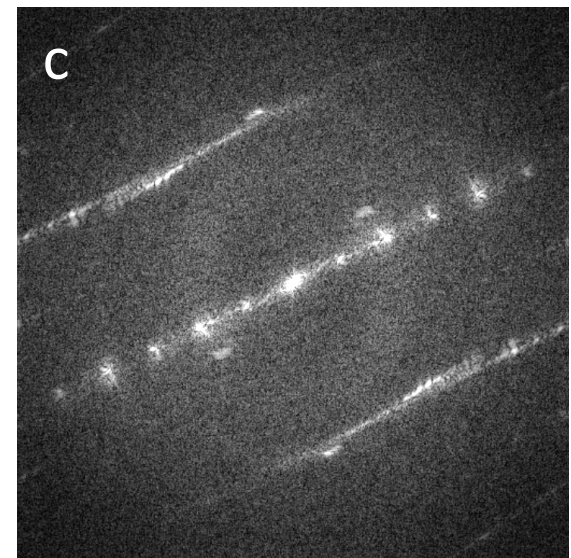
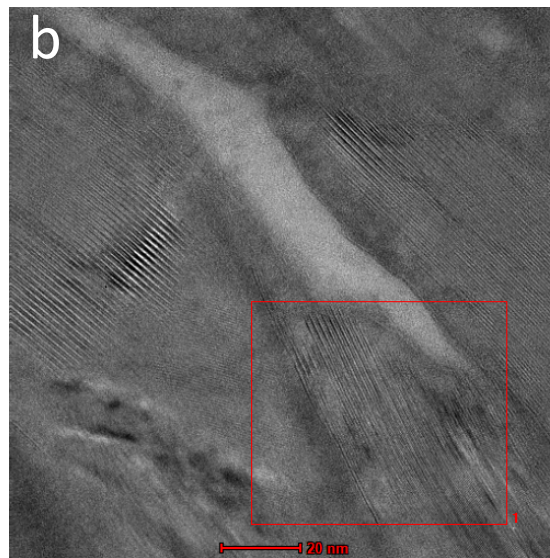
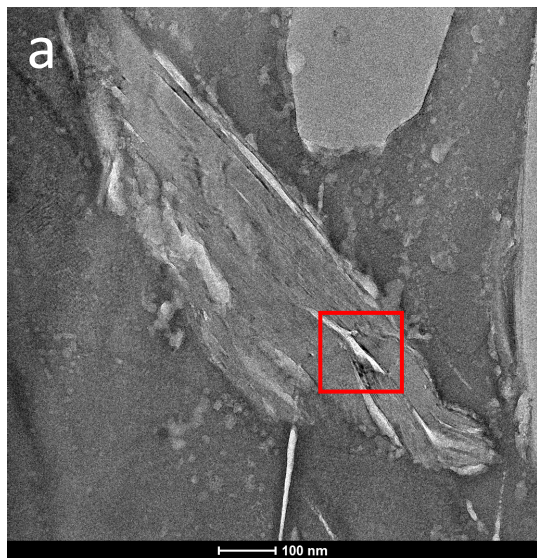
Total:		100.00	100.00	100.00	

Spectrum: 1 **4**

Element	Series	Net unn. [wt.%]	C norm. [wt.%]	C Atom. [at.%]	C Error (3 Sigma) [wt.%]
Arsenic	L-series 387	4.23	4.23	2.12	1.56
Iron	K-series 5024	49.98	49.98	33.53	5.11
Silicon	K-series 2527	18.41	18.41	24.56	1.20
Aluminium	K-series 2137	15.84	15.84	22.00	1.84
Magnesium	K-series 1670	11.54	11.54	17.79	1.42

Total:		100.00	100.00	100.00	

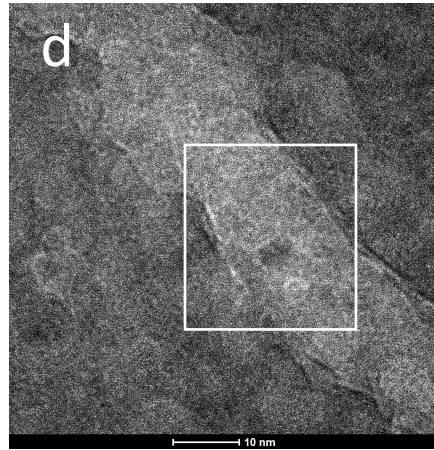
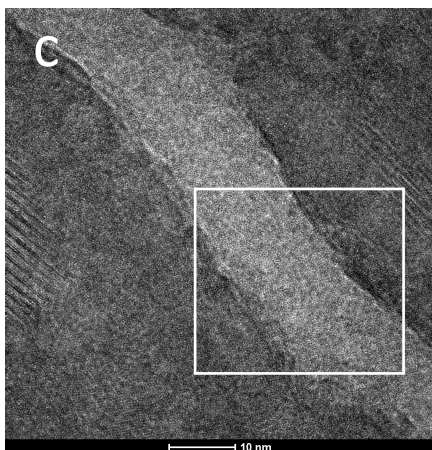
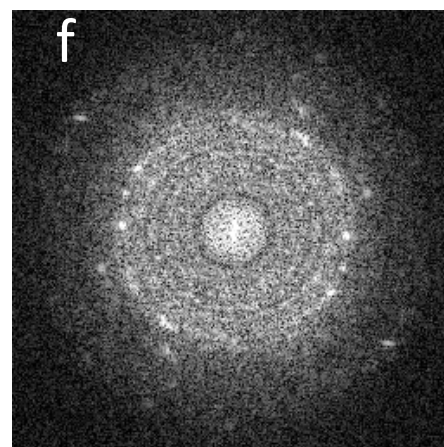
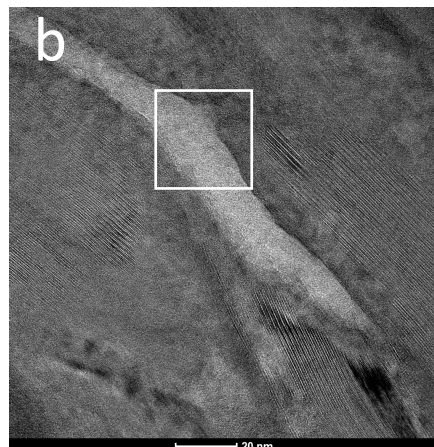
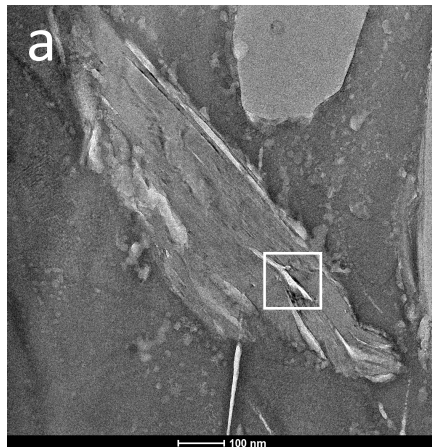
S33 Semi-Quantitative Chemical analysis for the chlorite grains indicated in S32



S34 (a)-(b) TEM images of the interior of an altered clinochlore crystal; the area shown in (b) is indicated with a red square in (a); a red square in (b) indicates the area from which the FFT pattern in (c) has been taken; (c) FFT pattern of the area indicated in (b); (d) d-spacings measured in the FFT pattern shown in (c).

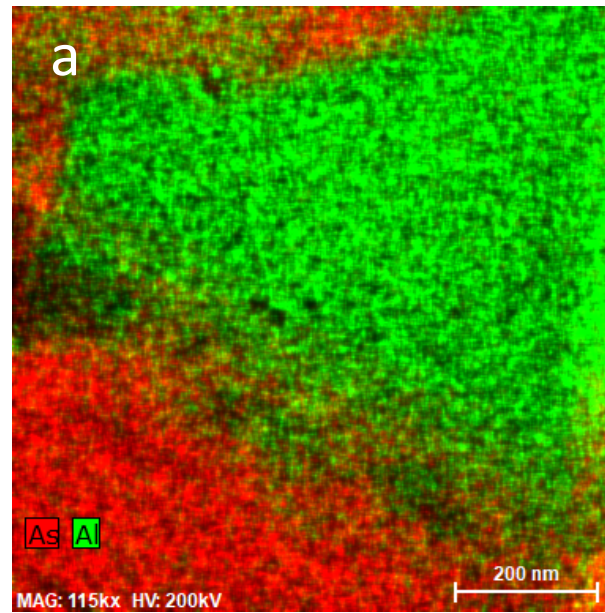
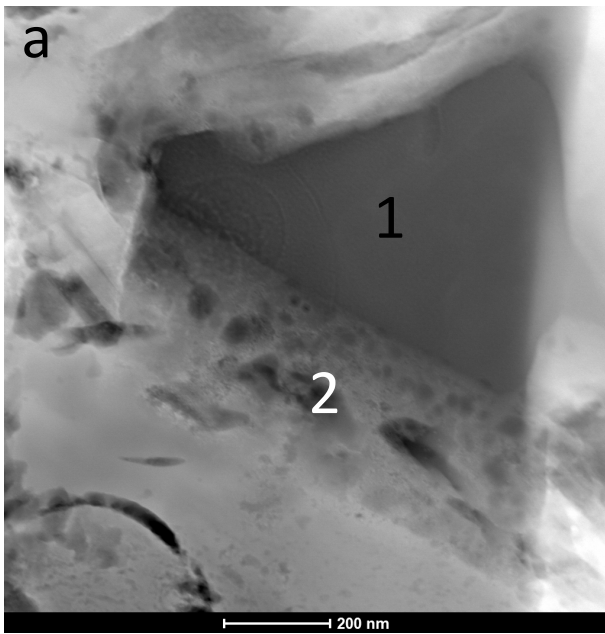
e

Clinochlore $(\text{Mg,Fe})_5\text{Al}(\text{AlSi}_3\text{O}_{10})(\text{OH})_8$	
D-spacing	(hkl)
14.4	(001)
7.20	(002)
4.80	(003)
3.60	(004)
2.90	(005)
4.33	(021)
3.25	(0-23)
2.75	(024)



g Arsenohopeite structure type	
D-spacing [Å]	(hkl)
4.90	(011)
4.11	(230)
3.50	(240)

S35 (a)-(d) TEM images of the interior of clinochore crystals containing (Co, Ni)-arsenates nanoparticles with the arsenohopeite structure type; the areas shown in (b), (c) and (d) are indicated with white squares in (a), (b) and (c), respectively; the area from where the FFT pattern in (f) was taken is indicated with a white square in (d); (f) FFT pattern from the area shown in (d); (g) d-spacings measured in the FFT pattern.



Spectrum: 1

1

Element	Series	Net un.	C norm.	C Atom.	C Error (3 Sigma)	
		[wt.%]	[wt.%]	[at.%]	[wt.%]	
Sodium	K-series	391	14.18	14.18	16.67	2.57
Aluminium	K-series	484	20.48	20.48	20.50	3.44
Silicon	K-series	1573	65.34	65.34	62.84	5.12
Total:		100.00	100.00	100.00		

Spectrum: 1

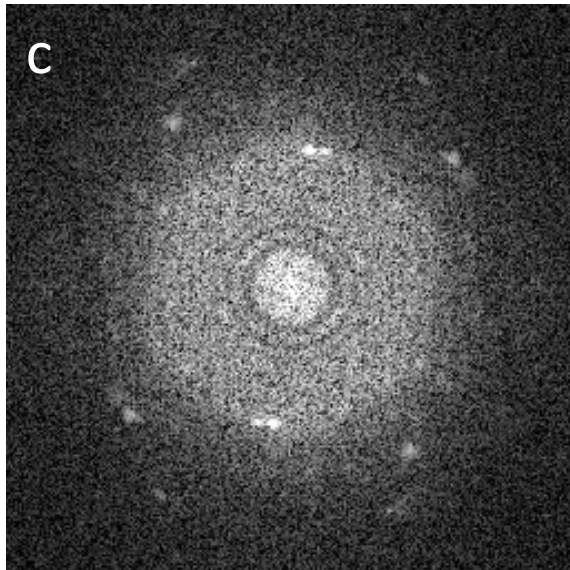
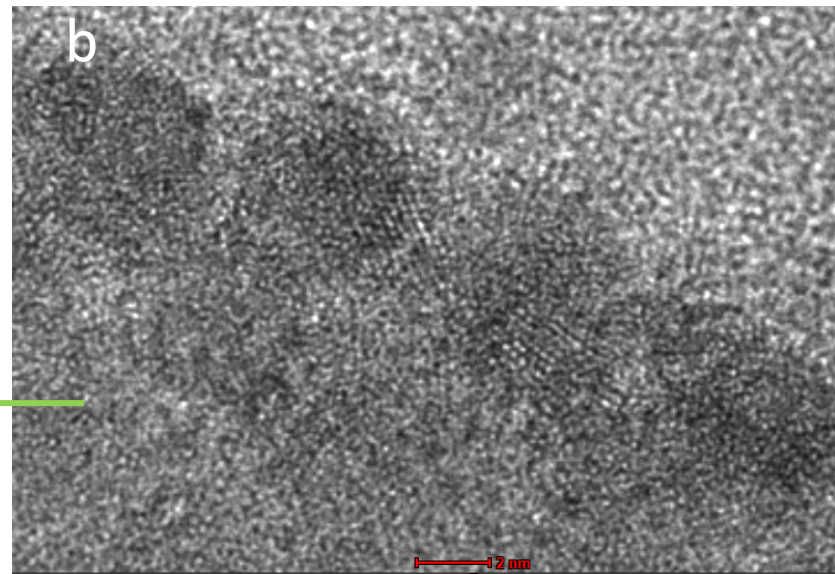
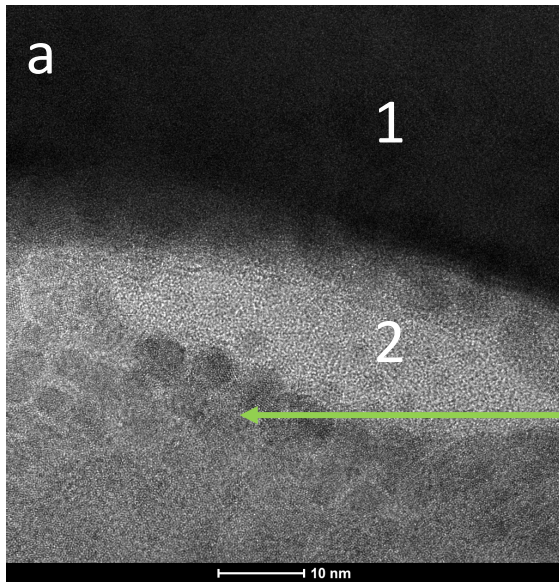
2

Element	Series	Net un.	C norm.	C Atom.	C Error (3 Sigma)	
		[wt.%]	[wt.%]	[at.%]	[wt.%]	
Iron	K-series	1867	3.46	3.46	2.82	0.48
Cobalt	K-series	9732	19.48	19.48	15.00	1.94
Nickel	K-series	9672	19.82	19.82	15.33	1.97
Zinc	K-series	2472	6.06	6.06	4.20	0.75
Arsenic	L-series	10239	20.86	20.86	12.64	6.38
Silicon	K-series	14209	19.31	19.31	31.20	0.57
Aluminium	K-series	4579	6.33	6.33	10.65	0.71
Sodium	K-series	2880	3.41	3.41	6.73	0.44
Calcium	K-series	824	1.27	1.27	1.43	0.26
Total:		100.00	100.00	100.00		

S36 (a) TEM STEM-EDS and (b) chemical

distribution map for As (red) and

Al (green) of a reaction rim around albite, the areas from where the semi-quantitative analyses (1) and (2) were taken are indicated in (a).



d

Minerals of the vivianite structure type	
D-spacing [Å]	(hkl)
6.71	(020)
2.60	(330)
2.03	(260)

S37 (a)-(b) TEM images of the reaction rim on the surface of albite; labelled “1” and (2) in (a), respectively; the area shown in (b) is indicated with a green arrow in (a); (c) FFT pattern of the area shown in (b); (d) d-spacings measured in the FFT pattern in (c).

Supplementary Data F

S 38 Visual Minteq calculations using the pore water chemistry C17 from Percival, J.B., Kwong, Y.T.J. Dumaresq, C.G., Michel, F.A. (2004) Transport and attenuation of arsenic, cobalt and nickel in an alkaline environment (Cobalt, Ontario) Geological Survey of Canada Open File 1680 and the thermodynamic data for FeOHCO_3 with $\log K = 10.76$ from Grivé, M., Duro, L., Bruno, J. (2014) Fe(III) mobilisation by carbonate in low temperature environments: Study of the solubility of ferrihydrite in carbonate media and the formation of Fe(III) carbonate complexes Applied Geochemistry 49, 57–67.

H+1	0
Ag+1	98.0
Al+3	364.7
As(V)	114800.0
Ba+2	14.2
Ca+2	40800.0
Cd+2	2.36
Co+2	3721.0
Cr(III)	16.57
Cu+2	1291.0
Fe+3	879.0
Hg(II)	226.6
Mg+2	3503.0
Mn+2	10.97
Mo(VI)	479.8
Na+1	283900.0
Ni+2	1035.0
P (PO4)	418.0
Pb+2	3091.0
Rb+1	25.58
S (SO4)	159000.0
Sb(V)	2949.0
Si (H4SiO4)	11590.0
Sr+2	144.0
Ti(IV)	54.4
V(V)	78.6
W(VI)	2.28
Zn+2	12.85

pH = 8

Total concentrations
 $\mu\text{g L}^{-1}$

S 39 Assumption 1: pore water in equilibrium with calcite,
Ionic strength = 0.0216

Output data for Fe-species:

Concentration Activity Log activity

Fe(CO ₃) ₃	2.4938E-10	6.8728E-11	-10.163
Fe(OH) ₂ ⁺	1.4844E-08	1.2864E-08	-7.891
Fe(OH) ₃ (aq)	7.1953E-10	7.2312E-10	-9.141
Fe(OH) ₄ ⁻	1.6644E-09	1.4423E-09	-8.841
Fe(SO ₄) ₂ ⁻	1.163E-18	1.0078E-18	-17.997
Fe ⁺³	2.6266E-18	7.2388E-19	-18.14
Fe ₂ (OH) ₂ ⁺⁴	6.6086E-23	6.6839E-24	-23.175
Fe ₃ (OH) ₄ ⁺⁵	7.0018E-28	1.9516E-29	-28.71
FeH ₂ PO ₄ ⁺²	1.9065E-20	1.0751E-20	-19.969
FeHPO ₄ ⁺	3.3779E-14	2.9272E-14	-13.534
FeOH ⁺²	1.2254E-12	6.9106E-13	-12.16
FeOHCO ₃	0.000015722	0.000015801	-4.801
FeSO ₄ ⁺	3.5786E-17	3.1011E-17	-16.508

Species distribution for Fe³⁺-species:

FeOHCO ₃	99.889
Fe(OH) ₂ ⁺	0.094
Fe(OH) ₄ ⁻	0.011

Output data for Fe-minerals:

Mineral log IAP Sat. index

Fe ₂ (SO ₄) ₃ (s)	-44.135	-40.401
FeAsO ₄ :2H ₂ O(s)	-25.031	-4.831
Ferrihydrite	5.859	2.659
Ferrihydrite (aged)	5.859	3.169
Goethite	5.859	5.368

S 40 Assumption 2: pore water in equilibrium with CO₂ atmosphere

Ionic strength = 0.0216

Output data for Fe-species:

Concentration Activity Log activity

Fe(CO ₃) ₃	1.2177E-10	3.4655E-11	-10.46
Fe(OH) ₂ ⁺	2.0807E-08	1.8095E-08	-7.742
Fe(OH) ₃ (aq)	1.0125E-09	1.0172E-09	-8.993
Fe(OH) ₄ ⁻	2.333E-09	2.0289E-09	-8.693
Fe(SO ₄) ₂ ⁻	1.848E-18	1.6072E-18	-17.794
Fe ⁺³	3.5781E-18	1.0183E-18	-17.992
Fe ₂ (OH) ₂ ⁺⁴	1.2351E-22	1.3226E-23	-22.879
Fe ₃ (OH) ₄ ⁺⁵	1.7827E-27	5.4326E-29	-28.265
FeH ₂ PO ₄ ⁺²	2.9558E-20	1.6909E-20	-19.772
FeHPO ₄ ⁺	5.2935E-14	4.6037E-14	-13.337
FeOH ⁺²	1.6994E-12	9.7212E-13	-12.012
FeOHCO ₃	0.000015715	0.000015789	-4.802
FeSO ₄ ⁺	5.3408E-17	4.6448E-17	-16.333

Output data for Fe-minerals:

Mineral	log IAP Sat. index	
FeAsO ₄ :2H ₂ O(s)	-24.877	-4.677
Ferrihydrite	6.007	2.807
Ferrihydrite (aged)	6.007	3.317
Goethite	6.007	5.516

Species distribution for Fe³⁺-species:

FeOHCO₃ 99.847

Fe(OH)₂⁺ 0.132

Fe(OH)₄⁻ 0.015

Appendix B: Mineralogy of the Cobalt Mining Camp

Table 1. Mineralogy identified from the ore and tailings of the Cobalt mining camp.

Ore Mineralogy			
Mineral name	Mineral formula	Mineral name	Mineral formula
Native silver	Ag ⁰	Acanthite	AgS ₂
Native bismuth	Bi ⁰	Proustite	Ag ₃ AsS ₃
Dyscrasite	Ag ₃ Sb	Stephanite	Ag ₅ SbS ₄
Argentite	Ag ₂ S	Allargentum	Ag _{1-x} S _x (x=0.09-0.16)
Cobaltite	CoAsS (**)	Chapmanite	Fe ₂ Sb(Si ₂ O ₅)O ₃ (OH)
Skutterudite	(Co,Fe,Ni)As ₂₋₃ (**)	Langisite	(Co,Ni)As
Niccolite	NiAs (**)	Larosite	(Cu,Ag) ₂₁ (Pb,Bi) ₂ S ₁₃
Mckinstryite	Ag _{5-x} Cu _{3+x} S ₄ (x=0-0.28)	Gersdorffite	NiAsS (**)
Pararammelsbergite	NiAs ₂	Bismuthinite	Bi ₂ S ₃ (**)
Arsenopyrite	FeAsS (**)	Chalcopyrite	CuFeS ₂ (**)
Cobaltoan arsenopyrite	(Fe,Co)AsS (**)	Argentobismutite	AgBiS ₂ (**)
Argentopyrite	AgFe ₂ S ₃ (**)	Safflorite	(Co,Ni,Fe)As ₂ (**)
Löllingite	FeAs ₂ (**)		
Tailings Mineralogy			
Mineral name	Mineral formula	Mineral name	Mineral formula
Albite	NaAlSi ₃ O ₈	Scorodite	Fe ³⁺ (AsO ₄)·2H ₂ O
Quartz	SiO ₂	Arsenohopeite	Zn ₃ (AsO ₄) ₂ ·2H ₂ O
Anorthite	CaAl ₂ Si ₂ O ₈	Goethite	α-Fe ³⁺ O(OH)
Dolomite	CaMg(CO ₃) ₂	Calcite	CaCO ₃
Clinochlore	Mg ₅ Al(AlSi ₃ O ₁₀)(OH) ₈	Alunite	KAl ₃ (SO ₄) ₂ (OH) ₆
Erythrite	Co ₃ (AsO ₄) ₂ ·8H ₂ O	Annabergite	Ni ₃ (AsO ₄) ₂ ·8H ₂ O
Cobaltoan olivenite	(Cu,Co) ₂ AsO ₄ (OH)	Titanite	CaTi(SiO ₄)O
Stilbite	NaCa ₄ [Al ₉ Si ₂₇ O ₇₂ ·nH ₂ O		
Roselite	Ca ₂ (Co ²⁺ ,Mg)(AsO ₄) ₂ ·2H ₂ O		
Ferropargasite	NaCa ₂ Fe ₄ Al(Si ₆ Al ₂)O ₂₂ (OH) ₂		
Muscovite	(K,Ca,Na)(Al,Mg,Fe) ₂ (Si,Al) ₄ O ₁₀ (OH) ₂		
Illite	(K,H ₃ O)Al ₂ Si ₃ AlO ₁₀ (OH) ₂		
Magnesoriebeckite	(Na,Ca) ₂ (Mg,Fe) ₅ Si ₈ O ₂₂ (OH) ₂		
Magnesoarfvedsonite	(Na)(Na ₂)(Mg ₄ Fe ³⁺)(Si ₈ O ₂₂)(OH) ₂		
Epidote	Ca ₂ (Al ₂ Fe ³⁺)(Si ₂ O ₇)(SiO ₄)O(OH)		

** occurs in ore and tailings. All mineral formulae were retrieved from <https://www.mindat.org/>.

Appendix C: X-ray Diffractograms

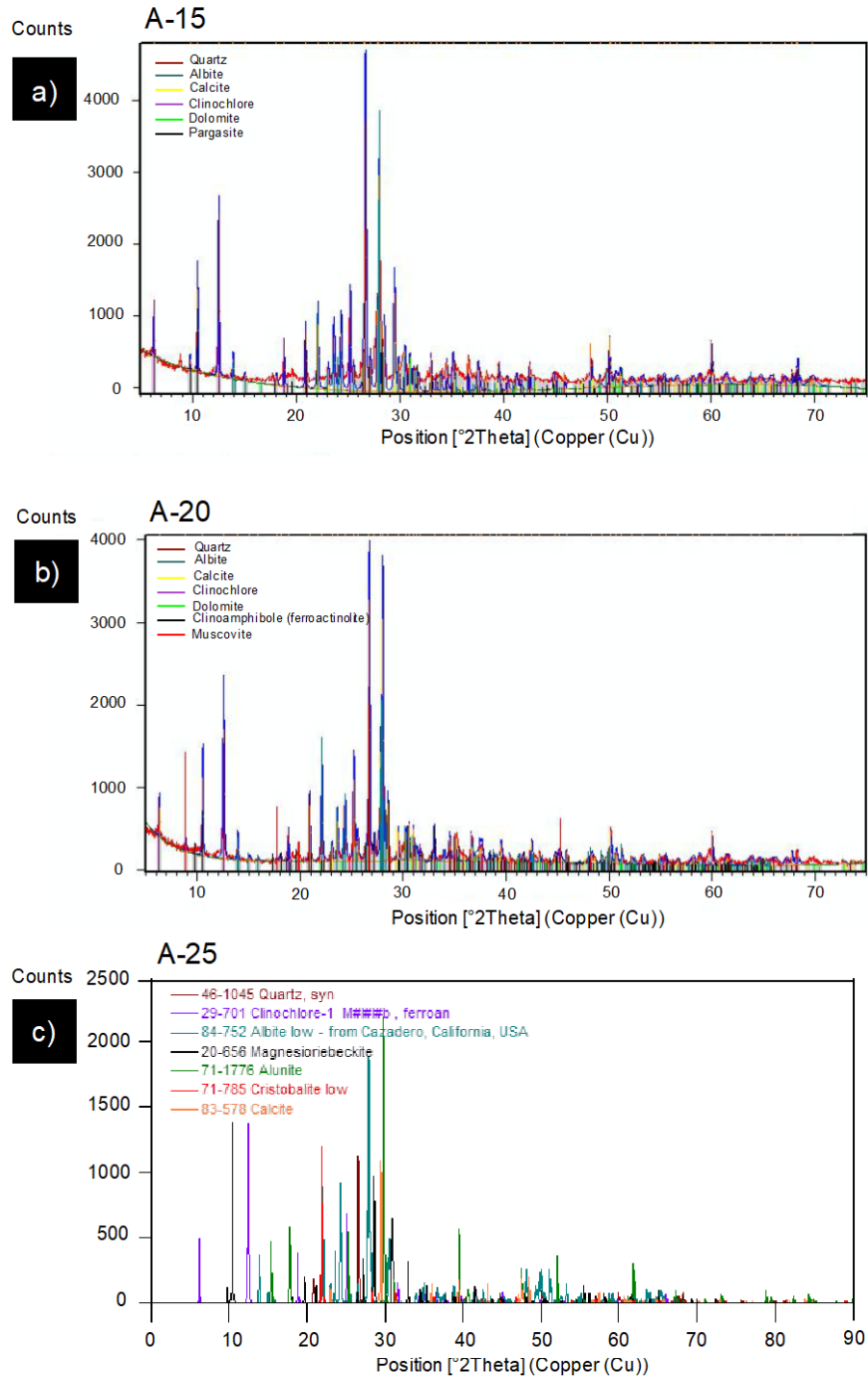


Figure 1. X-ray diffraction patterns from site A D = 15 (a), D = 20 (b) and D = 25 (c).

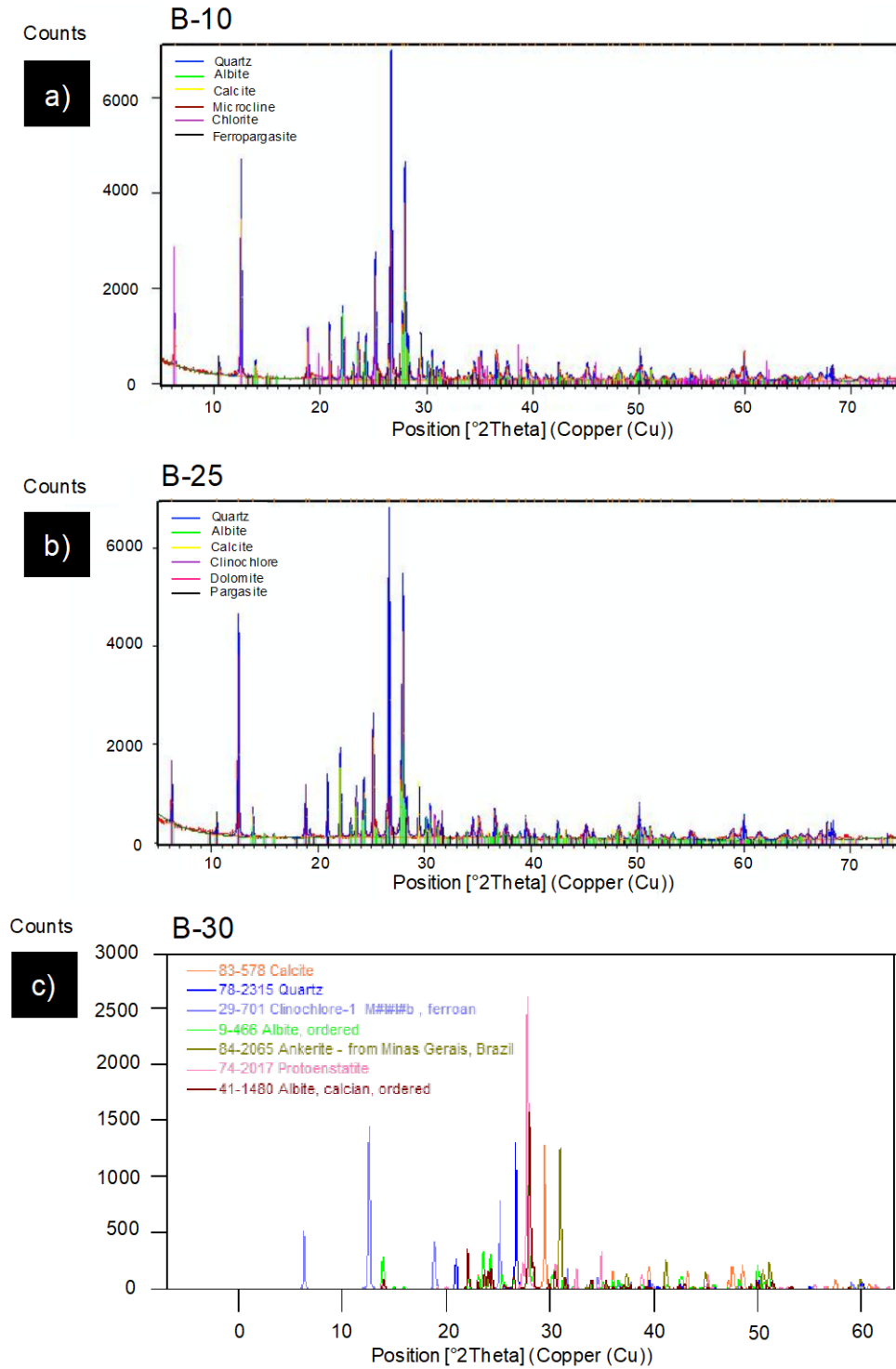


Figure 2. X-ray diffraction patterns from site B D = 10 (a), D = 25 (b) and D = 30 (c).

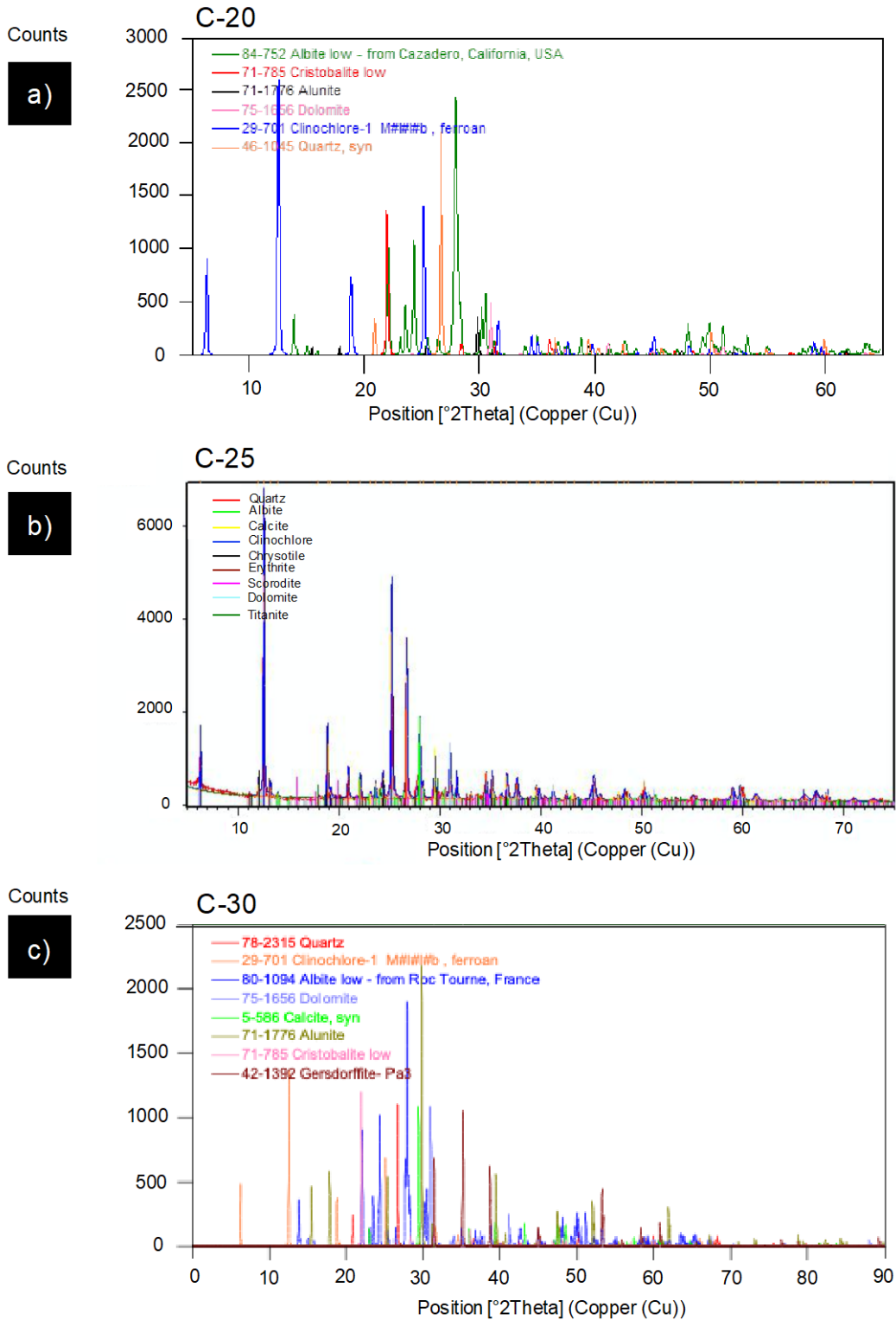


Figure 3. X-ray diffraction patterns from site C D = 20 (a), D = 25 (b) and D = 30 (c).

Appendix D: Raw Sequence Data and Rarefaction Curve

Table 1. A chart of the raw bacterial sequence data showing the total number of sequences, the percent of sequences filtered out, and the percent of sequences retained.

Sample ID	Total Number of Sequences	% Filtered	% Retained
A-05	49153	4.5	95.5
A-10	54213	3.9	96.1
A-15	27301	2.5	97.5
A-20	44540	3.3	96.7
A-25	48401	3.2	96.8
A-30	134261	3.9	96.1
B-05	19960	3.1	96.9
B-10	36860	3.5	96.5
B-15	31114	3.2	96.8
B-20	28089	3.5	96.5
B-25	33786	3.5	96.5
B-30	34573	3.3	96.7
C-05	17099	3.5	96.5
C-10	17153	3.0	97.0
C-15	21281	2.8	97.2
C-20	53910	3.2	96.8
C-25	52945	2.8	97.2
C-30	39746	2.6	97.4
NC	3202	3.4	96.6

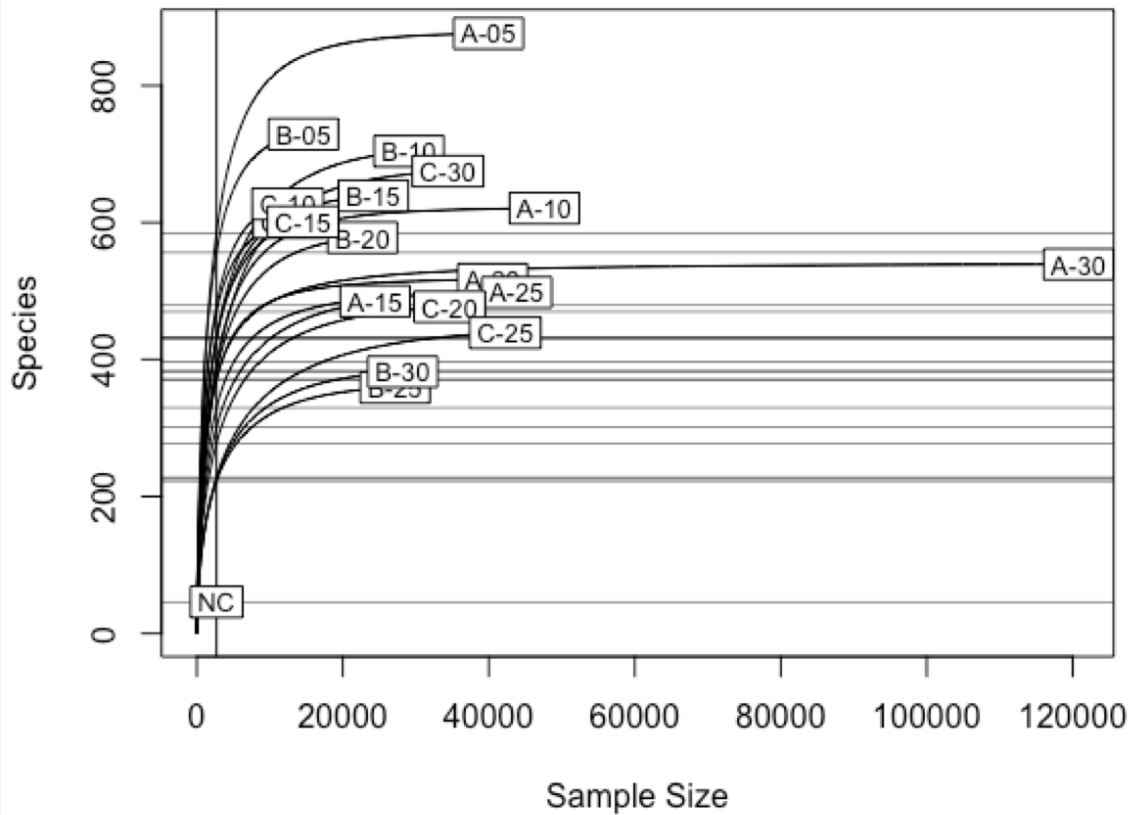


Figure 1. A rarefaction curve plot of tailings samples analyzed for 16S rRNA gene sequencing. The sample size (or sequencing depth) is on the X-axis, with species count on the Y-axis. Samples that have a curve that has plateaued means that the sequences were well-recovered, with some having a low species count meaning that there could have been a low DNA yield or the samples are not well diverse. Samples that have a curve that is beginning to plateau means that more sample diversity could have been captured, with (possibly) better extraction methods.

Appendix E: XANES Spectra

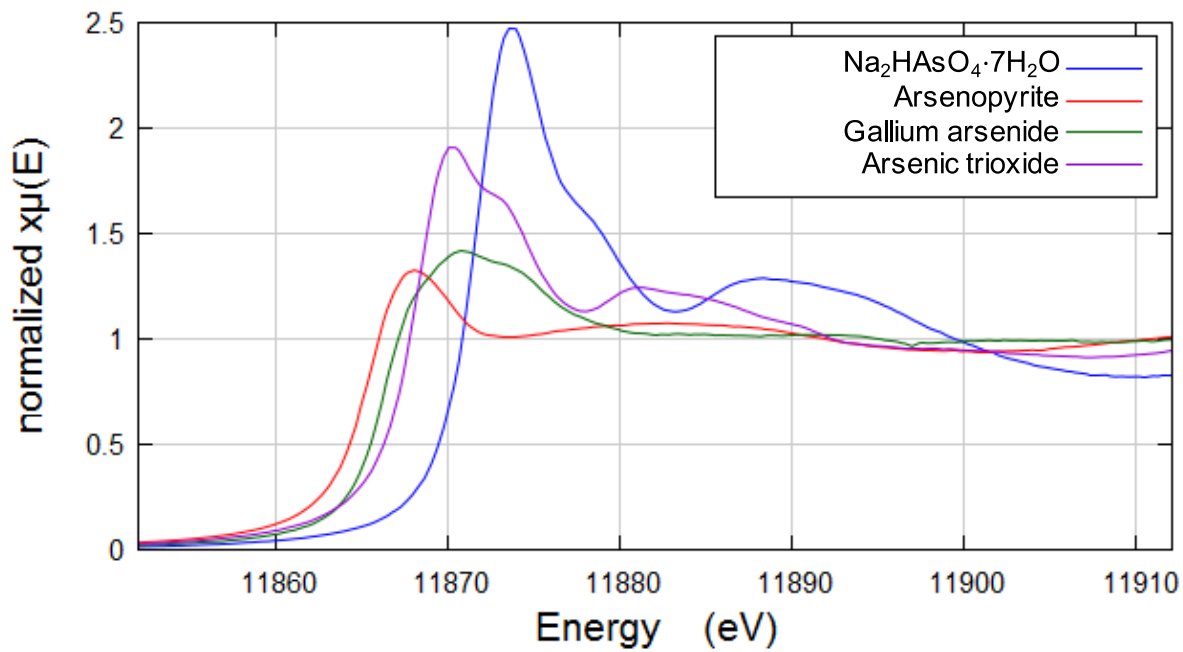


Figure 1. The triplicate averaged XANES spectra for the standards used.

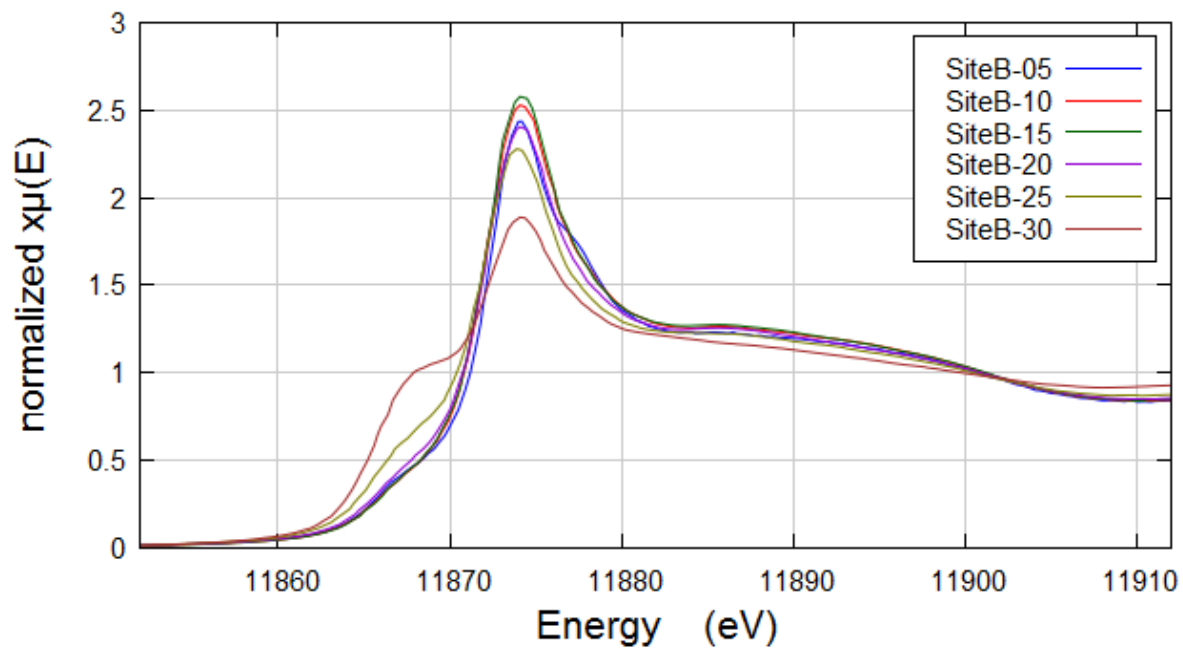


Figure 2. The triplicate averaged XANES spectra for site B tailings samples.

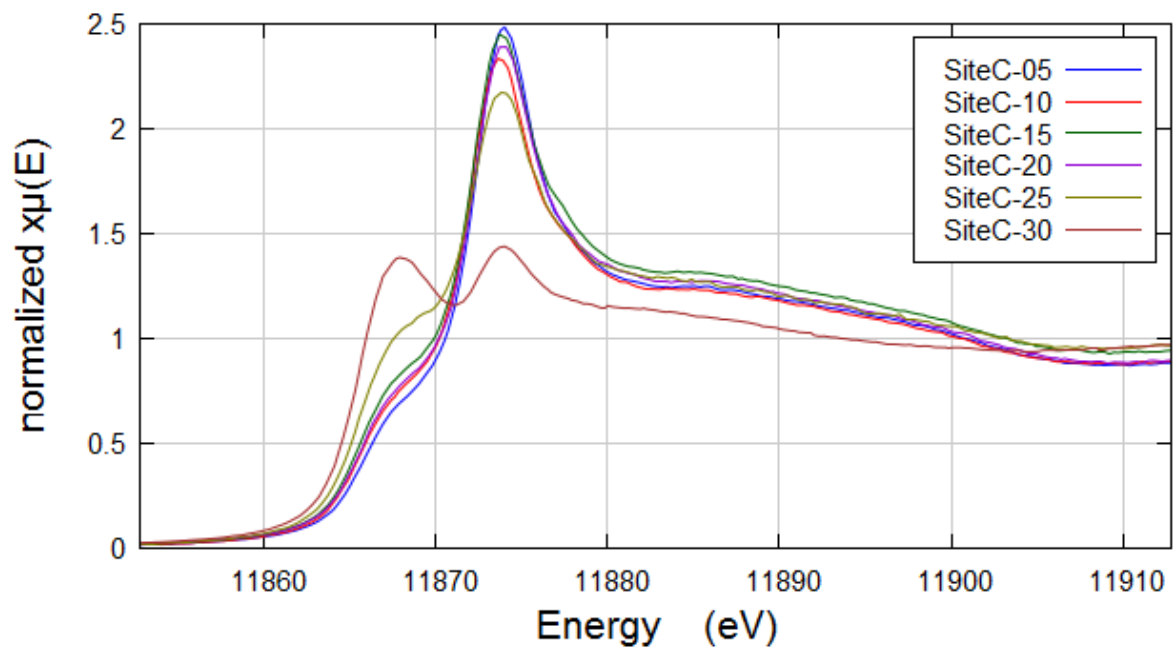


Figure 3. The triplicate averaged XANES spectra for site C tailings samples.

Appendix F: Analysis of Similarities (ANOSIM)

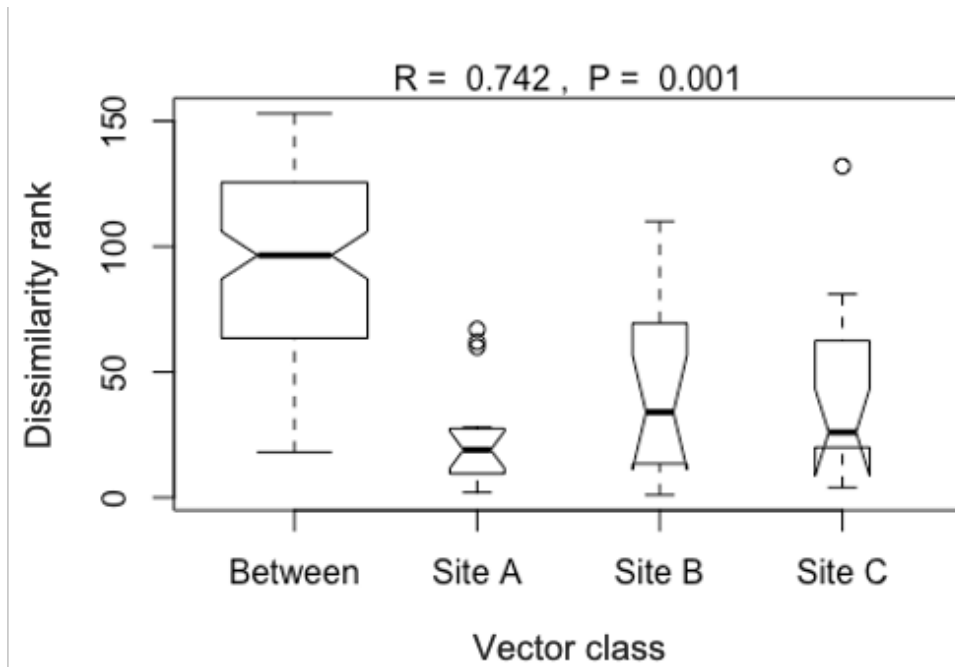


Figure 1. A graph resulting from the analysis of similarities (ANOSIM) test. The analysis was performed to identify dissimilarities between and within sites, using the microbial and geochemical data. An R-value of 0.742 with a p-value of 0.001 indicates a strong, statistically significant difference in the microbial communities based on the site grouping

Appendix G: Bulk Chemical Data

Table 1. Table showing the values or concentrations of the environmental and geochemical variables in each tailings sample.

ID	pH	Eh (V)	Ag (ppm)	As (wt%)	Ca (wt%)	Co (wt%)	Fe (wt%)	CO₂(T) (wt%)	S_(T) (wt%)	Co#	Fe#	S#
A-05	8.48	0.28	10.61	0.07	4.31	0.03	7.40	1.44	0.09	6.83	81.72	5.10
A-10	8.32	0.29	44.03	0.05	3.95	0.02	7.14	1.84	0.08	4.10	78.36	3.85
A-15	8.7	0.27	27.75	0.03	4.04	0.01	6.80	1.75	0.08	3.89	81.31	4.69
A-20	8.57	0.27	43.43	0.07	4.28	0.02	7.10	1.65	0.08	5.57	80.73	4.40
A-25	8.06	0.29	52.31	0.04	4.17	0.02	5.10	1.63	0.08	4.15	74.92	4.26
A-30	8.05	0.30	47.85	0.05	3.85	0.02	7.43	1.82	0.07	4.17	79.96	3.82
B-05	8.63	0.25	78.28	0.42	3.19	0.11	5.58	4.861	0.07	17.1	66.46	2.53
B-10	8.08	0.27	75.83	0.39	2.76	0.12	6.26	3.102	0.07	15.7	67.44	2.17
B-15	8.14	0.27	78.81	0.36	2.70	0.13	7.95	2.826	0.07	11.6	66.00	1.68
B-20	7.7	0.26	109.5	0.38	2.47	0.14	5.85	4.848	0.17	16.8	67.89	5.82
B-25	7.84	0.26	96.56	0.40	2.47	0.11	6.13	2.335	0.06	15.6	67.02	2.01
B-30	7.77	0.26	108.5	0.29	2.81	0.10	6.71	3.259	0.14	11.1	65.24	3.69
C-05	7.23	0.36	15.17	0.88	4.12	0.37	10.51	6.498	0.19	19.9	67.07	3.50
C-10	7.58	0.36	26.24	1.15	5.22	0.46	12.40	4.848	0.17	22.6	68.70	2.94
C-15	7.53	0.36	8.17	1.29	3.97	0.46	12.74	4.969	0.22	24.5	69.79	3.85
C-20	7.66	0.36	9.72	1.37	4.05	0.51	11.80	4.995	0.26	27.3	69.78	4.81
C-25	7.67	0.36	27.06	1.93	4.33	0.63	11.97	5.154	0.29	32.8	69.09	5.05
C-30	7.6	0.34	41.30	1.94	6.96	1.20	11.43	4.676	0.56	37.9	68.34	9.56

Table 2. Table showing the average As valence, the percent abundances of As-species and the ratio of positive to negative As species (AVR) (Equation 5).

Sample ID	Average As valence	As ⁵⁺ (%)	As ³⁺ (%)	As ¹⁻ (%)	AVR
B-05	4.27	87.77	0.00	12.23	7.17
B-10	4.90	94.80	5.2	0.00	0.00
B-15	4.92	96.10	3.90	0.00	0.00
B-20	4.47	86.03	7.63	6.33	14.79
B-25	3.93	71.10	17.10	11.83	7.45
B-30	2.18	43.97	13.57	42.47	1.35
C-05	4.04	73.27	16.03	10.70	8.34
C-10	3.71	62.80	23.6	13.63	6.34
C-15	4.28	68.97	28.53	2.50	39.00
C-20	3.86	67.20	20.77	12.03	7.31
C-25	3.52	51.70	31.07	17.20	4.81
C-30	0.25	11.83	13.57	74.60	0.34

Appendix H: Additional SEM results from sites B and C

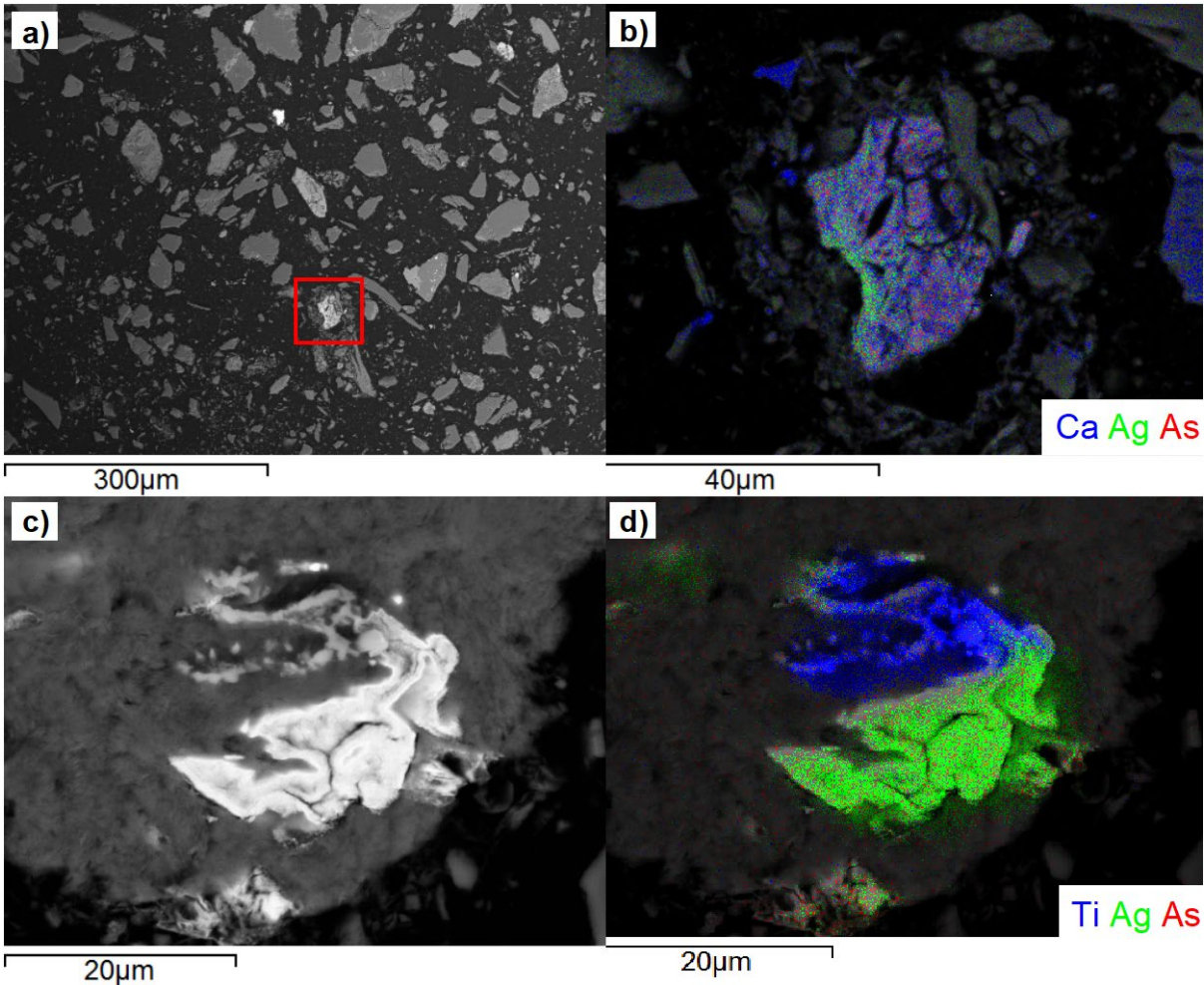


Figure 1. SEM photomicrographs and EDS-chemical maps for (a, b) a Ca-Fe-Ag-arsenate and (c, d) an unidentified As-Fe-S-Ag-O phase.

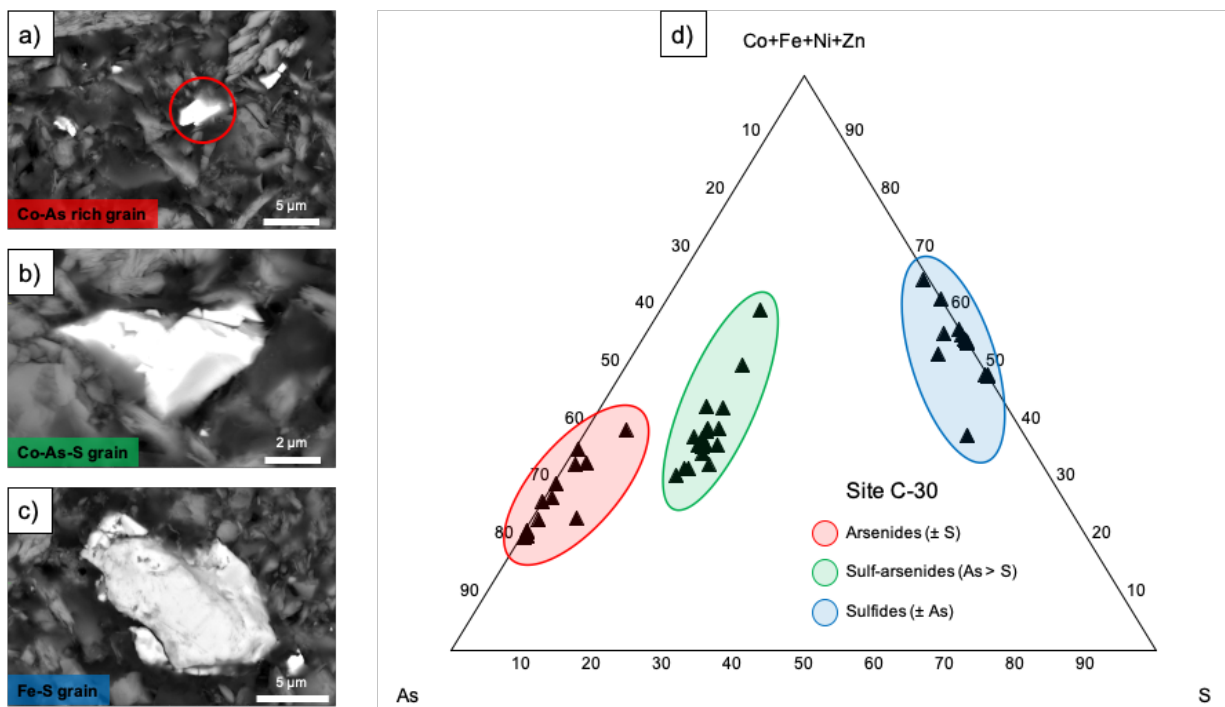


Figure 2. a) – c) SEM photomicrographs from D = 30 cm at site C, a) Co-arsenide, b) Co-sulfarsenide and c) Fe-sulfide, and d) a ternary diagram of the three different As-species identified on the SEM.

Appendix I: Additional Taxonomic Plots

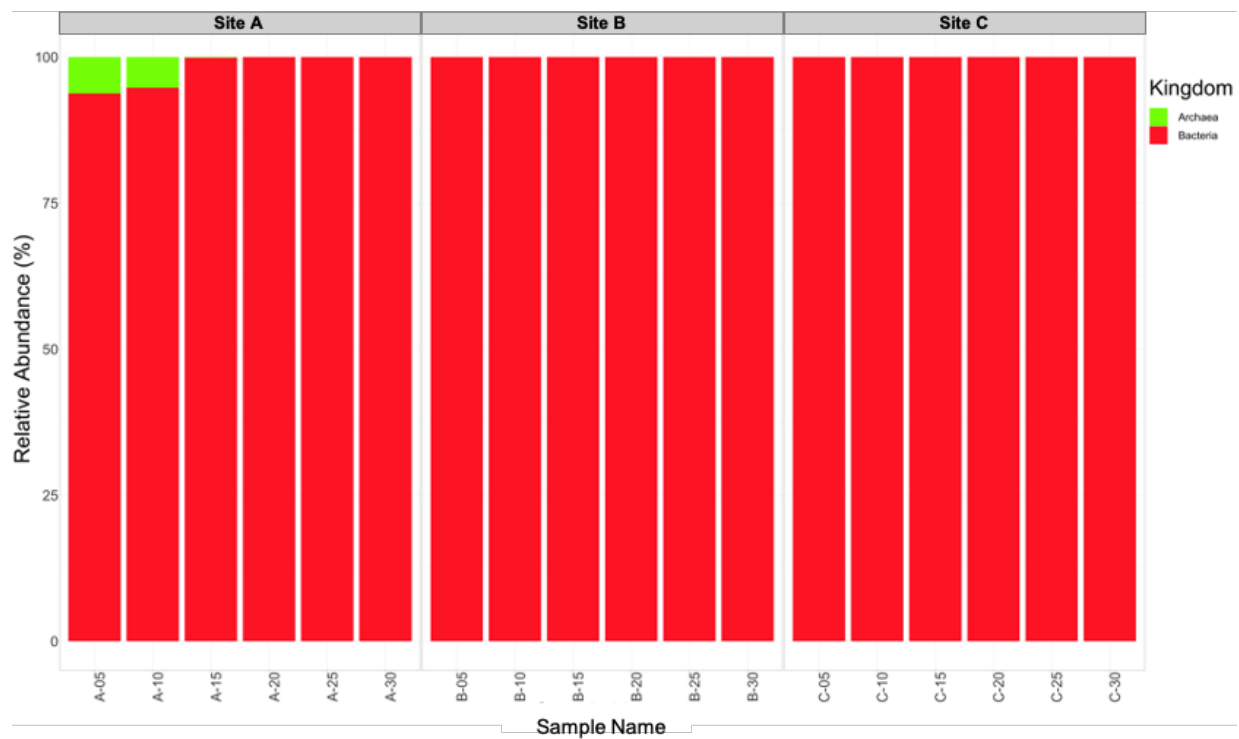


Figure 1. Normalized relative abundance taxonomic bar plot of microbial communities at the Kingdom level.

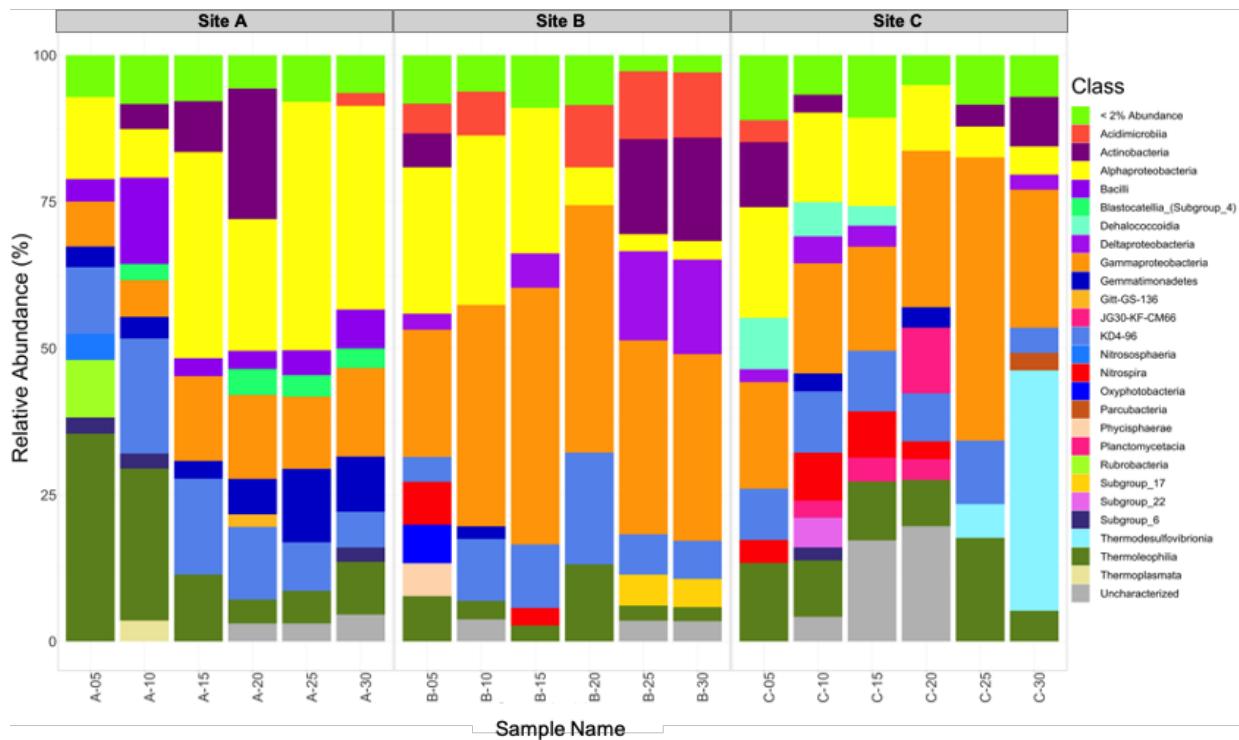


Figure 2. Normalized relative abundance taxonomic bar plot of microbial communities at the Class level.

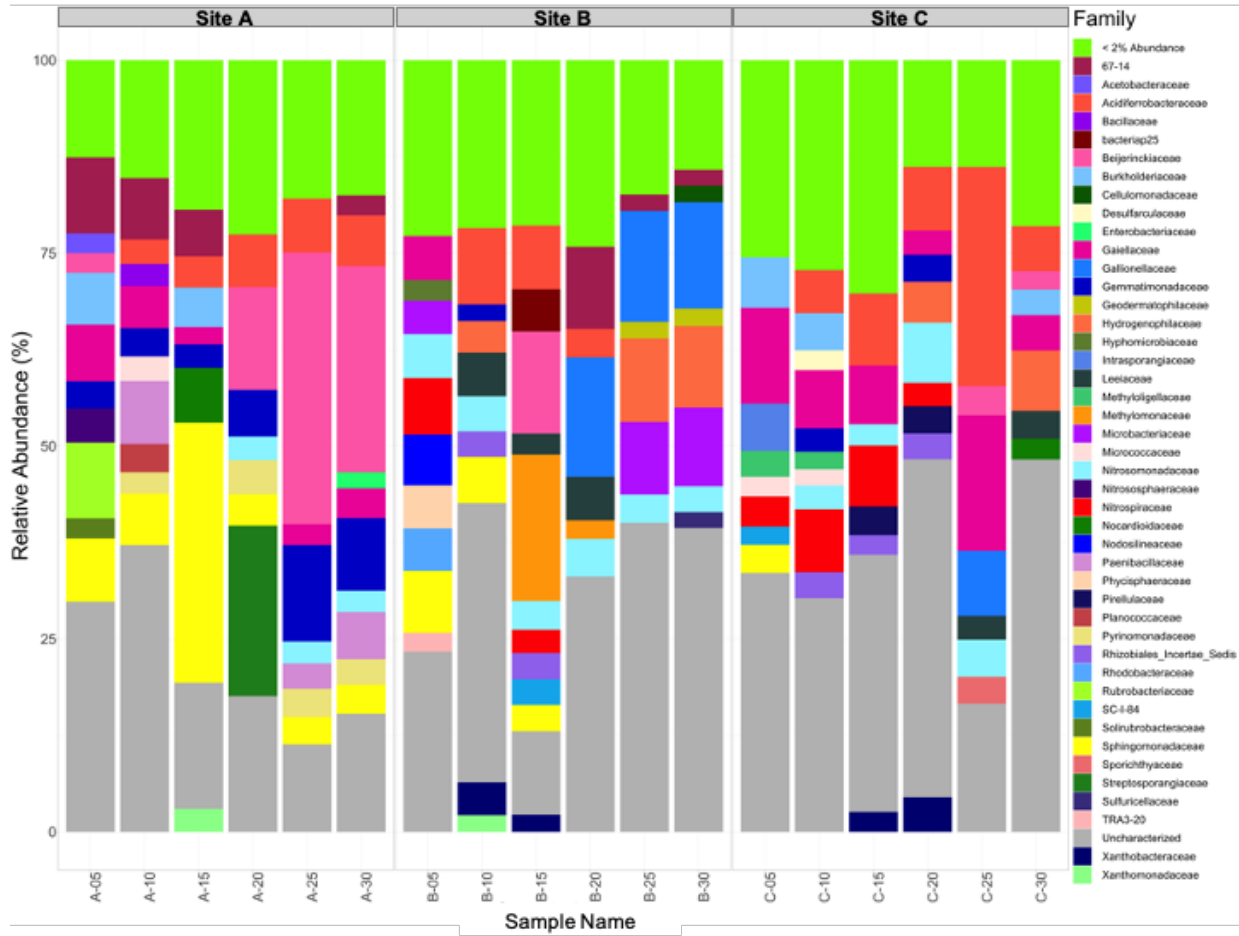


Figure 3. Normalized relative abundance taxonomic bar plot of microbial communities at the Family level.

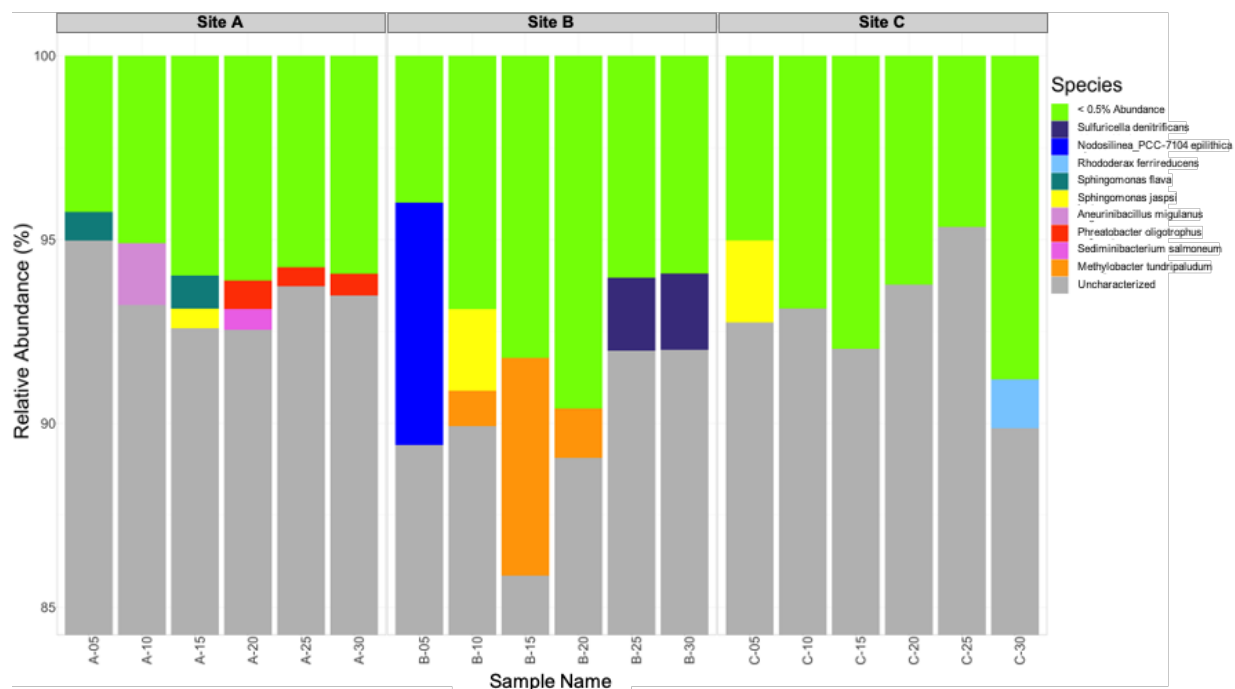


Figure 4. Normalized relative abundance taxonomic bar plot of microbial communities at the Species level.

Appendix J: Correlation Matrices

Table 1. Correlation matrix showing the correlations of environmental and geochemical variables to each other for material from site A.

SITE A	pH	Depth	Eh (V)	Ag (ppm)	As (wt%)	Ca (wt%)	Co (wt%)	Fe (wt%)	CO _{2(T)} (wt%)	S _(T) (wt%)	Co#	Fe#	S#
pH	1	-0.61	-0.94	-0.63	0.26	0.43	-0.025	0.37	-0.24	0.39	0.33	0.71	0.64
Depth	-0.61	1	0.34	0.78	-0.44	-0.41	-0.57	-0.350	0.42	-0.84	-0.52	-0.41	-0.59
Eh (V)	-0.94	0.34	1	0.45	-0.21	-0.49	0.16	-0.22	0.25	-0.2	-0.28	-0.63	-0.61
Ag (ppm)	-0.63	0.78	0.45	1	-0.5	-0.46	-0.6	-0.45	0.63	-0.85	-0.68	-0.71	-0.86
As (wt%)	0.26	-0.44	-0.21	-0.5	1	0.6	0.74	0.57	-0.62	0.73	0.94	0.53	0.42
Ca (wt%)	0.43	-0.41	-0.49	-0.46	0.6	1	0.61	-0.18	-0.9	0.64	0.77	0.13	0.77
Co (wt%)	-0.025	-0.57	0.16	-0.6	0.74	0.61	1	0.15	-0.81	0.9	0.85	0.13	0.54
Fe (wt%)	0.37	-0.35	-0.22	-0.45	0.57	-0.18	0.15	1	0.11	0.33	0.38	0.85	0.055
CO _{2(T)} (wt%)	-0.24	0.42	0.25	0.63	-0.62	-0.9	-0.81	0.11	1	-0.78	-0.85	-0.18	-0.84
S _(T) (wt%)	0.39	-0.84	-0.2	-0.85	0.73	0.64	0.9	0.33	-0.78	1	0.86	0.43	0.75
Co#	0.33	-0.52	-0.28	-0.68	0.94	0.77	0.85	0.38	-0.85	0.86	1	0.49	0.69
Fe#	0.71	-0.41	-0.63	-0.71	0.53	0.13	0.13	0.85	-0.18	0.43	0.49	1	0.49
S#	0.64	-0.59	-0.61	-0.86	0.42	0.77	0.54	0.055	-0.84	0.75	0.69	0.49	1

Table 2. A correlation matrix showing the correlations of environmental and geochemical variables to each other for material from site B.

SITE B	pH	Depth	Eh (V)	Ag (ppm)	As (wt%)	Ca (wt%)	Co (wt%)	Fe (wt%)	CO _{2(T)} (wt%)	S _(T) (wt%)	Co#	Fe#	S#	As Val	As ⁵⁺	As ³⁺	As ¹⁻	AVR
pH	1	-0.85	-0.39	-0.8	0.55	0.85	-0.21	-0.12	0.31	-0.6	0.26	-0.15	-0.52	0.37	0.48	-0.16	-0.29	-0.22
Depth	-0.85	1	0.058	0.84	-0.72	-0.6	-0.23	0.2	-0.42	0.47	-0.5	-0.3	0.33	-0.72	-0.81	0.019	0.65	0.074
Eh (V)	-0.39	0.058	1	-0.14	-0.31	-0.49	0.56	0.66	-0.4	0.043	-0.41	0.15	-0.046	0.4	0.35	0.41	-0.42	-0.41
Ag (ppm)	-0.8	0.84	-0.14	1	-0.54	-0.52	0.007	-0.19	0.13	0.83	-0.12	-0.02	0.77	-0.65	-0.71	-0.28	0.61	0.53
As (wt%)	0.55	-0.72	-0.31	-0.54	1	0.15	0.26	-0.54	0.26	-0.49	0.86	0.67	-0.24	0.71	0.7	0.35	-0.71	0.37
Ca (wt%)	0.85	-0.6	-0.49	-0.52	0.15	1	-0.5	-0.17	0.4	-0.3	0.044	-0.44	-0.3	-0.098	0.051	-0.61	0.19	-0.32
Co (wt%)	-0.21	-0.23	0.56	0.007	0.26	-0.5	1	0.1	0.3	0.31	0.3	0.67	0.41	0.71	0.68	0.37	-0.72	0.44
Fe (wt%)	-0.12	0.2	0.66	-0.19	-0.54	-0.17	0.1	1	-0.58	-0.19	-0.85	-0.53	-0.4	0.065	0.054	0.36	-0.069	-0.65
CO _{2(T)} (wt%)	0.31	-0.42	-0.4	0.13	0.26	0.4	0.3	-0.58	1	0.53	0.54	0.28	0.65	0.093	0.2	-0.64	-0.019	0.63
S _(T) (wt%)	-0.6	0.47	0.043	0.83	-0.49	-0.3	0.31	-0.19	0.53	1	-0.035	0.09	0.96	-0.4	-0.39	-0.52	0.41	0.54
Co#	0.26	-0.5	-0.41	-0.12	0.86	0.044	0.3	-0.85	0.54	-0.035	1	0.81	0.23	0.46	0.45	0.033	-0.46	0.68
Fe#	-0.15	-0.3	0.15	-0.018	0.67	-0.44	0.67	-0.53	0.28	0.093	0.81	1	0.32	0.64	0.57	0.35	-0.67	0.6
S#	-0.52	0.33	-0.046	0.77	-0.24	-0.3	0.41	-0.4	0.65	0.96	0.23	0.32	1	-0.25	-0.24	-0.48	0.25	0.72
As Val	0.37	-0.72	0.4	-0.65	0.71	-0.098	0.71	0.065	0.093	-0.4	0.46	0.64	-0.25	1	0.99	0.57	-0.99	0.083
As ⁵⁺	0.48	-0.81	0.35	-0.71	0.7	0.051	0.68	0.054	0.2	-0.39	0.45	0.57	-0.24	0.99	1	0.44	-0.96	0.054
As ³⁺	-0.16	0.019	0.41	-0.28	0.35	-0.61	0.37	0.36	-0.64	-0.52	0.033	0.35	-0.48	0.57	0.44	1	-0.65	-0.065
As ¹⁻	-0.29	0.65	-0.42	0.61	-0.71	0.19	-0.72	-0.069	-0.019	0.41	-0.46	-0.67	0.25	-0.99	-0.96	-0.65	1	-0.1
AVR	-0.22	0.074	-0.41	0.53	0.37	-0.32	0.44	-0.65	0.63	0.54	0.68	0.6	0.72	0.083	0.054	-0.065	-0.1	1

Table 3. A correlation matrix showing the correlations of environmental and geochemical variables to each other for material from site C.

SITE C	pH	Depth	Eh (V)	Ag (ppm)	As (wt%)	Ca (wt%)	Co (wt%)	Fe (wt%)	CO _{2(T)} (wt%)	S _(T) (wt%)	Co#	Fe#	S#	As Val	As ⁵⁺	As ³⁺	As ¹⁻	AVR
pH	1	0.74	-0.27	0.27	0.72	0.23	0.39	0.65	-0.89	0.34	0.63	0.78	0.34	-0.25	-0.38	0.75	0.22	-0.13
Depth	0.74	1	-0.76	0.57	0.97	0.53	0.83	0.16	-0.66	0.84	0.98	0.39	0.84	-0.71	-0.8	0.9	0.69	-0.29
Eh (V)	-0.27	-0.76	1	-0.86	-0.74	-0.9	-0.99	0.18	0.41	-0.97	-0.86	0.18	-0.95	0.98	0.99	-0.62	-0.98	0.42
Ag (ppm)	0.27	0.57	-0.86	1	0.65	0.9	0.82	-0.16	-0.36	0.74	0.71	-0.34	0.71	-0.86	-0.89	0.64	0.85	-0.66
As (wt%)	0.72	0.97	-0.74	0.65	1	0.51	0.79	0.19	-0.61	0.77	0.97	0.32	0.77	-0.66	-0.79	0.97	0.64	-0.32
Ca (wt%)	0.23	0.53	-0.9	0.9	0.51	1	0.88	-0.12	-0.47	0.82	0.65	-0.26	0.79	-0.94	-0.91	0.42	0.94	-0.5
Co (wt%)	0.39	0.83	-0.99	0.82	0.79	0.88	1	-0.11	-0.51	0.99	0.91	-0.05	0.98	-0.98	-0.99	0.67	0.97	-0.42
Fe (wt%)	0.65	0.16	0.18	-0.16	0.19	-0.12	-0.11	1	-0.74	-0.18	0.041	0.83	-0.22	0.23	0.1	0.17	-0.28	0.54
CO _{2(T)} (wt%)	-0.89	-0.66	0.41	-0.36	-0.61	-0.47	-0.51	-0.74	1	-0.45	-0.59	-0.71	-0.42	0.41	0.5	-0.56	-0.37	-0.036
S _(T) (wt%)	0.34	0.84	-0.97	0.74	0.77	0.82	0.99	-0.18	-0.45	1	0.9	-0.05	1	-0.96	-0.96	0.64	0.95	-0.38
Co#	0.63	0.98	-0.86	0.71	0.97	0.65	0.91	0.041	-0.59	0.9	1	0.21	0.9	-0.81	-0.89	0.9	0.8	-0.39
Fe#	0.78	0.39	0.18	-0.34	0.32	-0.26	-0.048	0.83	-0.71	-0.048	0.21	1	-0.049	0.22	0.11	0.3	-0.25	0.45
S#	0.34	0.84	-0.95	0.71	0.77	0.79	0.98	-0.22	-0.42	1	0.9	-0.05	1	-0.95	-0.95	0.64	0.95	-0.4
As Val	-0.25	-0.71	0.98	-0.86	-0.66	-0.94	-0.98	0.23	0.41	-0.96	-0.81	0.22	-0.95	1	0.98	-0.55	-1	0.5
As ⁵⁺	-0.38	-0.8	0.99	-0.89	-0.79	-0.91	-0.99	0.1	0.5	-0.96	-0.89	0.11	-0.95	0.98	1	-0.69	-0.97	0.46
As ³⁺	0.75	0.9	-0.62	0.64	0.97	0.42	0.67	0.17	-0.56	0.64	0.9	0.3	0.64	-0.55	-0.69	1	0.53	-0.44
As ¹⁻	0.22	0.69	-0.98	0.85	0.64	0.94	0.97	-0.28	-0.37	0.95	0.8	-0.25	0.95	-1	-0.97	0.53	1	-0.53
AVR	-0.13	-0.29	0.42	-0.66	-0.32	-0.5	-0.42	0.54	-0.036	-0.38	-0.39	0.45	-0.4	0.5	0.46	-0.44	-0.53	1

Appendix K: Output Tables from NMDS Plots

Table 1. Output table from the NMDS plot in Figure 11, showing which variables are most significant in controlling the microbial community composition. The square brackets indicate concentration of the particular element or compound. An R^2 and Pr (or p) value above 0.65 and less than 0.05 (respectively) is significant.

SITES A - C	NMDS1	NMDS2	R^2	Pr(>r)
pH	-0.608	-0.794	0.333	0.050 (.)
Depth	0.287	0.958	0.540	0.005 (**)
Eh	-0.023	1.000	0.284	0.081 (.)
[Ag]	0.493	-0.870	0.544	0.004 (**)
[As]	0.325	0.946	0.404	0.019 (*)
[Ca]	-0.287	0.958	0.335	0.038 (*)
[Co]	0.288	0.958	0.308	0.053 (.)
[Fe]	0.082	0.997	0.236	0.116
[CO _{2(T)}]	0.934	0.356	0.196	0.185
[S _(T)]	0.251	0.968	0.289	0.074 (.)
Co#	0.532	0.846	0.406	0.022 (*)
Fe#	-0.874	0.485	0.737	0.001 (***)
S#	-0.080	0.997	0.183	0.227

Significant codes: 0 (***), 0.001 (**), 0.01 (*), 0.05 (.), 0.1 ()

Table 2. Output table from the NMDS plot in Figure 12a, showing which variables are most significant in controlling the microbial community composition in site A. The square brackets indicate concentration of the particular element or compound. An R^2 and Pr (or p) value above 0.65 and less than 0.05 (respectively) is significant.

SITE A	NMDS1	NMDS2	R²	Pr(>r)
pH	-0.904	-0.428	0.231	0.644
Depth	0.799	0.601	0.961	0.011 (*)
Eh	0.974	0.226	0.034	0.956
[Ag]	0.598	-0.802	0.882	0.047 (*)
[As]	-0.804	-0.595	0.200	0.697
[Ca]	-0.853	-0.552	0.083	0.875
[Co]	-0.946	0.324	0.422	0.442
[Fe]	-0.987	0.158	0.193	0.779
[CO _{2(T)}]	0.471	-0.882	0.249	0.661
[S _(T)]	-0.984	0.177	0.767	0.081 (.)
Co#	-0.903	0.429	0.293	0.657
Fe#	-0.484	0.875	0.309	0.611
S#	-0.441	0.897	0.510	0.349

Significant codes: 0.01 (**), 0.01 (*), 0.05 (.), 0.1 ()

Table 3. Output table from the NMDS plot in Figure 12b, showing which variables are most significant in controlling the microbial community composition in site B. The square brackets indicate concentration of the particular element or compound. AVR (average valence ratio) is the ratio of the average positive versus negative arsenic species (Equation 5). An R² and Pr (or p) value above 0.65 and less than 0.05 (respectively) is significant. Significant codes: 0.01 (**), 0.01 (*), 0.05 (.), 0.1 ()

SITE B	NMDS1	NMDS2	R ²	Pr(>r)
pH	-0.513	0.859	0.915	0.031 (*)
Depth	0.855	-0.519	0.936	0.005 (**)
Eh	-0.260	-0.966	0.919	0.007 (**)
[Ag]	0.902	-0.431	0.579	0.225
[As]	-0.682	0.731	0.352	0.497
[Ca]	-0.313	0.949	0.775	0.087 (.)
[Co]	-0.563	-0.826	0.643	0.221
[Fe]	-0.142	-0.989	0.243	0.651
Co#	-0.543	0.840	0.180	0.724
Fe#	-0.612	-0.791	0.187	0.717
S#	0.433	-0.901	0.067	0.936
[CO _{2(T)}]	-0.577	0.817	0.326	0.571
[S _(T)]	-0.513	-0.858	0.1352	0.779
Average As valence	-0.937	-0.350	0.703	0.171
As ⁵⁺	-0.982	-0.186	0.811	0.118
As ³⁺	-0.061	-0.998	0.208	0.765
As ¹⁻	0.889	0.458	0.642	0.178
AVR	0.58110	0.81383	0.0219	0.975

Table 4. Output table from the NMDS plot in Figure 12c, showing which variables are most significant in controlling the microbial community composition in site C. The square brackets indicate concentration of the particular element or compound. AVR (average valence ratio) is the ratio of the average positive versus negative arsenic species (Equation 5). An R^2 and Pr (or p) value above 0.65 and less than 0.05 (respectively) is significant. Significant codes: 0.01 (**), 0.01 (*), 0.05 (.), 0.1 ()

SITE C	NMDS1	NMDS2	R^2	Pr(>r)
pH	0.769	-0.639	0.786	0.048 (*)
Depth	0.956	0.293	0.933	0.0278 (*)
Eh	-0.442	-0.897	0.833	0.0167 (*)
[Ag]	0.380	0.925	0.539	0.319
[As]	0.937	0.349	0.956	0.030 (*)
[Ca]	0.255	0.967	0.482	0.400
[Co]	0.557	0.831	0.770	0.046 (*)
[Fe]	0.30421	-0.953	0.325	0.558
Co#	0.852	0.524	0.925	0.026 (*)
Fe#	0.446	-0.895	0.719	0.126
S#	0.576	0.817	0.782	0.054 (.)
[CO _{2(T)}]	-0.878	0.477	0.385	0.558
[S _(T)]	0.560	0.829	0.791	0.042 (*)
Average As valence	-0.404	-0.915	0.690	0.090 (.)
As ⁵⁺	-0.523	-0.853	0.767	0.061 (.)
As ³⁺	0.986	0.165	0.874	0.061 (.)
As ¹⁻	0.38384	0.9234	0.687	0.093 (.)
AVR	-0.544	-0.839	0.075	0.844

Appendix L: Silver Concentration versus Depth

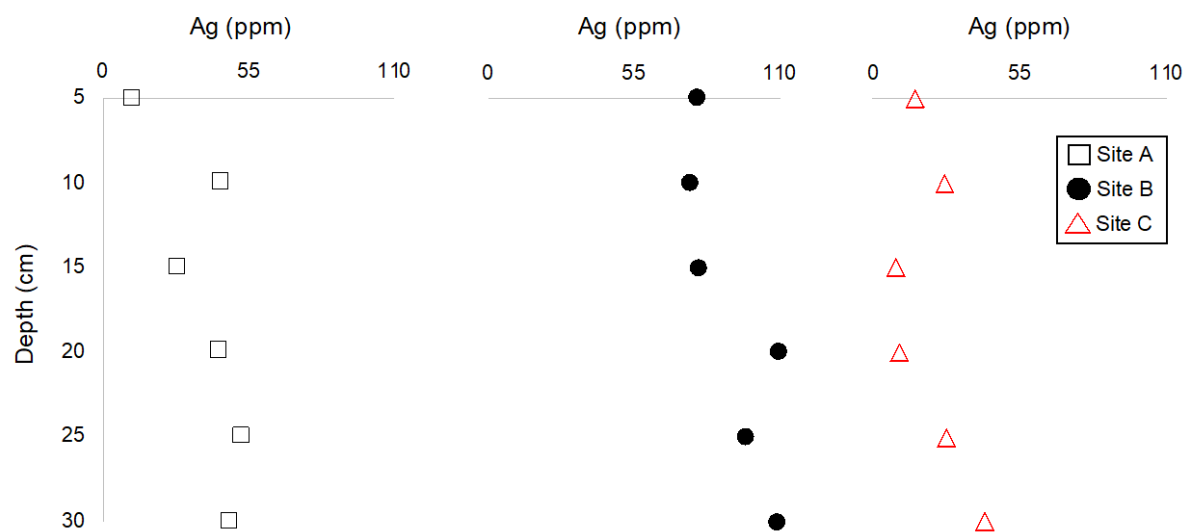


Figure 1. Depth profile plots showing the variation in Ag concentrations with depth (cm).

Appendix M: Eh Measurements

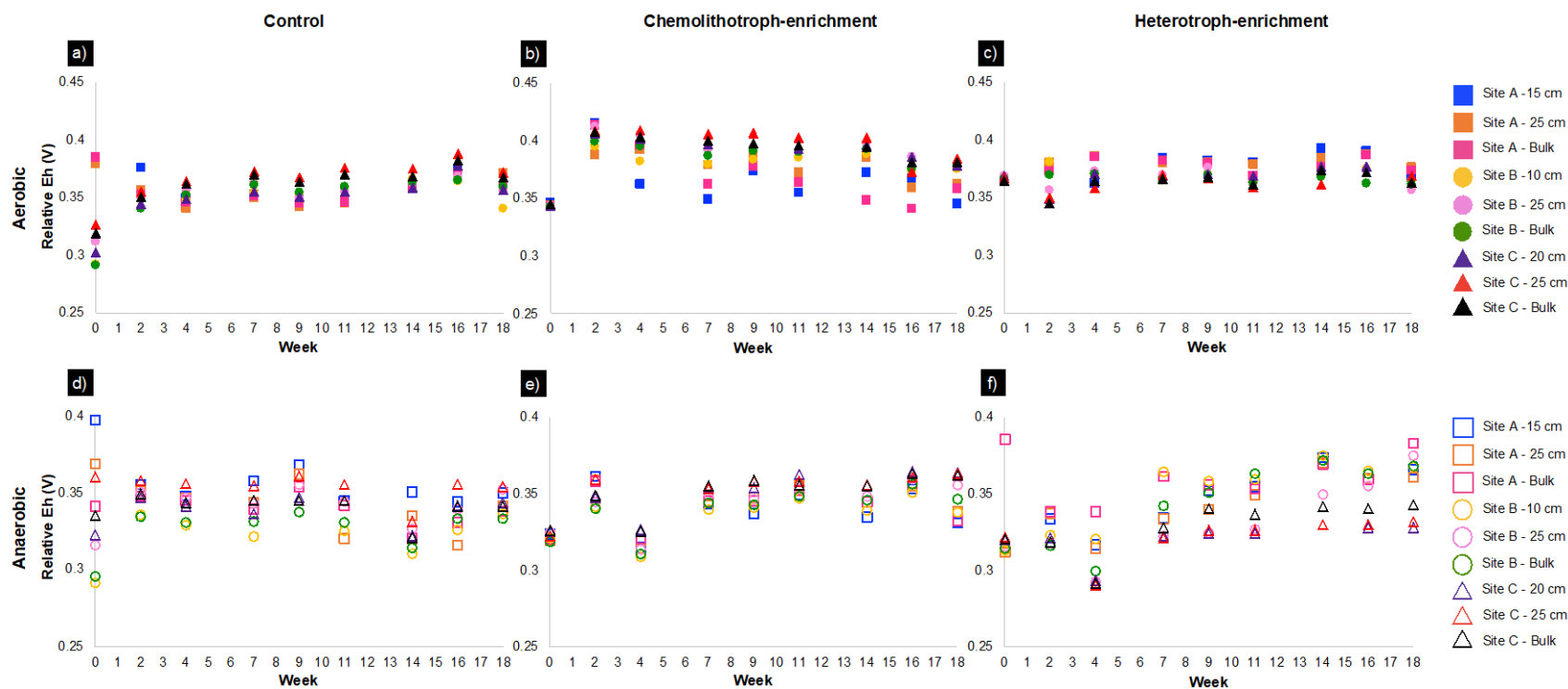


Figure 1. Eh measurements over the 18-week bioleaching experiment; a) the aerobic, control experiments, b) aerobic, chemolithotroph-enrichments, c) aerobic, heterotroph-enrichments, d) anaerobic, control, e) anaerobic chemolithotroph-enrichments, and f) anaerobic heterotroph-enrichments.

Appendix N: Raw Sequence Data and Rarefaction Curve

Table 1. Part 1 of 2: A chart of the raw bacterial sequence data showing the total number of sequences, the percent of sequences filtered out, and the percent of sequences retained.

Sample ID	Total # of Sequences	% Filtered	% Retained	Sample ID	Total # of Sequences	% Filtered	% Retained
AC-A-15-1	13823	2.8	97.2	C-A-15-1	27160	2.5	97.5
AC-A-15-2	15545	2.3	97.7	C-A-15-2	33838	2.5	97.5
AC-A-25-1	36460	2.7	97.3	C-A-25-1	18411	3.7	96.3
AC-A-25-2	25268	2.5	97.5	C-A-B-1	28975	2.4	97.6
AC-A-B-1	20353	4.4	95.6	C-A-B-2	21781	3.3	96.7
AC-A-B-2	19240	2.9	97.1	C-B-10-1	23941	2.6	97.4
AC-B-10-1	29797	2.3	97.7	C-B-10-2	21548	3.1	96.9
AC-B-10-2	21370	2.6	97.4	C-B-25-1	26287	2.6	97.4
AC-B-25-1	30662	2.2	97.8	C-B-25-2	31825	2.1	97.9
AC-B-25-2	37578	2.3	97.7	C-B-B-1	22174	2.8	97.2
AC-B-B-1	23620	2.3	97.7	C-B-B-2	19938	3.3	96.7
AC-B-B-2	30838	2.1	97.9	C-C-20-1	16677	2.6	97.4
AC-C-20-1	35599	2.0	98.0	C-C-20-2	21977	2.3	97.7
AC-C-20-2	21860	2.2	97.8	C-C-25-1	17228	2.5	97.5
AC-C-25-1	39702	2.0	98.0	C-C-25-2	16869	2.4	97.6
AC-C-25-2	18917	2.0	98.0	C-C-B-1	20231	5.0	95.0
AC-C-B-1	28211	2.1	97.9	C-C-B-2	22280	3.6	96.4
AC-C-B-2	29868	2.1	97.9	Ch-A-15-1	26902	3.6	96.4
ACh-A-15-1	26060	2.7	97.3	Ch-A-15-2	22581	6.0	94.0
ACh-A-15-2	20230	2.4	97.6	Ch-A-25-1	22217	4.0	96.0
ACh-A-25-1	14111	2.4	97.6	Ch-A-25-2	13174	3.2	96.8
ACh-A-25-2	24370	2.3	97.7	Ch-A-B-1	16128	3.6	96.4
ACh-A-B-1	25276	3.5	96.5	Ch-A-B-2	29264	4.2	95.8
ACh-A-B-2	16377	3.7	96.3	Ch-B-10-1	19856	2.5	97.5
ACh-B-10-1	24941	2.5	97.5	Ch-B-10-2	21656	2.3	97.7
ACh-B-10-2	26448	2.7	97.3	Ch-B-25-1	23128	2.2	97.8
ACh-B-25-1	13154	2.3	97.7	Ch-B-25-2	21241	2.6	97.4
ACh-B-25-2	30087	2.1	97.9	Ch-B-B-1	30295	2.1	97.9

Table 2. Part 2 of 2: A chart of the raw bacterial sequence data showing the total number of sequences, the percent of sequences filtered out, and the percent of sequences retained.

Sample ID	Total # of Sequences	% Filtered	% Retained	Sample ID	Total # of Sequences	% Filtered	% Retained
ACh-B-B-1	18245	9.6	90.4	Ch-B-B-2	21789	1.9	98.1
ACh-B-B-2	13752	2.5	97.5	Ch-C-20-1	17485	2.0	98.0
ACh-B-B-1	18245	9.6	90.4	Ch-B-B-2	21789	1.9	98.1
ACh-C-20-2	28267	2.0	98.0	Ch-C-25-1	22995	2.2	97.8
ACh-C-25-1	43323	2.2	97.8	Ch-C-25-2	20887	2.6	97.4
ACh-C-25-2	42915	2.5	97.5	Ch-C-B-1	35417	2.4	97.6
ACh-C-B-1	24699	3.4	96.6	Ch-C-B-2	20500	2.1	97.9
ACh-C-B-2	38631	4.1	95.9	H-A-15-1	20926	2.1	97.9
AH-A-15-1	70920	1.8	98.2	H-A-15-2	17965	2.5	97.5
AH-A-15-2	38299	2.9	97.1	H-A-25-1	37852	2.3	97.7
AH-A-25-1	60007	1.9	98.1	H-A-25-2	22397	2.2	97.8
AH-A-25-2	67565	1.6	98.4	H-A-B-1	25143	2.9	97.1
AH-A-B-1	48703	2.2	97.8	H-A-B-2	14065	2.8	97.2
AH-A-B-2	54640	2.3	97.7	H-B-10-1	44903	2.9	97.1
AH-B-10-1	73169	2.5	97.5	H-B-10-2	32144	3.1	96.9
AH-B-10-2	84642	2.5	97.5	H-B-25-1	18937	2.7	97.3
AH-B-25-1	129264	1.5	98.5	H-B-25-2	21903	2.9	97.1
AH-B-25-2	80043	1.9	98.1	H-B-B-1	32157	2.7	97.3
AH-B-B-1	82639	2.2	97.8	H-B-B-2	37189	2.6	97.4
AH-B-B-2	67433	2.2	97.8	H-C-20-1	14912	2.0	98.0
AH-C-20-1	83128	1.9	98.1	H-C-20-2	15882	2.7	97.3
AH-C-20-2	90517	1.8	98.2	H-C-25-1	17075	2.0	98.0
AH-C-25-1	52107	1.7	98.3	H-C-25-2	11761	2.4	97.6
AH-C-25-2	59118	1.6	98.4	H-C-B-1	16033	2.2	97.8
AH-C-B-1	39754	1.8	98.2	H-C-B-2	13237	2.9	97.1
AH-C-B-2	64987	1.9	98.1	NC	8793	10.6	89.4

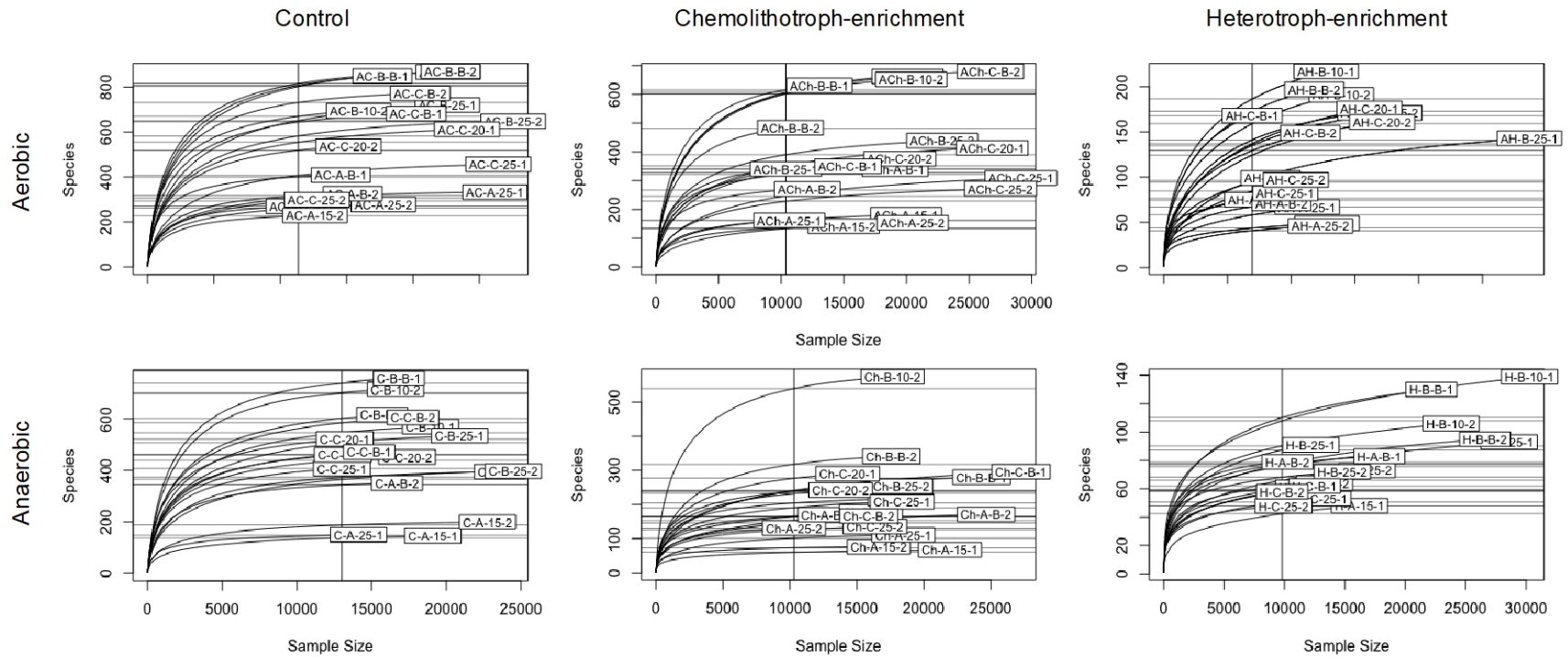


Figure 1. A rarefaction curve plot of tailings samples analyzed for 16S rRNA gene sequencing. The sample size (or sequencing depth) is on the X-axis, with species count on the Y-axis. Samples that have a curve that has plateaued means that the sequences were well-recovered, with some having a low species count meaning that there could have been a low DNA yield or the samples are not well diverse. Samples that have a curve that is beginning to plateau means that more sample diversity could have been captured, with potentially better extraction methods.

Appendix O: Concentrations of Total and Dissolved Cobalt and Arsenic Released Over Time

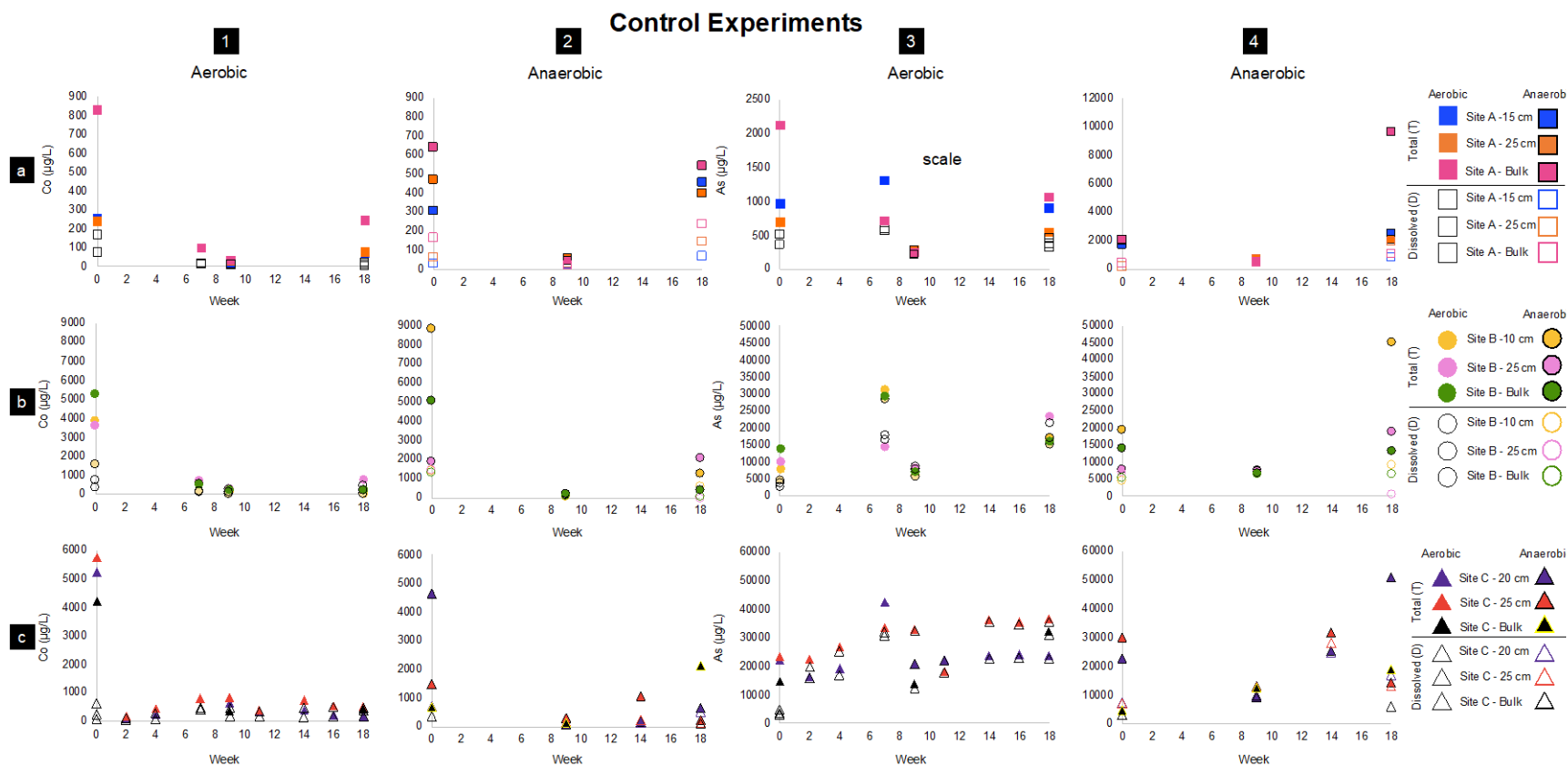


Figure 1. XY-plots of the total and dissolved amount of Co ($\mu\text{g/L}$) (columns 1 and 2 for the aerobic and anaerobic experiments, respectively) and As ($\mu\text{g/L}$) (columns 3 and 4 for the aerobic and anaerobic experiments, respectively) leached in the control-experiments. Please note the scale difference in column 3.

Chemolithotroph-enrichment Experiments

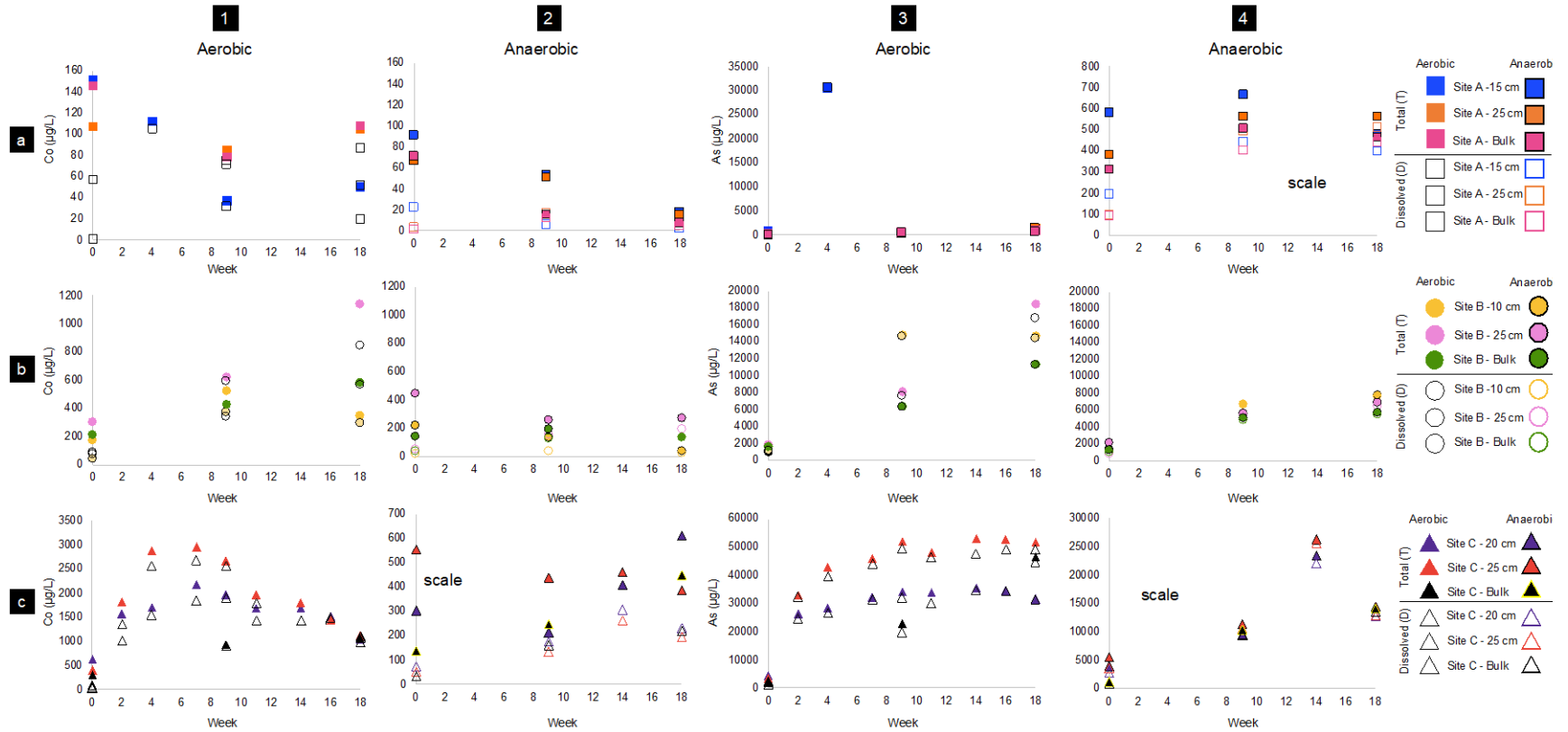


Figure 2. XY-plots of the total and dissolved amount of Co ($\mu\text{g/L}$) (columns 1 and 2 for the aerobic and anaerobic experiments, respectively) and As ($\mu\text{g/L}$) (columns 3 and 4 for the aerobic and anaerobic experiments, respectively) leached in the chemolithotroph-enrichment experiments. Please note the scale difference at: 2c, 4a, and 4c.

Heterotroph-enrichment Experiments

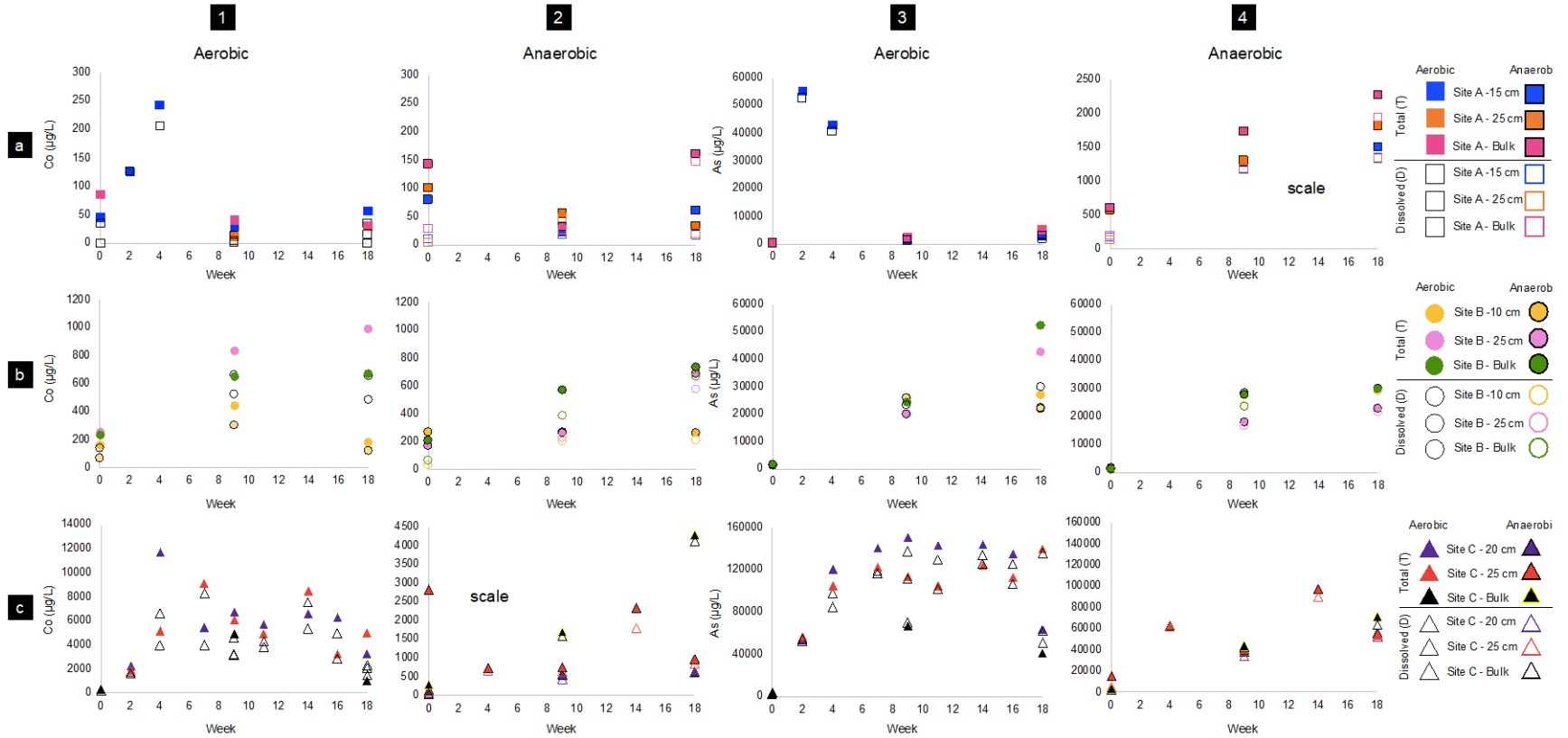


Figure 3. XY-plots of the total and dissolved amount of Co ($\mu\text{g/L}$) (columns 1 and 2 for the aerobic and anaerobic experiments, respectively) and As ($\mu\text{g/L}$) (columns 3 and 4 for the aerobic and anaerobic experiments, respectively) leached in the heterotroph-enrichment experiments. Please note the scale difference at 2c and 4a.

Appendix P: Total and Dissolved Metal Concentrations from Enrichment Experiments

Table 1. The cumulative percent of Co recovered from the 18-week control experiments. The naming scheme: experiment – site ID – centimetre or bulk – total (T) or dissolved (D).

Control Experiments: Cumulative Percent of Co Recovered									
Sample ID	Week 0	Week 2	Week 4	Week 7	Week 9	Week 11	Week 14	Week 16	Week 18
C-A-15-T	0.188			0.261	0.273				0.327
C-A-15-D	0.056			0.063	0.070				0.070
C-A-25-T	0.120				0.135				0.174
C-A-25-D	0.039				0.046				0.051
C-A-Bulk-T	0.418			0.467	0.484				0.606
C-A-Bulk-D	0.085			0.093	0.098				0.108
C-B-10-T	0.323			0.383	0.398				0.405
C-B-10-D	0.134			0.147	0.152				0.158
C-B-25-T	0.328			0.395	0.424				0.494
C-B-25-D	0.036			0.087	0.111				0.154
C-B-Bulk-T	0.447			0.494	0.516				0.538
C-B-Bulk-D	0.066			0.081	0.093				0.116
C-C-20-T	0.102	0.103	0.108	0.124	0.136	0.143	0.150	0.155	0.159
C-C-20-D	0.012	0.013	0.014	0.022	0.025	0.028	0.031	0.035	0.038
C-C-25-T	0.091	0.094	0.101	0.113	0.126	0.133	0.144	0.153	0.160
C-C-25-D	0.001	0.003	0.007	0.014	0.021	0.026	0.034	0.041	0.048
C-C-Bulk-T	0.069				0.075				0.081
C-C-Bulk-D	0.004				0.007				0.013
AC-A-15-T	0.227				0.265				0.604
AC-A-15-D	0.024				0.042				0.092
AC-A-25-T	0.236				0.266				0.467
AC-A-25-D	0.033				0.047				0.121
AC-A-Bulk-T	0.322				0.344				0.617
AC-A-Bulk-D	0.084				0.095				0.216
AC-B-10-T	0.729				0.740				0.845
AC-B-10-D	0.118				0.124				0.175
AC-B-25-T	0.170				0.184				0.371
AC-B-25-D	0.130				0.144				0.144
AC-B-Bulk-T	0.428				0.448				0.486
AC-B-Bulk-D	0.114				0.127				0.132
AC-C-20-T	0.090				0.093		0.096		0.108
AC-C-20-D	0.013				0.015		0.017		0.027
AC-C-25-T	0.023				0.028		0.044		0.048
AC-C-25-D	0.010				0.013		0.016		0.017
AC-C-Bulk-T	0.011				0.013				0.047
AC-C-Bulk-D	0.006				0.007				0.008

Table 2. The cumulative percent of As recovered from the 18-week control experiments. The naming scheme: experiment – site ID – centimetre or bulk – total (T) or dissolved (D).

Control Experiments: Cumulative Percent of As Recovered									
Sample ID	Week 0	Week 2	Week 4	Week 7	Week 9	Week 11	Week 14	Week 16	Week 18
C-A-15-T	0.282			0.659	0.731				0.991
C-A-15-D	0.107			0.280	0.347				0.441
C-A-25-T	0.190				0.270				0.419
C-A-25-D	0.100				0.178				0.281
C-A-Bulk-T	0.413			0.552	0.602				0.811
C-A-Bulk-D	0.101			0.214	0.257				0.349
C-B-10-T	0.206			1.001	1.162				1.592
C-B-10-D	0.120			0.842	0.985				1.369
C-B-25-T	0.267			0.653	0.874				1.497
C-B-25-D	0.073			0.551	0.782				1.351
C-B-Bulk-T	0.372			1.160	1.351				1.782
C-B-Bulk-D	0.100			0.543	0.758				1.219
C-C-20-T	0.163	0.284	0.425	0.735	0.888	1.052	1.226	1.404	1.578
C-C-20-D	0.037	0.152	0.275	0.500	0.651	0.814	0.981	1.150	1.316
C-C-25-T	0.123	0.240	0.379	0.553	0.724	0.819	1.008	1.194	1.385
C-C-25-D	0.016	0.119	0.252	0.420	0.589	0.682	0.868	1.049	1.235
C-C-Bulk-T	0.105				0.202				0.430
C-C-Bulk-D	0.025				0.113				0.333
AC-A-15-T	0.499				0.690				1.426
AC-A-15-D	0.050				0.216				0.453
AC-A-25-T	0.548				0.741				1.299
AC-A-25-D	0.059				0.243				0.764
AC-A-Bulk-T	0.398				0.505				2.389
AC-A-Bulk-D	0.092				0.195				0.414
AC-B-10-T	0.499				0.690				1.832
AC-B-10-D	0.120				0.306				0.544
AC-B-25-T	0.211				0.404				0.907
AC-B-25-D	0.189				0.376				0.395
AC-B-Bulk-T	0.380				0.566				0.922
AC-B-Bulk-D	0.145				0.322				0.495
AC-C-20-T	0.165				0.237		0.421		0.791
AC-C-20-D	0.052				0.121		0.302		0.426
AC-C-25-T	0.157				0.225		0.390		0.465
AC-C-25-D	0.035				0.102		0.248		0.316
AC-C-Bulk-T	0.033				0.120				0.253
AC-C-Bulk-D	0.022				0.088				0.131

Table 3. The cumulative percent of Co recovered from the 18-week chemolithotroph enrichments. The naming scheme: experiment – site ID – centimetre or bulk – total (T) or dissolved (D).

Chemolithotroph-Enrichments: Cumulative Percent of Co Recovered									
Sample ID	Week 0	Week 2	Week 4	Week 7	Week 9	Week 11	Week 14	Week 16	Week 18
Ch-A-15-T	0.112		0.195		0.222				0.259
Ch-A-15-D	0.000		0.077		0.101				0.115
Ch-A-25-T	0.054				0.096				0.149
Ch-A-25-D	0.000				0.037				0.081
Ch-A-Bulk-T	0.074				0.113				0.168
Ch-A-Bulk-D	0.029				0.064				0.090
Ch-B-10-T	0.014				0.058				0.087
Ch-B-10-D	0.003				0.034				0.059
Ch-B-25-T	0.027				0.082				0.184
Ch-B-25-D	0.008				0.060				0.135
Ch-B-Bulk-T	0.018				0.054				0.103
Ch-B-Bulk-D	0.006				0.035				0.082
Ch-C-20-T	0.012	0.043	0.076	0.119	0.157	0.190	0.223	0.253	0.273
Ch-C-20-D	0.002	0.022	0.052	0.088	0.125	0.153	0.182	0.210	0.230
Ch-C-25-T	0.006	0.035	0.081	0.128	0.170	0.201	0.230	0.252	0.270
Ch-C-25-D	0.001	0.022	0.063	0.105	0.146	0.175	0.197	0.221	0.239
Ch-C-Bulk-T	0.005				0.021				0.038
Ch-C-Bulk-D	0.001				0.016				0.034
ACh-A-15-T	0.067				0.106				0.119
ACh-A-15-D	0.016				0.021				0.022
ACh-A-25-T	0.033				0.058				0.066
ACh-A-25-D	0.002				0.010				0.014
ACh-A-Bulk-T	0.036				0.044				0.047
ACh-A-Bulk-D	0.001				0.006				0.009
ACh-B-10-T	0.018				0.029				0.032
ACh-B-10-D	0.001				0.004				0.006
ACh-B-25-T	0.039				0.062				0.086
ACh-B-25-D	0.004				0.018				0.035
ACh-B-Bulk-T	0.012				0.028				0.039
ACh-B-Bulk-D	0.003				0.014				0.025
ACh-C-20-T	0.006				0.010		0.018		0.030
ACh-C-20-D	0.002				0.005		0.011		0.015
ACh-C-25-T	0.009				0.016		0.023		0.029
ACh-C-25-D	0.001				0.003		0.007		0.010
ACh-C-Bulk-T	0.002				0.006				0.014
ACh-C-Bulk-D	0.001				0.003				0.007

Table 4. The cumulative percent of As recovered from the 18-week chemolithotroph-enrichments. The naming scheme: experiment – site ID – centimetre or bulk – total (T) or dissolved (D).

Chemolithotroph-Enrichments: Cumulative Percent of As Recovered									
Sample ID	Week 0	Week 2	Week 4	Week 7	Week 9	Week 11	Week 14	Week 16	Week 18
Ch-A-15-T	0.270		9.140		9.336				9.664
Ch-A-15-D	0.035		8.887		9.043				9.343
Ch-A-25-T	0.548				0.741				1.299
Ch-A-25-D	0.548				0.741				1.299
Ch-A-Bulk-T	0.140				0.346				0.626
Ch-A-Bulk-D	0.090				0.269				0.513
Ch-B-10-T	0.033				0.408				0.783
Ch-B-10-D	0.026				0.398				0.764
Ch-B-25-T	0.051				0.268				0.758
Ch-B-25-D	0.030				0.234				0.681
Ch-B-Bulk-T	0.044				0.216				0.520
Ch-B-Bulk-D	0.032				0.202				0.504
Ch-C-20-T	0.033	0.226	0.433	0.668	0.918	1.164	1.422	1.674	1.905
Ch-C-20-D	0.018	0.197	0.391	0.621	0.855	1.074	1.328	1.579	1.807
Ch-C-25-T	0.018	0.189	0.412	0.650	0.921	1.170	1.446	1.719	1.988
Ch-C-25-D	0.010	0.178	0.384	0.613	0.870	1.111	1.359	1.614	1.870
Ch-C-Bulk-T	0.018				0.178				0.506
Ch-C-Bulk-D	0.011				0.151				0.466
ACh-A-15-T	0.168				0.361				0.500
ACh-A-15-D	0.057				0.186				0.301
ACh-A-25-T	0.103				0.255				0.408
ACh-A-25-D	0.027				0.160				0.299
ACh-A-Bulk-T	0.061				0.160				0.251
ACh-A-Bulk-D	0.019				0.098				0.184
ACh-B-10-T	0.035				0.204				0.399
ACh-B-10-D	0.021				0.189				0.384
ACh-B-25-T	0.057				0.203				0.386
ACh-B-25-D	0.022				0.164				0.335
ACh-B-Bulk-T	0.034				0.170				0.323
ACh-B-Bulk-D	0.028				0.156				0.303
ACh-C-20-T	0.029				0.099		0.270		0.373
ACh-C-20-D	0.022				0.091		0.252		0.345
ACh-C-25-T	0.029				0.088		0.225		0.300
ACh-C-25-D	0.019				0.074		0.207		0.274
ACh-C-Bulk-T	0.009				0.082				0.180
ACh-C-Bulk-D	0.007				0.074				0.170

Table 5. The cumulative percent of Co recovered from the 18-week heterotroph-enrichments. The naming scheme: experiment – site ID – centimetre or bulk – total (T) or dissolved (D).

Heterotroph-Enrichments: Cumulative Percent of Co Recovered									
Sample ID	Week 0	Week 2	Week 4	Week 7	Week 9	Week 11	Week 14	Week 16	Week 18
H-A-15-T	0.034	0.127	0.306		0.328				0.371
H-A-15-D	0.000	0.093	0.244		0.253				0.280
H-A-25-T	0.043				0.050				0.064
H-A-25-D	0.017				0.020				0.020
H-A-Bulk-T	0.043				0.064				0.080
H-A-Bulk-D	0.000				0.001				0.009
H-B-10-T	0.014				0.050				0.065
H-B-10-D	0.006				0.031				0.041
H-B-25-T	0.023				0.097				0.186
H-B-25-D	0.013				0.071				0.130
H-B-Bulk-T	0.020				0.074				0.131
H-B-Bulk-D	0.012				0.056				0.097
H-C-20-T	0.006	0.049	0.277	0.383	0.513	0.623	0.752	0.874	0.937
H-C-20-D	0.003	0.038	0.167	0.243	0.306	0.380	0.484	0.580	0.620
H-C-25-T	0.005	0.034	0.115	0.259	0.354	0.431	0.565	0.616	0.695
H-C-25-D	0.002	0.027	0.090	0.220	0.292	0.360	0.479	0.524	0.547
H-C-Bulk-T	0.005				0.085				0.102
H-C-Bulk-D	0.002				0.054				0.091
AH-A-15-T	0.060				0.078				0.124
AH-A-15-D	0.009				0.023				0.037
AH-A-25-T	0.051				0.080				0.098
AH-A-25-D	0.003				0.028				0.039
AH-A-Bulk-T	0.073				0.089				0.171
AH-A-Bulk-D	0.015				0.028				0.104
AH-B-10-T	0.022				0.044				0.065
AH-B-10-D	0.002				0.018				0.036
AH-B-25-T	0.015				0.038				0.098
AH-B-25-D	0.005				0.025				0.076
AH-B-Bulk-T	0.017				0.065				0.126
AH-B-Bulk-D	0.005				0.037				0.093
AH-C-20-T	0.003				0.014				0.026
AH-C-20-D	0.001				0.010				0.021
AH-C-25-T	0.044		0.056		0.068		0.104		0.120
AH-C-25-D	0.002		0.012		0.022		0.050		0.064
AH-C-Bulk-T	0.005				0.033				0.103
AH-C-Bulk-D	0.001				0.027				0.095

Table 6. The cumulative percent of As recovered from the 18-week heterotroph-enrichments. The naming scheme: experiment – site ID – centimetre or bulk – total (T) or dissolved (D).

Heterotroph-Enrichments: Cumulative Percent of As Recovered									
Sample ID	Week 0	Week 2	Week 4	Week 7	Week 9	Week 11	Week 14	Week 16	Week 18
H-A-15-T	0.081	16.051	28.506		29.031				29.845
H-A-15-D	0.042	15.236	26.953		27.332				27.915
H-A-25-T	0.094				0.771				2.247
H-A-25-D	0.071				0.544				1.440
H-A-Bulk-T	0.061				0.512				1.494
H-A-Bulk-D	0.028				0.259				0.812
H-B-10-T	0.041				0.702				1.389
H-B-10-D	0.036				0.696				1.255
H-B-25-T	0.043				0.573				1.705
H-B-25-D	0.032				0.556				1.142
H-B-Bulk-T	0.044				0.698				2.107
H-B-Bulk-D	0.041				0.660				1.466
H-C-20-T	0.025	0.420	1.298	2.322	3.421	4.464	5.510	6.496	6.958
H-C-20-D	0.021	0.404	1.113	1.983	2.986	3.933	4.910	5.823	6.276
H-C-25-T	0.019	0.310	0.856	1.491	2.079	2.624	3.268	3.852	4.574
H-C-25-D	0.016	0.299	0.737	1.342	1.922	2.450	3.099	3.653	3.917
H-C-Bulk-T	0.028				0.498				0.785
H-C-Bulk-D	0.023				0.516				1.468
AH-A-15-T	0.168				0.533				0.965
AH-A-15-D	0.048				0.382				0.767
AH-A-25-T	0.152				0.502				0.988
AH-A-25-D	0.033				0.349				0.706
AH-A-Bulk-T	0.117				0.455				0.898
AH-A-Bulk-D	0.038				0.268				0.645
AH-B-10-T	0.038				0.755				1.514
AH-B-10-D	0.023				0.624				1.358
AH-B-25-T	0.031				0.502				1.104
AH-B-25-D	0.021				0.456				1.022
AH-B-Bulk-T	0.035				0.779				1.571
AH-B-Bulk-D	0.022				0.649				1.439
AH-C-20-T	0.016				0.294				0.695
AH-C-20-D	0.013				0.258				0.639
AH-C-25-T	0.078		0.402		0.609		1.110		1.390
AH-C-25-D	0.023		0.342		0.545		1.010		1.289
AH-C-Bulk-T	0.021				0.324				0.821
AH-C-Bulk-D	0.014				0.311				0.756

Appendix Q: Additional Taxonomic Plots after Bioleaching Experiments

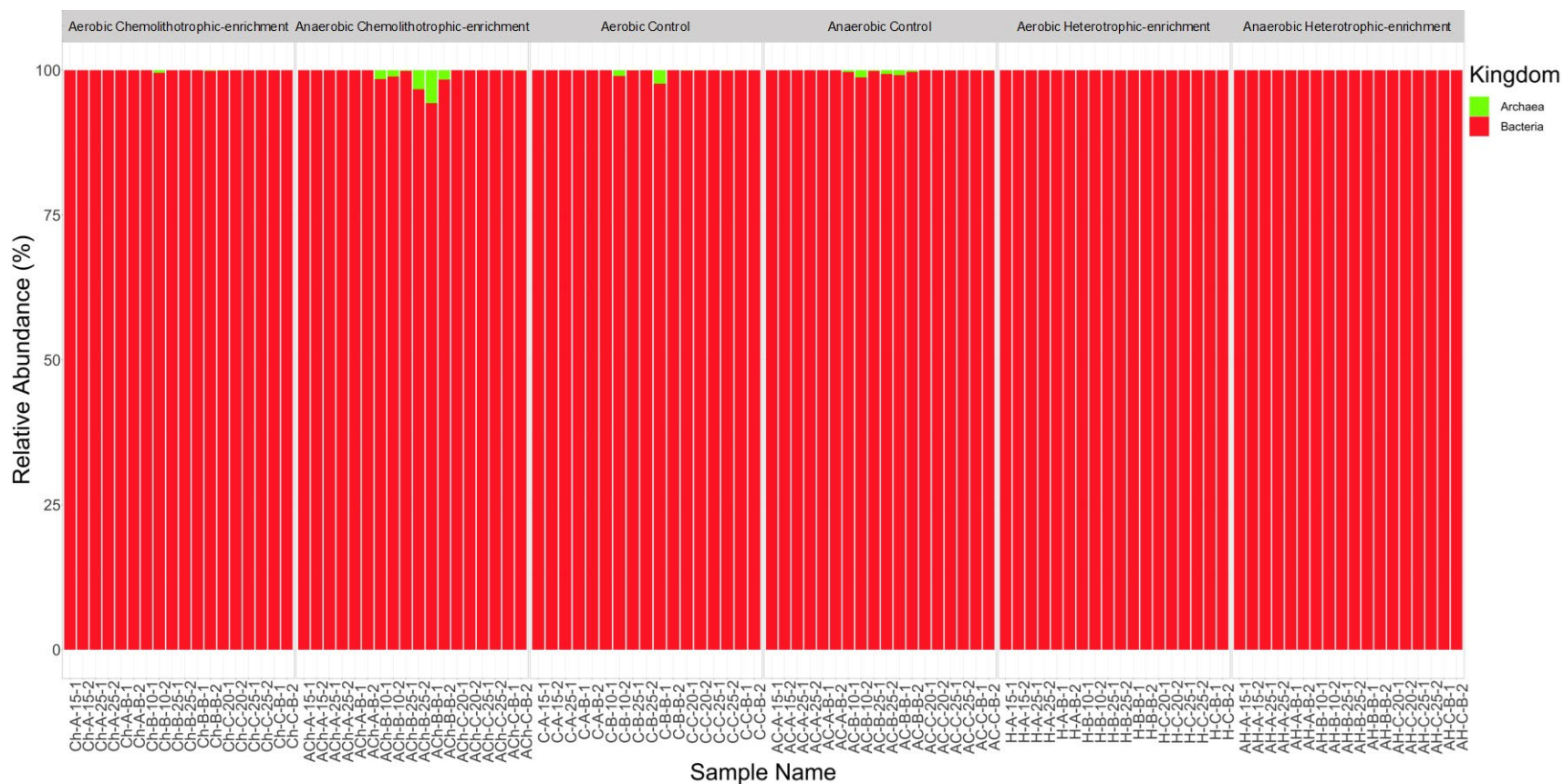


Figure 1. Normalized relative abundance taxonomic bar plot of the microbial communities present after bioleaching experiments at the Kingdom level.

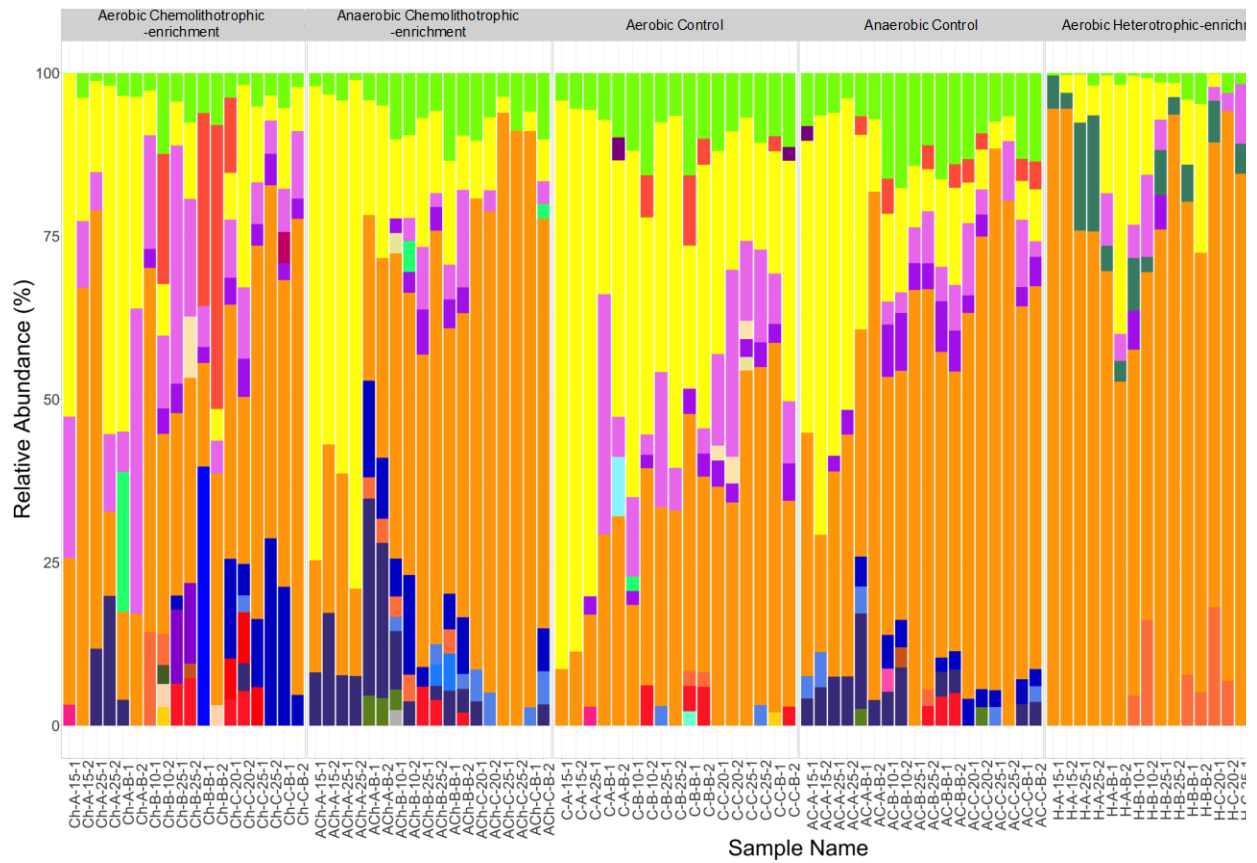


Figure 2. Normalized relative abundance taxonomic bar plot of the microbial communities present after bioleaching experiments at the Class level.

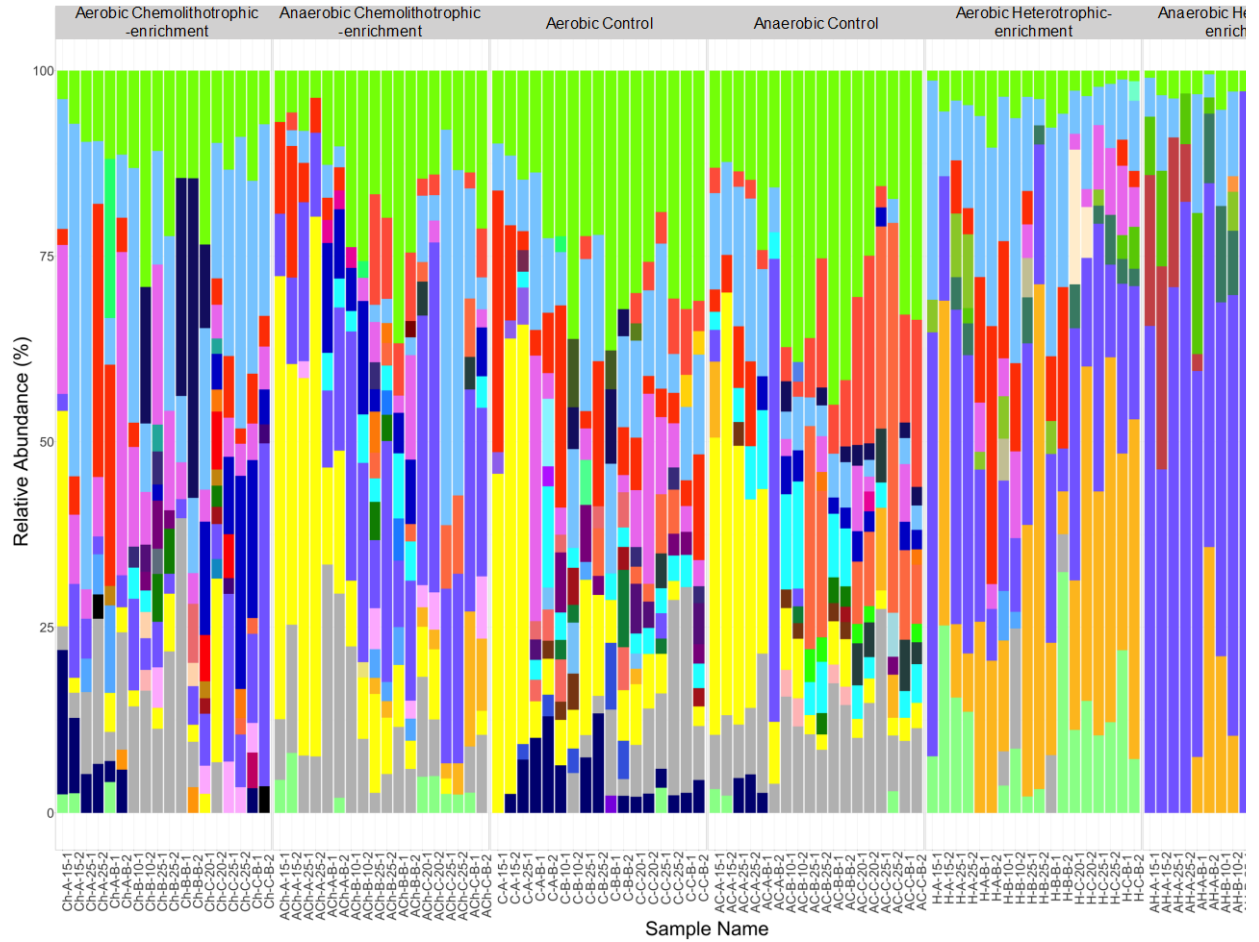


Figure 3. Normalized relative abundance taxonomic bar plot of the microbial communities present after bioleaching experiments at the Family level.

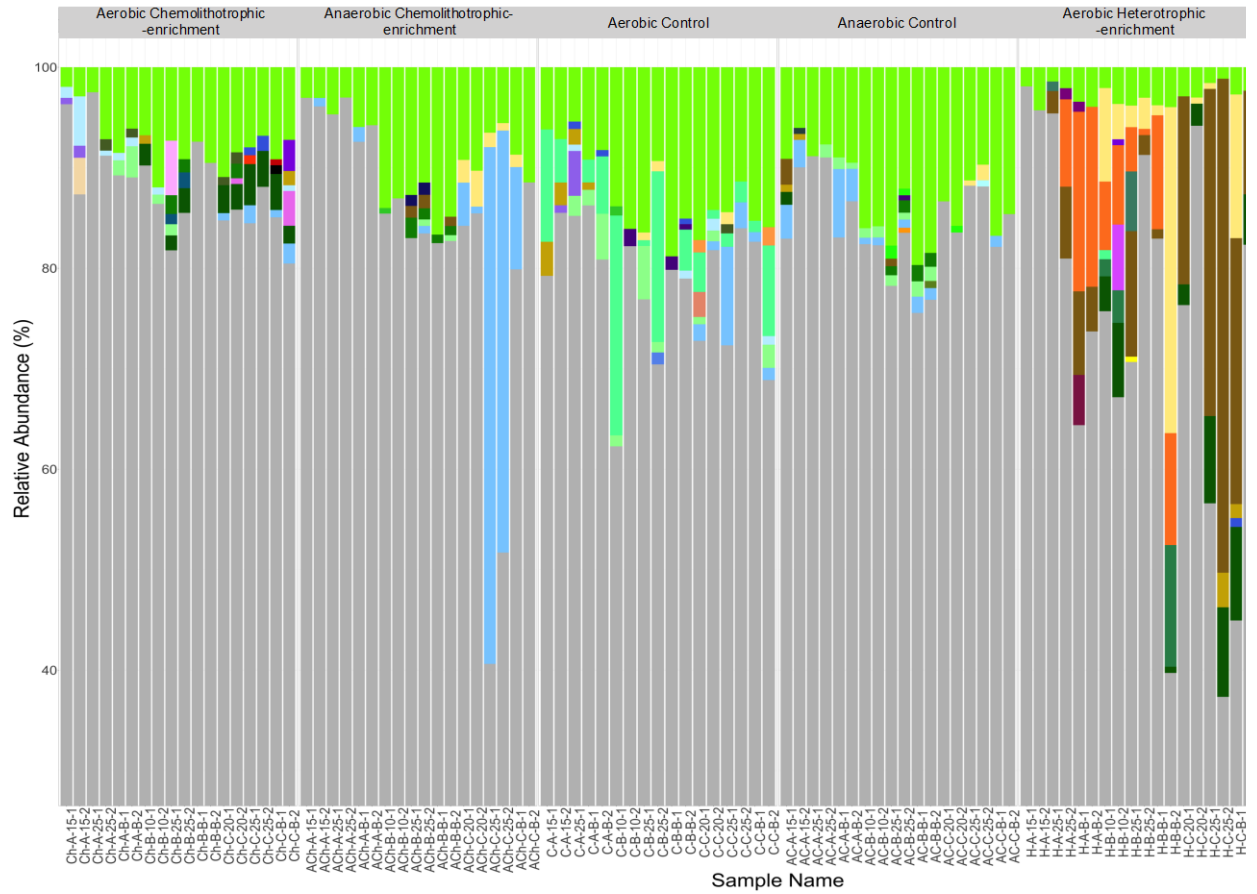


Figure 4. Normalized relative abundance taxonomic bar plot of the microbial communities present after bioleaching experiments at the Species level.